

9/78

(NASA-CR-157608) THE DEEP SPACE NETWORK
Progress Report, May and June 1978 (Jet
Propulsion Lab.) 188 p HC A09/MF A01

CSSL 22D

N78-32137
THRU
N78-32161
Unclas
G3/12 32842

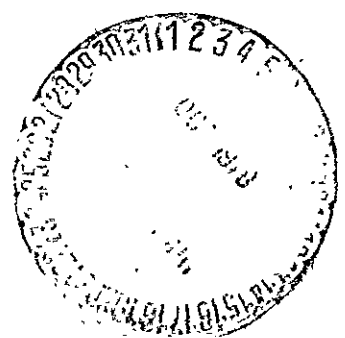
The Deep Space Network Progress Report 42-46

May and June 1978

August 15, 1978

National Aeronautics and
Space Administration

Jet Propulsion Laboratory
California Institute of Technology
Pasadena, California



The Deep Space Network Progress Report 42-46

May and June 1978

August 15, 1978

National Aeronautics and
Space Administration

Jet Propulsion Laboratory
California Institute of Technology
Pasadena, California

The research described in this publication was carried out by the Jet Propulsion Laboratory, California Institute of Technology, under NASA Contract No NAS7-100.

Preface

Beginning with Volume XX, the Deep Space Network Progress Report changed from the Technical Report 32- series to the Progress Report 42- series. The volume number continues the sequence of the preceding issues. Thus, Progress Report 42-20 is the twentieth volume of the Deep Space Network series, and is an uninterrupted follow-on to Technical Report 32-1526, Volume XIX.

This report presents DSN progress in flight project support, tracking and data acquisition (TDA) research and technology, network engineering, hardware and software implementation, and operations. Each issue presents material in some, but not all, of the following categories in the order indicated.

Description of the DSN

Mission Support

- Ongoing Planetary/Interplanetary Flight Projects
- Advanced Flight Projects

Radio Astronomy

Special Projects

Supporting Research and Technology

- Tracking and Ground-Based Navigation
- Communications—Spacecraft/Ground
- Station Control and Operations Technology
- Network Control and Data Processing

Network and Facility Engineering and Implementation

- Network
- Network Operations Control Center
- Ground Communications
- Deep Space Stations
- Quality Assurance

Operations

- Network Operations
- Network Operations Control Center
- Ground Communications
- Deep Space Stations

Program Planning

- TDA Planning

In each issue, the part entitled “Description of the DSN” describes the functions and facilities of the DSN and may report the current configuration of one of the seven DSN systems (Tracking, Telemetry, Command, Monitor & Control, Test & Training, Radio Science, and Very Long Baseline Interferometry).

The work described in this report series is either performed or managed by the Tracking and Data Acquisition organization of JPL for NASA.

Contents

DESCRIPTION OF THE DSN

Network Functions and Facilities	1-
N. A. Renzetti	
The DSN VLBI System, Mark I-79	5-
B. D. L. Mulhall	
NASA Code 311-03-43-10	
A Tutorial Introduction to Very Long Baseline Interferometry (VLBI) Using Bandwidth Synthesis	16
J. I. Molinder	
NASA Code 311-03-43-10	

MISSION SUPPORT

Ongoing Planetary/Interplanetary Flight Projects

Viking Extended Mission Support	29
R. L. Gillette	
NASA Code 311-03-22-50	
Pioneer Mission Support	33
D. W. H. Johnston	
NASA Code 311-03-21-90	
Helios Mission Support	37
P. S. Goodwin, G. M. Rockwell, and W. N. Jensen	
NASA Code 311-03-21-50	

SUPPORTING RESEARCH AND TECHNOLOGY

Tracking and Ground-Based Navigation

On Improved Ranging	40
J. W. Layland, A. I. Zygielbaum, and W. P. Hubbard	
NASA Code 310-10-61-16	
Establishing a Celestial VLBI Reference Frame—I. Searching for VLBI Sources	46
R. A. Preston et al.	
NASA Code 310-10-60-10	

Communications—Spacecraft/Ground

JPL 2²⁰ Channel 300 MHz Bandwidth Digital Spectrum Analyzer	57
G. A. Morris, Jr., and H. C. Wilck	
NASA Code 310-20-67-12	

Use of A Priori Statistics to Minimize Acquisition Time for RFI Immune Spread Spectrum Systems	62
J. K. Holmes and K. T. Woo	
NASA Code 310-20-67-13	

Station Control and Operations Technology

UNIBUS Monitor for PDP 11	70
M. D. Donner	
NASA Code 310-30-69-10	

DSS 13 Antenna Subsystem Automation	73
H. Phillips, I. Crane, and P. Lipsius	
NASA Code 310-30-68-11	

Network Control and Data Processing

FPLA Mechanization of Arithmetic Elements to Produce A + B or to Pass A Only	76
D. E. Wallis, H. Taylor, and A. L. Rubin	
NASA Code 310-40-72-08	

A Probabilistic Version of Sperner's Theorem, With Applications to the Problem of Retrieving Information From a Data Base	81
L. D. Baumert, R. J. McEliece, E. R. Rodemich, and H. Rumsey, Jr.	
NASA Code 310-40-72-08	

NETWORK AND FACILITY ENGINEERING AND IMPLEMENTATION

Network

VLBI-Laser Intercomparison Project	87
B. D. L. Mulhall	
NASA Code 311-03-42-91	

A Fast Computation of Complex Convolution Using a Hybrid Transform	92
I. S. Reed and T. K. Truong	
NASA Code 311-03-42-95	

The Gravitational Wave Detection Experiment: Description and Anticipated Requirements	100
A. L. Berman	
NASA Code 311-03-43-10	

Deep Space Stations

Preliminary Analysis of the Impact of Power Cycling on CTA-21 Equipment Reliability	109
E. R. Cole	
NASA Code 311-03-41-08	

The DSS Radio Science Subsystem—Data Handling of Very Long Baseline Interferometry (VLBI) Data	115
A. L. Berman	
NASA Code 311-03-43-10	

Absolute Flux Density Calibrations: Receiver Saturation Effects	123
A. J. Freiley, J. E. Ohlson, and B. L. Seidel	
NASA Code 311-03-41-05	

DSN Portable Zero Delay Assembly	130
E. J. Serhal, Jr., and T. Y. Otoshi	
NASA Code 311-03-42-54	

PROGRAM PLANNING

TDA Planning

Evaluation of the Developing DSN Life-Cycle Cost Standard Practice	139
M. McKenzie	
NASA Code 311-03-31-30	

VLBI HISTORY AND BIBLIOGRAPHY

A Brief Historical Introduction to Very Long Baseline Interferometry	146
B. Benjauthrit	
NASA Code 311-03-42-95	
An Extensive Bibliography on Long Baseline Interferometry	154
B. Benjauthrit	
NASA Code 311-03-42-95	

Network Functions and Facilities

N. A. Renzetti

Office of Tracking and Data Acquisition

The objectives, functions, and organization of the Deep Space Network are summarized; deep space station, ground communication, and network operations control capabilities are described.

The Deep Space Network was established by the National Aeronautics and Space Administration (NASA) Office of Space Tracking and Data Systems and is under the system management and technical direction of the Jet Propulsion Laboratory (JPL). The network is designed for two-way communications with unmanned spacecraft traveling approximately 16,000 km (10,000 miles) from Earth to the farthest planets and to the edge of our solar system. It has provided tracking and data acquisition support for the following NASA deep space exploration projects: Ranger, Surveyor, Mariner Venus 1962, Mariner Mars 1964, Mariner Venus 1967, Mariner Mars 1969, Mariner Mars 1971, and Mariner Venus-Mercury 1973, for which JPL has been responsible for the project management, the development of the spacecraft, and the conduct of mission operations; Lunar Orbiter, for which the Langley Research Center carried out the project management, spacecraft development, and conduct of mission operations; Pioneer, for which Ames Research Center carried out the project management, spacecraft development, and conduct of mission operations; and Apollo, for which the Lyndon B. Johnson Space Center was the project center and the Deep Space Network supplemented the Manned Space Flight Network, which was managed by the Goddard Space Flight Center. The network is currently providing tracking and data acquisition support for Helios, a joint U.S./West German project; Viking, for which Langley Research Center provides the project management, the Lander spacecraft, and conducts

mission operations, and for which JPL provides the Orbiter spacecraft; Voyager, for which JPL provides project management, spacecraft development, and conduct of mission operations; and Pioneer Venus, for which the Ames Research Center provides project management, spacecraft development, and conduct of mission operations. The network is adding new capability to meet the requirements of the Jupiter Orbiter Probe Mission, for which JPL provides the project management, spacecraft development and conduct of mission operations.

The Deep Space Network (DSN) is one of two NASA networks. The other, the Spaceflight Tracking and Data Network (STDN), is under the system management and technical direction of the Goddard Space Flight Center (GSFC). Its function is to support manned and unmanned Earth-orbiting satellites. The Deep Space Network supports lunar, planetary, and interplanetary flight projects.

From its inception, NASA has had the objective of conducting scientific investigations throughout the solar system. It was recognized that in order to meet this objective, significant supporting research and advanced technology development must be conducted in order to provide deep space telecommunications for science data return in a cost effective manner. Therefore, the Network is continually evolved to keep pace with the state of the art of telecommunications and data

handling. It was also recognized early that close coordination would be needed between the requirements of the flight projects for data return and the capabilities needed in the Network. This close collaboration was effected by the appointment of a Tracking and Data Systems Manager as part of the flight project team from the initiation of the project to the end of the mission. By this process, requirements were identified early enough to provide funding and implementation in time for use by the flight project in its flight phase.

As of July 1972, NASA undertook a change in the interface between the Network and the flight projects. Prior to that time, since 1 January 1964, in addition to consisting of the Deep Space Stations and the Ground Communications Facility, the Network had also included the mission control and computing facilities and provided the equipment in the mission support areas for the conduct of mission operations. The latter facilities were housed in a building at JPL known as the Space Flight Operations Facility (SFOF). The interface change was to accommodate a hardware interface between the support of the network operations control functions and those of the mission control and computing functions. This resulted in the flight projects assuming the cognizance of the large general-purpose digital computers which were used for both network processing and mission data processing. They also assumed cognizance of all of the equipment in the flight operations facility for display and communications necessary for the conduct of mission operations. The Network then undertook the development of hardware and computer software necessary to do its network operations control and monitor functions in separate computers. A characteristic of the new interface is that the Network provides direct data flow to and from the stations; namely, metric data, science and engineering telemetry, and such network monitor data as are useful to the flight project. This is done via appropriate ground communication equipment to mission operations centers, wherever they may be.

The principal deliverables to the users of the Network are carried out by data system configurations as follows:

- (1) The DSN Tracking System generates radio metric data, i.e., angles, one- and two-way doppler and range, and transmits raw data to Mission Control.
- (2) The DSN Telemetry System receives, decodes, records, and retransmits engineering and scientific data generated in the spacecraft to Mission Control.
- (3) The DSN Command System accepts spacecraft commands from Mission Control and transmits the commands via the Ground Communication Facility to a Deep Space Station. The commands are then radiated to the spacecraft in order to initiate spacecraft functions in flight.

- (4) The DSN Radio Science System generates radio science data, i.e., the frequency and amplitude of spacecraft transmitted signals affected by passage through media such as the solar corona, planetary atmospheres, and planetary rings, and transmits this data to Mission Control.

The data system configurations supporting testing, training, and network operations control functions are as follows:

- (1) The DSN Monitor and Control System instruments, transmits, records, and displays those parameters of the DSN necessary to verify configuration and validate the Network. It provides the tools necessary for Network Operations personnel to control and monitor the Network and interface with flight project mission control personnel.
- (2) The DSN Test and Training System generates and controls simulated data to support development, test, training and fault isolation within the DSN. It participates in mission simulation with flight projects.

The capabilities needed to carry out the above functions have evolved in the following technical areas:

- (1) The Deep Space Stations, which are distributed around Earth and which, prior to 1964, formed part of the Deep Space Instrumentation Facility. The technology involved in equipping these stations is strongly related to the state of the art of telecommunications and flight-ground design considerations, and is almost completely multimission in character.
- (2) The Ground Communications Facility provides the capability required for the transmission, reception, and monitoring of Earth-based, point-to-point communications between the stations and the Network Operations Control Center at JPL, Pasadena, and to the JPL Mission Operations Centers. Four communications disciplines are provided: teletype, voice, high-speed, and wideband. The Ground Communications Facility uses the capabilities provided by common carriers throughout the world, engineered into an integrated system by Goddard Space Flight Center, and controlled from the communications center located in the Space Flight Operations Facility (Building 230) at JPL.

The Network Operations Control Center is the functional entity for centralized operational control of the Network and interfaces with the users. It has two separable functional elements; namely, Network Operations Control and Network

Data Processing. The functions of the Network Operations Control are:

- (1) Control and coordination of Network support to meet commitments to Network users.
- (2) Utilization of the Network data processing computing capability to generate all standards and limits required for Network operations.
- (3) Utilization of Network data processing computing capability to analyze and validate the performance of all Network systems.

The personnel who carry out the above functions are located in the Space Flight Operations Facility, where mission operations functions are carried out by certain flight projects. Network personnel are directed by an Operations Control Chief. The functions of the Network Data Processing are:

- (1) Processing of data used by Network Operations Control for control and analysis of the Network.
- (2) Display in the Network Operations Control Area of data processed in the Network Data Processing Area.
- (3) Interface with communications circuits for input to and output from the Network Data Processing Area.
- (4) Data logging and production of the intermediate data records.

The personnel who carry out these functions are located approximately 200 meters from the Space Flight Operations Facility. The equipment consists of minicomputers for real-time data system monitoring, two XDS Sigma 5s, display, magnetic tape recorders, and appropriate interface equipment with the ground data communications.

omit

DSN VLBI Articles

This issue of the DSN Progress Report contains two articles which relate to current DSN VLBI activities.

The first article describes the functional requirements and system design of the DSN VLBI System, Mark I-79, a new system being implemented in the Network.

The second article provides a tutorial introduction to the technology of VLBI. The basic concepts are described, and equations are derived by which various parameters related to interferometry can be approximated.

At the back of this issue, the interested reader will find a brief VLBI history as well as an extensive VLBI bibliography.

D₂-17
N78-32139
(15)
(17B)

The DSN VLBI System, Mark I-79

B. D. L. Mulhall
TDA Engineering Office

The DSN VLBI System has been established as a new Network System. This article describes the system and discusses the system functional requirements.

I. Introduction

Very long baseline interferometry is a new capability being implemented in the Network to support flight project navigation requirements and provide station frequency standard stability monitoring of sufficient accuracy to effectively validate hydrogen maser performance.

In order to manage this major new implementation, the DSN VLBI System was established, and a review of the system functional requirements was held on 24 February 1978. A description of the system and the phases of its implementation follow.

II. Definition

Very long baseline interferometry is a method of measuring the time of arrival of a radio signal at two locations very distant from each other on the Earth's surface. From the measurement of difference in time of arrival, the position of the radio source and/or several other parameters of the problem can be determined. These other parameters include Universal Time One (UT1) (the instantaneous rotational angle of the Earth), polar motion, the relative position of the two stations, and the time offset and rate of change of the clocks at the two stations.

III. System Characteristics

The DSN VLBI System can be characterized as a new implementation in the 64-meter subnet and the Network Operations and Control Center. The implementation modifies existing station equipment; implementation of the 34-meter subnet is planned later (e.g., the multimission open-loop receivers, the occultation data assembly, and the digital recorder assembly). New hardware and software will be implemented in the Network Data Processing Area at JPL Pasadena.

VLBI requires at least two stations and a central facility for correlation and estimation processors.

The station diagram consists of an antenna pointed at the signal being used to make the measurement, low-noise microwave amplifiers, and receivers for receiving the signal and converting it to zero offset. At this point, analog-to-digital converters and multiplexers convert the data to digital form and direct them to the appropriate device for recording. The diagrams show various implementation phases. These are Block 1 (Phase 1, 2, and 3) and Block 2.

Block 1 handles data differently than does Block 2. As shown in Fig. 1, the Block 1 system records the data on computer-compatible tape for playback and transmission to

the Ground Communications Facility (GCF) wideband data lines.

The DSS configuration for Block 1, Phase 1 is shown in Fig. 3. GCF transmission capability will be achieved by July 1979 by employing the Block IV receiver and DSN Advanced System IF to video converters to provide data to the DSS Radio Science Subsystem. By July 1980, the multimission open-loop receiver will be transferred. This configuration (Fig. 4) is called Block 1, Phase 2. The Block 1 configuration is completed with Phase 3 by the addition of the Block 1 processor (Fig. 6).

The Block 2 interferometer (Fig. 2) requires such large volumes of data and is used so relatively infrequently that the data are recorded on a digital instrumentation recorder, the digital recorder assembly. These tapes are then shipped or transported to the correlation facility. Figure 3 shows the DSS configuration with the Block 3 Monitor and Control Subsystem, which centralizes the collection of configuration and calibration data.

The correlation facilities are also divided by Blocks 1 and 2 in Figs. 1 and 2. These two processor facilities employ the same design and equipment, special-purpose hardware for correlation, control computer, and correlation software. However, as before, the method of providing data to the correlator is significantly different for Block 1 than for Block 2. In the case of Block 1, the computer edits the data received over wideband data lines and provides two serial streams of bits representing the information recorded at the two separate stations. These data are accepted by the correlator and the cross-correlation is performed. This facility serves only DSN operational functions, and consequently, will be located in the Network Data Processing Area (NDPA).

In the case of Block 2, the same correlator design is employed; however, the data are provided by playback from the digital recorder assembly. This facility will be located outside of the Network Operations Control Center (NOCC) at another location within JPL, Pasadena.

IV. DSS Configuration

The DSS configuration (Figs. 3, 4, and 5) includes the portions of the Ground Communications Facility (GCF) that exist at the station. The configuration at both VLBI stations is identical.

The signal is received and passes through the Antenna Microwave Subsystem. In this subsystem, the phase calibrator tones generated by the Receiver-Exciter Subsystem are injected as high up, as near the front end, as possible. These

tones provide a calibration of any drift between the injection point and the analog-to-digital converters. The Antenna Microwave Subsystem also provides water vapor radiometer data to the DSS Monitor and Control Subsystem for logging.

The signal next passes to the Receiver-Exciter Subsystem, where the signal is converted from RF to 300 MHz IF. The signal is then divided into eight IF-to-video converters. These IF converters are in turn interfaced to the A-to-D converters in the DSS Radio Science Subsystem. At this point the data either go through a multiplexer to the occultation data assembly for recording for Block 1 functions or the digital recording assembly for Block 2 functions. After the observation, if Block 1 configuration is in use, the data are played back from the real-time record, blocked up in GCF blocks, and provided to the station wideband data assembly for transmission. If Block 2 functions are being used, the recording on the digital recording assembly is shipped back to the correlation facility.

The Monitor and Control Subsystem has the functions of configuring the stations and collecting various calibration and configuration data. These calibration and configuration data are provided to the digital recording assembly for logging and transmission over wideband lines with the actual VLBI data or they are provided over high-speed lines for monitoring purposes. If Block 2 data are being recorded, then the computer recorder on the occultation data assembly is used for collecting the calibration and configuration data and providing them with the digital recording assembly tape. The Monitor and Control also receives predicts from the Network Operations and Control Center, which are disseminated to the appropriate subsystems, including Antenna Mechanical, for pointing the antenna.

V. Ground Communications Facility and Network Operations and Control Center Configurations

Figures 6 and 7 show the entire GCF, including the station portion and the NOCC configuration. The NOCC configuration is further divided between the equipment in the network data processing terminal and the network data processing area. The network data log provided by the GCF can be used for collecting the VLBI and the calibration and configuration data for Block 1. The VLBI real-time monitor collects configuration and calibration data to verify the performance of the network in real time.

The VLBI data are replayed and metered out to the VLBI correlator assembly that is under the control of the VLBI processor assembly, a computer with the correlation program running in it. The two data streams are cross-correlated and the resulting fringes are recorded by the VLBI processor

assembly. After the correlation process, the post-correlation tape is replayed through the same computer and post-correlation and estimation processing are performed. The final product is clock sync, UT1, the polar motion.

The Block 2 correlator does not employ the GCF transmission, and consequently, the tapes of the digital recording assembly and occultation data assembly are brought to this facility, where the correlation process is quite similar using the same design correlator and identical software except for additional features and functions required of Block 2 over Block 1 capability.

The Display Subsystem provides station configuration data to the network operations and, from this area, controls are sent to the station. In the Support Subsystem, the VLBI predicts program is used to generate the sequence of events for the station, including the antenna pointing angles, which are then transmitted through GCF for Blocks 1 and 2 data acquisition.

VI. Block 2 VLBI Future Requirements

The future of the Block 2 VLBI processor beyond the DSN requirements for radio source catalog maintenance are being studied and defined. The evolutionary growth of this facility, so that it can serve the radio astronomy community and the National Geodetic Survey requirements as well as the DSN needs, is briefly described.

Table 1 shows the evolutionary steps for the processor for radio astronomy applications. The columns list the number of stations or radio telescopes which can be simultaneously correlated, the number of BWS channels that can be correlated in parallel, and finally, the need dates for the expanded capability. The first step would be the two-station, 8-channel correlator capability. This capability employs digital instrumentation recorders with 24 tracks, which are capable of extension to 28 tracks. In order to reduce tape usage, the eight BWS channels are blocked up after A and D conversion and written across the 24 tracks. This requires deskewing upon playback.

The first step in increasing capability would be to add Mark II compatibility for system validation and for processing of Mark II tapes, which will still be in use when the processor becomes operational. The need for this Mark II capability could be as early as 1979, even though the processor is not operational at that time. At the same time, capability should be provided to read eight tracks of data directly off the tape and provide each track to the respective correlator channel so that the processor would be capable of performing Mark III processing with multiple passes through the tape. The capabil-

ity for parallel reading without deskewing could also be used as early as 1979.

The second step would be either to expand to three stations and three baselines with eight channels or expand the two telescope processors to 28 channels, all of which would be read directly off independent tracks of the 28-track recorder. The expansion from eight to 28 tracks increases processor throughput by a factor of 3.5 if all 28 tracks are parallel BWS channel recordings. On the other hand, going from two to three stations increases throughput by a factor of 3 (three baselines versus one). This latter step is considerably more expensive, since an additional tape drive is required.

By 1981, a third step could be justified in terms of the needs of the radio astronomy community. This third step would be to provide three baseline correlators with 28 BWS channels per station. At this time, a decision point is reached. For the ultimate capability, the number of radio telescopes in the radio astronomy network needs to be identified. Presently, there are four, perhaps five, radio telescopes in the United States which will shortly be equipped with Mark III instrumentation. By 1981, we should be able to say if the number of radio telescopes in the Network Users Group will increase to eight or possibly ten.

Based on the ultimate number of potential telescopes, the decision can be made to proceed to increase the processor to four, possibly five, stations, leaving room for ultimate expansion to the final number. At this point also, the existing hardware correlator assembly probably needs to be repackaged to make room available for cabling to interconnect all the other station correlators so that in Step 4, when expansion is made to four or five telescopes, the repackaging would leave enough room for additional cabling and modules to allow all the necessary cross-correlations to be performed in parallel.

The expansion in BWS channels beyond 28 may also be required, but this decision can probably be made later. The increase in hardware for expansion in channels goes by n , while the increase for expansion in telescope goes by n^2 , and consequently the ultimate number of stations to be processed simultaneously is a more critical decision than the ultimate number of BWS channels.

Table 2 shows the growth of processor capability required primarily for geodetic but also for geodynamic (UT1-polar motion) applications. Some differences between these requirements and the astronomy requirements are:

- (1) BWS channel widths for radio astronomy range from 0.125 MHz to 2 MHz (possibly both narrower and

wider widths will be required), while geodesy requires 2 MHz to 25 MHz channel bandwidth.

- (2) Radio astronomy requires independent track recording, while geodesy requires maximum tape efficiency while keeping the ability to speed up or slow down the data rate during the observation, depending on the source

strength. This requires blocking the data and writing across all tracks regardless of the tape speed.

The immediate impact of these Block 2 processor plans is the design requirement to be able to expand the correlator to multiple baseline. The Block 1 processor is not affected since it will remain a two-station device.

Table 1. Radio astronomy applications

Step	Number of telescopes	Number of BWS channels	Date needed
0	2	8 (blocked and written over 24 tracks)	
1a		(Mark II compat.)	1979
1b	2	8 (parallel, each track recorded independently)	1979
2 } 2 }	3 2	8 28	
3	3	28	1981
	(Decision points for ultimate number of telescopes)		
4	4 (5?)	28	1983

Table 2. Geodetic and/or geodynamic applications

Step	Number of antennas	Number of BWS channels	BWS channel width	Date needed
1	2	2	2 - 25 MHz	1981
2	2	6	2 - 8 MHz	1981
3	6	6	2 - 8 MHz	1982/3

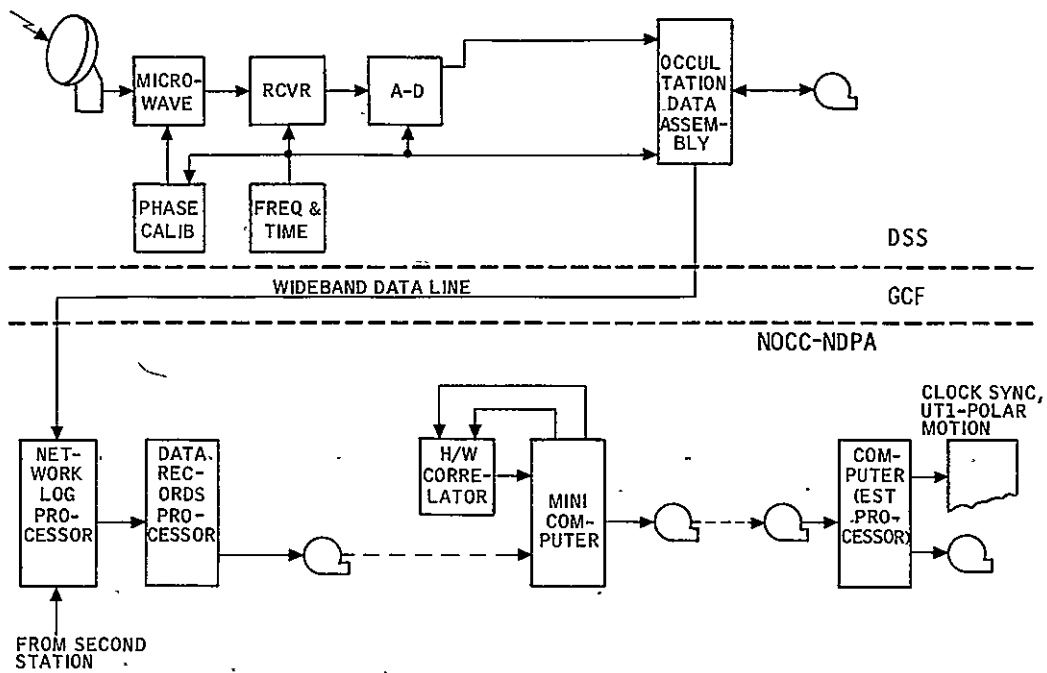


Fig. 1. Block 1 configuration

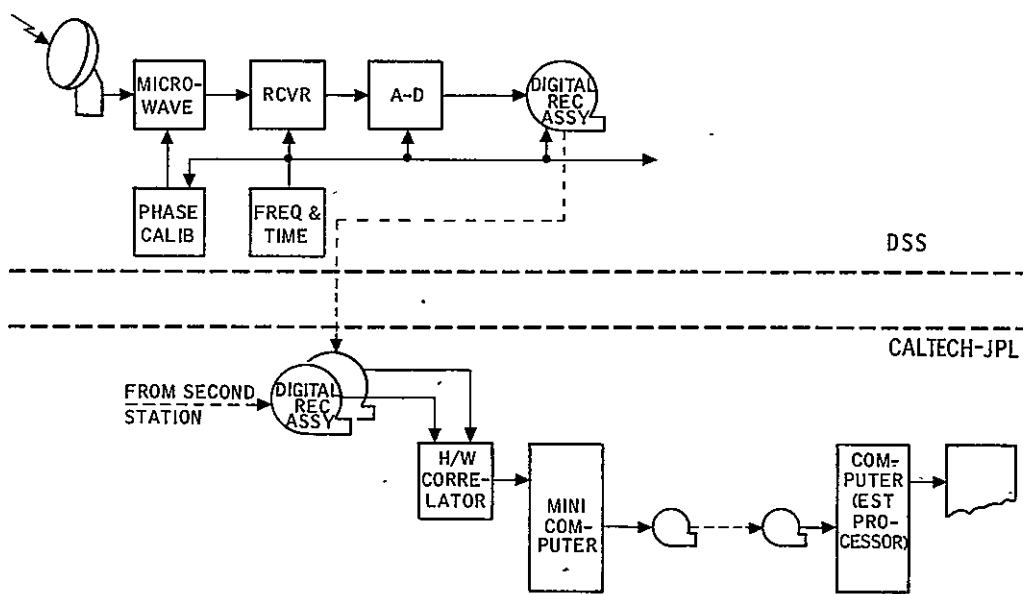


Fig. 2. Block 2 configuration

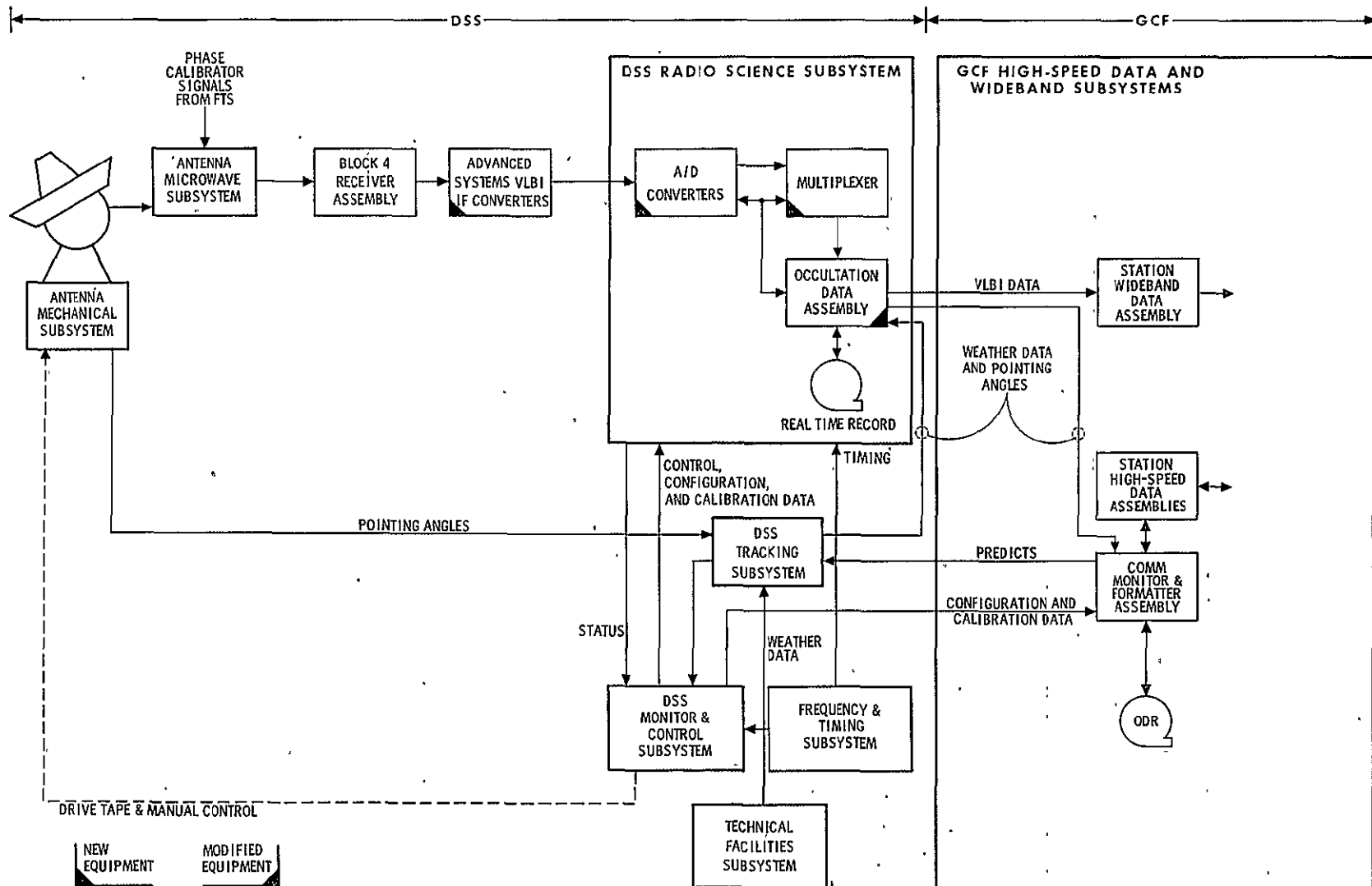


Fig. 3. DSS-GCF block diagram, Block 1, Phase 1

ORIGINAL PAGE IS
OF POOR QUALITY

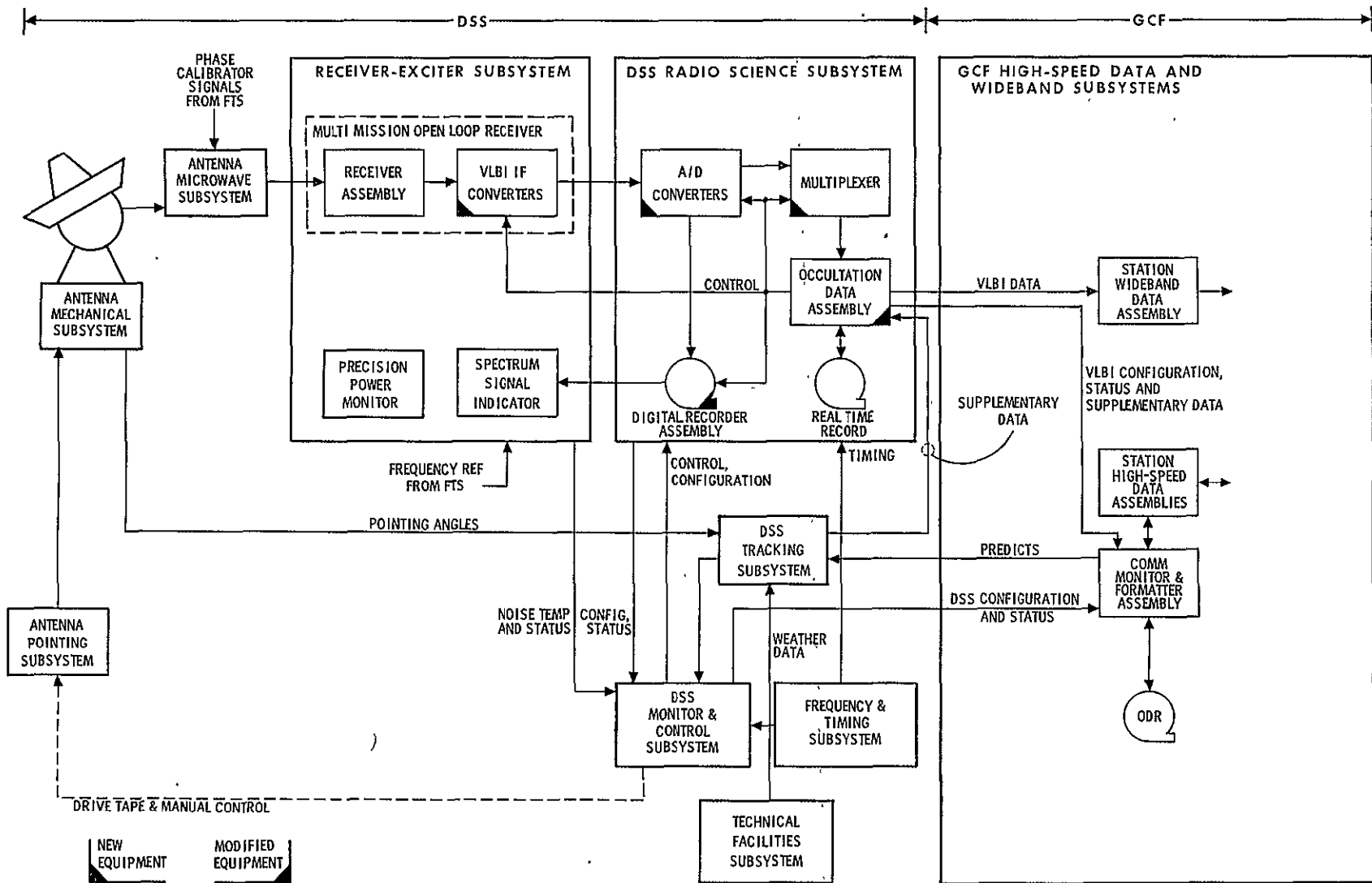


Fig. 4. DSS-GCF block diagram, Block 1 and 2 VLBI configuration before Block 3 DMC

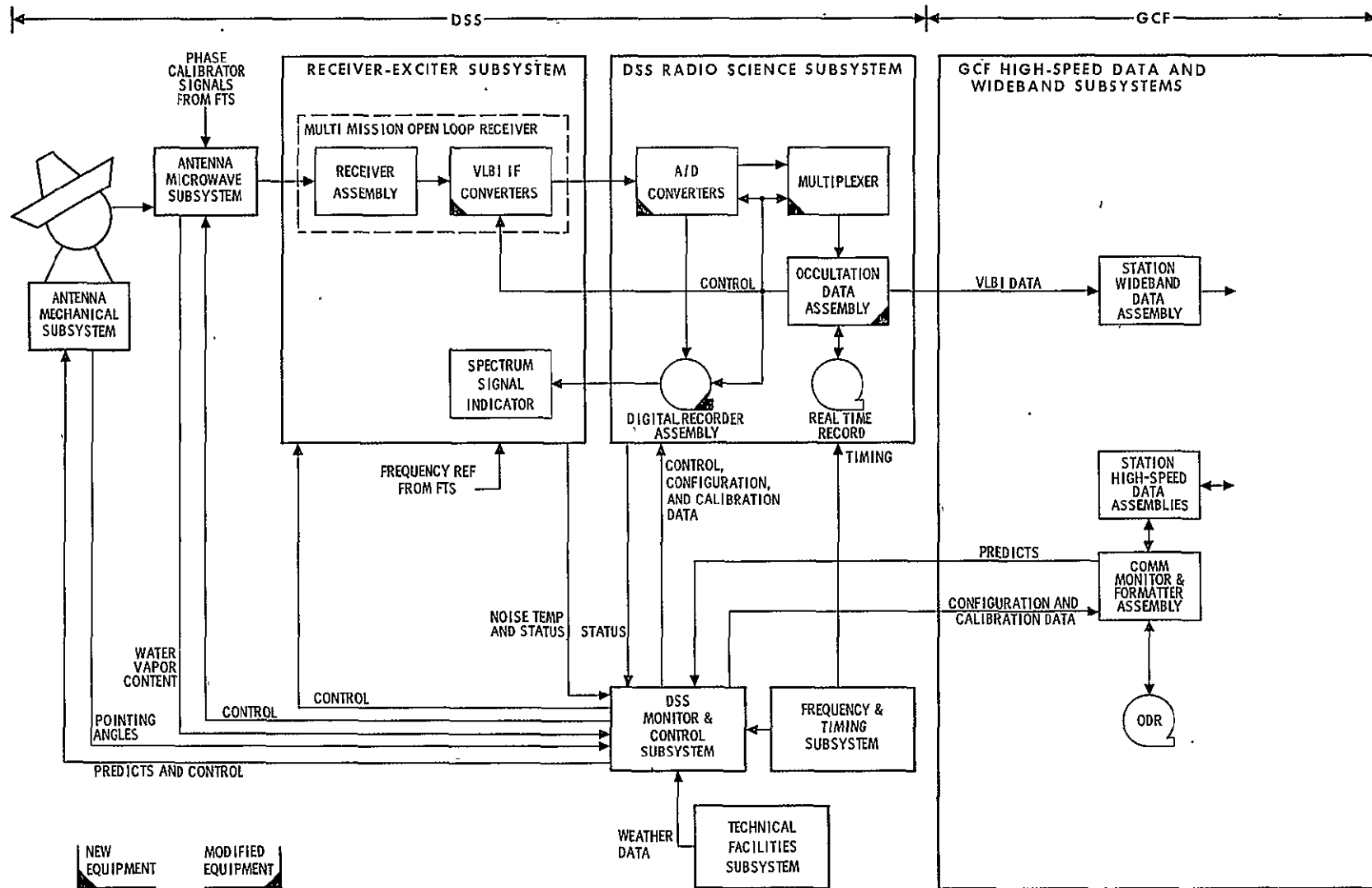


Fig. 5. DSS-GCF block diagram, with Block 3 DMC

ORIGINAL PAGE IS
OF POOR QUALITY

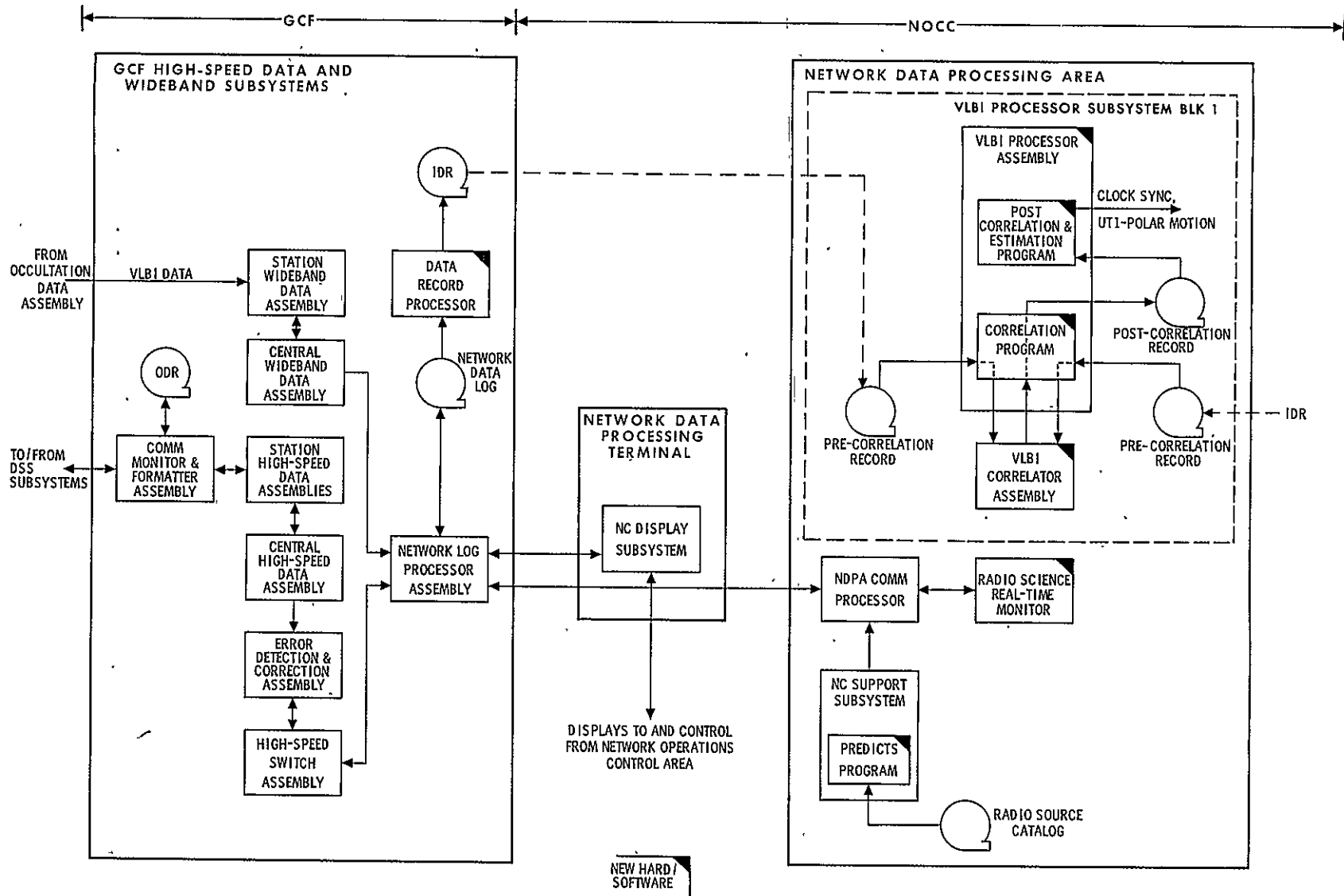


Fig. 6. GCF-NOCC block diagram, Block 1 processor

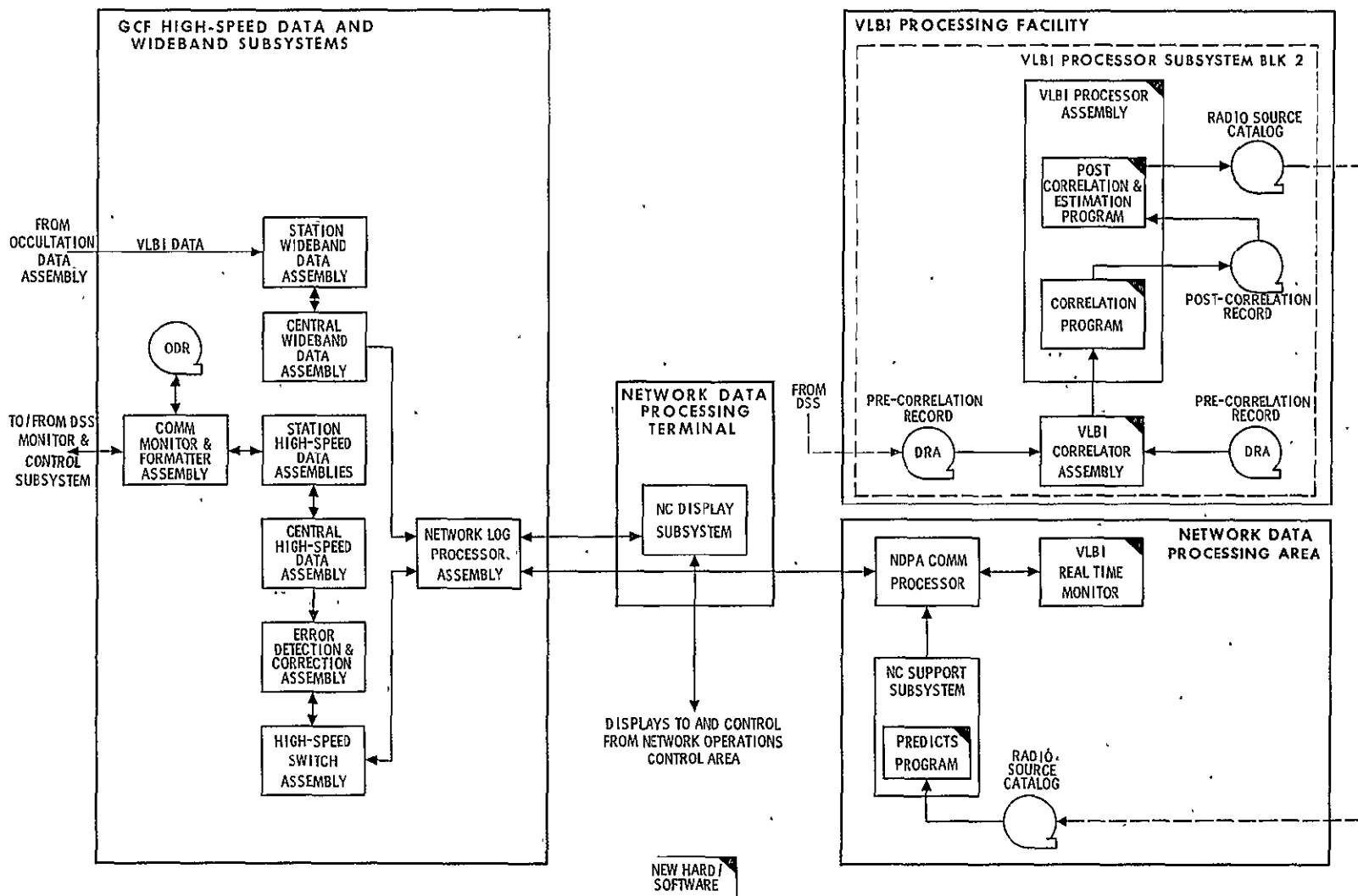


Fig. 7. GCF-NOCC block diagram, Block 2 processor

ORIGINAL PAGE IS
OF POOR QUALITY

D3-17 - (178)
(28)

N78-32140

DSN Progress Report 42-46

May and June 1978

A Tutorial Introduction to Very Long Baseline Interferometry (VLBI) Using Bandwidth Synthesis

J.L. Molinder

TDA Engineering and Harvey Mudd College

This article gives a tutorial presentation of the basic principles underlying Very Long Baseline Interferometry (VLBI) using bandwidth synthesis. Although many subtle details are ignored, the article presents the basic signal processing approach and summarizes results showing the tradeoff of measurement accuracy with spanned bandwidth, source strength, antenna size and efficiency, system noise temperature, and data volume. Results pertaining to minimization of required antenna time for a given baseline measurement accuracy are also discussed.

I. Introduction

A concise description of VLBI, given in Ref. 1, is repeated below.

In very long baseline interferometer (VLBI) measurements, the radio signal produced by a distant source is recorded simultaneously at two radio antennas. Because of a difference in raypaths, the signal will be delayed in time at one antenna relative to the other. By cross correlating the two signals, the time delay and/or its time derivative may be determined. In addition, correlated amplitude measurements can yield source strength and structure. If the radio signal is generated by an extragalactic object, the radio source may be regarded as a fixed object because of its great distance. In this case, the time dependence of the time delay is generated by the Earth's motion but depends, of course, on the source location and the baseline vector between the two antennas. In general, measurement of the time delay

and/or its derivative for many sources can lead to a least-squares determination of source locations, the baseline vector, and Earth motion parameters, such as UT1 and polar motion.

Although much has been written about VLBI, a need was felt for a tutorial introduction to the basic principles involved. It is much easier to understand the more detailed analyses of VLBI after the central ideas are understood. Thus this tutorial concentrates only on the basic principles and ignores many subtle details that are discussed thoroughly in the literature.

II. Monochromatic Source (Ref. 2)

Consider two antennas separated by a distance (baseline) B receiving a signal from a distant extraterrestrial source. The geometry is shown in Fig. 1. If the source is assumed to be monochromatic and noise (receiver and background) is

neglected, the received signals at the two antennas can be represented as

$$V_1(t) = A_1 \cos 2\pi f_s t$$

and

$$V_2(t) = A_2 \cos 2\pi f_s (t - \tau_g) \quad (1)$$

where

A_1, A_2 represent the strength of the received signals at antennas 1 and 2, respectively

$\tau_g = (B \cos \psi)/c$ is the time delay (typically a slowly varying function of time due to the earth's rotation) in the reception of a given wavefront at antenna 2 relative to antenna 1

c is the velocity of light

These signals are processed by the system shown schematically in Fig. 2 to produce a cross-correlation function $R(\tau_g, \tau_m, t)$. From Fig. 2,

$$\begin{aligned} V_{im}(t) &= [A_1 \cos 2\pi f_s t] [M_1 \cos (2\pi f_{LO1} t - \theta_1)] \\ &= \frac{A_1 M_1}{2} \cos [2\pi(f_s - f_{LO1})t + \theta_1] \\ &\quad + \frac{A_1 M_1}{2} \cos [2\pi(f_s + f_{LO1})t - \theta_1] \end{aligned} \quad (2)$$

where

f_{LO1} is the effective local oscillator mixing frequency at station 1

M_1 is the amplitude of the local oscillator at station 1

θ_1 represents phase shifts due to the receiver and local oscillator (Phase shifts due to other propagation effects such as the ionosphere can also be included in this term.)

The low-pass filter is designed to pass the difference term and reject the sum term. (Assume for simplicity that the filter gain is 1 for the difference frequency. Equivalently it can be lumped in with M_1 and θ_1 .) Thus the recorded signal at station 1 is given by

$$V_{1L}(t) = \frac{A_1 M_1}{2} \cos [2\pi(f_s - f_{LO1})t + \theta_1] \quad (3)$$

In an entirely similar fashion,

$$V_{2L}(t) = \frac{A_2 M_2}{2} \cos [2\pi(f_s - f_{LO2})t - 2\pi f_s \tau_g + \theta_2] \quad (4)$$

As indicated in Fig. 2, $V_{1L}(t)$ and $V_{2L}(t)$ are typically recorded on magnetic tape (digitally in most cases, as discussed later) and shipped to a central facility for correlation and further processing.

Correlation consists of advancing the recorded signal $V_{2L}(t)$ from station 2 by a model time τ_m that approximates the expected geometric delay τ_g , taking the product of the signals and again low-pass filtering. This is equivalent to multiplying $V_{1L}(t)$ and $V_{2L}(t + \tau_m)$ and low-pass filtering. From Eq. (4),

$$\begin{aligned} V_{2L}(t + \tau_m) &= \frac{A_2 M_2}{2} \cos [2\pi(f_s - f_{LO2})(t + \tau_m) - 2\pi f_s \tau_g + \theta_2] \\ &= \frac{A_2 M_2}{2} \cos [2\pi(f_s - f_{LO2})t \\ &\quad + 2\pi(f_s - f_{LO2})\tau_m - 2\pi f_s \tau_g + \theta_2] \end{aligned} \quad (5)$$

Taking the product of $V_{1L}(t)$ and $V_{2L}(t + \tau_m)$, expanding into sum and difference terms, and noting that the low-pass filter removes the sum (high-frequency) term yields

$$R(\tau_g, \tau_m, t) = K \cos \phi_f(t) \quad (6)$$

where

$$K = \frac{A_1 A_2 M_1 M_2}{8}$$

and

$$\begin{aligned} \phi_f(t) &= 2\pi(f_{LO2} - f_{LO1})t - 2\pi(f_s - f_{LO2})\tau_m \\ &\quad + 2\pi f_s \tau_g + \theta_1 - \theta_2 \end{aligned}$$

The cross-correlation function $R(\tau_g, \tau_m, t)$ is processed further (as will be discussed in a later section) and the delay τ_g as well as the delay rate $\dot{\tau}_g$, which are the basic VLBI data types, are determined by analyzing the phase of the cross-correlation function. Note that $\phi_f(t)$ may also be written in the form

$$\begin{aligned} \phi_f(t) &= 2\pi(f_{LO2} - f_{LO1})t + 2\pi f_s \Delta\tau \\ &\quad + 2\pi f_{LO2} \tau_m + \theta_1 - \theta_2 \end{aligned} \quad (7)$$

where

$$\Delta\tau = \tau_g - \tau_m$$

A. Angular Sensitivity

The geometric delay τ_g enters into the phase of the cross-correlation function $\phi_f(t)$ as the term $2\pi f_s \tau_g$. Suppose it is possible to detect a variation in the phase $\phi_f(t)$ of 2π radians (a one-fringe change). This corresponds to a change in geometric delay (assuming the other terms of $\phi_f(t)$ do not change) given by

$$2\pi f_s \Delta\tau_g = 2\pi \quad (8)$$

or

$$\Delta\tau_g = \frac{1}{f_s}$$

Now the relationship between small changes in τ_g and small changes in the angle to the source ψ can be approximated by

$$\Delta\tau_g \cong \frac{\partial\tau_g}{\partial\psi} \Delta\psi \quad (9)$$

Substituting $\tau_g = (B \cos \psi)/c$ yields

$$\Delta\tau_g = \frac{-B \sin \psi}{c} \Delta\psi \quad (10)$$

or

$$\Delta\psi = \frac{-c}{B \sin \psi} \Delta\tau_g$$

Using $\Delta\tau_g = \frac{1}{f_s}$ gives

$$\Delta\psi \cong \frac{-c}{B \sin \psi} \frac{1}{f_s} = \frac{-\lambda}{B \sin \psi} \quad (11)$$

since $c/f_s = \lambda$, where λ is the wavelength of radiation at frequency f_s .

As an example, suppose $B = 10,000$ km and $\lambda = 13$ cm (corresponding to an S-band signal). Then

$$\Delta\psi \cong \frac{-1.3 \times 10^{-1}}{1 \times 10^7 \sin \psi} = \frac{-1.3 \times 10^{-8}}{\sin \psi} \text{ rad}$$

$$= \frac{-0.0027}{\sin \psi} \text{ arc sec} \quad (12)$$

As stated in Ref. 2, "This illustrates the potential of VLBI: a change in position of 10^{-3} arc sec causes detectable changes in the cross correlation. At the present though, there is an ambiguity in determining which fringe the source is on." That ambiguity problem is brought out in the next two sections.

B. Phase Measurement

The cross-correlation function $R(\tau_g, \tau_m, t)$ is multiplied by the cosine and sine of a model phase $\phi_m(t)$ and integrated over an interval of T seconds (the integrator eliminates the sum frequency term of the product) to produce the so-called cosine and sine-stopped fringes

$$\mu_c(t, \tau_m) = \frac{K}{2} \cos [\phi_f(t) - \phi_m(t)]$$

and

$$\mu_s(t, \tau_m) = \frac{K}{2} \sin [\phi_f(t) - \phi_m(t)] \quad (13)$$

The phase of the cross-correlation function can, in principle, be determined (within a multiple of 2π) as

$$\phi_f(t) - \phi_m(t) = \tan^{-1} \frac{\mu_s(t, \tau_m)}{\mu_c(t, \tau_m)}$$

or

$$\phi_f(t) = \phi_m(t) + \tan^{-1} \frac{\mu_s(t, \tau_m)}{\mu_c(t, \tau_m)} \quad (14)$$

In actual practice the phase is determined by fitting sinusoids to the cosine and sine-stopped fringes.

III. Polychromatic Source and Bandwidth Synthesis

As noted above, the phase of the cross-correlation function $R(\tau_g, \tau_m, t)$ due to geometric delay can be determined only within a multiple of 2π (i.e., $\phi_f(t) = 2\pi f_s \tau_g + 2\pi n$). If the source consists of several spectral lines (polychromatic) it is possible to determine the delay by combining measurements from the cross-correlation functions of the individual spectral lines. As an example, suppose the source consists of two spectral lines at frequencies f_{s1} and f_{s2} . The phases of the cross-correlation functions due to the geometric delay term are then measured as

$$\phi_{f1}(t) = 2\pi f_{s1} \tau_g + 2\pi m$$

and

$$\phi_{f2}(t) = 2\pi f_{s2} \tau_g + 2\pi n \quad (15)$$

where m and n are integers (see Fig. 3). If the a priori uncertainty in slope S of phase versus frequency is less than $\Delta S_{1,2} = 2\pi(f_{s2} - f_{s1})$, then corresponding phase points may be connected (i.e., the relative phase ambiguity resolved) and the delay τ_g is determined by the slope of the connecting line, since

$$\tau_g = \frac{\phi_{f2} - \phi_{f1}}{2\pi(f_{s2} - f_{s1})}$$

or

$$\tau_g = \frac{S}{2\pi} \quad (16)$$

It is important to note that the uncertainty in S includes uncertainties in both τ_g and instrumental delays. The instrument delay uncertainty can be essentially eliminated by using a phase calibrator. In addition, there is of course some uncertainty in the measurement of the phase $\phi_f(t)$ due to noise as indicated by the error bars in Fig. 3. (Noise is considered in a later section.) If the uncertainty in the measurement of $\phi_f(t)$ at a given frequency is σ_{ϕ_f} then the uncertainty in τ_g (neglecting certain errors due to ionospheric effects) is given by

$$\sigma_{\tau_g} = \frac{\sqrt{2} \sigma_{\phi_f}}{2\pi(f_{s2} - f_{s1})} \quad (17)$$

where the $\sqrt{2}$ results from incoherent differencing of phase errors. The point is that for a given σ_{ϕ_f} , the larger the term $f_{s2} - f_{s1}$ (commonly called the spanned bandwidth), the smaller will be the delay uncertainty σ_{τ_g} . This technique is known as bandwidth synthesis.

In this simple example, increasing the spanned bandwidth would also require more accurate a priori information in order to resolve the relative phase ambiguity. This dilemma can be avoided if an additional intermediate channel is added as shown in Fig. 3. Assume the relative phase ambiguity is resolved between channels 1 and 3 using a priori information. The more precise estimate of τ_g determined by using channels 1 and 3 may now be used to resolve the ambiguity between the outside channels 1 and 2. Obviously several intermediate channels may be required to resolve the relative phase

ambiguities depending on the spanned bandwidth, accuracy of the a priori information, and uncertainty in individual phase measurements.

IV. Wideband Source and Noise

A. Cross-Correlation Function

In most cases the source used in VLBI (a natural radio source for example) is broadband and can be approximated as white noise over the band of interest. In this case the correlation function can be shown (Ref. 1) to be of the form

$$R(\tau_g, \tau_m, t) = D(\Delta\tau) \cos \phi_f(t) \quad (18)$$

where

$$\Delta\tau = \tau_g - \tau_m$$

$$\phi_f(t) = 2\pi(f_{LO2} - f_{LO1})t + 2\pi f_s \Delta\tau + 2\pi f_{LO2} \tau_m + \theta_1 - \theta_2$$

Note that the correlation function differs from the monochromatic case in that the amplitude of the correlation function $D(\Delta\tau)$ is a function of $\Delta\tau = \tau_g - \tau_m$ rather than a constant. For example, if the receiver has a rectangular bandpass of width W centered at f_s , the amplitude of the correlation function is given by (Ref. 1)

$$D(\Delta\tau) = K_1 W \frac{\sin \pi W \Delta\tau}{\pi W \Delta\tau} \quad (19)$$

where K_1 is a constant. This dependence on model delay reflects the accuracy with which the two signals have been aligned in time.

Note further that, in the case of a broadband source, delay information can be obtained by analyzing the amplitude as well as the phase of the cross-correlation function. To determine τ_g from the amplitude of the cross-correlation function, the model delay τ_m is adjusted to maximize $D(\Delta\tau)$, at which point $\Delta\tau = \tau_g - \tau_m = 0$ or $\tau_g = \tau_m$.

The accuracy with which delay can be determined using the amplitude of the cross-correlation function depends on the width of the peak of $D(\Delta\tau)$ versus $\Delta\tau$. In the case of a rectangular bandpass, the first zero of $D(\Delta\tau)$ (see Fig. 4) occurs at $\pi W \Delta\tau = \pi$ or $\Delta\tau = 1/W$. Thus the accuracy with which delay can be determined using this technique is proportional to the reciprocal of the channel bandwidth. Typically this bandpass shape can be used to estimate the delay τ_g with

an accuracy of $0.01/2W$ to $0.1/2W$ seconds (2.5 to 25 nsec for $W = 2\text{MHz}$).

B. Bandwidth Synthesis

Rather than use the amplitude of the cross-correlation function to determine the delay, which would require recording a wide-bandwidth signal, several narrower bandwidth channels are used (see Fig. 5). Cross-correlation functions are computed for each channel, and the delay is determined by analyzing the phases of the cross-correlation functions and using bandwidth synthesis as explained above for the polychromatic source. However, the amplitude of the single-channel cross-correlation function can be used to improve a priori knowledge of τ_g prior to performing bandwidth synthesis. It can be shown that for a given delay uncertainty σ_{τ_g} , bandwidth synthesis requires less data than the amplitude technique for many cases of practical interest (Ref. 3).

J. B. Thomas has drawn up an alternate way of looking at the bandwidth synthesis process shown schematically in Fig. 6. First of all, the amplitude of the correlation function is used to give an unambiguous delay measurement based on the channel bandwidth W (2 MHz in this case). This delay measurement can then be used to resolve the delay ambiguity resulting from the most closely spaced channel pair (5 MHz in this example). The delay ambiguity results from the phase slopes spaced by $\Delta S_{1,3}$ in Fig. 3 [$\Delta\tau_{1,3} = (1/2\pi) \Delta S_{1,3}$]. Once the ambiguity in the most closely spaced channel pair is resolved, the more accurate measured delay obtained is in turn used to resolve the ambiguity in the more widely spaced channel pair (20 MHz in this case). Note, that both the uncertainty in the delay measurement and the ambiguity spacing decrease as the channel separation increases (see Eqs. 16 and 17) as indicated in Fig. 6.

V. Effect of Noise and Digital Processing

When noise is included, the cross-correlation function may be written

$$R(\tau_g, \tau_m, t) = D(\Delta\tau) \cos \phi_f(t) + n(t) \quad (20)$$

where $n(t)$ is a random function due to receiver and background noise. A rather involved analysis (Refs. 4 and 5) shows that

$$\frac{S}{N} = \frac{D(\Delta\tau)_{\max}}{\sigma_n} = \frac{D(0)}{\sigma_n} = \sqrt{\frac{T_{a1} T_{a2} WT}{T_{s1} T_{s2}}} \quad (21)$$

where

$$\frac{S}{N} = \text{stopped fringe signal-to-noise ratio}$$

$$\sigma_n = \text{rms fringe noise}$$

$$T_{a1}, T_{a2} = \text{effective radio source temperatures (K) at stations 1 and 2, respectively}$$

$$T_{s1}, T_{s2} = \text{total system noise temperature (K) at stations 1 and 2, respectively}$$

$$W = \text{channel bandwidth (Hz)}$$

$$T = \text{total integration time (sec)}$$

In the actual implementation of this technique each channel is hard-limited and sampled (1-bit quantization) at a rate $2W$. The effect of hard-limiting for low signal-to-noise ratios is to reduce the signal to noise ratio S/N by a factor of $2/\pi$ (Ref. 4) and thus for the actual system

$$\frac{S}{N} = \frac{2}{\pi} \sqrt{\frac{T_{a1} T_{a2} WT}{T_{s1} T_{s2}}} \quad (22)$$

Note that maximum S/N requires that the model delay τ_m must be accurate enough to keep $D(\Delta\tau)$ near its maximum $D(0)$ to provide the most accurate measurement in the presence of noise as described below. In addition, further processing requires "seeing" fringes, which in practice requires that S/N be at least 5 and preferably 10.

A. Phase and Delay Measurement Accuracy (Refs. 5 and 6)

The error in determining $\phi_f(t) - \phi_m(t)$ from the stopped fringes may be illustrated by noting that $\mu_c(t, \tau_m)$ and $\mu_s(t, \tau_m)$ are projections of a vector consisting of the signal vector plus a noise vector on two orthogonal axes as shown in Fig. 7, where

$$\mu_c(t, \tau_m) = \frac{D(0)}{2} \cos [\phi_f(t) - \phi_m(t)] + \frac{n_c(t)}{2}$$

and

$$\mu_s(t, \tau_m) = \frac{D(0)}{2} \sin [\phi_f(t) - \phi_m(t)] + \frac{n_s(t)}{2} \quad (23)$$

Since the noise is spherically symmetric, it follows (see Fig. 7) that for small rms phase deviations,

$$\sigma_{\phi_f} = \tan^{-1} \left(\frac{\text{noise}}{\text{signal}} \right) \cong \frac{\text{noise}}{\text{signal}} = \frac{1}{S/N} = \frac{N}{S} \quad (24)$$

A more rigorous analysis (Ref. 5) yields the same result, and thus (assuming the relative phase ambiguities have been resolved) the system noise-limited delay accuracy σ_{τ_g} is given by

$$\sigma_{\tau_g} = \frac{\sqrt{2} \sigma_{\phi_f}}{2\pi(f_{s2} - f_{s1})} \quad (25)$$

where f_{s1} , f_{s2} now refer to the center frequencies of channels 1 and 2, respectively. Defining the spanned bandwidth $B_s = f_{s2} - f_{s1}$ yields

$$\sigma_{\tau_g} = \frac{\sqrt{2} \sigma_{\phi_f}}{2\pi B_s} = \frac{\sqrt{2}}{4B_s} \sqrt{\frac{T_{s1} T_{s2}}{T_{a1} T_{a2} WT}} \quad (26)$$

Substituting (Ref. 7)

$$T_{ai} = \frac{1}{2} \frac{10^{-26}}{K} J \epsilon_i \frac{\pi}{4} d_i^2 \quad i = 1, 2 \quad (27)$$

where

$\frac{1}{2}$ = antenna polarization loss

J = correlated flux of radio source in Janskys (Jansky = 10^{-26} W/m² Hz)

ϵ_i = antenna efficiency

d_i = antenna diameter in meters

K = Boltzmann's constant ($K = 1.38 \times 10^{-23}$ Joule/Kelvin)

gives

$$\sigma_{\tau_g} = \frac{1.24 \times 10^3}{B_s J d_1 d_2} \sqrt{\frac{T_{s1} T_{s2}}{\epsilon_1 \epsilon_2 WT}} \text{ sec} \quad (28)$$

It is sometimes convenient to give σ_{τ} in cm by multiplying by the speed of light (3×10^{10} cm/sec). If, in addition, the spanned bandwidth B_s is measured in MHz (10^6 Hz) and if the sampling rate is twice the channel bandwidth so that the number of megabits of data N is given by

$$N = \frac{2WT}{10^6} \text{ Mbits} = S_r T$$

where

S_r = mean sampling rate in megabits/sec for each channel

T = total integration time in seconds

B_s = spanned bandwidth in MHz

Then

$$\sigma_{\tau_g} \text{ (cm)} = \frac{K_2}{B_s J d_1 d_2} \sqrt{\frac{T_{s1} T_{s2}}{\epsilon_1 \epsilon_2 S_r T}} \text{ cm} \quad (29)$$

where

B_s = spanned bandwidth in MHz

J = correlated flux of radio source in Janskys

ϵ_i = antenna efficiency $i = 1, 2$

d_i = antenna diameter in meters

$K_2 = 5.26 \times 10^4$

Again it is important to note that Eq. (29) gives the standard deviation in the measurement of the delay τ_g due to thermal noise only. Other error sources such as instrumental effects, propagation (ionosphere), modelling, etc., must also be considered. The real importance of the equation is to show the manner in which various parameters affect VLBI accuracy.

As an example, using the following values for a typical Mark II observation,

$K_2 = 5.26 \times 10^4$

$J = 1$ Jansky

$T_{s1} = T_{s2} = 30$ K

$S_r = 4$ Mbps

$B_s = 40$ MHz

$d_1 = d_2 = 64$ m

$\epsilon_1 = \epsilon_2 = 0.55$

$T = 150$ sec (2-1/2 min)

yields

$$\sigma_{\tau_g} \text{ (cm)} = \frac{5.26 \times 10^4}{(40)(1)(64)(64)} \sqrt{\frac{(30)(30)}{(0.55)(0.55)(4)(150)}} = 0.7 \text{ cm}$$

Note that if the spanned bandwidth and antenna parameters are held fixed, σ_{τ_g} varies as $(S_r T)^{-1/2} = N^{-1/2}$, where N = total number of bits for the observation. In the above example,

$$N = S_r T = 4(150) = 600 \text{ Mbits} = 6 \times 10^8 \text{ bits}$$

The sampling rate S_r is proportional to the channel bandwidth (2 MHz for the Mark II VLBI system) and thus, if the channel bandwidth is increased, the integration time T can be decreased while maintaining a given σ_{τ_g} as long as $N = S_r T$ is held constant. A wider channel bandwidth may allow a more accurate single-channel delay to be computed, however, which affects the resolution of phase ambiguities in the bandwidth synthesis process.

It should also be pointed out that T refers to integration time, during which the same radio signal from the source is recorded at two stations. If short segments of the signal are recorded, careful timing is required to insure signal overlap.

VI. Measurement of Source Position and Earth Motion Parameters

As stated in Ref. 1 for an extragalactic radio source, "the time dependence of the time delay is generated by the earth's motion but depends, of course, on the source location and the baseline vector between the two antennas." For example, the relationship between the geometric time delay τ_g , baseline B , and source position is given by (Ref. 2)

$$\tau_g = \frac{B}{c} [\sin \delta \sin \delta_b + \cos \delta \cos \delta_b \cos(\alpha_b - \alpha)] \quad (30)$$

where

B = length of the baseline

δ = declination of the source

δ_b = declination of the baseline

α = right ascension of the source

α_b = right ascension of the baseline

c = velocity of light

In addition, the instantaneous spin axis of the earth (which is the reference for the source and baseline coordinates in Eq. 30 above) changes both with respect to an inertial reference frame (precession and nutation) and the earth's crust (polar motion).

A number of delay measurements at various times and for various sources can be used to make a least-squares determination of source coordinates, the baseline vector, and earth motion parameters. A discussion of some of the tradeoffs involved in this type of measurement is given in the next section using the baseline as an example.

A. Baseline Accuracy

The standard deviation of the error in baseline measurement is approximately given by (Refs. 8 and 9)

$$\sigma = \sigma_x A \sqrt{\frac{N_p}{N_{\text{obs}}}} \quad (31)$$

where

N_p = number of parameters solved for in the multi-parameter fit

N_{obs} = number of observations

A = constant ranging from 1 to 4 depending on a covariance analysis based on source locations, etc.

and

$$\sigma_x^2 = \sigma_{\tau_g}^2 + \sigma_o^2$$

where

σ_{τ_g} = that given previously

σ_o = standard deviation of other uncertainties such as ionospheric effects, tropospheric effects, uncertainties in source positions (if taken as given), frequency standard deviations from linear performance in time, etc.

For example, consider solving for three earth parameters and four clock parameters using 28 observations, with $\sigma_{\tau_g} = 0.7$ cm (see previous calculation) and $A = 4$. Assume for simplicity that $\sigma_o = 0$; then

$$\sigma = (0.7)(4) \sqrt{\frac{7}{28}} = 1.4 \text{ cm}$$

The total number of bits required in this case is given by

$$N_T = N_{\text{obs}} S_r T = 28 \times 6 \times 10^8 = 1.68 \times 10^{10} \text{ bits}$$

B. Delay Rate Accuracy

For a given standard deviation in phase σ_{ϕ_f} , the standard deviation in delay rate may be approximated by noting that, from Eq. (6),

$$\dot{\phi}_f(t) = 2\pi f_s \dot{\tau}_g + 2\pi(f_{LO2} - f_{LO1}) \quad (32)$$

and thus

$$\sigma_{\dot{\phi}_f} = 2\pi f_s \sigma_{\dot{\tau}_g}$$

or

$$\sigma_{\dot{\tau}_g} = \frac{\sigma_{\dot{\phi}_f}}{2\pi f_s} \text{ sec/sec} \quad (33)$$

Since for an integration interval of T seconds, $\dot{\phi}_f$ can be approximated by taking the difference in phase over the integration interval and dividing by T ,

$$\sigma_{\dot{\phi}_f} \cong \frac{\sqrt{2}\sigma_{\phi_f}}{T} \text{ radians/sec} \quad (34)$$

and thus

$$\sigma_{\dot{\tau}_g} = \frac{\sqrt{2}\sigma_{\phi_f}}{2\pi f_s T} \text{ sec/sec} \quad (35)$$

Note that there is no ambiguity problem in determining delay rate and the effective spanned bandwidth for delay rate is the rf channel frequency f_s . Since σ_{ϕ_f} varies as $T^{-1/2}$, $\sigma_{\dot{\tau}_g}$ varies as $T^{-3/2}$. Note that although for a given spanned bandwidth and antenna parameters, $\sigma_{\dot{\tau}_g}$ depends only on the number of bits $N = S_r T$ (thus allowing a tradeoff between integration time and channel bandwidth), $\sigma_{\dot{\tau}_g}$ depends explicitly on the integration time T (varying as T^{-1} for a fixed $\sigma_{\dot{\tau}_g}$). From Eq. (26),

$$\sigma_{\phi_f} = \frac{2\pi B_s}{\sqrt{2}} \sigma_{\dot{\tau}_g} \quad (36)$$

Substituting into Eq. (35),

$$\sigma_{\dot{\tau}_g} = \frac{B_s}{f_s T} \sigma_{\dot{\tau}_g} \text{ sec/sec} \quad (37)$$

or

$$\sigma_{\dot{\tau}_g} = \frac{B_s}{f_s T} \sigma_{\dot{\tau}_g} \text{ (cm) cm/sec}$$

Dividing by the wavelength of the signal at frequency f_s ,

$$\sigma_{\dot{\tau}_g} = \frac{B_s}{f_s T \lambda} \sigma_{\dot{\tau}_g} \text{ (cm)} = \frac{B_s}{cT} \sigma_{\dot{\tau}_g} \text{ (cm) Hz.}$$

Using the previous Mark II example yields

$$\sigma_{\dot{\tau}_g} = \frac{40 \times 10^6}{(3 \times 10^{10})(150)} 0.7 = 6.22 \times 10^{-6} \text{ Hz.}$$

Accurate measurement of $\dot{\tau}_g$ strengthens the multiparameter fit for baseline measurement, especially the z-component (along the earth's rotation axis), as schematically indicated by Fig. 8. A tradeoff of τ vs $\dot{\tau}$ accuracy for a given baseline component accuracy thus exists. This affects observation strategy and has not been analyzed in detail as yet, since the experimental data on typical $\sigma_{\dot{\tau}_g}$ at X-band are only now becoming available.

VII. Required Antenna Time for a Given Baseline Accuracy

As discussed previously, the standard deviation of the error in baseline measurement is given by Eq. (31):

$$\sigma = \sigma_x A \sqrt{\frac{N_p}{N_{\text{obs}}}}$$

where

$$\sigma_x^2 = \sigma_{\dot{\tau}_g}^2 + \sigma_o^2$$

and

$$\sigma_{\dot{\tau}_g} = \frac{K_2}{B_s J d_1 d_2} \sqrt{\frac{T_{s1} T_{s2}}{\epsilon_1 \epsilon_2 S_r T}} \quad (38)$$

Following an analysis by D. Rogstad, the total antenna time T_{ant} and number of bits N_T required for a given baseline accuracy are given by

$$T_{\text{ant}} = N_{\text{obs}} (T + t_m) \quad (39)$$

and

$$N_T = N_{\text{obs}} S_r T \quad (40)$$

where t_m is the average time required to move from one source to another ($\cong 4$ min for a 64-m/64-m antenna pair), and T is the integration time per source (assumed uniform). For convenience, define

$$\sigma_s = \frac{K_2}{B_s J d_1 d_2} \sqrt{\frac{T_{s1} T_{s2}}{\epsilon_1 \epsilon_2 S_r t_m}} \quad (41)$$

Then

$$\frac{\sigma_{\tau_g}}{\sigma_s} = \sqrt{\frac{t_m}{T}} \quad \text{or} \quad \sigma_{\tau_g}^2 = \sigma_s^2 \frac{t_m}{T} \quad (42)$$

and

$$\sigma^2 = (\sigma_{\tau_g}^2 + \sigma_o^2) \frac{A^2 N_p}{N_{\text{obs}}} = \left(\sigma_s^2 \frac{t_m}{T} + \sigma_o^2 \right) \frac{A^2 N_p}{N_{\text{obs}}} \quad (43)$$

Clearly, there is a tradeoff between T and N_{obs} in maintaining a constant σ . Rogstad has determined the minimum value

of $T_{\text{ant}} = N_{\text{obs}}(T + t_m)$ subject to a constraint on σ (or σ^2). The result (which can be derived using Lagrange multipliers) is

$$T_{\text{ant}} = N_p A^2 \left(\frac{\sigma_o}{\sigma} \right)^2 t_m \left(1 + \frac{\sigma_s}{\sigma_o} \right)^2 \text{ sec}$$

This corresponds to

$$N_T = N_p A^2 \left(\frac{\sigma_o}{\sigma} \right)^2 S_r t_m \left(\frac{\sigma_s}{\sigma_o} \right) \left(\frac{\sigma_o}{\sigma_s} + 1 \right) \text{ bits}$$

Normalized curves of the results are given in Ref. 9, as well as a discussion of how σ_o should be handled. Rogstad has subsequently obtained further results in this area.

VIII. Summary

This tutorial is intended to give the reader an appreciation of the basic principles of VLBI. It should not be used as the sole basis of further analysis. A great deal of technical literature exists for those interested in further information and more detailed analyses. Especially recommended as a starting point are the articles by J. G. Williams (Ref. 2), A. E. E. Rogers (Ref. 10), and J. B. Thomas (Ref. 1, 4, and 11).

Acknowledgements

The author is especially indebted to J. L. Fanselow and J. B. Thomas for their patient explanations and review of this tutorial. In addition, J. B. Thomas graciously allowed the use of Fig. 5 and the alternate way of looking at bandwidth synthesis that he drew up for an article to be published in the future.

References

1. Thomas, J. B., "An Analysis of Long Baseline Radio Interferometry," *The Deep Space Network Progress Report*, Technical Report 32-1526, Volume VIII, Jet Propulsion Laboratory, Pasadena, California, February 1972.
2. Williams, J. G., "Very Long Baseline Interferometry and Its Sensitivity to Geophysical and Astronomical Effects," *Jet Propulsion Laboratory Space Programs Summary 37-62*, Volume II, February 1970.
3. Fanselow, J. L., "Superiority of Bandwidth Synthesis Over the Burst Mode Technique for Determining Time Delay in VLBI," IOM 391.5-517, December 1, 1975 (JPL internal document).
4. Thomas, J. B., "An Analysis of Long Baseline Radio Interferometry, Part III," *The Deep Space Network Progress Report*, Technical Report 32-1526, Volume XVI, Jet Propulsion Laboratory, Pasadena, California, August 1973.
5. Thomas, J. B., "System Noise Effects in VLBI Measurements," Engineering Memorandum 315.6, October 25, 1976 (JPL internal document).
6. Molinder, J. I., and Mulhall, B. D. L., "Minutes of the DSN VLBI Implementation Team Meeting of 16 December 1976," IOM AE-76-197, 17 December 1976 (JPL internal document).
7. Brown, D. S., "VLBI Fringe Phase SNR and Bit Calculations," IOM 315.1-222, 14 December 1977 (JPL internal document).
8. VLBI Validation Report, Pre-Session No. 1, April 1, 1977, Document 890-60 (JPL internal document).
9. Molinder, J. I., and Mulhall, B. D. L., "Minutes of the DSN VLBI Implementation Team Meeting of 20 January 1977," IOM AE-77-11, 24 January 1977 (JPL internal document).
10. Rogers, Alan E. E., "Very Long Baseline Interferometry with Large Effective Bandwidth for Phase-Delay Measurements," *Radio Science*, Volume 5, Number 10, October 1970.
11. Thomas, J. B., "An Analysis of Long Baseline Radio Interferometry, Part II," *The Deep Space Network Progress Report*, Technical Report 35-1526, Volume VIII, Jet Propulsion Laboratory, Pasadena, California, May 1972.

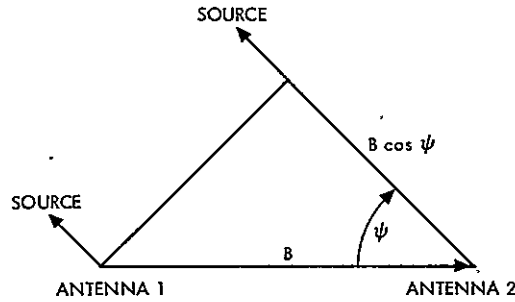
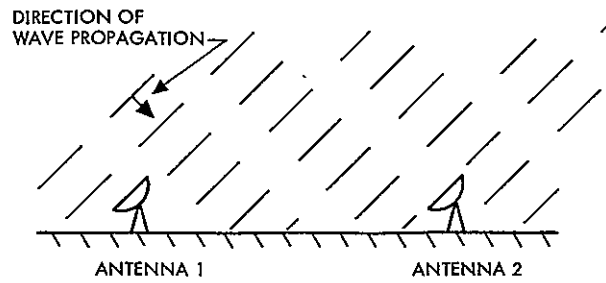
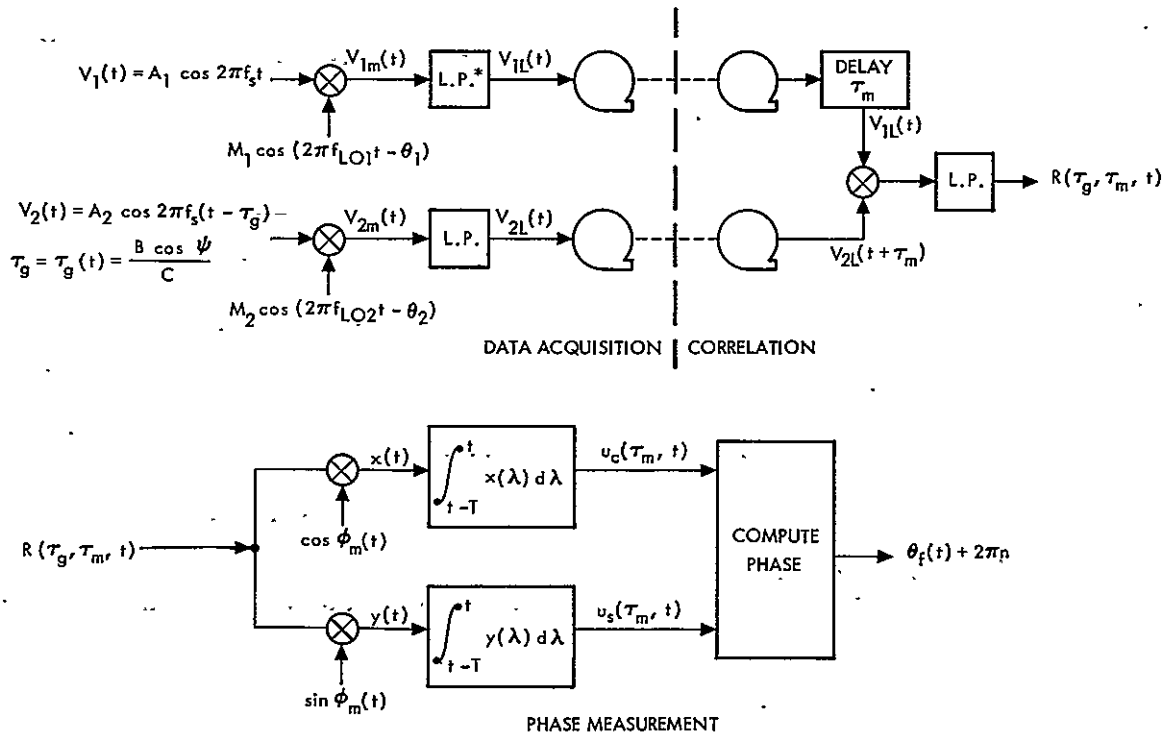


Fig. 1. VLBI Geometry



*LOW-PASS FILTER

Fig. 2. VLBI signal processing

ORIGINAL PAGE IS
OF POOR QUALITY

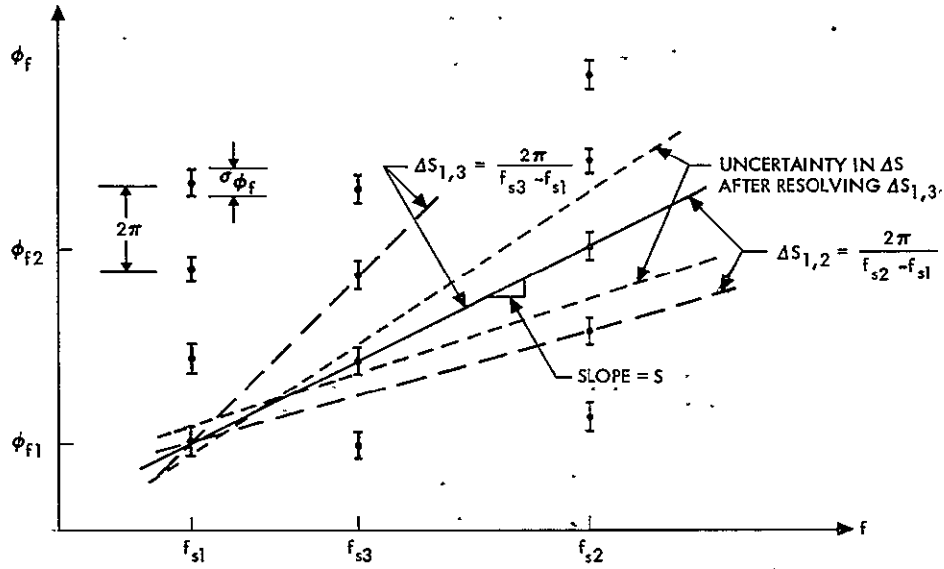


Fig. 3. VLBI relative phase ambiguity resolution and bandwidth synthesis

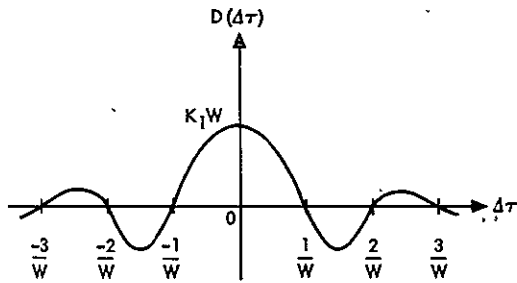


Fig. 4. Amplitude of cross-correlation function $D(\Delta\tau)$ vs bit stream misalignment ($\Delta\tau$)

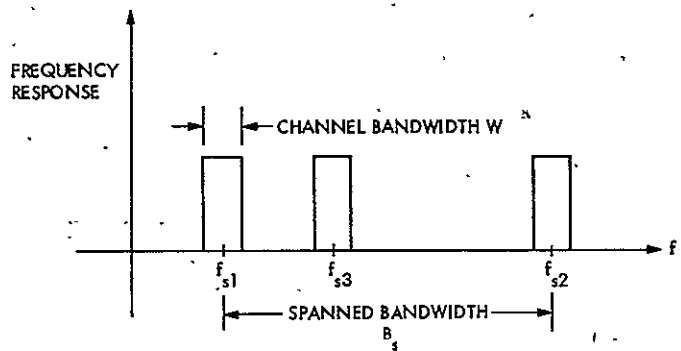


Fig. 5. Frequency response of bandwidth synthesis VLBI system

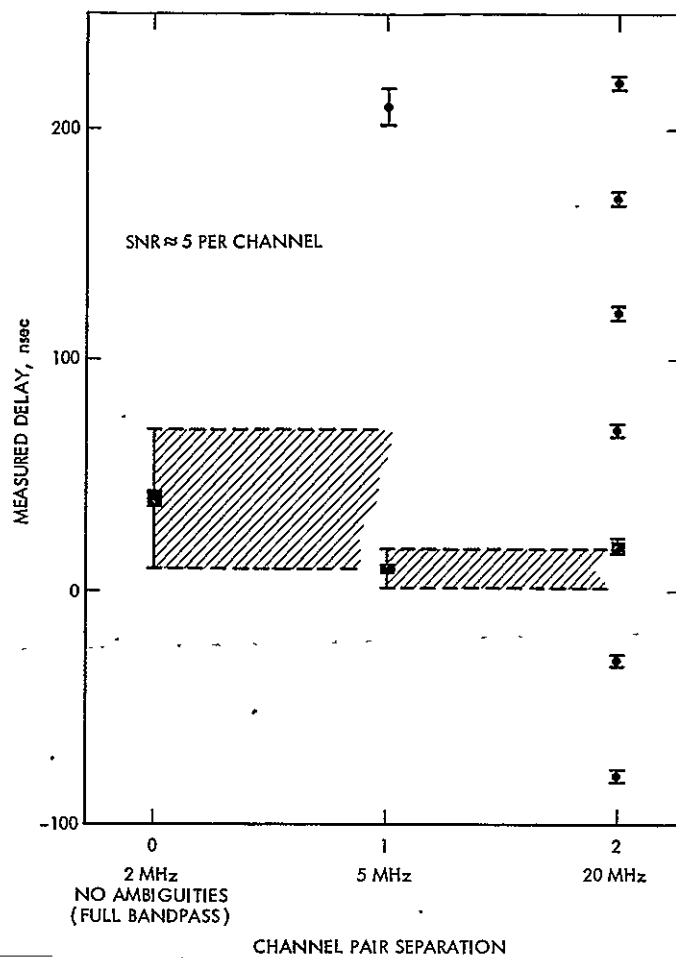


Fig. 6. Schematic example of ambiguity resolution in bandwidth synthesis

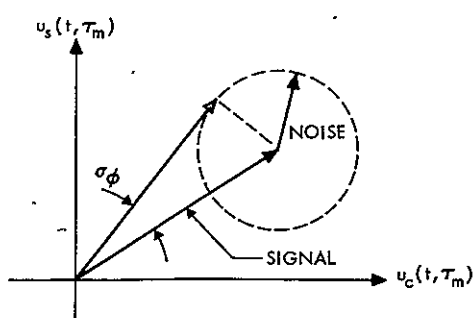


Fig. 7. Effect of noise on accuracy of phase measurement

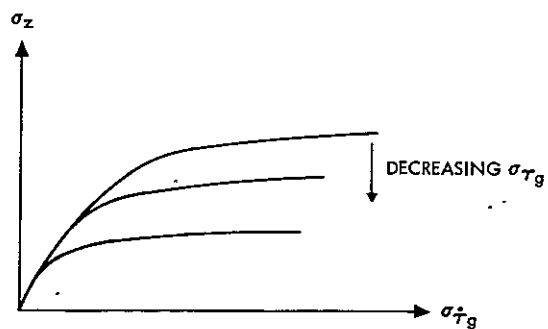


Fig. 8. Standard deviation in Z-component of baseline as a function of σ_{τ_g} and σ_{t_g}

D4-14
32

N78-32141

Viking Extended Mission Support

R. L. Gillette

Deep Space Network Operations Section

This report covers the period from 1 March through 30 April 1978. It reports on DSN support of Viking spacecraft activities during the period and continues reporting on the DSN Viking Command and Tracking support. It also continues the reports on the status of Viking DSN Mark III Data Subsystem Implementation Project (MDS) related testing.

I. Viking Operations

A. Status

The Viking Orbiter 1 spacecraft continued to make detailed photomaps of Mars during this reporting period and to return scientific data on Martian cloud patterns, temperatures, and water vapor in the atmosphere.

To conserve gas, the Viking Orbiter 2 scientific observations of the poles of Mars were discontinued during this reporting period and the spacecraft commanded into a roll drift mode of operation. In this mode Orbiter 2 cannot observe Mars or support relay links from Lander 2. However its radio signals were used to map gravity variations on Mars, caused by pockets of dense material called Mascons, which slightly change the orbital speed of the spacecraft.

The Viking Landers continued their investigation into the composition of the Martian soil. Plans were completed for automatic operation of both Landers with little or no instructions from Earth starting in early June.

B. Orbiter 2 Aft-Bioshield Jettison

The Viking Orbiter 1 (VO-1) aft-bioshield (Fig. 1) was separated shortly after Lander separation in 1976. The shock impact on the VO-1 radio subsystem was a momentary change

in the uplink signal level, indicating a momentary out-of-lock even with an uplink signal present. Also, a transient occurred in the traveling wave tube helix current, which required a half hour to recover. Because of these effects, and a failure in a gyro power supply on Viking Orbiter 2 (VO-2) at Lander separation, the VO-2 aft-bioshield was not separated during the Viking primary mission. The science community was interested in having this separation done during the extended mission, so as to provide a wider field of view for instrument operation.

The decision was made to separate the bioshield on March 3, 1978. The 64-meter Deep Space Station (DSS 63) located in Spain was the primary tracking station supporting the bioshield jettison with the 26-meter Spanish Deep Space Station (DSS 61) assigned as a backup if needed for commanding.

The separation sequence went entirely without problems. The first indication of a successful separation was an abrupt change in the spacecraft two-way doppler from DSS 63. The VO-2 aft-bioshield separation is the last major spacecraft event planned on either Orbiter.

C. Spacecraft Problems

The VO-2 spacecraft developed a serious gas leak in the attitude control system in late March resulting in loss of half

of the spacecraft's remaining gas supply. To conserve gas the Orbiter's redundant attitude control system was switched on. To prevent depletion of the remaining gas due to leaks in the roll jets of the redundant attitude system, VO-2 was commanded into a roll drift mode of operation while scientists prepared the most useful science sequences for the remaining lifetime of the spacecraft.

D. Radio Science

Radio Science activities and experimentation continued during March and April. These activities include near-simultaneous Lander/Orbiter ranging, VO-1 and VO-2 Earth occultation coverage, and the Gravity Field Experiment.

II. Network Support

Table 1 shows the Viking Extended Mission (VEM) tracking support for March and April 1978. Noticeable during this period is the increase of 64-meter support (DSS 14, 43, 63) during April. This is primarily due to the gas leak problem on VO-2 requiring the additional 8-dB antenna gain from the 64-meter network over the 26-meter network to make up for the 21-dB signal loss when VO-2 was commanded into a roll drift mode and the transmitter configured to the spacecraft low-gain antenna.

Table 2 gives the total number of commands transmitted by the DSN for Viking Project during March and April 1978.

III. DSN Mark III Data Subsystem (MDS) Implementation Testing and Status

As indicated in the last report of this series, MDS test and training had been completed at all DSN stations except DSS 11 at Goldstone, California. DSS 11 was released on 15 January to begin their MDS upgrade and complete test and training during this reporting period.

A. DSS 11 Test Status

Test and training activities for Viking started in March and consisted of three Operational Verification Tests (OVTs) and a DSN/MCCC System Integration Test (SIT).

Only the third of the three Viking OVTs was considered successful. Problems in the Simulation Conversion Assembly (SCA) at DSS 11 and the Test and Training Computer in the Network Operations Control Area (NOCA) at JPL prevented testing of the telemetry system. Both the SCA and the Test and Training Computer are used by the DSN to simulate a spacecraft and generate simulated spacecraft telemetry data.

The first System Integration Test scheduled for 29 March was cancelled due to SCA problems and a last minute priority placed on the Viking Mission Computers by the Viking Project to support real-time operations. A Viking SIT retest on 7 April was considered successful.

After several successful demonstration passes with the Viking spacecraft, DSS 11 was placed under DSN Viking Configuration Control, effective 26 April.

Table 1. VEM tracking support 1978

DSS	March		April	
	Tracks	Hours	Tracks	Hours
11	19	167	-	-
12	5	22	1	8
14	37	272	47	365
42	30	201	30	192
43	15	68	27	163
44	6	43	-	-
61	25	281	15	159
62	3	22	3	29
63	30	293	42	440
Total	170	1369	165	1356

Note: Number of tracks represent the summation of all Viking spacecrafts tracked. Track time, in hours, represents actual scheduled station support.

Table 2. Commands transmitted during March and April 1978

DSS	Commands	
	March	April
11	119	-
12	1	374
14	1326	3032
42	261	1079
43	124	275
44	3	-
61	1073	1503
62	461	73
63	2597	4005
Total	5965	10341

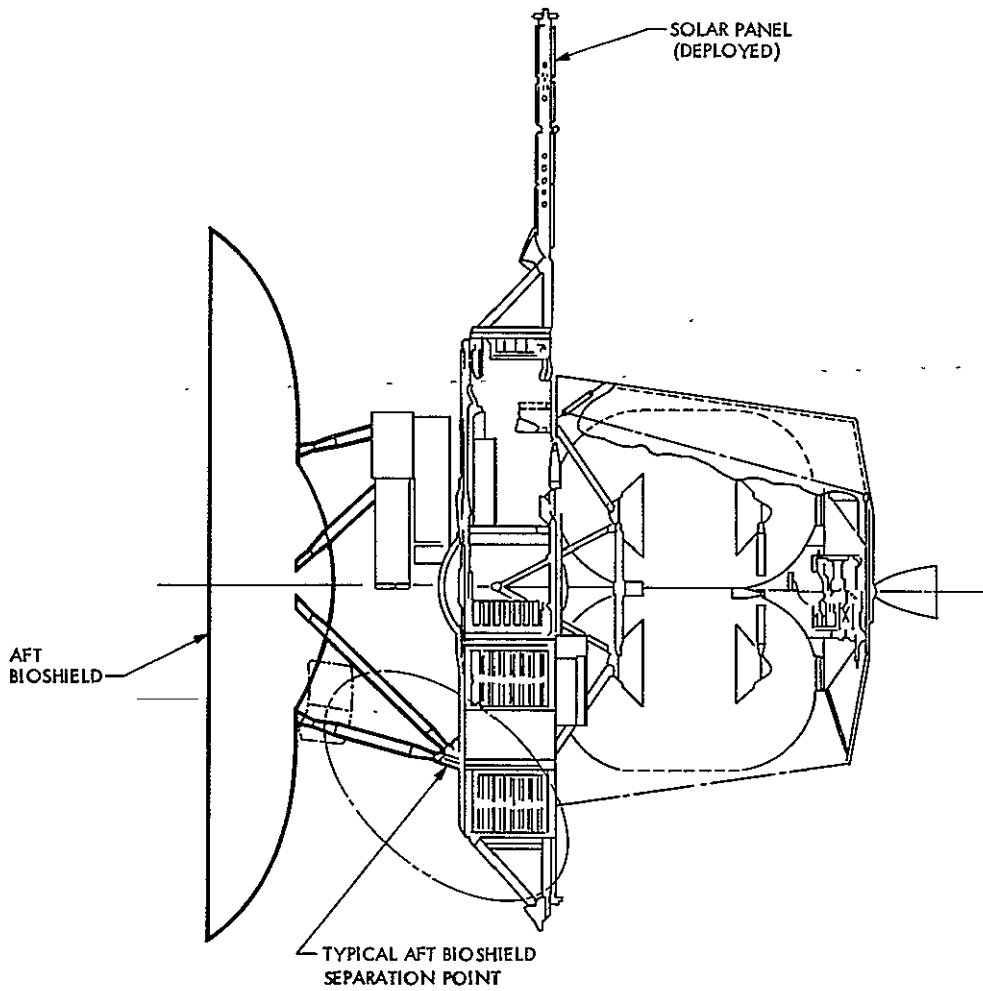


Fig. 1. Location of aft bioshield separation points

ORIGINAL PAGE IS
OF POOR QUALITY

D5-36
14-14B

Pioneer Mission Support

D. W. H. Johnston
DSN Operations Section

This article covers the time period from 1 January 1978 through 31 May 1978. Ongoing Pioneer Project operations (Pioneers 6 through 11) are briefly mentioned. The DSN prelaunch preparations and launch operations for the Pioneer Venus Orbiter are described in detail, along with a brief update on the Pioneer Venus Multiprobe launch and encounter preparations.

I. Pioneers 6, 7, 8, 9, 10, 11

Pioneers 6-9 have only been tracked on a few rare occasions, due to the higher priority of other DSN users, and all the spacecrafts' status appear to be unchanged. Pioneer 10 and 11 are being tracked almost daily; Pioneer 10 mostly by DSS 63, and Pioneer 11 mostly by DSS 42 and DSS 62. Precession maneuvers on Pioneer 10 and 11 are routinely being conducted approximately every four weeks.

- (3) Start support of MOS Operational tests (in January 1978)
- (4) Start DSN Initial Acquisition tests at launch minus 30 days
- (5) Support prelaunch Operational Readiness Tests (ORTs).

II. Pioneer 12 (Pioneer Venus Orbiter)

A. Prelaunch Training and Testing for Launch and Cruise

The DSN prelaunch test and training program was planned to follow the established sequence of:

- (1) Start DSN Operational Verification Tests (OVTs) (on 1 Oct. 1977)
- (2) Start support of ARC Ground Data System (GDS) tests (on 1 Nov. 1977)

The initial DSN OVTs uncovered some problems such as the inability of the Telemetry Processor Assembly (TPA) to process Pioneer Venus uncoded telemetry, and several station and NOCC problems associated with the newly implemented high-speed data 22-bit error polynomial. These problems were discussed in detail in *The DSN Progress Report 42-45* (Pioneer Venus 1978 Mission Support for April 1978).

The above problems delayed the DSN readiness for GDS support by approximately one month; however, the principal obstacle in preparing for the Orbiter launch was severe problems with the ARC simulation, telemetry, and command software. To expedite the development of the ARC software a series of single system "data flow" tests were initiated in January 1978, occasionally supported by DSS 11, 44, 62 and

MIL-71; but the bulk of these numerous tests were conducted between ARC and CTA-21.

The DSN OVT schedule was also extended to keep the DSS new proficiency at an acceptable level, and these added OVTs were also utilized as a data source to provide ARC with opportunities to further develop their telemetry and command software.

Formal GDS tests started on 1 March 1978 and MOS tests on 20 March 1978; and the ORTs in May 1978, with no significant DSN problems.

3. Pioneer Venus Orbiter Launch

- (1) The Pioneer Venus Orbiter Initial Acquisition study was published and sent to the Pioneer Acquisition station (DSS 44) and the back-up station (DSS 42) on 15 April 1978 prior to the Initial Acquisition OVTs. The Initial Acquisition OVTs were conducted successfully, with both stations confirming that station and JPL crews scheduled to support the launch were fully trained.
- (2) All DSN launch-required facilities were green prior to launch. There was, however, a major antenna failure during a rain storm at DSS 44, with repairs completed only 24 hours prior to launch.
- (3) Predicts had to be regenerated at L-20 minutes due to a 5 kHz change in predicted frequencies supplied by Ames.
- (4) After a reasonably smooth minus count the Atlas Centaur lifted off at 13:13:00.073 GMT. The launch to parking orbit was nominal with Main Engine Cutoff (MECO) 1 occurring 7.4 seconds before predicted time. The Centaur second burn was nominal with MECO 2 and spacecraft separation occurring 4.5 seconds before predicted time. Spacecraft injection appeared to be very nominal with midcourse correction calculations from preliminary data calculated to be about 3 meters per second.
- (5) During the minus count only two communication problems of any significance occurred. The spacecraft telemetry 7.2 kilobit/s HSD line was down for 24 minutes which caused the Project to reschedule a command memory readout. The ACN 6.2 kilobit/s spacecraft data line to the Cape was red for 8 minutes.
- (6) During the plus count all ETR, STDN, and ARIA supported all data intervals essentially as planned. No major losses of data occurred. Mark events 1 through 13 were read out.

- (7) ACN support for possible commanding was flawless, however, the PMOCC elected to not send the command to start the science sequence because of ambiguous telemetry indications. This was the most significant post-launch problem and first became apparent when processing the post-separation ACN data by the PMOCC showed a tremendous number of spacecraft problems. At the same time the Hughes computer at the Cape, processing supposedly the same data, showed all was well on the spacecraft. This ambiguity in the spacecraft status caused the Project to not send the command from ACN to start the science sequence. The first DSS 44 data processed by the PMOCC showed all was well and the science sequence was started from that station.

This discrepancy in processing of ACN data was caused by an error in the high-speed data system Block Error Decoders (BED) located at Ames and was not isolated until one month after launch. The BEDs were relabeling high-speed data blocks found to have errors as error-free blocks.

- (8) The initial acquisitions by DSS 44 and 42 were textbook except for a momentary loss at the backup station (DSS 42) when the antenna ran into the DEC prelimits during autotrack on the acquisition aid antenna. DSS 44 acquired the uplink with only 5 Hz left of the planned uplink sweep at VCO level.
- (9) The only anomaly during the first pass was an indication of the spacecraft rejecting a ground command that was never sent after DSS 62 AOS. This anomaly was later determined to have been caused by excessive radiated transmitter power causing the command detector (CMD) to interpret noise as a command. This CMD was then rejected due to checksum errors. DSS 44 radiated 500 watts (SCM) during the initial acquisition pass and DSS 62 acquired at 1 kW as planned. Subsequent to the above diagnosis, uplink power was reduced to 300 watts at all stations until launch plus 2 days when the power was increased (over DSS 11) to 1 kW.

Magnetometer boom deployment, first precision maneuver, and high gain antenna spin-up were supported without incident. Extensive science calibration related activities have also been continuing.

- (10) Two other major events after launch were the Trajectory Correction maneuver on 1 June and the first attempt at executing the High Gain Antenna and X-band calibration over DSS 11 and 14 on 8 and 9 June. The X-band downlink signal level was 10 dB lower than expected. Subsequent testing showed the loss was due to bandwidth spreading resulting from

the uplink command modulation being turned around into the X-band.

Although this report has concentrated on problems encountered, the overall launch support was considered very successful and the view has been generally expressed that this was the smoothest planetary launch to date.

III. Pioneer Venus Multiprobe

A. Launch Preparation

The Multiprobe launch preparation is a relatively small task compared to the Orbiter launch, as the stations involved are tracking the Orbiter daily and both spacecraft are very similar in the launch/cruise mode as far as the DSN is concerned.

The only DSN tests planned are initial acquisition OVTs with DSS 42 and 44; and support of a single MOS test on 12 July 1978; and two ORTs on 27 July and 2 August respectively.

The only change from the Orbiter launch is that DSS 42 will be prime, with DSS 44 as back up. The reason for this is that the spacecraft will rise and set in the DSS 44 West "Keyhole" resulting in the DSS 42 rise earlier than DSS 44 and also resulting in DSS 42 setting approximately one hour ten minutes later than DSS 44, permitting an overlap with DSS 62.

B. Multiprobe Entry Planning

As a result of the four 8-hour Multiprobe Entry procedure development tests in March 1978 (discussed in *The DSN Progress Report 42-45*) conducted at DSS 14, the following procedures have been generated and will be used in the remaining Multiprobe Entry preparation activities:

- (1) A detailed step-by-step sequence of events covering the entire Multiprobe Entry portion of the mission was developed.
- (2) A first cut at an E-3 hour checklist (E = time of entry of the probes into the Venus atmosphere; nominally at an altitude of 200 kilometers) was developed. The start of this check at DSS 14 and 43 is coincidental with the time at which the station configuration is finally frozen (i.e., no further rectification of hardware failures). The

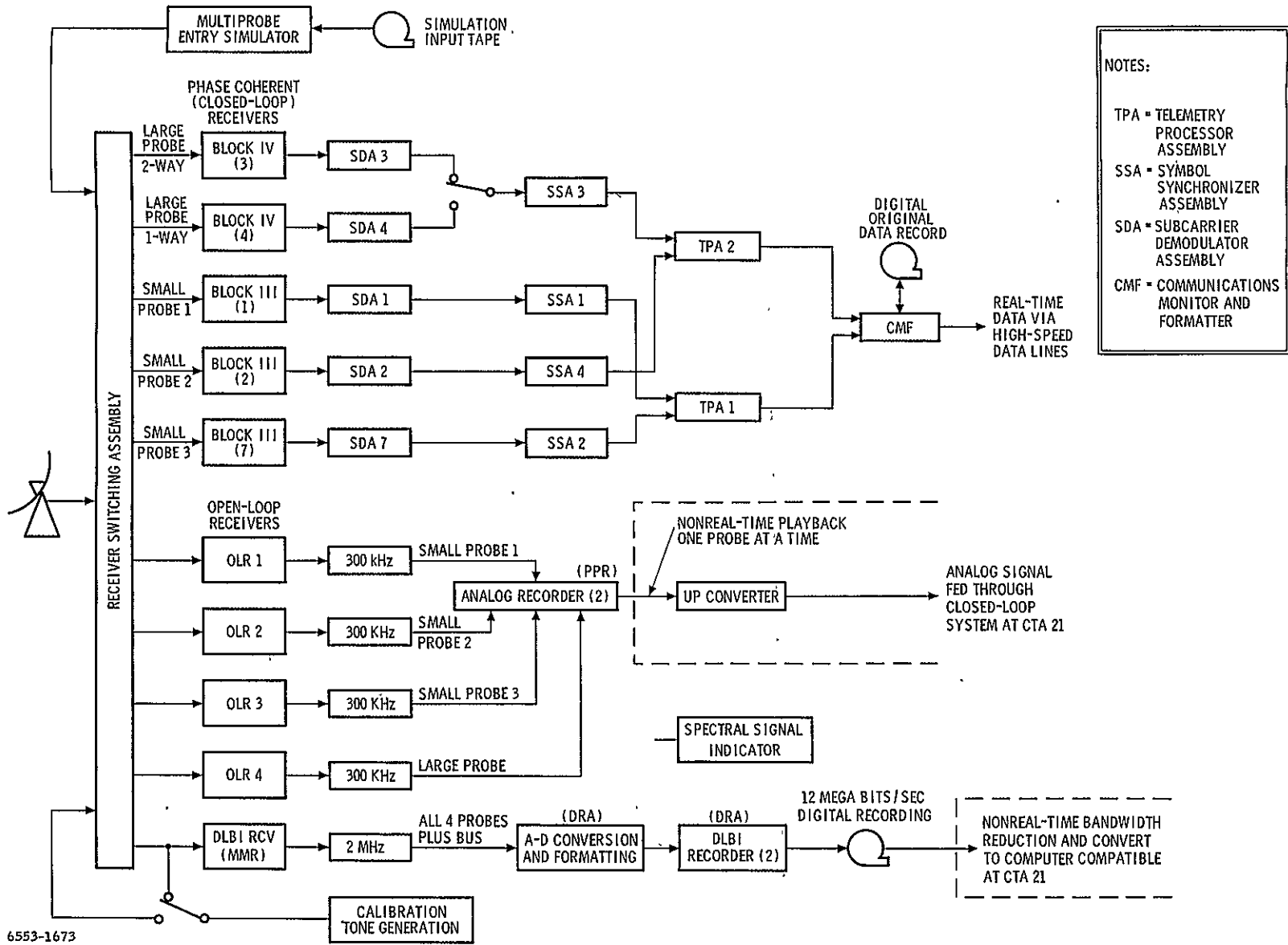
check consists of a switch-by-switch "preflight" followed by acquisition of the bus downlink signal by the five closed loop receivers and five open loop receivers. This signal is processed by the four (closed loop receiver) telemetry strings and routed via HSDL to JPL for verification (see Fig. 1). Simultaneously, the closed loop receiver doppler is processed and transmitted to JPL and the four open loop receivers and Multi Mission Receiver (MMR) similarly acquire the bus signal, confirmed on the Spectral Signal Indicators (SSIs), and record the open loop doppler and telemetry on the DRA and PPR recorders. The open loop signal recorded on the PPR recorders is replayed via the up-converter into the closed loop receivers and again routed back to JPL. This positively confirms correct configuration of all the closed and open loop data paths. Finally, the checklist requires the termination of the bus signal tracking and all other signal sources, the loading of new tapes, and the loading of all required probe parameters and frequencies, etc.

- (3) The E-1 hour checklist is virtually a final recheck of switch positions and frequencies prior to probe acquisition.
- (4) These procedures plus the extensive multiprobe encounter prepass calibrations will be exercised in tests starting in July 1978 and continuing every other week to December 1978, specifically involving the station crews who will be supporting the actual encounter.

The initial exercises at DSS 14 in March indicated that a 16-man crew is required to operate at DSS 14 and DSS 43 during the encounter, so the above tests are planned at a time when the prime crews are "back to back," enabling both crews to work an extra four hours in parallel along with the off shift personnel needed to produce the full complement of 16.

C. ALSEP Tracks

The ALSEP tracks are being executed to produce VLBI data in order to check out the VLBI Wind Measurement experiment which involves station equipment, CTA-21 processing and MIT processing. The tracks involve various combinations of DSS 14, 43, and STDN Santiago and Guam tracking stations. This series of test tracks was described in *The DSN Progress Report 42-45*; and the next article in this series will include a detailed status of the results of the tests conducted from February through July 1978.



NOTES:

- TPA = TELEMETRY PROCESSOR ASSEMBLY
- SSA = SYMBOL SYNCHRONIZER ASSEMBLY
- SDA = SUBCARRIER DEMODULATOR ASSEMBLY
- CMF = COMMUNICATIONS MONITOR AND FORMATTER

ORIGINAL PAGE IS OF POOR QUALITY

6553-1673

Fig. 1. Pioneer Venus '78 multiprobe entry

Helios Mission Support

P. S. Goodwin
TDA Mission Support

G. M. Rockwell and W. N. Jensen
Deep Space Network Operations Section

This article reports on activities of the DSN Network Operations organization in support of the Helios Project from 15 April 1978 through 15 June 1978.

I. Introduction

This article is the twenty-second in a continuing series of reports that discuss Deep Space Network support of Helios Mission Operations. Included in this article is information on Helios-1's seventh perihelion, Helios-2's fifth perihelion, and other mission-related activities.

II. Mission Operations and Status

The Helios-1 spacecraft passed through its seventh perihelion on 29 April 1978 at 06:13:30 Universal Time Coordinated (UTC). The perihelion pass was not covered by a DSN station, but rather by DSS 67/68 at Weilheim, Germany. The spacecraft was at a bit rate of 512 bits per second (bps) coded in Format 1, configured in medium power mode and with all experiments on. All spacecraft subsystems and experiments were in excellent condition.

Helios-2 passed through its fifth perihelion on 30 April 1978 at 05:08 UTC, and as was the case with Helios-1, coverage was by DSS 67/68. The bit rate was at 256 bps coded Format 2. The spacecraft was in a medium power mode and all experiments were on. All of Helios-2 subsystems and experiments appeared to be in excellent condition.

On 3 June 1978, the Helios Project requested that the DSN 64-meter stations use 20-kilowatt (kW) power for uplinking to Helios-2. The reason for this was due to the Sun-Earth-Probe (SEP) angle decreasing below 4 degrees. Since 23 May 1978, the highly active Sun began to influence uplink and downlink signals heavily, with ever-increasing frame deletions. On 3 June 1978, two commands were lost over DSS 43 (Canberra, Australia) prior to the 20-kW uplink request, which prevented the spacecraft from configuring to the gap coverage read-in bit rate. This resulted in a 13-hour loss of data. In addition to the 20-kW mode, the Project will transmit all critical commands three times, which has proved helpful in the past during similar conditions. Also, the telemetry bit rate was lowered to 128 bps, which is the lowest bit rate capable of reading out the spacecraft memory to cover gaps between stations. The above configuration will exist until mid-July,

An unexpected blackout entry occurred on 8 June 1978 over DSS 63 (Madrid, Spain). Station 63 had trouble maintaining telemetry lock at 128 bps and the situation did not improve when the rate was lowered to 64 bps. DSS 67/68 (Weilheim, Germany) was asked to acquire, and the results were the same as experienced at DSS 63. As a result, the project configured the spacecraft's memory for a 22-day storage period assuming a symmetrical exit angle, and the

spacecraft was commanded to an 8 bps read-in mode on 8 June 1978 at 18:07 UTC. The subsequent passes at DSS 43 and DSS 63 showed a very degraded signal and proved "almost blackout" conditions at an SEP angle of approximately 3.1 degrees. This region will be exited on 29 June 1978.

Overall coverage of both Helios spacecraft for this period is listed in Table 1.

III. Special Activities

A. DSN Mark III Data Subsystem (MDS) Update

As reported in the last article, DSS 11 MDS update was completed (Ref. 1) and the station placed under configuration control to support Helios flight operations on 26 April 1978. This completes the DSN MDS implementation.

B. Support of On-Board and Ground Experiments

The DSN 64-meter stations have continued practicing polarimetry and Meteorological Monitor Assembly (MMA) procedures (Ref. 1). During the blackout period of Helios-2, discussed earlier in this article, Faraday rotation data (Experiment 12) will be collected during all 64-meter Helios-2 tracks.

This utilizes the same procedures for polarimetry and MMA procedures mentioned above. These data will also be correlated with pulsar data collected by the 100-meter antenna at Effelsberg, Germany, on 12, 13 and 14 June. In addition to this period of high interest, the time of closest approach (smallest SEP angle) of 17, 18 and 19 June, is most critical to experimenters and good data is hoped for.

Concerning Experiment 10 (micrometeoroid counter and analyzer), the experiment on Helios-2 was turned off on 5 June, after the experimenter suspected a problem, due to a current rise in Sensor-A of the experiment package. The date of Experiment 10 turn-on and checkout has not yet been determined at this writing.

C. German Space Operations Center (GSOC) 22-Bit-Error Polynomial Code (EPC) Conversion

In October, 1978, GSOC is scheduled to convert to 22-bit EPC to conform to the DSN 22-bit configuration. The first test of the system, referred to by GSOC as the Mission Control and Computer Center (MCCC) bypass, was conducted on 2 June 1978. Data were successfully passed from DSS 62 (Cebreros, Spain) through the high-speed switch at JPL to GSOC while in the 22-bit EPC. Future checkout of the system is planned prior to final conversion in October.

Reference

1. Goodwin, P. S., Jensen, W. N., Rockwell, R. M., "Helios Mission Support" in *The Deep Space Network Progress Report 42-45*, pp. 101-103, Jet Propulsion Laboratory, Pasadena, California, June 15, 1978.

Table 1. Helios tracking coverage

Month	Spacecraft	Station type	Number of tracks	Tracking time (hours, minutes)
April	Helios-1	26-meter	42	252:07
		64-meter	3	13:56
	Helios-2	26-meter	39	232:05
		64-meter	21	116:36
May	Helios-1	26-meter	55	333:41
		64-meter	1	5:06
	Helios-2	26-meter	22	124:00
		64-meter	29	140:20

D7-44
32-20N

N78-32144

On Improved Ranging

J. W. Layland, A. I. Zygielbaum, and W. P. Hubbard
Communications Systems Research Section

The currently deployed ranging systems are subject to a variety of waveform distortion errors and equipment vagaries which limit the accuracy of the range data used for Navigation and Radio Science. In light of this fact, this article presents arguments, both subjective and experimental, for increasing the accuracy of the currently deployed ranging system by the adoption of an approximately 1 MHz sine wave for the precision-defining signal for ranging. Inferences are also drawn for the design of more precise and wider bandwidth ranging systems in the future.

I. Introduction

We have, in recent months, reviewed the instrumental limitations to range measurement accuracy. Two specific objectives were sought: devising cost-effective improvements to the current generation of ranging systems, and establishing guidelines for future ranging system development. Our analysis and supporting experimentation indicate that within the bandwidth constraints of the current, or NASA Standard Transponder, a 1 MHz range code plus appropriate filtering in the ground systems should improve the accuracy achievable to the order of 1 meter (6 ns). In the long term, further improvements to range accuracy can be achieved only by increasing the bandwidth of the entire end-to-end ranging system. Since many elements of a two-way ranging instrument are common with three-way or differential one-way instruments, the information we have obtained should also provide useful guidance to the design of these related systems.

One unexpected result of our work was confirmation of the previously suspected sensitivity of the ranging system to errors

caused by changes in Tracking Station equipment configuration. In our current test series, errors induced by changes in the uplink modulator were as large as 11 meters (70 ns). This type of error may be a prime contributor to the ranging system problems currently under investigation by both Viking and Voyager projects.

II. Near-Term Improvements

In the design of precise measurement systems, it is virtually imperative to utilize the entire available bandwidth with signals that are readily detected and processed in a way which directly contributes to improving the accuracy of the measurements. This is not done in the current ranging systems, in which both the fundamental and third harmonic of the precision-defining range code fall within the passband of current transponders. While the third harmonic *could* be processed to enhance ranging accuracy, this processing is not done, nor is it readily implemented. With the current range-code detection schemes, the third harmonic contributes

nothing to measurement precision, and could be removed by filtering (Ref. 1). Its principal function in the current system has been to allow a numerically simple conversion from range-code correlations to estimated range. In actuality, the presence of the third harmonic creates the opportunity for severe distortion errors to arise, so that its removal would improve accuracy, though not precision. Phase-shift and filter effects vary between stations and between transponders, to cause configuration-dependent bias errors and waveform distortion effects which are the limiting error sources of the current system.

Let us suppose that the received ranging waveform consists of the fundamental and third harmonic from a square-wave. As noted above, we have previously shown that simply throwing away the third harmonic does not degrade the precision of the range delay estimate with respect to thermal noise. However, aside from ambiguities, it is easy to show that a range delay estimate can be constructed using this third harmonic alone which has exactly the same precision as the delay estimate derived from the fundamental component. Since the fundamental can resolve the three-fold ambiguities of the third harmonic, and since their thermal noise errors are independent, the two delay estimates could be combined to effect a $\sqrt{2}$ improvement in precision over either one alone.

If, however, the transponder in question can pass the third harmonic of the conventional 500 KHz range code with little attenuation, it can also pass the fundamental of a 1 MHz range code with little or no attenuation. Doubling the range-code frequency provides a direct factor-of-two improvement in delay-estimate precision with respect to the conventional 500 kHz range code as conventionally processed. It also provides a $\sqrt{2}$ improvement in delay-estimate precision over the best processing for the conventional range code. As the third harmonic of the 1 MHz code now does not pass through the transponder, further improvements require first increased transponder bandwidths, and subsequently increased bandwidth throughout the system.

There is an additional advantage to the 1 MHz code which results because none of the code harmonics pass through the transponder. Professor L. Rauch has recently pointed out (Ref. 2) that nonlinear elements such as exist in the transponder's modulator and power amplifiers can induce phase-shifts in the fundamental component of a waveform which depend upon the phase of the harmonics entering the nonlinear element. With all harmonics removed from the range code prior to such nonlinearities, delay errors induced by the harmonics should be minimized. We anticipate that use of the 1 MHz range code, coupled with filters in the ground receiving system which pass only the fundamental of this code, will greatly reduce sensitivity to DSN equipment variations which

manifest themselves in changes in the harmonic structure of the waveform.

Knowing that the third harmonic of the conventional 500 kHz range code is passed by the transponders, it has been suggested that a range code of that frequency be used to gain an additional factor-of-1.5 increase in range precision. This gain is unlikely to be achieved for two reasons: First, the third harmonic is attenuated by 3 dB in several of the present physical transponders, and second the 1.5 MHz signal is now close to the transponder filter band-edge and thus more subject to phase-shifts due to environmental changes in the transponder.

It is worth noting here that if a PN range code were used instead of square-wave, only those spectral lines below the first zero of the spectrum are at a phase which helps improve signal delay resolution, while those between the first and second spectral null (may) degrade resolution. This is exactly analogous to the behavior of a square-wave as discussed above, where the third harmonic, falling between the first and second spectral nulls, is nonbeneficial in resolving range delay with a correlation-type estimator. When we earlier asked (Ref. 3) for the best unit-power waveform to be tracked by a delay-locked loop in terms of residual phase jitter, the answer was almost identical to a PN which had been filtered to include only the frequency region below the first spectral null. The length of that PN depended upon the SNR that was to be achieved by the delay-lock tracker, which effected the band-limit constraint for that system.

The PN, however, is a waveform with many spectral components within the main lobe of its spectrum. Any nonlinearities in the ranging circuit will generate cross-modulation terms between these components which coincide with some other component. This creates the potential for waveform distortion effects similar to those we have now, albeit at a lower magnitude. If we keep the waveform spectrally simple, i.e., a sine-wave which occupies nearly the full bandwidth available, the distortion effects induced by nonlinearities can be scrubbed off by filtering at appropriate places within the system.

The conclusion we wish to draw from this can be summarized as follows: To get the best possible results for ranging, the available bandwidth should be completely utilized by those signal components which are most useful. For the near term, a 1 MHz range code will substantially improve the accuracy achievable with current transponders. Our recent test results, to be described next, reinforce this opinion. A future article will discuss other currently limiting error sources, and the anticipated effect of increasing the available ranging bandwidth.

III. Experimental Results

Several experiments were recently conducted to measure the so-called ranging "waveform-distortion" error and test the concepts previously proposed (Ref. 1) as a cure. These experiments utilized the Mu-II Ranging System (Ref. 4) installed at the Telecommunications Development Laboratory (TDL). The first of four groups of experiments determined the precision of the current ranging system. The remaining three experiments measured the improvement in precision gained by (1) filtering all but the fundamental frequency of the 500 kHz range code prior to demodulation, (2) utilizing a 1 MHz range code, and (3) using a 1 MHz range code filtered as in (1).

The results of our investigations indicate that a filtered 1 MHz code (3 above) reduces the waveform distortion to below 1 ns of error. This also increases the ranging system immunity to errors induced by equipment variation in receivers, excitors, and transmitters.

A. The Setup

Figure 1 illustrates the various experiment configurations. The Mu-II Ranging System range code modulated a carrier which was echoed either by a wideband zero-delay device or the proof test model of the MVM'73 transponder. Mu-II Channels 1 and 2 were respectively connected to 10 MHz IF signals from the Block IV and Block III receivers. One of a pair of passband filters was inserted into either the Block IV or Block III to Mu-II IF cable to provide a band-limited received range code. The filter characteristics are shown in Fig. 2 for the "500 kHz" filter and Fig. 3 for the "1 MHz" filter.

B. Experiments and Results

The general test plan consisted of utilizing both the zero delay device and the MVM'73 transponder in conjunction with each of the following four test conditions:

- (1) 500 kHz code, unfiltered
- (2) 500 kHz code, with filtered IF signal
- (3) 1 MHz code, unfiltered
- (4) 1 MHz code, with filtered IF signal

The data from tests (1) and (2) or test (3) and (4) were obtained simultaneously by connecting one channel of the Mu-II directly to the Block III (IV) IF signal and inserting a filter in the Block IV (III) IF signal attached to the other channel. Comparison of Block III and Block IV data showed error differences on the order of tenths of nanoseconds. Because differences between the two Mu-II channels were of the same magnitude, the taking of data simultaneously is reasonable and justified by minimizing the test time. It must be noted that

Mu-II channel 1 exhibited an unexpected periodic error, which appears as periodic hash on the data graphs displayed below. From extensive testing we infer that this error is due to hysteresis in the channel 1 A/D converter and interaction between the three Mu-II coders. The hysteresis was predicted by Layland (Ref. 5). Coder interaction was discovered experimentally. Because these inseparable errors are small (<1 ns), they will be ignored in this article.

Each of the tests described below involved stepping the local model of the received range code in 7 ns steps over a span of one quarter of the period of the highest frequency code (clock). At each step, the code phase measurement $\hat{\theta}$ is compared to the actual phase θ . The graphs are the error function $\theta - \hat{\theta}$ and are in units of nanoseconds. This is a direct display of the so-called "waveform-distortion" error.

1. **500 kHz code, zero delay device.** This configuration is identical to current DSN ranging (Planetary Ranging Assembly - PRA) zero-delay calibrations. Figure 4a is the error function without filtering. The peak-to-peak error is 18.5 ns. A dramatic improvement is shown in Fig. 4b. By adding the "500 kHz filter," the error is reduced to 1.5 ns.

2. **500 kHz code, transponder.** The peak-to-peak error in Fig. 5a is about 7.4 ns. This is the error of the unfiltered ranging system. Adding the "500 kHz filter" (Fig. 5b) reduces the error to about 2.1 ns. This is a substantial improvement over the current ranging system.

3. **1 MHz code, zero-delay device.** Tests with a 1 MHz range code confirmed the expected improvements. Using the zero-delay device, a peak-to-peak error of 3.9 ns (Fig. 6a). Using the "1 MHz filter" reduced this error to 1.0 ns (Fig. 6b).

4. **1 MHz code, transponder.** This final test set further justifies the use of a 1 MHz code and filter. Without the filter (Fig. 7a), the error is 14.2 ns. When the "1 MHz" filter is used, the error (Fig. 7b) is only 0.6 ns.

C. End-To-End Distortion Immunity

The "end-to-end ranging system" includes the ranging machine, exciter, transmitter, receiver, spacecraft transponder, zero delay devices, and all cables, switches, connectors, etc., in the ranging path. Each component in this path is capable of inducing, to varying degrees, range code distortions in both the frequency and time domains. Jumps in DSN station range calibrations and spacecraft range residuals evidence the relative susceptibility of the range system to equipment vagaries.

The exciter modulator is one major source of waveform distortion. Two standard DSN modulators were compared in terms of relative spacecraft delay versus modulation index.

The left side of Fig. 8 shows an almost 70 ns worst-case disparity between modulators. Use of the 1 MHz code and filter reduced this to about 10 ns. A similar modulator measurement was made earlier (Ref. 1) using only the 500 kHz code and "500 kHz filter." The worst-case difference was 10 ns without the filter and 3 ns with it. During the current series of tests, using the 500 kHz code with no filter produced the 70 ns disparity noted earlier. A 30 ns worst-case difference resulted when the "500 kHz filter" was used. These current numbers were easily repeatable to within 1-2 ns during the six-month period while we sought to explain the differences between the 500 kHz results now and in 1975. We now believe that these discrepancies are due to the extensive modification to TDL which occurred between the two test series.

In addition, we strongly suspect that the numbers previously seen correspond only with the behavior of a superbly tended calibration laboratory which TDL was in 1975. Our current measurements follow a period when TDL has been "mothballed" without continuous expert attention, and may in fact be more representative of the ranging system behavior to be expected in the operational DSN tracking stations. The delicate nature of the current range system is obvious.

Utilizing a 1 MHz range code and IF filter increases system immunity to equipment variation.

IV. Comments

We have demonstrated that use of a 1 MHz range code and a narrow-passband IF filter can reduce waveform distortion error by a factor of as much as 20. Along with this improvement in ranging precision, ranging accuracy is enhanced by nullifying many errors caused by equipment vagaries. In our opinion, the IF filter and concomitant modification of ranging system software (and in the case of the Planetary Ranging Assembly, hardware) are the most cost-effective way of improving the current generation ranging system.

The lessons we have learned here are also important for the development of the next generation ranging system. Clearly we need to increase the available bandwidth, and as we do, we should occupy that bandwidth almost completely with a sinusoidal ranging tone for precise definition of range.

Acknowledgements

We would like to thank J. Weese for his extraordinary efforts in making and keeping TDL operational for our experiments.

References

1. Martin, W. L., and Layland, J. W., "Binary Sequential Ranging With Sinewaves," *JPL-DSN-PR 42-31*, Feb. 15, 1976, pp. 30-40.
2. Rauch, L., Private Communication.
3. Layland, J. W., "The Optimum Cross Correlation Function for a First-Order Tracking Loop Under Unit Power Constraint," *JPL-SPS 37-51*, Vol. III, June 1968, pp. 240-244.
4. Martin, W. L., and Zygielbaum, A. I., *MU-II Ranging JPL-TM 33-768*, May 15, 1977.
5. Layland, J. W., "Digital Demodulation With a Non-Ideal Quantizer," *JPL-DSN-PR 42-32*, April 15, 1976, pp. 100-105.

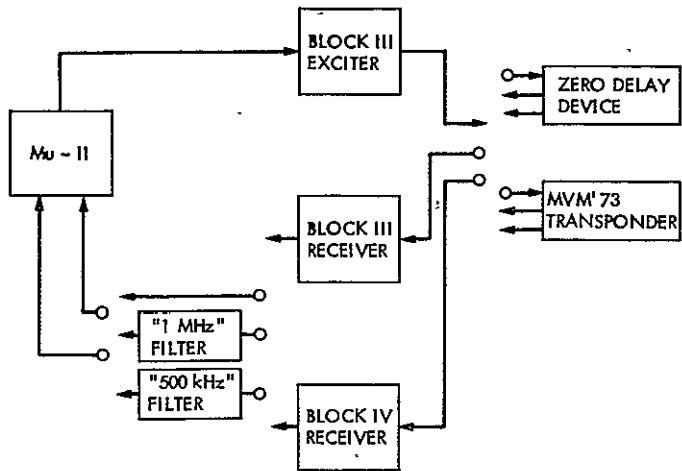


Fig. 1. TDL configuration

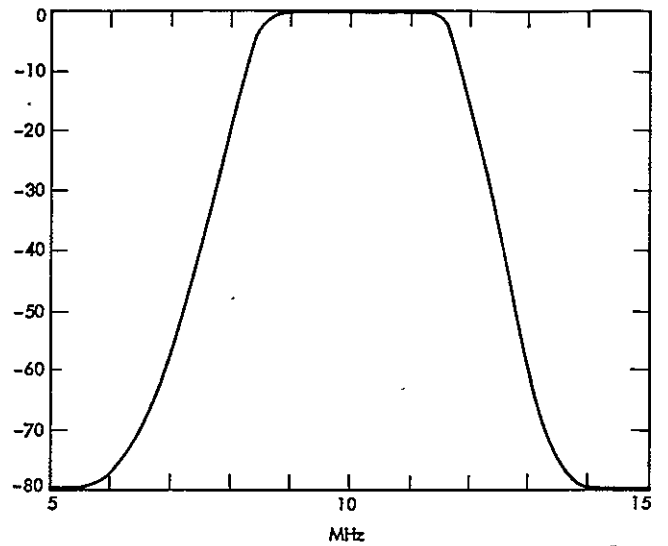


Fig. 3. "1 MHz filter" bandpass

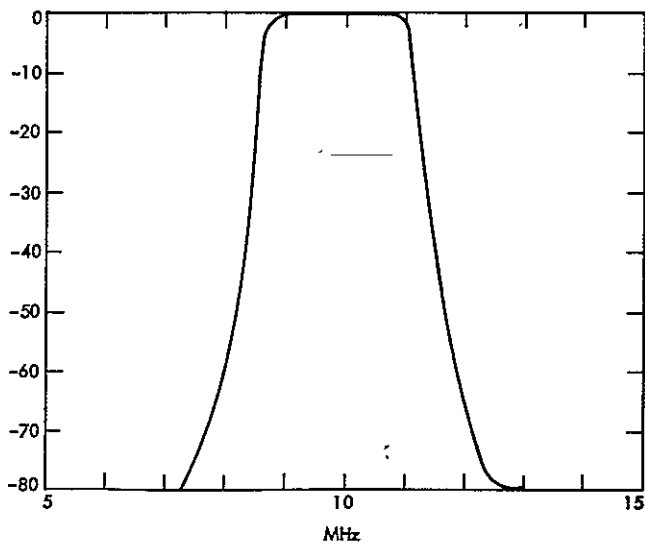


Fig. 2. "500 kHz filter" bandpass

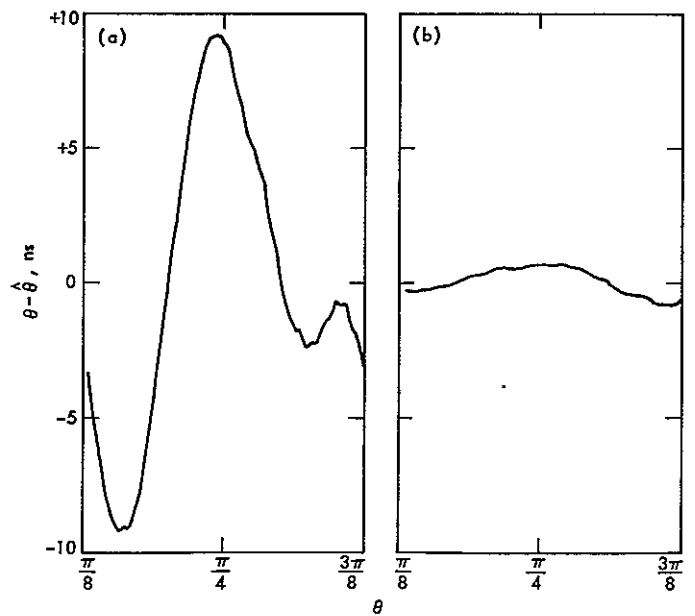


Fig. 4. Phase error—500 kHz code, zero delay device:
(a) Unfiltered, (b) 400 kHz filter

ORIGINAL PAGE IS
OF POOR QUALITY

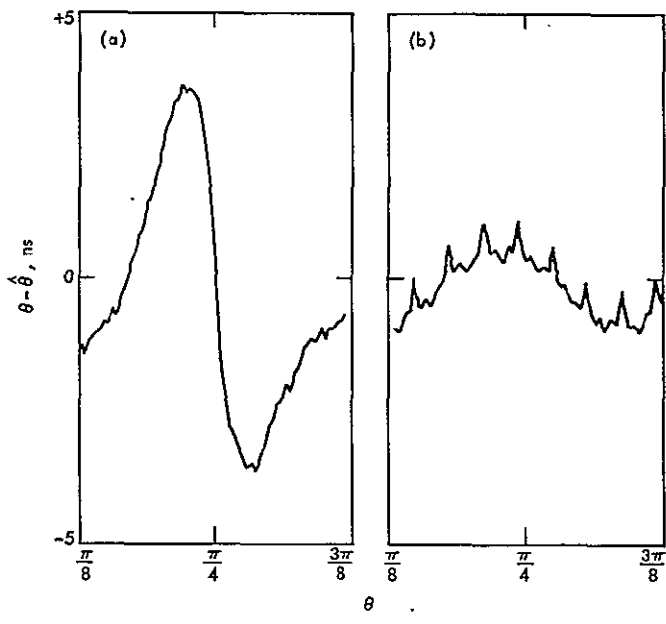


Fig. 5. Phase error—500 kHz code, transponder: (a) Unfiltered, (b) 500 kHz filter

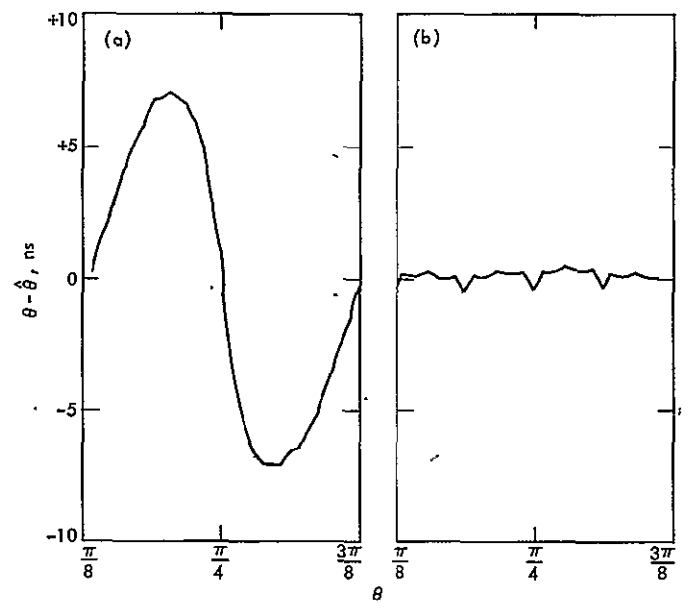


Fig. 7. Phase error—1 MHz code, transponder: (a) Unfiltered, (b) 1 MHz filter

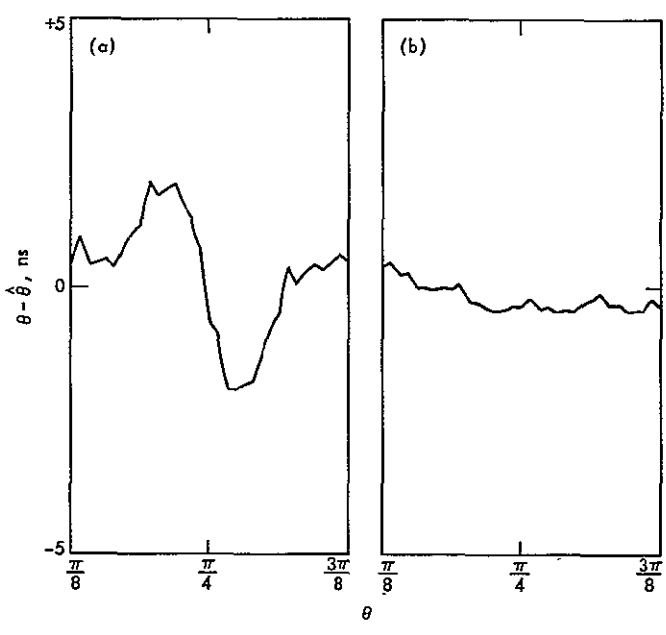


Fig. 6. Phase error—1 MHz code, zero delay device: (a) Unfiltered, (b) 1 MHz filter

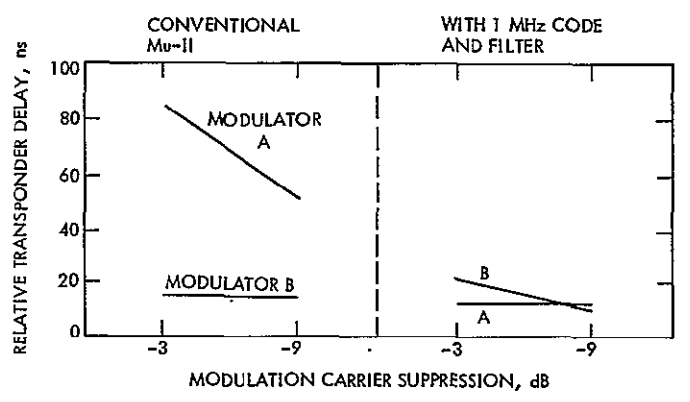


Fig. 8. Range variation caused by modulator change

Establishing a Celestial VLBI Reference Frame— I. Searching for VLBI Sources

R. A. Preston, D. D. Morabito, J. G. Williams, M. A. Slade, A. W. Harris,
S. G. Finley, L. J. Skjerve, and L. Tanida
Tracking Systems and Applications Section

D. J. Spitzmesser
Deep Space Network Operations Section

B. Johnson
Aeronautics-Ford, Newport Beach, California

D. L. Jauncey
C.S.I.R.O., Division of Radiophysics, Sydney, NSW, Australia

A. Bailey, R. Denise, J. Dickenson, R. Livermore,
A. Papij, A. Robinson, and C. Taylor
Tidbinbilla Deep Space Communications Complex, Australia

F. Alcazar, B. Luaces, and D. Munoz
Madrid Deep Space Communications Complex, Spain

The Deep Space Network is currently engaged in establishing a new high-accuracy VLBI celestial reference frame. This article discusses the present status of the task of finding suitable celestial radio sources for constructing this reference frame. To date, 564 VLBI sources have been detected, with 166 of these lying within 10° of the ecliptic plane. The variation of the sky distribution of these sources with source strength is examined.

I. Introduction

The Deep Space Network (DSN) is currently engaged in establishing a new high-accuracy celestial reference frame composed of compact extragalactic radio sources, principally quasars. These radio sources are observed by means of the

technique of Very Long Baseline Interferometry (VLBI), whereby two antennas separated by distances of up to an earth diameter, simultaneously observe the same source (Ref. 1). This article will discuss the effort which has been undertaken to find a suitable set of celestial radio sources from which the VLBI reference frame may be constructed.

In the past, astrometric or geodetic studies which required the use of a celestial reference frame had to rely on an optical star reference frame (that is, a set of optical stars whose relative positions were well known). Such reference frames were limited to accuracies of about 0.1 arcseconds (5×10^{-7} radians) in relative source positions due to the effects of atmospheric turbulence on optical observations and the relative angular ("proper") motions of the stars in the sky. Since VLBI sources are extragalactic and thought to be on average about 10^6 times farther away than optical stars, proper motions should be negligible. In addition, the VLBI technique should reach angular measurement accuracies approaching 0.001 arcseconds (5×10^{-9} radians). Hence, VLBI radio reference frames should possess accuracies which exceed those of optical reference frames by one or two orders of magnitude (Refs. 2, 3).

Of what use is such an accurate celestial reference frame? Some examples:

- (1) *Calibrating Deep Space Probe Radio Metric Tracking Data* — The DSN is currently developing an operational VLBI system to synchronize clock epochs and rates among the worldwide DSN spacecraft tracking stations and to monitor earth rotational irregularities in order to properly calibrate radio metric navigation data from interplanetary spacecraft (Ref. 4). In addition, the measured variations in earth spin rate and pole position are important clues to understanding the dynamics of the earth's crust and interior (Refs. 5, 6, 7).
- (2) *Navigating Interplanetary Spacecraft* — The DSN is currently involved in a demonstration of the value of VLBI measurements of spacecraft position for improving the navigation of the Voyager spacecraft (Ref. 8). Computer simulations have shown that VLBI would provide significant navigational enhancements to future interplanetary missions as well (e.g.: Galileo, VOIR).
- (3) *Measuring Planetary and Lunar Orbital Motions* — Improved knowledge of planetary and lunar motion by means of observations of spacecraft in orbit about or on the surface of these bodies will provide higher navigational accuracy for deep space probes as well as useful information for studies of solar system dynamics. At present, JPL researchers are observing the motion of both the moon and Mars by VLBI techniques (Ref. 9).
- (4) *Monitoring Earth Crustal Motions* — At JPL, project ARIES is currently demonstrating that VLBI can be used to monitor local crustal motions in order to study their relationship to seismic events (Refs. 10, 11). Eventually, VLBI will be used to measure the relative motion of crustal blocks on a global scale.

- (5) *Earth Surveying* — The National Geodetic Survey is considering using VLBI techniques to assist in its effort to accurately determine the relative separations of widely spaced survey markers.

With this justification, we can now consider what the logical steps in the development of a VLBI reference frame would be:

- (1) Conduct a sky search for celestial VLBI sources which might be useful.
- (2) Choose the "best" subset of these sources for forming the VLBI reference frame.
- (3) Determine accurate relative positions of these sources.

Although it is conceptually possible to pursue these tasks in purely sequential order, in practice we have performed these activities to a large extent in parallel. Nonetheless, to date, the most intensive effort has gone into searching for sources, and that is the subject of the remainder of this article.

II. The Search Concept

The search for VLBI sources first became an organized pursuit in the summer of 1974. Up to that point, perhaps 60 celestial VLBI sources had been found by DSN efforts as well as astronomers at other institutions. It became evident that this number of sources would not suffice for future VLBI requirements, and moreover, that this was probably only a small fraction of the total number of VLBI sources in the sky, and hence, probably not an optimum set from which to form a VLBI reference frame. The search began slowly, but in the past two years, increased in intensity. Up to the present time, more than 30 individual observing sessions have been organized.

III. What is a VLBI Source?

The strength of a celestial radio source, or its total flux density, can be expressed as:

$$S_T = \iint_{\text{over the source}} B(\theta, \phi) d\theta d\phi$$

where

$$S_T = \text{total flux density in Jansky} \\ (1 \text{ Jansky} = 10^{-26} \text{ watts/m}^2/\text{Hz})$$

θ, ϕ = orthogonal angular celestial coordinates measured from a designated source center in radians

$B(\theta, \phi)$ = the angular brightness distribution of the source in Jansky/steradian

The VLBI strength of a celestial radio source, or its correlated flux density, can be expressed as (Ref. 12):

$$S_c = \left| \iint_{\text{over the source}} B(\theta, \phi) e^{-i(2\pi)(u\theta + v\phi)} d\theta d\phi \right|$$

where

S_c = correlated flux density in Jansky

u, v = the components of the baseline vector separating the two observing antennas, along θ, ϕ plane of sky coordinates, in RF wavelengths

So, for a particular observation, the correlated flux density is merely the amplitude of one component of a complex two-dimensional spatial Fourier transform of the angular brightness distribution of the source. If the source angular size is significantly smaller than the spatial wavelengths of the transform component, $1/u$ and $1/v$, then it is easy to derive that the correlated flux density is equal to the total flux density. If most of the power emanating from a source comes from angular areas that are large compared to the spatial wavelengths, then virtually none of the total flux density of the source appears as correlated flux density. So, to observe a significant fraction of the total flux density as correlated flux density, much of the total flux density must come from regions smaller than $1/u$ and $1/v$.

Our baselines lengths were about 7×10^7 RF wavelengths, and so the spatial wavelengths, $1/u$ and $1/v$, were generally on the order of a few milliarcseconds. Hence, the radio sources we detect as VLBI sources have a significant amount of their total flux density contained in components that are no more than a few milliarcseconds in angular extent. Only a small percentage of celestial radio sources have such tiny strong components. More typically, radio sources are many seconds of arc to several minutes of arc in angular extent.

What types of celestial sources have such small components? Within our own galaxy there are not many VLBI sources of interest to us. A few molecular clouds emit maser radiation from compact regions (Ref. 13). However, because the molecules radiate at only discrete spectral lines, are extremely time variable, and are relatively nearby, these sources are not the object of our search. Since stars are usually very weak radio sources, few stars have been detected with

present VLBI systems (Ref. 14). The only confirmed, reliable, and wideband VLBI source of reasonable strength within our own galaxy is the galactic center source (Ref. 15).

Exterior to our galaxy, VLBI sources within our limits of detectability fall into three categories:

- (1) *Quasars* — The most distant class of extragalactic objects. Optically, they are stellar in appearance, with emission and absorption spectral lines shifted far to the red. By current cosmological thought, the large redshifts are indicative of great distance, generally billions of light years. The extraordinary power output per unit volume exhibited by quasars is not explained by current theories. A prominent suggestion is that the large energies are released by matter falling into massive black holes, perhaps as large as $10^8 - 10^{10}$ solar masses. Ground based VLBI studies indicate that not only do some of these objects possess angular radio structure at the milliarcsecond level, but that this structure can be time-variable over a few months with apparent internal velocities exceeding the speed of light (Ref. 16). Most of the VLBI sources we find are identified as quasars, when optical identifications exist.
- (2) *BL Lacertae Type Objects* — These radio sources appear to be similar to quasars, but their atomic emission lines are nonexistent or weak. They are generally somewhat more compact and time-variable than quasars (Ref. 17). Astronomers feel they may be the bright cores of distant elliptical galaxies.
- (3) *Galactic Cores* — Many galaxies possess an active central region from which radio emission emanates. VLBI observations have shown that galactic cores can contain angular structure at the milliarcsecond level and, in one case, structural changes which indicate apparent internal velocities exceeding the speed of light (Ref. 16). The VLBI features are often aligned with larger scale features of the source, which suggest that both small and large scale radio structure may have originated from similar explosive events in the core at different epochs. Of perhaps more terrestrial interest is the fact that our own galaxy has an active VLBI core.

The noted similarities of quasars, BL Lacertae objects, and galactic cores may be an indication that all three are merely different classes of a single type of celestial phenomenon, perhaps at different evolutionary stages.

IV. Selection of Candidate Sources

If one were to examine the entire sky for VLBI sources to the level of sensitivity we desire, the task might take several

decades. Hence, our search was relegated to observing known celestial radio sources to see which of these might be VLBI sources.

In order to keep from searching all known celestial radio sources for VLBI components, we have used existing information on radio sources as clues to source size. The following criteria proved useful in determining which sources might have structure confined to the milliarcsecond-level:

- (1) *Spectrum* – Power does not fall off with increasing frequency as rapidly as more typical radio sources in the range 1–10 GHz. An even stronger indicator is if the spectrum is flat, sloped upward, or peaked in this range. Of all the indicators of milliarcsecond structure, spectral properties have proved the most useful.
- (2) *Variability* – Identified as radio or optical variable.
- (3) *Optical Identification* – Identified as extragalactic.
- (4) *Size Limits* – A short baseline interferometer can determine if a source has components smaller than its resolution limit (resolution does not exceed a few arcseconds).
- (5) *Interplanetary Scintillation* – Radio sources that show scintillations when viewed through the solar corona possess components with angular sizes $\lesssim 0.1$ arcsecond.
- (6) *Detection in High Frequency Surveys* – A larger percentage of sources detected in surveys between 1 and 10 GHz are VLBI sources than is the case at lower frequencies.

We searched the literature for information on celestial radio sources. This was not a simple task, as the information is scattered through hundreds of articles. Nor is the literature static. Many of the high frequency radio surveys have only been performed during the last few years, and some of the sky is still unsurveyed at high frequency. Fortunately, a few high frequency radio surveys (e.g.: Parkes, NRAO-Bonn, Ohio State) provide data on a large fraction of the sky. In general, we chose as candidates only those sources whose total flux densities were greater than 0.7 Jansky at 2.3 GHz.

To date, our literature searches have yielded about 1100 celestial radio sources which might prove to be VLBI sources. Of these, we have performed VLBI observations on almost 900 sources, and have detected 564 as VLBI sources.

V. The Observations

The observations were all performed with pairs of antennas within the DSN which were separated by intercontinental distances. In practice, this meant observing on the Goldstone-

Australia or Goldstone-Spain baselines as pairs of antennas on the Spain-Australia baseline cannot simultaneously observe a very large area of sky. Generally, 64 – 26-meter antenna pairs were used, but occasionally 64 – 64-meter combinations were substituted. All the observations were performed at 2290 MHz. The receiver chain generally consisted of an S-band traveling wave maser followed by a special phase-stable S-band VLBI receiver which converted the signal to an IF of 50 MHz. The Mark II VLBI recording system, which was developed by the National Radio Astronomy Observatory, then recorded a 1.8 MHz data bandwidth by digitally sampling at a 4-Mbs rate (Ref. 18). Digital sampling and phase stability of the receiver chain were controlled by rubidium or hydrogen maser atomic clocks. System temperatures were measured at both antennas for each source so that the data could be properly calibrated.

VI. Data Processing

Matching tapes from the two antennas were then cross-correlated on a special hardware/software computer at the National Radio Astronomy Observatory in Charlottesville, Virginia. Computer manipulation of the output of this correlator yielded the correlation constant, ρ , for each observation, or the fraction of bits on the two tapes that were correlated. Correlation constants were then converted into correlated flux densities, S_c , by means of the expression:

$$S_c = 2.6\rho \sqrt{T_1 T_2 \left(\frac{dS}{dT}\right)_1 \left(\frac{dS}{dT}\right)_2}$$

where

S_c = correlated flux density in Jansky

T_i = the measured system temperature at antenna i in K

$\left(\frac{dS}{dT}\right)_i$ = the inverse sensitivity of antenna i in Jansky/K (i.e., how strong does a source have to be in total flux density (Jansky) to raise the system temperature 1K)

The uncertainty in the correlated flux density measurements due to random noise effects may be expressed as:

$$\sigma_{S_c} = 6.3 \times 10^3 \sqrt{\frac{T_1 T_2}{e_1 e_2} \frac{1}{D_1 D_2} \frac{1}{\sqrt{Bt}}}$$

where

e_i = the antenna efficiency of antenna i (dimensionless)

D_i = the diameter of antenna i in meters

B = the recorded bandwidth in Hz

t = the coherent integration time in seconds

Most sources were observed for at least three minutes, but for data processing the observations were broken into one minute segments. From this we see that the 5σ detection limit for this search for VLBI sources was about 0.1 Jansky. In addition, one would expect the random uncertainty in detected source strength to be about 0.02 Jansky. However, in practice, systematic errors at the 5 or 10% level dominate the random contribution for most sources.

If a priori source positions are in error, the tapes must be correlated over a range of relative tape delay and delay rate offsets in order to detect a VLBI source. Appropriate searches in these parameters were performed so that the sky was completely searched within 0.5 arcminutes of all nominal source positions. Almost all a priori source position errors should be covered by this degree of position searching. In addition, once detections were achieved, the measured delay and delay rate offsets allowed positional errors to be measured to about one arcsecond, a good level from which to start building a VLBI reference frame.

VII. Results

The reduction of our data is not yet at a complete stage. Accurate source strengths and positions have been calculated for less than half of our detected sources. For the remainder we have strengths accurate to about 20%. Nonetheless, it is useful at this stage to study the general sky distribution of detected sources as a function of source strength. In later articles we will publish catalogs of detected sources.

VIII. The General Sky Distribution

Figures 1a, 1b, and 1c display the general sky distribution of detected VLBI sources as a function of VLBI source strength. The plots show the entire sky, with ± 12 hours of right ascension, or celestial longitude, being displayed horizontally, and $\pm 90^\circ$ of declination, or celestial latitude, being displayed vertically. These maps are equal area representations, so that local spatial densities in one area may be compared to local densities in another.

It should be noted that displaying these source distributions as a function of source strength is fraught with problems, since the strengths of the sources may be uncertain for a number of reasons:

- (1) Due to incomplete data reduction, our source strengths are only accurate to about 20% for more than half of the sources.
- (2) The total flux density and structure of these sources are often time-variable over months or years.
- (3) The correlated flux density may change as a baseline turns with earth rotation. This is due to the fact that changes in the projection of the baseline into the plane of the sky in the source direction can cause different spatial frequencies of the source's brightness distribution to be sampled.
- (4) Differences in correlated flux density between different baselines may also be apparent due to the sampling of different spatial frequencies.

Hence, in displaying VLBI sky maps as a function of source strength, our gradations in source strength should be kept quite coarse. Even then, the categories are not crisp. However, although the plots may not show the true strength of a particular source at a certain epoch and on a certain baseline, they do indicate the general densities of sources as a function of strength.

Figure 1a shows the global distribution of all 564 detected sources. The lower limit of correlated flux strength is about 0.1 Jansky. Several things are evident from this plot:

- (1) In general, the distribution is dense and rather uniform.
- (2) Pairs of DSN antennas cannot commonly view the sky below $\approx -45^\circ$ declination.
- (3) The north polar area is more sparsely populated. This is directly due to a lack of sufficient high frequency surveys in this region to easily identify candidate sources to observe.
- (4) The areas near the plane of the galaxy (not shown) are more sparsely populated. This is particularly evident between $\pm 30^\circ$ declination at right ascensions of about -5 and $+7$ hours. This is due to the fact that high frequency radio surveys often skip the galactic regions and that interstellar charged particles near the galactic plane can cause intrinsically small sources to be scattered to larger angular sizes.

We should point out that this is not nearly a complete map of the VLBI sky at the level of 0.1 Jansky. Since one of our criteria for choosing candidate sources was to generally only keep sources with total flux densities greater than 0.7 Jansky, we have missed a large number of very compact sources with lower total flux densities.

Figure 1b shows the distribution of 184 sources with correlated flux densities greater than 0.5 Jansky. This is also a rather dense and even distribution, and is a more complete representation of the VLBI sky than was the 0.1 Jansky map.

The DSN Block 1 VLBI System is being developed to calibrate radio metric navigation data from deep space probes (Ref. 4). The sensitivity of this system to VLBI source strength is 0.5 Jansky. In order to conserve antenna time, this system is intended to produce the appropriate calibrations with only 1 or 2 hours of observing on each of two baselines. During that short time span, a single pair of DSN antennas will see only a small segment of sky in common. In order to properly estimate the desired parameters, there must be a good distribution of sources within this small common area of sky. This must be true at any time of day. Hence, this system requires a source catalog of about 100 sources. The number of sources we have found with strengths greater than 0.5 Jansky is nicely matched to the number of required sources.

Figure 1c displays the distribution of 50 sources with correlated flux densities greater than 1.0 Jansky. This is also quite a complete representation of the VLBI sky, but the distribution is no longer very dense. Note that less than 10% of the total number of detected VLBI sources have correlated flux strengths greater than 1.0 Jansky.

The falloff in number of sources with increasing source strength is shown more clearly in the histogram of Fig. 2. The number of sources at source strengths less than 0.5 Jansky is smaller than the true sky distribution, due to our candidate selection criteria and our approximate sensitivity limit of 0.1 Jansky. At the high end of the source strength scale, we see that only 10 sources are stronger than 2.0 Jansky and none are stronger than 4.0 Jansky. The middle range of this histogram, say, 0.5 to 2.0 Jansky, can be approximately described by the expression:

$$N = 50S_c^{-1.9}$$

where

N = the number of sources stronger than a correlated flux strength of S_c Jansky

If this relationship holds at lower source strengths as well, then we might expect to find perhaps 4000 sources with correlated flux strengths greater than 0.1 Jansky, or seven times our present number of detections.

IX. The Ecliptic Distribution

Figures 3a, 3b, and 3c display the distribution of VLBI sources within 10° of the ecliptic plane. These maps are plotted on rectangular grids rather than equal area representations. The ecliptic plane appears as a sinusoidal-like trace across these plots.

The ecliptic plane is important in solar system astrometric VLBI work, for it is here that planets and spacecraft mostly travel. The motions of these objects may be accurately monitored against the background of VLBI sources by means of the technique of Differential VLBI (Δ VLBI). With Δ VLBI, a spacecraft and an extragalactic VLBI source can be simultaneously observed on the same VLBI baseline. When the VLBI measurements of the two sources are subsequently differenced, most error contributions cancel to a high degree, providing an accurate measure of the angular separation of the two sources. Since the remaining sizes of many of these errors after cancellation are proportional to the angular separation of the two sources, a high density of extragalactic VLBI sources along the ecliptic plane is desirable, so that a source close to the spacecraft is always available. It also follows that operational Δ VLBI systems will probably be required to work at more sensitive levels than is required for the operational system which calibrates radio metric navigation data, so that spacecraft/extragalactic VLBI source separations can be reduced. Ideally, one might desire as many as 100 sources in an ecliptic reference frame, so that a spacecraft would never be more than a few degrees from a useful source.

Figure 3a shows all 166 detected sources within 10° of the ecliptic. The distribution is rather dense and uniform except for the two areas where the galactic plane crosses the ecliptic plane at about 6 and 18 hours of right ascension. It may be possible to increase the density of sources in the galactic regions by observing at X-band rather than S-band, as the scattering effect is thought to be inversely proportional to approximately frequency squared. Also shown are the positions along the ecliptic of the critical events in the Voyager and Galileo missions where Δ VLBI might provide significant navigational advantages.

Figure 3b shows the distribution of 51 sources within 10° of the ecliptic plane which have correlated flux densities greater than 0.5 Jansky. The distribution now becomes relatively sparse in some areas. Figure 3c shows the distribution of the 14 sources with strengths greater than 1.0 Jansky. The distribution is now very sparse as demonstrated by the fact that no sources appear anywhere near the Voyager encounters of Jupiter and the whole Galileo Jupiter orbit phase is almost quasar-free.

X. Summary

We are engaged in a task of searching for a suitable set of celestial radio sources from which a high precision VLBI reference frame may be constructed. The observational portion of this program is nearly completed. We have shown here sky distributions of the 564 detected VLBI sources greater than about 0.1 Jansky and the subset of 166 of these sources which lie within 10° of the ecliptic. These distributions are reasonably dense at the level of 0.5 Jansky and below. The DSN operational VLBI system for calibrating radio metric

navigation data will utilize sources stronger than 0.5 Jansky. An operational Δ VLBI system would probably have to employ weaker sources.

Significant data reduction and some observing remains to complete the task of searching for VLBI sources. Published catalogs of VLBI sources, source positions, and correlated flux densities will follow this article. The tasks of choosing the "best" of the available VLBI sources and determining accurate relative positions of the chosen sources are now receiving increased emphasis.

Acknowledgement

We are indebted to the efforts of Radio Science Support Group at the Goldstone DSN complex and to the competent assistance of the personnel at Deep Space Stations 13, 14, 42, 43, 62, and 63. We would also like to thank the Station Directors at these stations for supporting our program, namely E. Jackson (DSS 13), C. Koscielski (DSS 14), T. Reid (DSS 42, 43), J. Urech (DSS 62), and J. Fernandez (DSS 63).

References

1. Kellermann, K. I., "Intercontinental Radio Astronomy," *Scientific American*, 226, 2, pp. 72-83, 1972.
2. Rogers, A. E. E., et al., "Extragalactic Radio Sources: Accurate Positions from Very-Long-Baseline Observations," *Ap. J.*, 186, 1973.
3. Clark, T. A., et al., "Radio Source Positions from Very-Long-Baseline Interferometry Observations," *A.J.*, Vol. 81, No. 8, 1976.
4. Mulhall, B. D. L., "DSN VLBI System Status and Plans," *DSN Progress Report* 42-46, July-August, 1978.
5. Shapiro, I. I., et al., "Transcontinental Baselines and the Rotation of the Earth Measured by Radio Interferometry," *Science*, 186, pp. 920-922, 1974.
6. Fanselow, J. L., et al., "The Goldstone Interferometer for Earth Physics," *DSN Technical Report* 32-1526, Vol. V, pp. 45-57, 1971.
7. Shapiro, I. I., and C. A. Knight, "Geophysical Applications of Long-Baseline Radio Interferometry," *Earthquake Displacement Fields and Rotation of the Earth*, L. Manshina et al., Eds., Reidel Pub. Co., pp. 284-301, 1970.
8. Brunn, D. L., et al., "VLBI Spacecraft Tracking System Demonstration, Part I: Design & Planning," *DSN Progress Report* 42-45, May-June, 1978.

9. Slade, M. A., et al., "ALSEP-Quasar Differential VLBI," *The Moon*, 17, pp. 133-147, 1977.
10. Ong, K. M., et al., "A Demonstration of a Transportable Radio Interferometric Surveying System With 3-cm Accuracy on a 307-m Base Line," *JGR*, Vol. 81, No. 20, pp. 3587-3593, 1976.
11. MacDoran, P. F., "Radio Interferometry for International Study of the Earthquake Mechanism," *Acta Astronautica*, Vol. 1, pp. 1427-1444, 1974.
12. Thomas, J. B., "An Analysis of Long Baseline Radio Interferometry," *JPL Technical Report 32-1526*, Vol. VII.
13. Cook, A. H., *Celestial Masers*, Cambridge University Press, 1977.
14. Clark, T. A., et al., "An Unusually Strong Radio Outburst in ALGOL-VLBI Observations," *Ap. J.*, 206, pp. L107-L111, 1976.
15. Kellermann, K. I., et al., "The Small Radio Source at the Galactic Center," *Ap. J.*, 214, L61-L62, 1977.
16. Wittels, J. J., et al., "Fine Structure of 25 Extragalactic Radio Sources," *Ap. J.*, 196, pp. 13-39, 1975.
17. Disney, M. J., and Veron, P., "BL Lacertae Objects," *Sci. Amer.*, 237, No. 2, 1977.
18. Clark, B. G., "The NRAO Tape-Recorder Interferometer System," *Proceedings of the IEEE*, Vol. 61, No. 9, pp. 1242-1248, 1973.

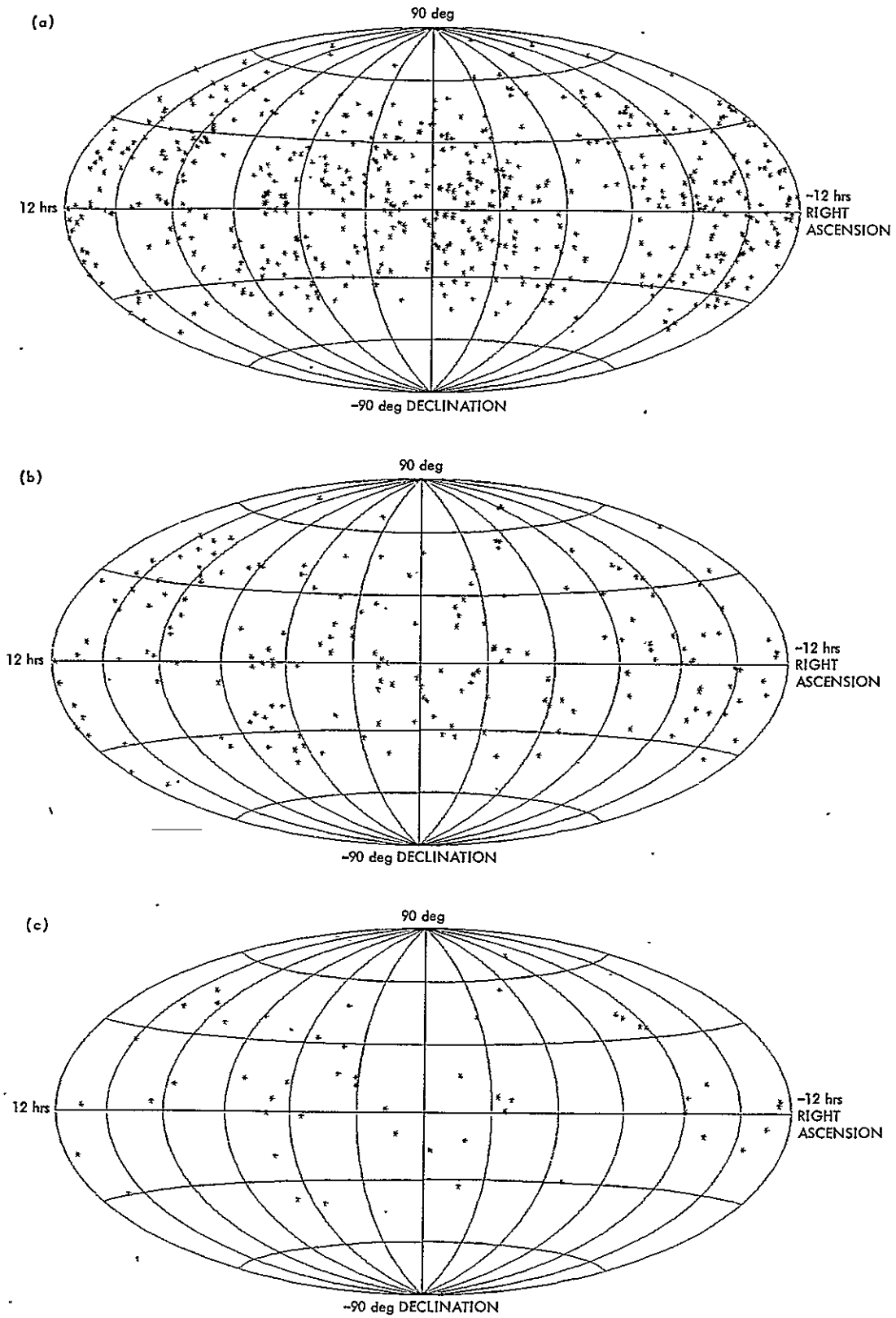


Fig. 1. Sky distribution of VLBI sources: (a) 564 sources ≥ 0.1 Jansky, (b) 184 sources ≥ 0.5 Jansky, (c) 50 sources ≥ 1.0 Jansky

ORIGINAL PAGE IS
OF POOR QUALITY

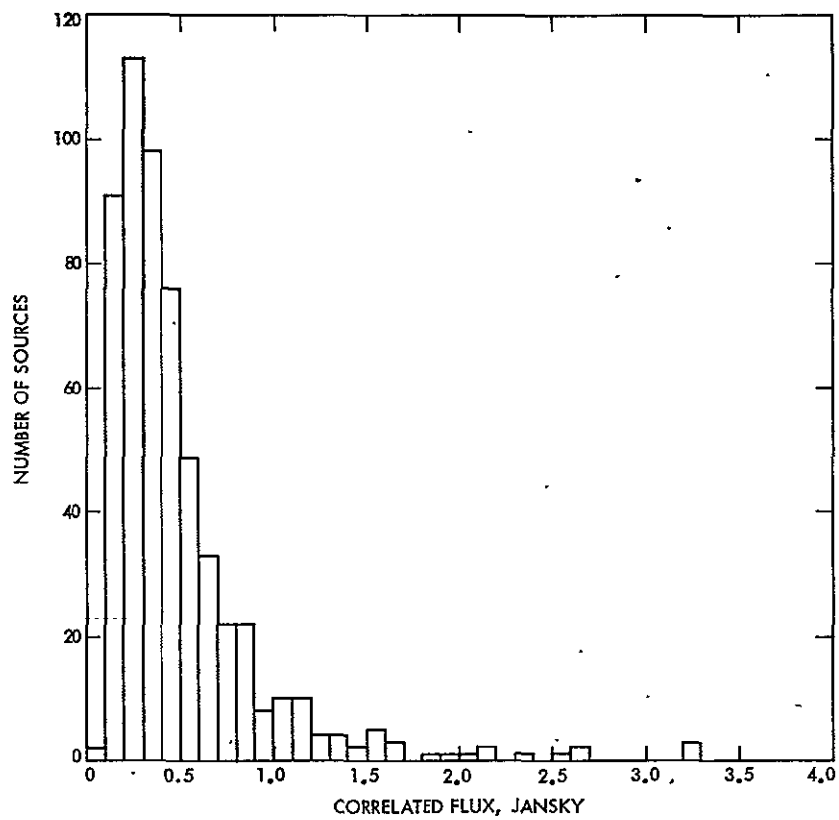


Fig. 2. Histogram of number of VLBI sources versus correlated flux

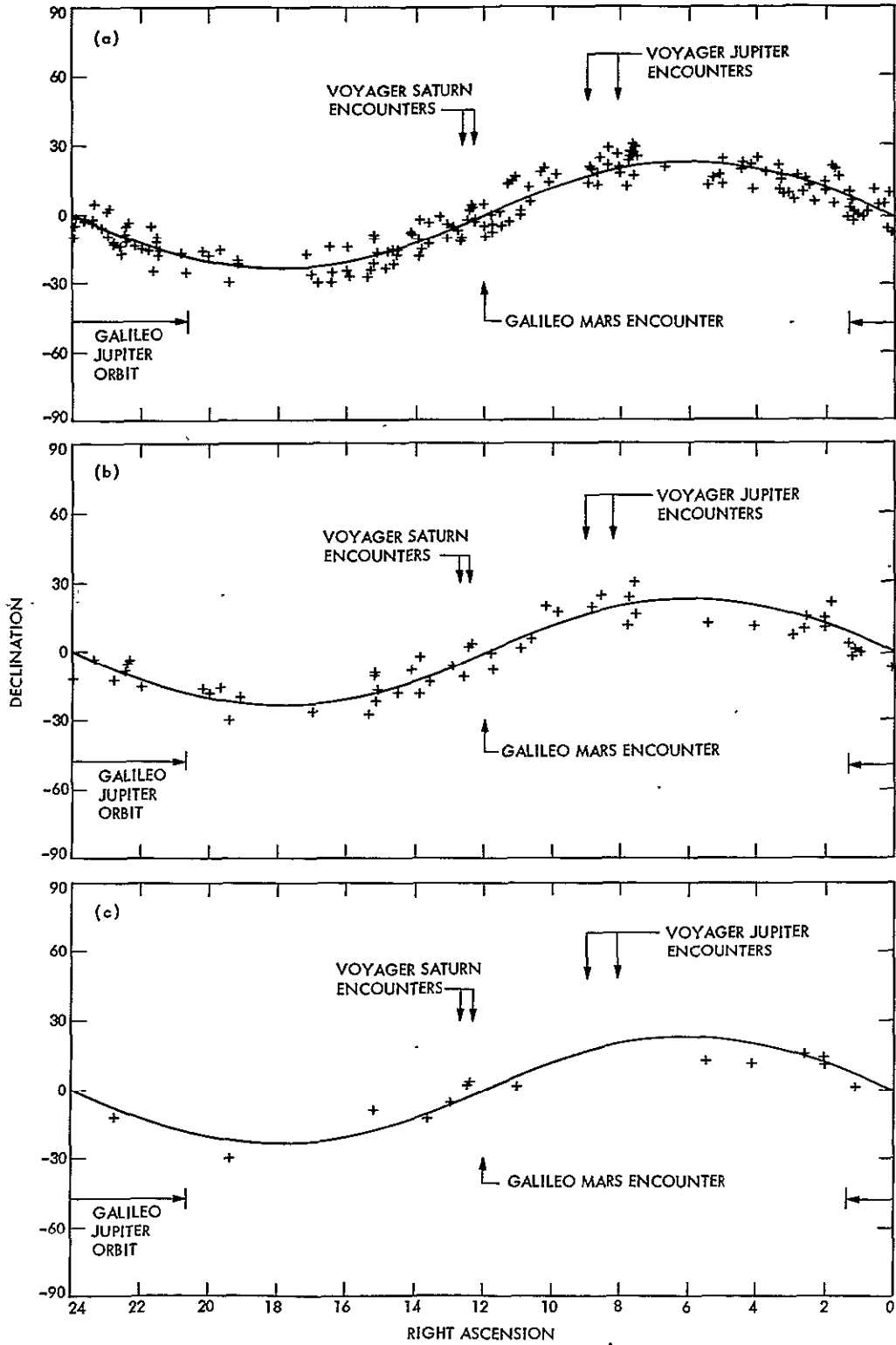


Fig. 3. VLBI sources within $\pm 10^\circ$ of ecliptic: (a) 166 sources ≥ 0.1 Jansky, (b) 51 sources ≥ 0.5 Jansky, (c) 14 sources ≥ 1.0 Jansky

ORIGINAL PAGE IS
OF POOR QUALITY

JPL 2^{20} Channel 300 MHz Bandwidth Digital Spectrum Analyzer

G. A. Morris, Jr., and H. C. Wilck
Communications Systems Research Section

A million (2^{20}) channel, 300 MHz bandwidth, digital spectrum analyzer is being constructed at the Jet Propulsion Laboratory. The design, fabrication, and maintenance philosophy of the modular, pipelined, Fast Fourier Transform (FFT) hardware are described. The spectrum analyzer will be used to examine the region from 1.4 GHz to 26 GHz for Radio Frequency Interference (RFI) which may be harmful to present and future tracking missions of the Deep Space Network. The design will have application to the Search for Extraterrestrial Intelligence (SETI) signals and radio science phenomena.

I. Introduction

A million channel digital spectrum analyzer with 300 MHz of bandwidth is under construction at the Jet Propulsion Laboratory. The 300 MHz bandwidth was chosen to take advantage of a 300 MHz bandwidth K-band traveling wave maser which is used with parametric up-converters to cover the frequency range from 1.4 GHz to 26 GHz. The purpose of the spectrum analyzer is to detect and identify radio frequency interference which may be harmful to present and future spacecraft tracking missions of the Deep Space Network.

The block diagram of the spectrum analyzer is shown in Fig. 1. The RF system consists of an antenna, parametric

up-converter, maser, and receiver with 300 MHz bandwidth IF output. An analog filter bank is used to separate the 300 MHz into 32 complex channels of 10 MHz bandwidth each. A pipelined, decimation in frequency FFT is used to process two of these 10 MHz channels simultaneously. The power spectrum is obtained by squaring the real and imaginary parts of the complex spectrum. The power spectrum is accumulated for a number of spectra to reduce the data bandwidth to a manageable value for input to a general purpose computer.

An extensive computer simulation was performed to determine the optimum hardware implementation to support the 60 dB dynamic range required. As a result of this

simulation, the hardware is implemented using 8 bit A/D converters, 12 bit memories in the first four stages, 16 bit memories in the remaining 11 stages, and 16 bit, fixed point, hard scaled calculations in all stages.

II. Analog Filter Bank

The bank of analog filters, shown in Fig. 2, is used to break the 300 MHz total bandwidth into 32 channels of 10 MHz bandwidth each. The input IF signal is distributed to the 32 complex mixers together with the output from a comb generator. This comb generator supplies the 32 local oscillator frequencies separated by 10 MHz. The complex mixer is made of two mixers and a 90° phase shifter between the local oscillator input and one of the mixers. The in-phase (real) and quadrature (imaginary) outputs of the mixer each pass through a 5 MHz low pass filter to an 8 bit A/D converter. These 10 MHz A/D converters are now readily available at relatively low cost because of their use in digital conversion of TV signals.

The low pass filters are 3 dB down at the band edge, resulting in aliasing between adjacent 10 MHz channels. This aliasing is compensated for by a postprocessing algorithm in the general purpose computer.

III. FFT Block Diagram

The FFT, shown in Fig. 3, consists of 15 pipelined stages (Ref. 1), each composed of a memory unit and a "butterfly" arithmetic unit. Only three types of modules are used in the entire FFT. The memory modules used for the first four stages have a maximum capacity of 16K complex words of 12 bits. The other 11 memory modules have a maximum capacity of 1024 complex words of 16 bits. The same 16 bit arithmetic module type is used in all stages.

The memory modules are programmed with a dual-in-line header to provide the appropriate delay and trig coefficients for each stage in the pipeline.

The input to the FFT uses the "Biplex" method (Ref. 2) to simultaneously process two independent 10 MHz channels in the pipelined architecture FFT. This method results in the full-time utilization of all memory and arithmetic elements. The complete spectrum analyzer contains 16 of these dual 15-stage pipelined FFT's.

IV. Memory Units

A block diagram which is common to both types of memory units is shown in Fig. 4. A memory unit is composed of two delay memories and multiplexers which allow straight through or crossed input-output connection as required in the pipelined algorithm. The memory unit also contains the trig coefficient generator. A delay equalization stage is incorporated to compensate for different timing delays in the two paths through the arithmetic unit.

The differences between the two types of memory units concern the size and type of delay memory and type of trig generator.

The first four memory units, called 16K max on the FFT block diagram (Fig. 3) use CCD memories with a capacity of 16K complex words of 12 bits. They are implemented by multiplexing four Fairchild CCD461A integrated circuits to obtain 10 MHz bandwidth. The remaining 11 units, called 1K max, use random access memories (Intel 2125AL) with a capacity of 1024 words of 16-bits.

The trig generator in the first four stages uses differences between successive coefficients, stored in ROM, to calculate the coefficients. This technique is usable because the decimation in frequency algorithm requires trig coefficients in the order of increasing angle. Storing differences rather than coefficients results in smaller ROM size and reduced total integrated circuit count. The trig generator in the remaining 11 stages actually stores the coefficients in ROM.

The trig coefficients used are always negative numbers so that -1 is included in the 2's complement number field. Appropriate sign changes are incorporated in the arithmetic unit to allow this convention.

V. Arithmetic Unit

The FFT radix 2 butterfly arithmetic unit is shown in Fig. 5. The complex adder/subtractor butterfly is placed in front of the complex multiplier in the decimation in frequency algorithm. The adder/subtractor operates on 16 bits of input data to deliver 17 bits of output. The output is scaled and rounded to retain the 16 most significant bits. The adder is implemented with the 74S283 and the subtractor with the 74S381.

The complex multiplier is composed of four real multipliers followed by an adder (74S283) and subtractor (74S381) to combine the partial products. The real multipliers are imple-

mented with the TRW MPY-16A. Two of these multipliers are connected in parallel and multiplexed to obtain a 10 MHz multiply rate. This is simple because of the input and output registers contained within the MPY-16A. The complete complex multiplier contains eight of the MPY-16A's. A fractional multiply is performed, and the 16 most significant bits are retained. The internal circuitry of the MPY-16A is used to round the result.

VI. Fabrication

A dual 32K point FFT prototype is now under construction at JPL. The prototype modules are constructed on wire wrap boards approximately 15 by 35 cm.

VII. Maintenance Philosophy

Testers are being designed to completely exercise the logic of the memory and arithmetic units of the FFT. These testers are used in manufacturing and depot level maintenance.

In the field, digital test signals, instead of the A/D converter outputs, can be injected into the FFT. The output of any module can then be compared to the expected output which is obtained from the general purpose computer. The failed unit is isolated by this technique and repaired by replacement. Failed modules are returned to a depot for repair. Since there are only three module types in the FFT, only a small inventory of spares is required. All diagnostic tests are conducted at full clock rate.

References

1. Rabiner, L. R., and Gold, B., *Theory and Application of Digital Signal Processing*, Prentice Hall, Inc., New Jersey, 1975, pp. 602-609.
2. Emerson, R. F., "Biplex Pipelined FFT", in *The Deep Space Network Progress Report 42-34*, Jet Propulsion Laboratory, Pasadena, California, 1976, pp. 54-59.

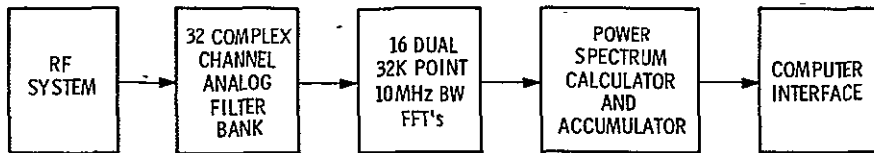


Fig. 1. Spectrum analyzer block diagram

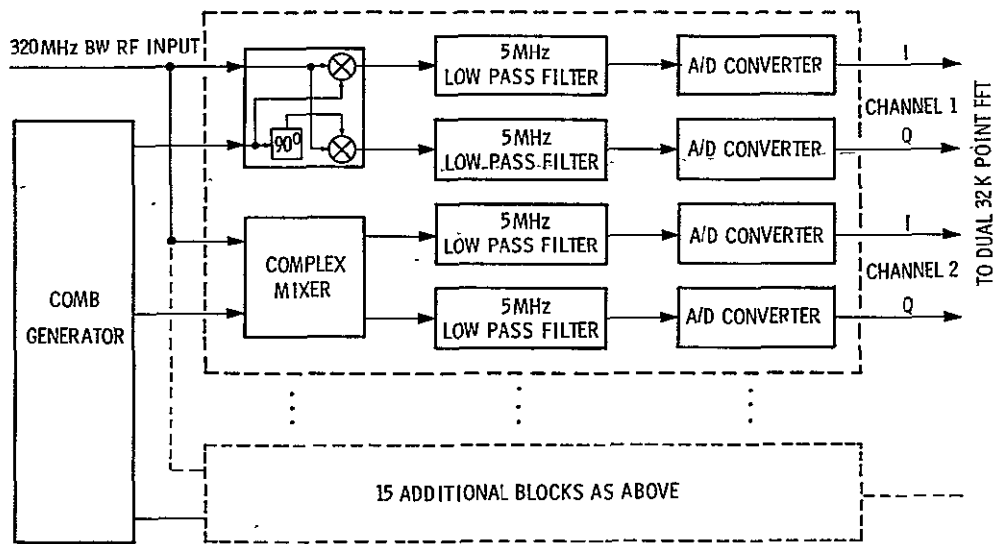


Fig. 2. Analog filter bank

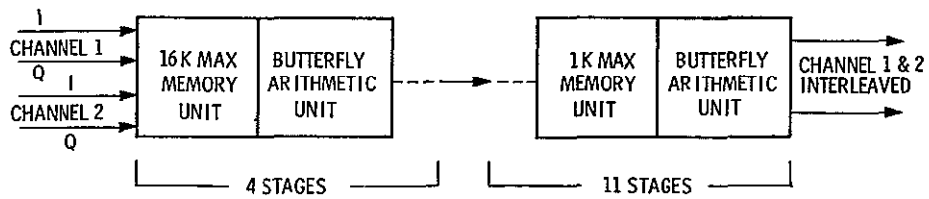


Fig. 3. FFT block diagram

ORIGINAL PAGE IS
OF POOR QUALITY

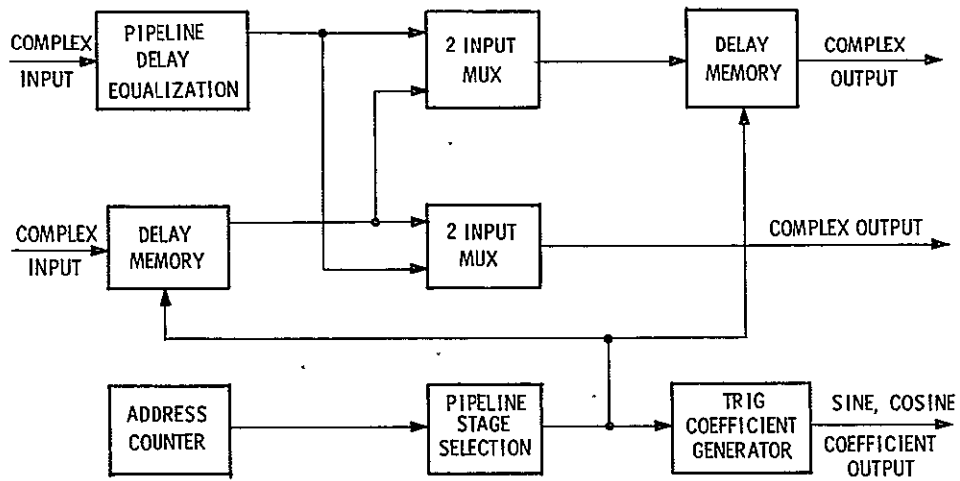


Fig. 4. Butterfly memory unit

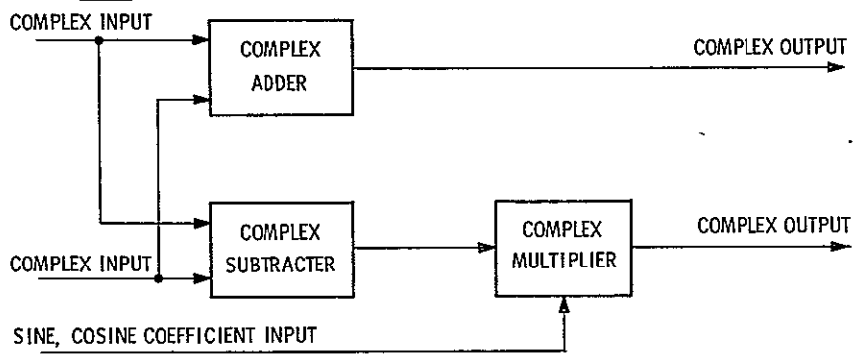


Fig. 5. Butterfly arithmetic unit

D16-69
65-12A

N78-32147

Use of A Priori Statistics to Minimize Acquisition Time for RFI Immune Spread Spectrum Systems¹

J. K. Holmes and K. T. Woo
Communications Systems Research Section

A theory is given which allows one to obtain the optimum acquisition sweep strategy of a PN code despreaders when the a priori probability density function is not uniform. This theory has application to psuedo noise spread spectrum systems which could be utilized in the DSN to combat Radio Frequency Interference (RFI). In a sample case, when the a priori probability density function is Gaussian, the acquisition time is reduced by about 41% compared to a "uniform sweep" approach.

I. Introduction

The acquisition circuitry of a desreader (a PN code acquisition and tracking system) is commonly designed so that complete passes are made across the code range uncertainty, as shown in Fig. 1a, during the initial search for the code epoch. This search, which is commonly implemented by retarding one half a chip at a time, then integrating and comparing to a threshold (Fig. 2), continues until the signal is acquired. This scheme is efficient when the a priori location of the signal in the uncertainty region has a uniform probability density function. However, when the a priori density function is peaked, it is more likely to find the signal in the peaked region than elsewhere, so the full sweep approach may not be the best one.

This article is concerned with a method that allows one to determine the optimum sweep pattern to minimize the acquisition time, while achieving a required probability of signal detection, for a given a priori probability density of the signal location. The calculation is carried out for a Gaussian a priori signal location probability density function as illustrated in Fig. 1b. However, the approach is general so that it can be applied to any given a priori signal location probability density function.

The basis of this method relies on the fact that any meaningful statistics (Ref. 1, for example) of acquisition time, which is the time required to search the code until acquisition, depends directly upon the number of chips (code symbols) to be searched. Therefore searching where there is the greatest likelihood that the signal will be found first reduces the total number of positions to be searched.

¹Portions of this work were performed for the TDRSS Project at TRW Systems.

II. Probability of Detection After N Sweeps

Consider a symmetric search centered at the mean of a symmetric, unimodal, a priori probability density function as shown in Fig. 1c for the case of $N=3$ sweeps. Denote Q_N as the probability of acquiring at the end of N sweeps. Typically Q_N would be 0.9 or 0.5, for example. Let $L_1, L_2, L_3, \dots, L_N$ denote the lengths (in number of cells) of the code range uncertainty to be searched during the N sweeps, and assume that $L_N \geq L_{N-1} \geq \dots \geq L_1$. Let $p(x)$ be the a priori probability density of the location of the signal. Further, let S_i denote the event that the signal is not detected in any one of the first i sweeps over regions with lengths L_1, L_2, \dots, L_i . Also, we shall use the notation S_0 to denote the event that the signal is not detected with zero sweeps, which is of course a sure event. It is clear that the conditional probability density of the signal location x , given that no sweep has yet been made, is equal simply to the a priori density $p(x)$, i.e.,

$$p(x|S_0) = p(x) \quad (1)$$

This density is illustrated in Fig. 3a. Suppose no signal is detected during the first sweep over L_1 , i.e., suppose the event S_1 has occurred. The conditional density $p(x|S_1)$ is equal to, by use of Baye's rule,

$$p(x|S_1) = \frac{p(S_1|x)p(x)}{P(S_1)} \quad (2)$$

In (2) the conditional (or a posteriori) probability density $p(S_1|x)$, is clearly given by

$$p(S_1|x) = \begin{cases} 1 - P_d & \text{if } x \in L_1 \\ 1 & \text{if } x \notin L_1 \end{cases} \quad (3)$$

where P_d is the probability of detection given the signal is there. The notations $x \in L_1$ and $x \notin L_1$ denote the fact that the location of the signal is within the set L_1 or not in L_1 , and $P(S_1)$ is the probability of the event S_1 :

$$P(S_1) = 1 - P_d P(L_1) \quad (4)$$

where $P(L_1)$ denotes the probability that the signal location x is within the set L_1 :

$$P(L_1) = \int_{-L_1/2}^{L_1/2} p(x) dx \quad (5)$$

Substituting (3), (4) into (2) we thus have

$$p(x|S_1) = \begin{cases} \frac{(1 - P_d)p(x)}{1 - P_d P(L_1)} & \text{if } x \in L_1 \\ \frac{P(x)}{1 - P_d P(L_1)} & \text{if } x \notin L_1 \end{cases} \quad (6)$$

This conditional density is illustrated in Fig. 3b. It is easy to show that

$$\int_{-\infty}^{\infty} P(x|S_1) dx = \frac{(1 - P_d)P(L_1)}{1 - P_d P(L_1)} + \frac{1 - P(L_1)}{1 - P_d P(L_1)} = 1 \quad (7)$$

The joint probability density of x and the event S_1 is thus given by (from Eqs. 2 and 6):

$$p(x, S_1) = p(x|S_1)P(S_1) = \begin{cases} (1 - P_d)p(x) & \text{if } x \in L_1 \\ p(x) & \text{if } x \notin L_1 \end{cases} \quad (8)$$

since $P(S_1) = 1 - P_d P(L_1)$. The joint probability of S_1 and $x \in L_1$ is given by

$$P(L_1, S_1) = \int_{-L_1/2}^{L_1/2} p(x, S_1) dx = (1 - P_d)P(L_1) \quad (9)$$

Since $L_2 \geq L_1$, the joint probability of S_1 and $x \in (L_2 - L_1)$ is given by (from Eq. 8)

$$\begin{aligned} p(L_2 - L_1, S_1) &= \int_{-L_2/2}^{-L_1/2} P(x, S_1) dx + \int_{L_1/2}^{L_2/2} P(x, S_1) dx \\ &= P(L_2 - L_1) = P(L_2) - P(L_1) \end{aligned} \quad (10)$$

Further, let P_i , $i = 1, 2, \dots, N$ denote, respectively, the probabilities that the signal is acquired during the i^{th} sweep, but not in the first, second, \dots , $(i-1)^{\text{th}}$ sweeps. If we can compute these P_i 's, then Q_N is clearly equal to the sum

$$Q_N = P_1 + P_2 + P_3 + \dots + P_N \quad (11)$$

It is clear that the probability of acquiring in the first sweep is given by

$$P_1 = P_d P(L_1) \quad (12)$$

The probability P_2 by definition, then, is equal to the joint probability

$$\begin{aligned} P_2 &= \text{Prob [acq. in second sweep, fail to acq. in first sweep]} \\ &= P_d P(L_2 - L_1, S_1) + P_d P(L_1, S_1) \\ &= P_d [P(L_2) - P(L_1)] + P_d (1 - P_d) P(L_1) \end{aligned} \quad (13)$$

In computing (13) we have used Eqs. (9) and (10). Following identical arguments one obtains the joint probability density

$$p(x, S_2) = \begin{cases} (1 - P_d)^2 p(x) & \text{if } x \in L_1 \\ (1 - P_d) P(x) & \text{if } x \in (L_2 - L_1) \\ p(x) & \text{if } x \notin L_2 \end{cases} \quad (14)$$

It is then easy to compute the a posteriori probability density function after two sweeps:

$$p(x|S_2) = \begin{cases} \frac{(1 - P_d)^2 p(x)}{P(S_2)} & x \in L_1 \\ \frac{(1 - P_d) p(x)}{P(S_2)} & x \notin L_1, x \in L_2 \\ \frac{p(x)}{P(S_2)} & x \notin L_2 \end{cases} \quad (15)$$

This density function is shown in Fig. 3c. From (14) one obtains, for $L_3 \geq L_2 \geq L_1$,

$$\begin{aligned} P_3 &= P_d P(L_3 - L_2, S_2) + P_d P(L_2 - L_1, S_2) + P_d P(L_1, S_2) \\ &= P_d [P(L_3) - P(L_2)] + P_d (1 - P_d) [P(L_2) - P(L_1)] \\ &\quad + P_d (1 - P_d)^2 P(L_1) \end{aligned} \quad (16)$$

In general, P_i can be written for $i = 1, 2, \dots, N$ as.

$$P_i = P_d \sum_{n=1}^i (1 - P_d)^{i-n} [P(L_n) - P(L_{n-1})] \quad (17)$$

with $P(L_0) \equiv 0$. When (17) is substituted into (11) we obtain, after some simple algebra:

$$Q_N = \sum_{i=1}^N P_i = P_d (1 - P_d)^N \sum_{k=1}^N \frac{P(L_k)}{(1 - P_d)^k} \quad (18)$$

The fact that we can write P_i in the form of Eq. (17) is intuitively clear. We can argue through the case of P_3 , as given in (16). The region of search during the third sweep can be divided into three nonoverlapping regions = $L_3 - L_2$, $L_2 - L_1$, and L_1 . By the time the third sweep is initiated, the region L_1 has already been searched twice. Hence the joint probability that signal is detected in this region during the third sweep but not during the first two sweeps is $P_d (1 - P_d)^2 P(L_1)$. Similarly, the probability that signal is detected in the region $L_2 - L_1$ during the third sweep, but not during the first two sweeps, is $P_d (1 - P_d) [P(L_2) - P(L_1)]$, since this region has only been searched once before the initiation of the third sweep. The region $L_3 - L_2$ has not yet been searched, and thus the probability of detecting the signal in this region is simply $P_d [P(L_3) - P(L_2)]$. P_3 is the probability of detecting the signal in any one of these three nonoverlapping regions during the third sweep, and is thus equal to the sum of these three terms, which is precisely the result of (15).

III. Optimum Symmetric Search Strategy

Suppose we design a search algorithm with search lengths L_1, L_2, \dots, L_N in the first N sweeps, and suppose the resulting probability of signal acquisition in these N sweeps is Q_N , which is computed in Section II as a function of the a priori probability density of the signal location, the number of sweeps N , and the search lengths. Denote the acquisition time that is required for the probability of signal acquisition to reach Q_N by T_{Q_N} . For example, $T_{0.9}$ is the time required to arrive at a Q_N of 0.9. The basis of the following optimization procedure is that, regardless the actual value of Q_N , the acquisition time T_{Q_N} is proportional to the number of chips searched, which is proportional to the total search sweep length

$$\sum_{i=1}^N L_i$$

Therefore our problem becomes: Determine the optimum search lengths L_1, L_2, \dots, L_N so that Q_N equals the desired acquisition probability and

$$L_T = \sum_{i=1}^N L_i$$

is minimized, thereby minimizing our acquisition time. Our method of solution is to use the LaGrange Multiplier method. Let

$$F = P_d \sum_{k=1}^N P(L_k)(1 - P_d)^{N-k} - \lambda \sum_{k=1}^N L_k \quad (19)$$

where λ is the unknown LaGrange Multiplier. Up to this point the theory is quite general, the only requirement being that the a priori density be unimodal and symmetric and that $P(L_k)$ be differentiable. Since this problem was motivated by the desire to improve acquisition time for the spread spectrum receivers and since a reasonable estimate for the a priori location of the signal is Gaussian, we shall illustrate the theory by assuming that the a priori density function is Gaussian. Now with this assumption we have

$$P(L_i) = 2 \int_0^{L_i/2} \frac{1}{\sqrt{2\pi}\sigma} \exp\left(-\frac{t^2}{2\sigma^2}\right) dt = \text{erf}\left(\frac{L_i}{2\sqrt{2}\sigma}\right) \quad (20)$$

Differentiating, we obtain

$$\frac{\partial F}{\partial L_i} = -\lambda + P_d(1 - P_d)^{N-i} \frac{\partial P(L_i)}{\partial L_i} = 0 \quad (21)$$

Since

$$\frac{\partial P(L_i)}{\partial L_i} = \frac{1}{\sqrt{2\pi}\sigma} \exp\left(-\frac{L_i^2}{8\sigma^2}\right) \quad (22)$$

we can solve (21) to obtain

$$l_i = 2\sqrt{2} \sqrt{\ln \left[\frac{1}{\lambda'(1 - P_d)^i} \right]} \quad (23)$$

where

$$\lambda' = \frac{\lambda\sqrt{2\pi}\sigma}{P_d(1 - P_d)^N} \quad (24)$$

$$l_i = \frac{L_i}{\sigma} \quad (25)$$

Substituting for l_i (the normalized chip search numbers) back into the equation for Q_N allows us in principle to solve for λ' :

$$Q_N = 2P_d \sum_{k=1}^N (1 - P_d)^{N-k} \times \int_0^{\sqrt{2}\sqrt{\ln [1/\lambda'(1 - P_d)^k]}} \frac{1}{\sqrt{2\pi}} \exp\left(-\frac{t^2}{2}\right) dt \quad (26)$$

This equation appears nearly impossible to solve analytically; however it can be solved simply on a digital computer by trial and error, picking λ' so that Q_N equals the desired probability. This must be done for all N ; of course in practice a few values of N will be sufficient. Before we discuss the results of the computer solutions let us consider the improvement over an unoptimized sweep.

IV. Uniform A Priori Density Sweep Strategy

The usual strategy for sweeping to obtain acquisition is to start at the end of the uncertainty region, where the range delay is minimum, and then retard the range in increments of typically one-half chip. By sweeping from the minimum delay to the maximum delay the chances of acquiring a multipath signal are diminished. If the probability of detection, given that the received code and the reference code are aligned, is given by P_d and if the a priori probability density function is uniformly distributed, then the cumulative probability of acquisition is as shown in Fig. 4. If, for example, a probability of 0.5 is chosen as the desired probability of acquisition, then the curve could be read off of the abscissa and the associated time, denoted by $T_{0.5}$, would be the time it takes to acquire with a probability of 0.5.

A measure of the improvement of the optimized scheme over the uniform sweep scheme can be measured as follows. Denote T_Q^U as the time to acquire with a probability of Q using the uniform sweep approach. Next, let T_Q^O denote the time to

acquire with the optimized sweep. Then the improvement factor of the optimized sweep over the uniform sweep is given by

$$r_Q = \frac{T_Q^U}{T_Q^O} \quad (27)$$

The acquisition time is then $T_Q^U r_Q^{-1} = T_Q^O$. Clearly $r_Q \geq 1$ since unity is achieved with the uniform sweep strategy, and therefore the method never increases acquisition time. Our result is for $Q = 0.5$ as a representative case.

V. Numerical Results

As discussed in Section III, to obtain the optimum sweep lengths we have to first solve for λ' from (26), from which the optimum sweep lengths are given, for $i = 1, 2, \dots, N$, by

$$L_i = 2\sqrt{2} \sigma \sqrt{\ln \frac{1}{\lambda'} - (i-1) \ln(1-P_d)} \quad (28)$$

As evident from (28), the solution of λ' must satisfy the condition:

$$\ln \frac{1}{\lambda'} - \ln(1-P_d) \geq 0 \quad (29)$$

in order for L_i to be meaningful. Thus it is convenient to define the left-hand side of (29) to be of the form

$$\ln \frac{1}{\lambda'} - \ln(1-P_d) \equiv e^x \quad (30)$$

so that instead of solving (26) for λ' we can solve for the root of the following equation:

$$f(x) = P_d \sum_{k=1}^N (1-P_d)^{N-k} \times \operatorname{erf} \sqrt{e^x - (k-1) \ln(1-P_d)} - Q_N \quad (31)$$

which can be obtained numerically by the Newton's iterative solution, computing successive iterations according to

$$x_{k+1} = x_k - \frac{f(x_k)}{f'(x_k)} \quad (32)$$

where the derivative of $f(x)$ can be evaluated from (31) to be

$$f'(x) = P_d \sum_{k=1}^N (1-P_d)^{N-k} \frac{e^{x - [e^x - (k-1) \ln(1-P_d)]}}{\sqrt{\pi [e^x - (k-1) \ln(1-P_d)]}} \quad (33)$$

Before we illustrate the procedure by numerical example a discussion on the choice of N is in order. First we note that in order for a given N to give finite optimum sweep lengths, N must satisfy

$$Q_N \leq P_d \sum_{k=1}^N (1-P_d)^{N-k} \quad (34)$$

since the right-hand side of (34) is the probability of signal acquisition with infinite sweep lengths (i.e., for the case $x = \infty$). Next, an upper bound on N can also be given by noting the fact that the smallest value of x is $-\infty$, so that N must satisfy, from (31),

$$Q_N \geq P_d \sum_{k=1}^N (1-P_d)^{N-k} \operatorname{erf} \sqrt{(k-1) \ln \frac{1}{1-P_d}} \quad (35)$$

Equations (34) and (35) give lower and upper bounds of N , for given values of P_d and Q_N , within which optimum solutions of sweep lengths are feasible. The following examples illustrate the results obtained by this optimum search technique as compared to the uniform search algorithm.

Example 1

Suppose $P_d = 0.25$ and the desired $Q_N = 0.5$. The admissible number of sweeps N for this case is 3 and 4. The sweep lengths in terms of σ (standard deviation of the signal location probability density) are shown in Table 1. Also shown in Table 1 is the ratio between the uniform search acquisition

time and the acquisition time using this optimum procedure. The search region in the uniform sweeps is assumed to be $\pm 3\sigma$. The four-sweep search gives an improvement ratio of 1.73 over the uniform sweep search algorithm, i.e., a reduction acquisition time of 41%.

Example 2

Suppose $P_d = 0.5$ and $Q_N = 0.9$. It is found that only $N = 4$ or $N = 5$ are admissible since solutions do not exist for all other N . Table 2 gives the sweep lengths and the corresponding improvement ratios over uniform searches.

As illustrated by these two examples the improvement factor of this optimum search strategy over the uniform search varies according to P_d , Q_N and N . Nevertheless, the improvement factor is always ≥ 1 .

VI. Conclusions

We have presented a method that can be used to optimize (minimize) the acquisition time for a PN-type spread spectrum system when the a priori probability density function is not uniform. Specifically we have calculated, for an assumed a priori Gaussian density function, that, when the 0.5 probability acquisition-time was used as a measure, the acquisition time was reduced by 40% for a cell detection probability of 0.25 when three sweeps were used. For the same parameters and with four sweeps the acquisition time was reduced by 41%. When the acquisition time probability was set to 0.9 instead of 0.5 the reduction was 25% of the uniform sweep time.

This technique has application to the DSN if psuedo-noise spread spectrum systems are utilized to combat RFI.

References

1. J. K. Holmes and C. C. Chen, "Acquisition Time Performance of PN Spread-Spectrum Systems," *IEEE Trans. on Communications*, No. 8, Aug. 1977.
2. M. Holmes, Private Communication, Oct. 1977.
3. C. Gumacos "Analysis of an Optimum Sync Search Procedure," *IEEE Trans. on Communications*, pp. 89-99, March 1963.

Table 1. $P_d = 0.25, Q_N = 0.5$

	Opt search with 3 sweeps	Opt. search with 4 sweeps
L_i/σ	2.54	1.19
	2.96	1.93
	3.33	2.46
		2.89
Improvement ratio over uniform search	1.66	1.73

Table 2. $P_d = 0.5, Q_N = 0.9$

	Opt. search with 4 sweeps	Opt. search with 5 sweeps
L_i/σ	2.63	0.56
	3.53	2.42
	4.24	3.38
	4.85	4.12
		4.74
Improvement ratio over uniform search	1.34	1.34

ORIGINAL PAGE IS
OF POOR QUALITY

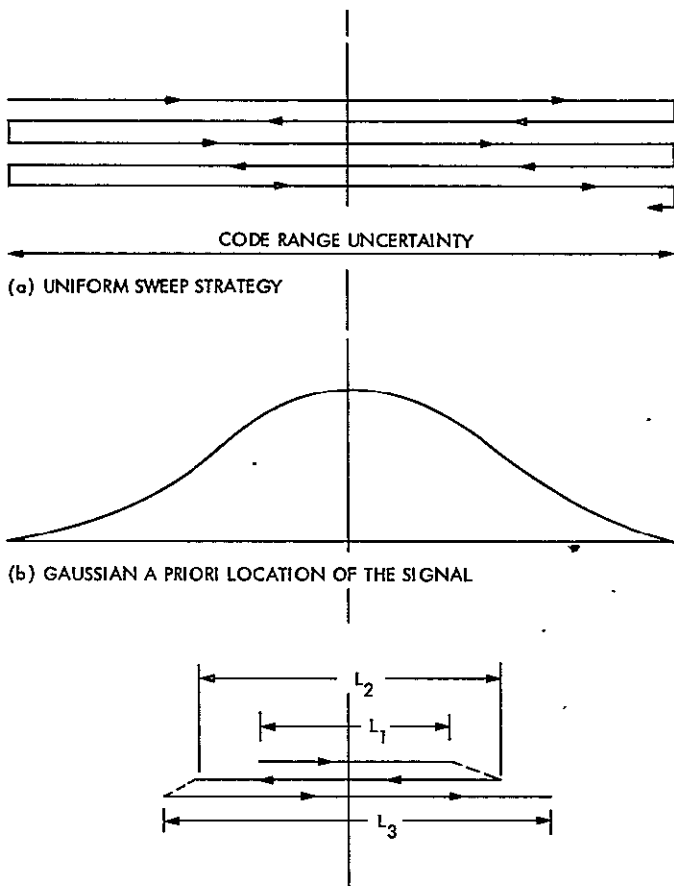


Fig. 1. A priori signal location and search strategies

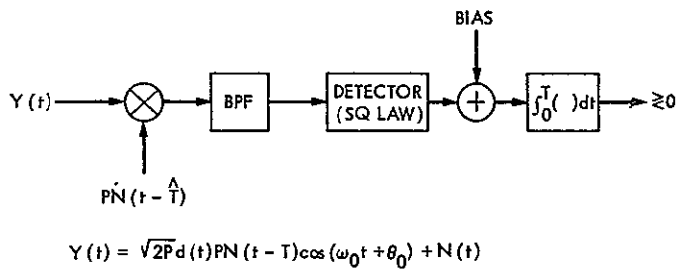


Fig. 2. Typical simplified fixed dwell time acquisition system

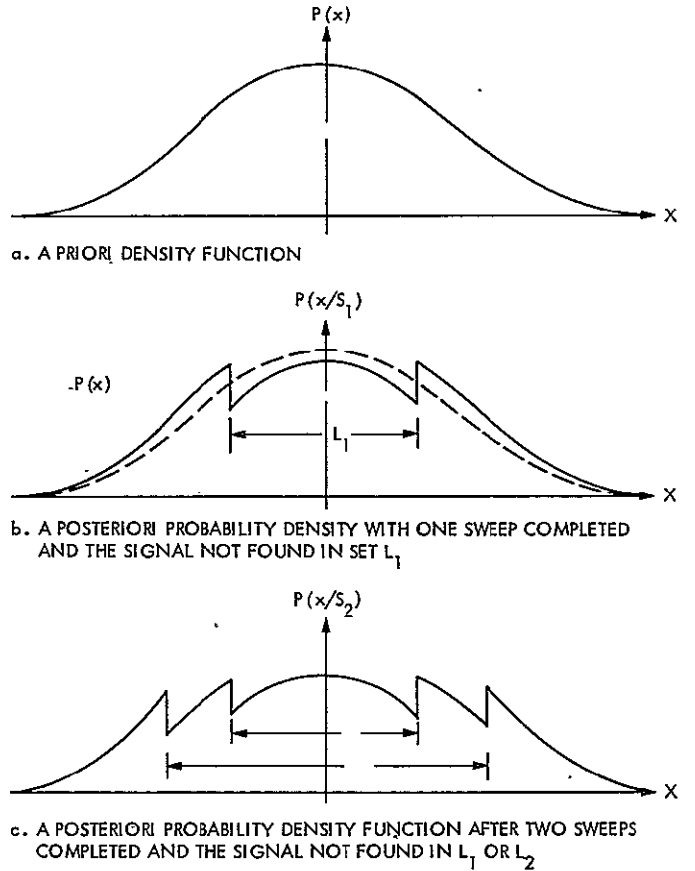


Fig. 3. Evolution of the a priori density function

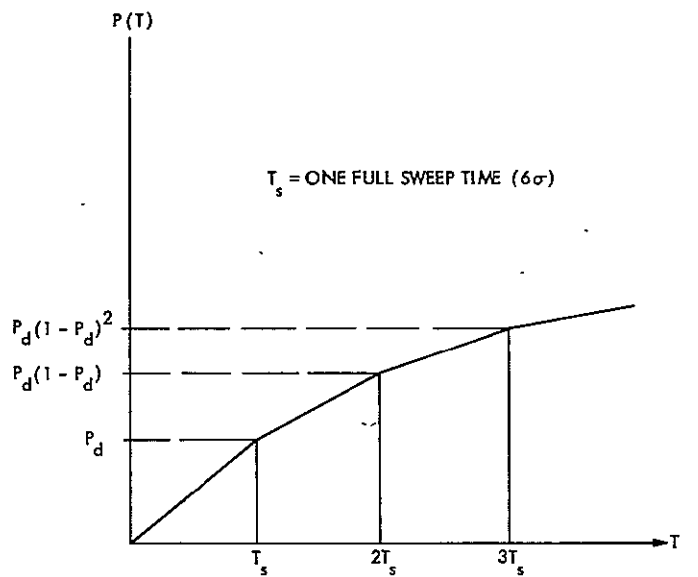


Fig. 4. Cumulative probability of acquiring in time T for the uniform sweep scheme

UNIBUS Monitor for PDP 11¹

M. D. Donner

Communications Systems Research Section

A UNIBUS Monitor has been designed and constructed to facilitate development of hardware interfaces with the PDP 11 minicomputer. The Monitor provides useful displays of UNIBUS conditions and provides the user with a flexible diagnostic tool. It can also serve as a simple display and data entry device, permitting extremely simple input/output for development software.

I. Introduction

A UNIBUS Monitor has been designed and constructed to facilitate development of hardware interfaces with the PDP 11 minicomputer (Figs. 1 and 2). The Monitor provides useful displays of UNIBUS conditions and provides the user with a flexible diagnostic tool. It can also serve as a simple display and data entry device, permitting extremely simple input/output (I/O) for development software. At this time the Monitor is being used with the DSN Planetary Radar System, which uses a PDP 11.

II. The Problem

While the PDP 11's UNIBUS system simplifies peripheral and I/O interfacing and handling, it also introduces a single point of failure which can bring down a whole system. If a peripheral or I/O device fails in a way that interferes with UNIBUS functioning, it is possible that the processor will be unable to execute the code. In a situation like this it would be

convenient to be able to view the UNIBUS status directly without having to probe all 56 UNIBUS signal lines individually. In a static situation this would be comparatively simple; simply hook an indicator light up to each signal line. Since the UNIBUS is a dynamic system involving various time-varying signals which typically change too fast for an engineer or technician to see, some capability must be added in the monitor to recognize and display this dynamic activity in a useful way.

III. The Solution

A. Single Address, Synchronous

In this mode (*MONITOR* switch – “OFF,” *SYNCHRO/I/O* switch – “SYNCHRO,” *SA/RANGE* switch – “SA”) the UNIBUS Monitor watches for bus transactions involving the bus address specified by the top row of octal lever wheel switches. If the *A* lines contain that address the monitor latches the *A* lines on the arrival of *MSYN*. If the *C* lines indicate a *DATO* or *DATOB* operation, the *D* lines are latched at the same time. If the operation is a *DATI* or *DATIP*, the *D* lines are latched on the arrival of *SSYN*.

¹UNIBUS and PDP are registered trademarks of the Digital Equipment Corporation.

B. Range, Synchronous

This mode is similar to mode A (*MONITOR* – “OFF,” *SYNCHRO/IO* – “SYNCHRO,” *SA/RANGE* – “RANGE”) except that instead of responding only to the address dialed into the *A* switches, the Monitor responds to all addresses less than or equal to the *A* switches and greater than or equal to the *D* switches.

C. Single Address, IO

In this mode (*MONITOR* – “OFF,” *SYNCHRO/IO* – “IO,” *SA/RANGE* – “SA”) the UNIBUS Monitor serves as a UNIBUS peripheral, responding as a peripheral or input/output device would. It responds to the address contained in the upper row of lever wheel switches. When the *A* lines contain the correct address and *MSYN* is asserted by the bus master, the UNIBUS Monitor latches down the *A* lines and responds with *SSYN*. On *DATO* or *DATOB* operations the Monitor latches down the *D* lines at the same time as the *A* lines. On *DATI* and *DATIP* operations the Monitor asserts the contents of the lower row of lever switches onto the *D* lines until *MSYN* is released. In *IO* mode the monitor observes the UNIBUS handshaking protocols according to Digital Equipment Corp. specifications.

D. Range, IO

This mode (*MONITOR* – “OFF,” *SYNCHRO/IO* – “IO,” *SA/RANGE* – “RANGE”) is essentially the same as Mode C except that the Monitor responds to the range of addresses between *A* and *D* inclusive. On *DATI* and *DATIP* instructions the contents of the lower row of switches are asserted onto the *D* lines as in Mode C. In this mode the lower address boundary and the returned data are the same, but this shouldn't cause any problem.

E. Monitor Mode

In this mode both the *D* and *A* latches are held enabled. No dynamic responses are made. All addresses are displayed for as long as they are present. This mode is useful for taking a look at the UNIBUS in static situations, such as when the processor is stalled.

F. Non-Modal Displays

All the other UNIBUS signals are displayed on LEDs directly on the front panel with no dynamic interactions with the bus. In addition, the *C* lines are decoded into the four bus transactions, *DATO*, *DATOB*, *DATI*, *DATIP*, and displayed. Also, the *MSYN*, *SSYN*, *SACK*, and *BUS GRANT* lines have pulse stretching one shots so that the signal and an “activity” indicator are both displayed. In the case of the *BUS GRANT* lines the one shot is triggered by the assertion of any grant line; there is only one activity indicator for the grant lines. One particular reason for activity indicators on the *GRANT* lines and on *SACK* is that should a UNIBUS device fail with its *BUS REQUEST* asserted and be incapable of responding to the *BUS GRANT*, the processor will attempt over and over to grant the request without success, timing out and starting over again each time. The *GRANT ACTIVITY* indicator will catch this kind of failure.

IV. Conclusion

After construction and testing the UNIBUS Monitor was taken out to DSS 14, where it was installed with the planetary radar equipment. In this application the Monitor soon proved its usefulness in analyzing UNIBUS communication performance.

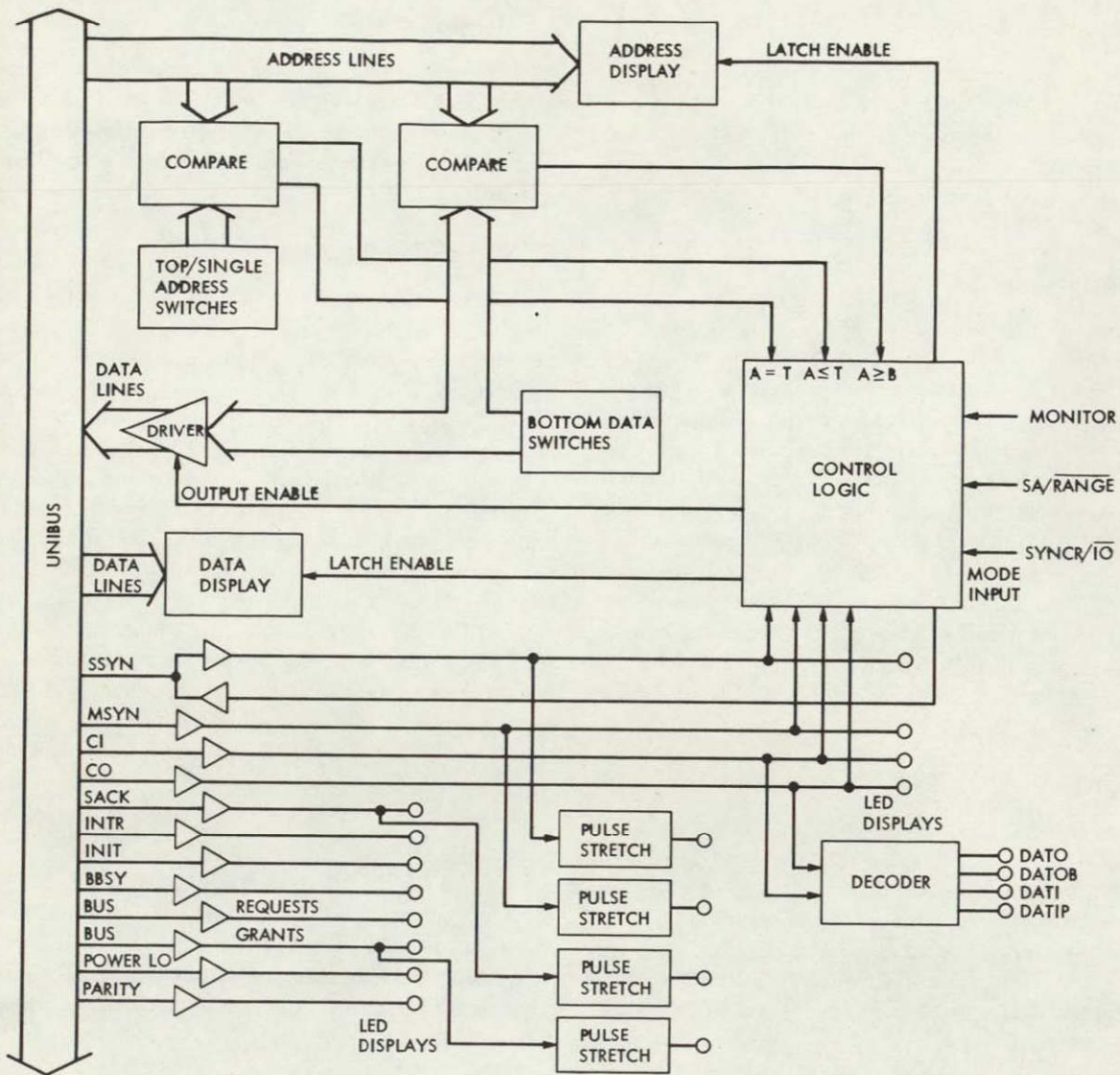


Fig. 1. UNIBUS Monitor block diagram

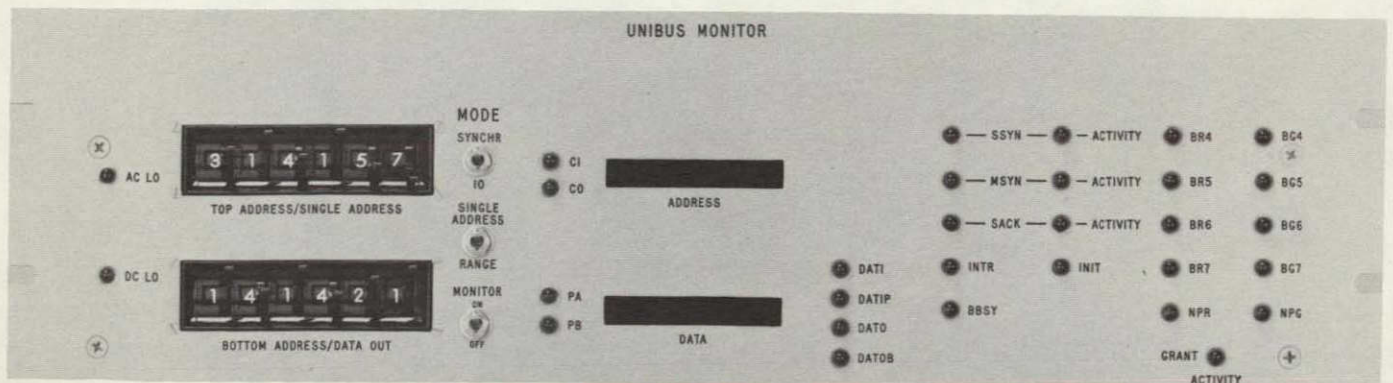


Fig. 2. UNIBUS Monitor panel

ORIGINAL PAGE IS
OF POOR QUALITY

D12-75
33-070

N78-32149

DSS 13 Antenna Subsystem Automation

H. Phillips, I. Crane, and P. Lipsius
DSN Engineering Section

Unattended station operation has been implemented at DSS 13, permitting full operational control from NOCC. Sensors have been installed in the mechanical subsystem to monitor critical functions. These are arranged to permit automated premission checkout of the subsystem, automated reaction to component failure, and identification of failed components under control of the antenna pointing computer. This monitoring installation will serve as a prototype for monitoring equipment to be installed throughout the DSN.

I. Introduction

Unattended station operation has been implemented at DSS 13, permitting full operational control from the Network Operations Control Center (NOCC). Sensors have been installed in the mechanical subsystem to monitor critical functions. These are arranged to permit automated premission checkout of the subsystem, automated reaction to component failure, and identification of failed components under control of the antenna pointing computer. This monitoring installation will serve as a prototype for monitoring equipment to be installed in the DSN.

II. Automated Premission Checkout

The function of a premission checkout is to assure that all of the antenna subsystem equipment required for tracking and for automated response to an equipment failure is functioning. The automated checkout, controlled by the Modcomp pointing computer, was planned to be carried out in the following steps:

- (1) Verify that the wind velocity on site is within acceptable limits.
- (2) Verify that the level in the servo hydraulic fluid reservoir is within the prescribed limits.
- (3) Start the servo high-pressure pumps and the filter circulating pumps and verify that these are operating.
- (4) Verify hydraulic pressure at the azimuth and elevation servo valves.
- (5) Start the gear drive lubrication pumps and verify lubrication pressure or flow.
- (6) Test the drive brakes as follows:
 - (a) Set in a zero rate command for each axis.
 - (b) Release the brakes for each axis, and verify that the brakes release.
 - (c) Reset the brakes for each and verify that they set.
- (7) Check the drive operation as follows:

- (a) Release the brakes and sound the horn. *
- (b) In low-speed mode, command a small rate in each axis.
- (c) Calculate $\Delta\theta/\Delta t$ for each axis over a small period and verify that the antenna is moving at the commanded rate.
- (d) Read the analog rate signal from the antenna and verify that it is within tolerance compared to the calculated $\Delta\theta/\Delta t$.
- (e) Command a zero rate and set the brakes.

III. Monitoring During Operations

Monitoring during operations is required to determine if the mechanical components are operating within normal parameters and to initiate, by computer control, defensive action to prevent a catastrophic failure. The sensing points

were chosen to isolate major potential failure points, and to provide the computer with the information necessary to initiate a defensive reaction when called for. The functions monitored and the action to be taken on a sensed failure are listed in Table 1. The actual sensed points are listed in Table 2.

IV. Present Status

All of the monitoring equipment has been installed on the antenna and is presently operational. The microcomputer for collecting data and transmitting operational data has been installed and is operational. A demonstration of remote operation controlled from NOCC has been conducted. Operational experience is now being developed to validate the checkout. Monitor and failure response rationale data are also being developed on the normal operating range of the various parameters prior to implementing the final monitoring software in the antenna controller.

Table 1. Monitoring during antenna operation

Parameter	Action on failure
Reservoir oil level change	
Slow leakage rate	Drive to stow
Large leakage rate	Stop pumps immediately
High-pressure pump and motor operation	
Motor current excessive	Shut off system
Pressure output excessive	Shut off system
Low pressure at servo valves	Shut off high-pressure pump and filter circulation pumps
Gear drive lubricant flow failure	Drive to stow, set brakes
System oil temperature excessive	Drive to stow, set brakes
Wind velocity excessive	Drive to stow, set brakes
Cable wrap-up limits	Command zero rate, set brakes
Tracking error excessive	Shift to low rate command in high-speed mode and drive to stow
DC power supplies failure (control room)	Automatic servo system shutdown if both power supplies fail
Remote DC power supply	Automatic servo system shutdown

Table 2. Sensor implementation

In control room	Clockwise cable wrapup limit
	Counterclockwise cable wrapup limit
	Azimuth 1 brake status
	Azimuth 2 brake status
	Elevation left brake status
	Elevation right brake status
	Azimuth high-speed mode select
	Elevation high-speed mode select
	Disable circuit status
	Power supply 1 status
	Power supply 2 status
	Azimuth prelimit status
	Elevation prelimit status
At antenna	Elevation low-speed servo valve pressure differential
	Elevation system pressure
	Elevation high-speed servo valve pressure differential
	Elevation high-speed system supply pressure
	Elevation low-speed system supply pressure
	Azimuth high-speed servo valve differential pressure
	Azimuth low-speed servo valve differential pressure
	Azimuth high-speed system supply pressure
	Azimuth low-speed system supply pressure
	Fluid level (hydraulic tank)
	Wind speed (southwest wind tower)
	Wind speed (southeast wind tower)
	Wind direction (southwest wind tower)
	Wind direction (southeast wind tower)
	Hydraulic oil temperature
	Lube oil pressure
	75-horsepower starter status
	125-horsepower starter status
	Pump flow 75 horsepower (left)
	Pump flow 75 horsepower (right)
Pump flow 125 horsepower (left)	
Pump flow 125 horsepower (right)	
Hydromech building 28 V DC power supply status	

FPLA Mechanization of Arithmetic Elements to Produce A + B or to Pass A Only

D. E. Wallis, H. Taylor, and A. L. Rubin
Communications Systems Research Section

This article describes a 4-bit and a 3-bit adder which can be implemented under special hardware restrictions. The chip to be used is Field-Programmable Logic Array (FPLA) with 12 input lines, 50 AND gates inside, and output through only 6 OR gates. The context in which it is being used requires an "enable" function which can suppress one of the two numbers to be added. The 3-bit enabled adder is compatible with lookahead-carry mechanizations using the 74S182. It will be used in the accumulator for the RFI project.

I. Discussion and Result

The 4-bit adder is pictured in Fig. 1. The point of interest is the reduction in the number of AND gates accomplished by sharing six Boolean terms between S_1 and C_2 . A sequence of these 4-bit adders to add two $4n$ -bit numbers in ripple-carry fashion would be rather slow, because each next adder would have to wait for the previous carry.

The 3-bit adder is pictured in Fig. 2. Sixteen of these will add two 48-bit numbers faster than twelve of the 4-bit adders. The increase in speed is achieved by a well known "look ahead" arrangement. Each 3-bit adder puts out a \bar{P} bit and a \bar{G} bit instead of a carry bit. The \bar{G} bit will have value 0 if and only if a carry will be generated. The \bar{P} bit will have value 0 if \bar{G} has value 1 and a carry would be propagated. Using the \bar{P} s and \bar{G} s from all the 3-bit adders at once, the whole arrangement can get the sum of two 48-bit numbers in only 5 gate-delay times.

The main point of interest in the 3-bit adder is the sharing of AND gates by way of the function F. This makes it possible to implement all the functions desired with the given chip.

The other point of interest is that F does not depend on C_0 . This means that F will find its final value during the time that C_0 is being computed in the lookahead network. Thus when C_0 arrives all the gates affected by C_0 will find their values in just 1 gate-delay time.

The practical problem was to mechanize a 48-bit digital integrator (or accumulator) whose memory could be read and cleared at the same time that a new datum d_i was added to begin a new integral. The memory type being used was not, itself, clearable. The form of the integrator is as shown in Fig. 3.

The available 74S381 4-bit arithmetic/logical unit (ALU) almost met the requirements. The 74S381 can be controlled so as either to add its two inputs (A and B), or to transmit zero output. The zero output clears the memory, as desired, but the time-coincident incoming datum d_i is lost and does not initialize the next summation.

What was required, then, was an ALU which could add two numbers A and B, or transmit one of them (called "pass A"). No such ALU was available commercially. It seemed, however,

C-2

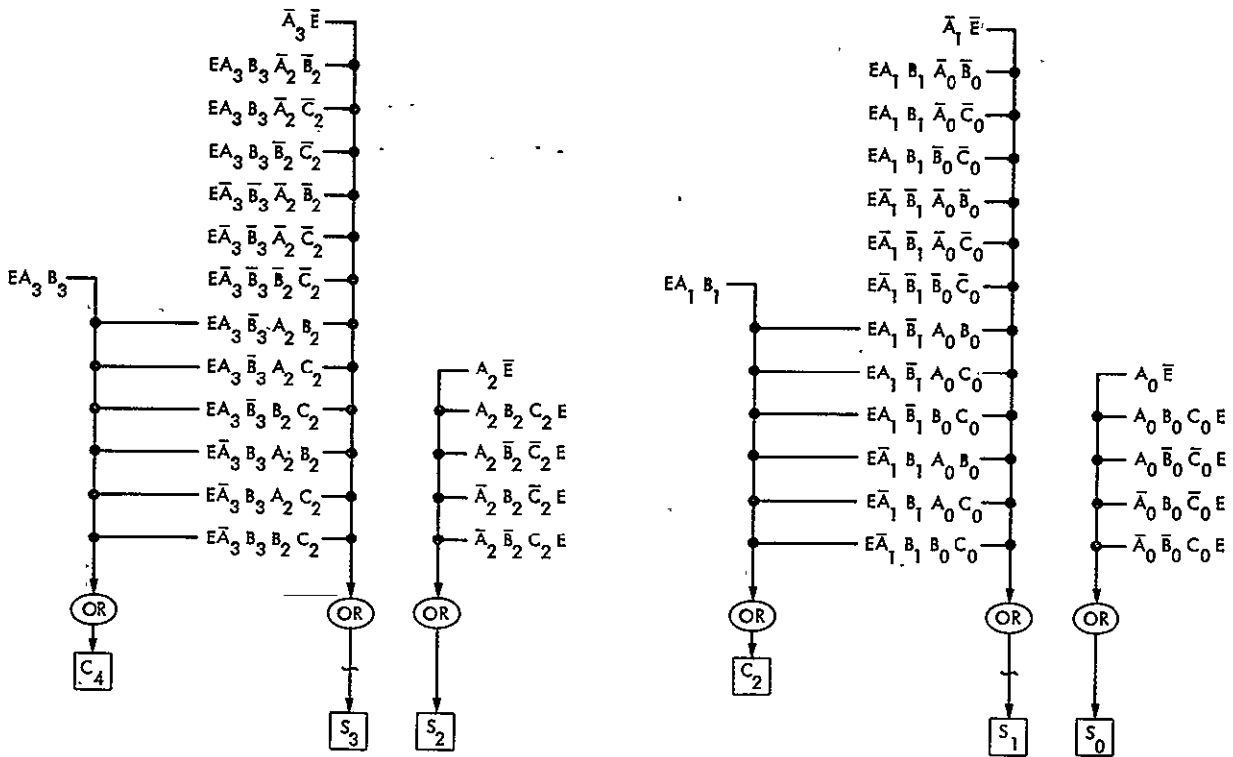


Fig. 1. 4-bit (dual 2-bit) adder, with enable

ORIGINAL PAGE IS
OF POOR QUALITY

that an acceptable ALU could be created by programming a field-programmable logic array (FPLA) such as the 74S330, whose package size and pinout were compatible with the 74S381.

The 74S330 has 50 AND gates, each of which may be programmed to AND any of 12 input variables using arbitrary assignments of which "rail" or true/false sense of each input variable would be effective on each AND gate. Further, any combination of the AND gate outputs can be ORed into any of six internal OR gates. Each OR gate is made available as an output from the 74S330, and each OR output can be programmed so as to invert its output, if desired.

The 48-bit adder logic was to be built on a circuit board having little room ("real estate") for extra components. It was, therefore, necessary to maximize the number of bits which could be added by each 74S330. Further, the adder had to be a "fast" adder, i.e., compatible with carry lookahead techniques, such as those based on the 74S182 lookahead generator. It soon became apparent that the availability of

only 50 AND gates in the FPLA was going to be a major limitation in the adder word-size or adder speed or both. Thus a combinatorial study was made in an attempt to obtain an optimal design for an adder based on the 50-gate FPLA.

First choice would have been a 4-bit adder with the \bar{P} , \bar{G} , and E functions. We think that is impossible although we do not know how to prove it.

The design chosen after several trials was the 3-bit adder of Fig. 4.

Arthur L. Rubin has obtained the following result. Subject to the requirements of the chip 74S330, a 3-bit adder with \bar{P} , \bar{G} , and E which makes no use of a tie around (such as the connection of the output F to other FPLA inputs, as seen in Fig. 2) from the output of the chip (and hence avoids the one extra gate delay) cannot be designed with fewer than 50 AND gates. Achieving the 3-bit adder of Fig. 4 on one chip makes the 48-bit adder as fast as possible.

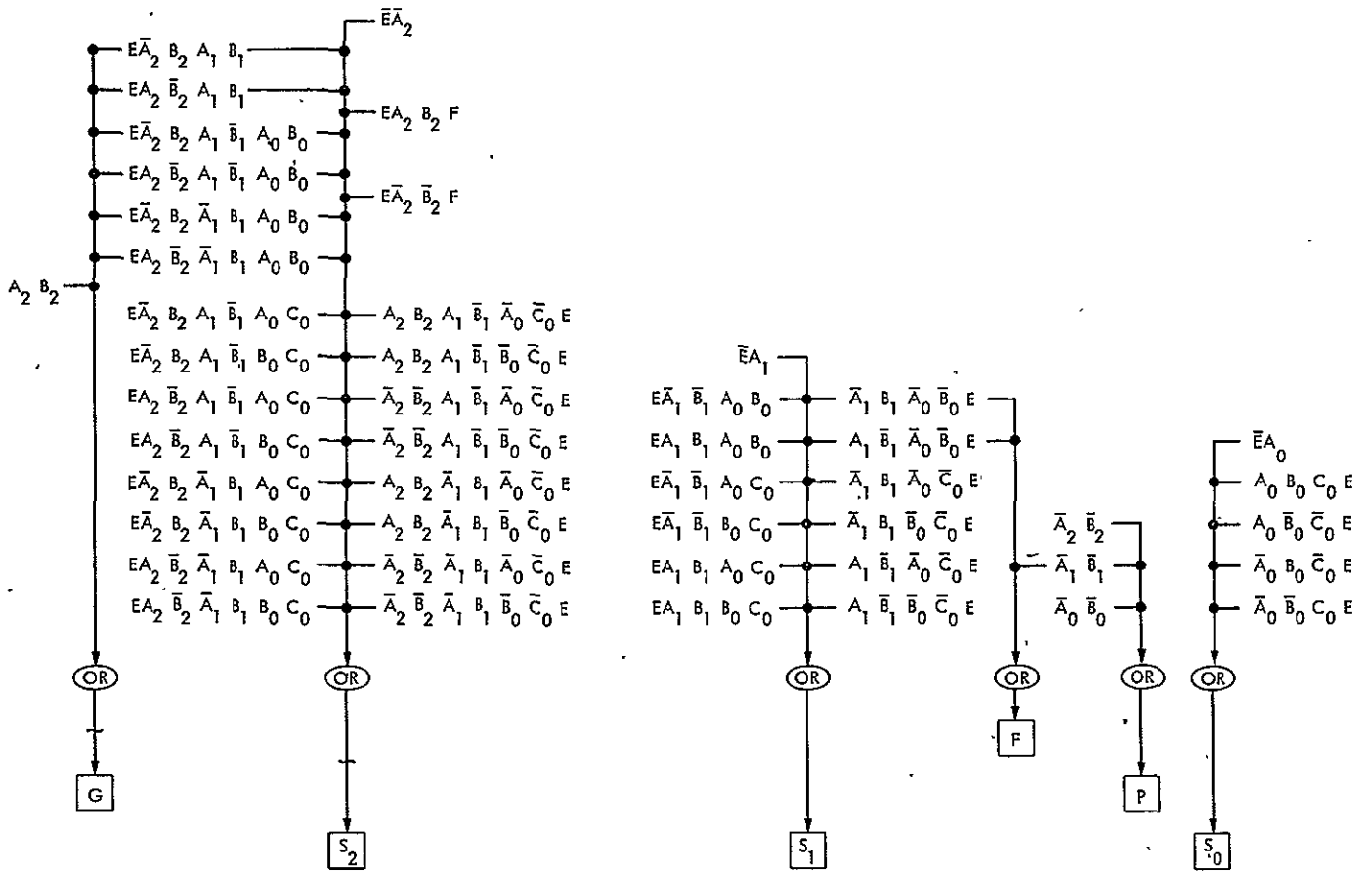


Fig. 2. 3-bit, lookahead-compatible adder, with enable, using an intermediate output F connected to higher-order sum-terms

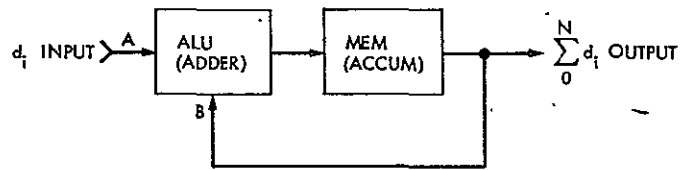


Fig. 3. Schematic diagram of digital accumulator using an adder

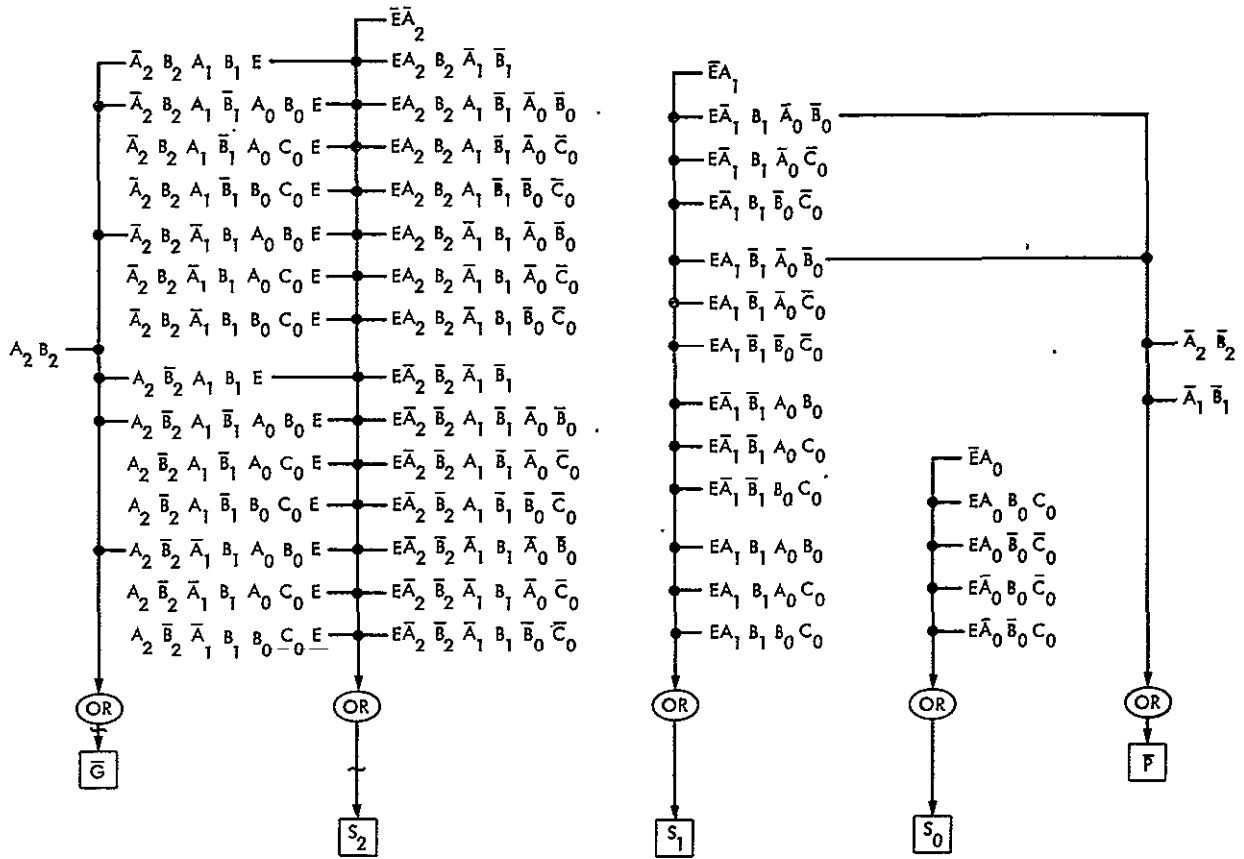


Fig. 4. 3-bit, fastest lookahead-compatible adder, with enable, using no intermediate outputs

ORIGINAL PAGE IS
OF POOR QUALITY

A Probabilistic Version of Sperner's Theorem, With Applications to the Problem of Retrieving Information From a Data Base

L. D. Baumert, R. J. McEliece, E. R. Rodemich, and H. Rumsey, Jr.
 Communications Systems Research Section

We show how the design of an optimal "merged keycode" information retrieval system involves finding the probability distribution on n -bit binary words that minimizes $P\{X \leq Y_1 \cup \dots \cup Y_r\}$ where X, Y_1, \dots, Y_r are selected independently according to the given probability distribution. We then find the minimizing probability distribution in the case $r = 1$.

I. Introduction

In retrieving information from a large data base, such as will exist in the DSN's digital RFI Surveillance System (Ref. 1), the technique of *merged keycodes* (Ref. 2) is often useful. In this technique each record in the data base is assumed to have a certain number of attributes. Each possible attribute A is assigned a binary code (whose length is normally that of one computer word) $C(A)$. If the record R possesses attributes A_1, A_2, \dots , it is then assigned the merged keycode $C(R) = C(A_1) \cup C(A_2) \cup \dots$, where the symbol \cup denotes the logical OR operation.

If one wants to locate all records in the data base possessing a fixed set of attributes, say B_1, B_2, \dots, B_s , one computes the merged keycode $D = C(B_1) \cup \dots \cup C(B_s)$, and then tags each record R such that $D \leq C(R)$. Clearly the set of records with the desired attributes is a subset of the tagged records. However, some of the tagged records will not have the desired attributes; such records are called *false drops*. It is obviously desirable to minimize the number of false drops, other things being equal.

Under certain circumstances, it is reasonable to model the above situation as follows. A fixed number, say r , binary codewords are selected independently according to a certain probability distribution P , which is to some extent controlled by the system design. Denote these codewords by Y_1, Y_2, \dots, Y_r — they represent the keycodes of the attributes of a randomly selected record. Let $X_1, \dots, X_s, s \leq r$ denote the keycodes corresponding to the attributes in a random query of the data base. We assume the X_i are chosen independently according to the same probability distribution P . The probability of false drop is then

$$P\{X_1 \cup \dots \cup X_s \leq Y_1 \cup \dots \cup Y_r\} = P\{X_1 \leq Y_1 \cup \dots \cup Y_r\}^s$$

Thus we are led to ask: What is the probability distribution on n -bit binary words that minimizes the probability $P\{X_1 \leq Y_1 \cup \dots \cup Y_r\}$ for various values of r ?

In this article, we will solve this question for the case $r = 1$. It is hoped that the techniques developed can be brought to

bear for larger values of r . In the remainder of this section, we will describe our main result.

Let Ω be a finite set with n elements, and let $V = V(\Omega)$ denote the collection of all subsets of Ω . For $x \in V$, $|x|$ will denote the cardinality of x . The relations of set inclusion and proper set inclusion will be denoted by $x \leq y$ and $x < y$, respectively. The empty set, viewed as an element of V , will be denoted by 0 , and Ω itself, as an element of V , by 1 .

Let $p(x)$ be a probability distribution on V , and let X and Y be elements of V chosen randomly and independently according to p . We denote by $P\{X \leq Y\}$ the probability that X will be a subset of Y . Our main result is the following.

Theorem 1. If $n > 1$, then for any probability distribution,

$$P\{X \leq Y\} \geq \left(\binom{n}{\lfloor \frac{n}{2} \rfloor} \right)^{-1}$$

Furthermore equality holds for the probability distribution defined by

$$p(x) = \begin{cases} \left(\binom{n}{\lfloor \frac{n}{2} \rfloor} \right)^{-1} & \text{if } |x| = \lfloor \frac{n}{2} \rfloor \\ 0 & \text{otherwise} \end{cases}$$

In the remainder of this section, we make some remarks about Theorem 1 and its proof. The proof itself occupies Sections II–V.

- (1) The restriction $n > 1$ is necessary, since with $n = 1$, the probability distribution $p(0) = p(1) = 1/2$ gives $P\{X \leq Y\} = 3/4$, whereas

$$\left(\binom{n}{\lfloor \frac{n}{2} \rfloor} \right)^{-1} = 1$$

- (2) Let $Y = \{y_1, \dots, y_M\}$ be a set of M pairwise non-comparable elements of V , i.e., $y_i \leq y_j$ iff $i = j$. If we define a probability distribution $p(x)$ by

$$p(x) = \begin{cases} \frac{1}{M} & \text{if } x \in Y \\ 0 & \text{otherwise} \end{cases}$$

then clearly $P\{X \leq Y\} = P\{X = Y\} = 1/M$. Hence by Theorem 1,

$$M \leq \binom{n}{\lfloor \frac{n}{2} \rfloor}$$

This is Sperner's famous bound (see Ref. 3, for example) on the maximum number of non-comparable elements in V . Thus (for $n > 1$) Theorem 1 can be viewed as a generalization of Sperner's bound.

- (3) For even values of n , it is possible to show that the particular probability distribution cited in the statement of Theorem 1 is the only one for which equality holds. For odd $n \geq 3$, the obvious alternate distribution

$$p(x) = \begin{cases} \left(\binom{n}{\lfloor \frac{n}{2} \rfloor} \right)^{-1} & \text{if } |x| = \lfloor \frac{n}{2} \rfloor + 1 \\ 0 & \text{otherwise} \end{cases}$$

also achieves equality. For odd $n \geq 5$ this is the only other equality-achieving distribution. However, for $n = 3$ there are infinitely many extremal distributions:

$$p(x) = \begin{cases} a & \text{if } |x| = 1 \\ 1/3 - a & \text{if } |x| = 2 \\ 0 & \text{if } |x| = 0 \text{ or } 3, \text{ for } 0 \leq a \leq 1/3 \end{cases}$$

(These facts can all be proved by making a careful study of our proof of Theorem 1. For the sake of brevity, however, we shall omit the details.)

- (4) Our proof contains two main ideas. First, by using more-or-less standard calculus techniques, one can obtain very strong necessary conditions satisfied by any extremal probability distribution. This we do in Section II. Second, we derive in Section IV (after some preliminary material in Section III) a lemma dealing with the expected number of maximal chains through a point of V which is selected according to a given probability distribution. This lemma was motivated in part by Lubell's classic proof (Ref. 3) of Sperner's theorem. Finally in Section V, these two ideas are combined to give our proof of Theorem 1.

(5) A possible alternate form of Theorem 1 would concern minimizing the probability that X and Y are comparable. It turns out that this problem is much easier to handle; the result is

$$P\{X \leq Y \text{ or } X \geq Y\} \geq \left(\frac{\binom{n}{2}}{\binom{n}{2}}\right)^{-1}$$

for all n , and equality occurs only for a uniform probability distribution on the subsets of cardinality

$$\left\lfloor \frac{n}{2} \right\rfloor \text{ or } \left\lceil \frac{n+1}{2} \right\rceil$$

However, this inequality follows already from a theorem of Motzkin and Strauss (Ref. 4), together with Sperner's original theorem.

II. Lagrange Multipliers

The probability $Q(p) = P\{X \leq Y\}$ is given by the sum

$$Q(p) = \sum\{p(x)p(y) : x \leq y\} \quad (1)$$

We are asked to minimize the function Q of the 2^n variables $(p(x), x \in V)$, subject to the following constraints:

$$\sum_{x \in V} p(x) = 1 \quad (2)$$

$$p(x) \geq 0, \text{ all } x \in V \quad (3)$$

Suppose p is a probability distribution that minimizes $Q(p)$ subject to (2) and (3), and let $G = \{x : p(x) > 0\}$. Temporarily we regard p and G as being fixed. Consider now the new problem of minimizing the function,

$$Q_G(q) = \sum\{q(x)q(y) : x \leq y, x, y \in G\} \quad (4)$$

where q is a real-valued function defined on G , subject to the single linear constraint

$$\sum_{x \in G} q(x) = 1 \quad (5)$$

(N.B. q is *not* required to be a probability distribution.)

Let $B = \min\{p(x)^2 : x \in G\}$, and let U denote the Euclidean neighborhood of the function p (restricted to G) defined by

$$U = \left\{q : \sum_{x \in G} (q(x) - p(x))^2 < B\right\} \quad (6)$$

Clearly if $q \in U$, then $q(x) > 0$ for all $x \in G$. Thus by the assumed extremal property of p , we have

$$Q_G(q) \geq Q_G(p), \text{ for all } q \in U \text{ satisfying (5)} \quad (7)$$

Thus p (restricted to G) gives a local minimum of the function Q_G , subject to the constraint (5), and so by the Lagrange multiplier rule there exists a constant λ such that

$$\frac{\partial Q_G}{\partial p(x)} = \lambda, \text{ for all } x \in G \quad (8)$$

Using (1), this becomes

$$2p(x) + \sum_{y < x} p(y) + \sum_{y > x} p(y) = \lambda, \text{ for all } x \in G \quad (9)$$

Furthermore, since $P\{X \leq Y\} = P\{X \geq Y\}$ by symmetry,

$$\begin{aligned} 2P\{X \leq Y\} &= P\{X \leq Y\} + P\{X \geq Y\} \\ &= \sum_{x \in G} p(x) \left\{ \sum_{y \leq x} p(y) + \sum_{y \geq x} p(y) \right\} \\ &= \sum_{x \in G} p(x) \left\{ 2p(x) + \sum_{y < x} p(y) + \sum_{y > x} p(y) \right\} \\ &= \lambda \sum_{x \in G} p(x) = \lambda, \text{ by (9)} \end{aligned}$$

Thus we have identified the constant λ in (9), and so we have

$$2p(x) + \sum_{y < x} p(y) + \sum_{y > x} p(y) = 2P\{X \leq Y\}, \quad (10)$$

for all $x \in G$

Equation (10) is the condition which must be satisfied by any extremal probability distribution that we will return to in Section V.

Note: Equation (9) follows immediately from the Kuhn-Tucker theorem of nonlinear programming (Ref. 5), and indeed one can also conclude from K-T that the left side of (9) is $\geq \lambda$ if $x \notin G$. We have included this elementary derivation only to make our exposition more self-contained.

III. Preliminaries About Chains

A *chain* of length r in V is an $(r + 1)$ -tuple $c = (x_0, x_1, \dots, x_r)$ of elements from V such that $x_0 < x_1 < \dots < x_r$. If in addition we have $|x_{i+1}| = |x_i| + 1$, c is said to be a *maximal chain* (of length r) from x_0 to x_r . Such a chain is said to *pass through* each of the points x_0, x_1, \dots, x_r .

If (y_0, y_1, \dots, y_m) is any chain in V , we denote by $MC(y_0, \dots, y_m)$ the set of all maximal chains from y_0 to y_m which pass through each of the y_i 's. The number of maximal chains in $MC(y_0, \dots, y_m)$ is denoted by $f(y_0, \dots, y_m)$. Thus

$$f(y_0, \dots, y_m) = |MC(y_0, \dots, y_m)| \quad (11)$$

If $(y_0, \dots, y_k, \dots, y_m)$ is a chain, it is clear that every maximal chain in $MC(y_0, \dots, y_m)$ can be decomposed uniquely into a chain from $MC(y_0, \dots, y_k)$ followed by a chain from $MC(y_k, \dots, y_m)$. Hence

$$f(y_0, \dots, y_k, \dots, y_m) = f(y_0, \dots, y_k) f(y_k, \dots, y_m) \quad (12)$$

and by induction it follows that

$$f(y_0, \dots, y_m) = \prod_{i=0}^{m-1} f(y_i, y_{i+1}) \quad (13)$$

In view of (13), in order to compute $f(c)$ for a general chain c , it suffices to consider the case where $c = (x, y)$ consists of only two elements. This we now do.

Let $x = x_0 < x_1 < \dots < x_r = y$ be a maximal chain from x to y and let $x_{i+1} - x_i = \{w_i\}$, $i = 0, 1, \dots, r - 1$. Then $(w_0, w_1, \dots, w_{r-1})$ is a permutation of the elements

in the set $y - x$. Conversely, if (w_0, \dots, w_{r-1}) is any permutation of $y - x$, and if we define $x_i = x \cup \{w_0, w_1, \dots, w_{i-1}\}$, then (x_0, \dots, x_r) will be a maximal chain from $x_0 = x$ to $x_r = y$. Hence there is a one-to-one correspondence between chains from x to y and permutations of $y - x$:

$$f(x, y) = |y - x|! \quad (14)$$

$$f(y_0, \dots, y_m) = \prod_{i=0}^{m-1} |y_{i+1} - y_i|! \quad (15)$$

As a final bit of notation, for $x \in V$ let $N(x)$ be the number of maximal chains from 0 to 1 passing through x . Then

$$\begin{aligned} N(x) &= f(0, x, 1) \\ &= f(0, x) f(x, 1) \\ &= |x|! (n - |x|)! = n! / \binom{n}{|x|} \end{aligned} \quad (16)$$

Note that as a function of x , $N(x)$ achieves its minimum value when $|x| = n/2$ for n even, and $|x| = (n \pm 1)/2$ for n odd. Thus if we define $\alpha(n) = [n/2]! (n - [n/2])!$, we have

$$N(x) \geq \alpha(n), \text{ all } x \in V, \quad (17)$$

with equality iff $x = [n/2]$ or $n - [n/2]$.

IV. A Basic Lemma

Let G be a subset of V . If $c = (x_0, \dots, x_r)$ is a chain in V , and at least one element of c lies in G , we define $L_G(c)$ ("the last element of c lying in G "), as follows:

$$L_G(c) = x_k, \text{ where } k = \max \{i: x_i \in G\} \quad (18)$$

If no element of c lies in G , $L_G(c)$ is undefined.

Further, we define for each $x \in V$,

$$N_G(x) = |\{c \in MC(0, 1): L_G(c) = x\}| \quad (19)$$

Thus $N_G(x)$ is the total number of maximal chains from 0 to 1 whose last element in G is x . If now for each $x \in V$ we define $g(x)$ by

$$g(x) = |\{c \in MC(x, 1): L_G(c) = x\}| \quad (20)$$

i.e., $g(x)$ is the number of maximal chains from x to 1 whose last element in G is x itself, it follows that

$$N_G(x) = f(0, x) g(x) \quad (21)$$

If p is a probability distribution on V , and if X is an element of V chosen randomly according to p , the number of maximal chains from 0 to 1 passing through X , $N(X)$ is a random variable whose expectation is given by $E(N(X)) = \sum \{p(x)N(x): x \in V\}$. The following lemma gives another formula for $E(N(X))$ which is crucial in our proof of Theorem 1.

Lemma 1

Let p be a probability distribution on V , and let $G = \{x \in V: p(x) > 0\}$. Then

$$\sum_{x \in V} p(x)N(x) = \sum_{y \in G} N_G(y) \sum_{x \leq y} p(x) \left(\frac{|y|}{|x|} \right)^{-1}$$

Proof

Using the fact that $p(x) = 0$ if $x \notin G$, and (16), we have

$$\sum_{x \in V} p(x)N(x) = \sum_{x \in G} p(x) f(0, x) f(x, 1) \quad (22)$$

We now classify the chains in $MC(x, 1)$ according to their last element in G . If $y \geq x$, then the number of maximal chains from x to 1 whose last element in G is y is $f(x, y)g(y)$. Thus

$$f(x, 1) = \sum_{y \geq x} f(x, y)g(y) \quad (23)$$

Replacing $f(x, 1)$ in (22) by the sum (23), and interchanging the order of summation, we get

$$\begin{aligned} \sum_{x \in V} p(x)N(x) &= \sum_{y \in G} g(y) \sum_{x \leq y} p(x) f(0, x) f(x, y) \\ &= \sum_{y \in G} f(0, y) g(y) \sum_{x \leq y} p(x) \frac{f(0, x) f(x, y)}{f(0, y)} \end{aligned}$$

But by (21), $f(0, y)g(y) = N_G(y)$. And by (14),

$$\frac{f(0, x) f(x, y)}{f(0, y)} = \frac{|x|! |y - x|!}{|y|!} = \left(\frac{|y|}{|x|} \right)^{-1}$$

This proves Lemma 1.

V. Proof of Theorem 1

We are now in a position to give a short proof of Theorem 1. The idea of the proof is to estimate the expected number of maximal chains through a randomly selected point of V in two ways. On one hand, this expectation is certainly at least $\alpha(n)$ by (17). On the other hand, using the machinery we have developed in Sections II-IV, we will show that this expectation (at least for an extremal probability distribution) is at most $P\{X \leq Y\} \cdot n!$. The resulting bound, $P\{X \leq Y\} \geq \alpha(n)/n!$, is the bound of Theorem 1. Let us now see how this proof goes in detail.

Let p be a probability distribution that minimizes $Q(p) = P\{X \leq Y\}$, and let $G = \{x \in V: p(x) > 0\}$. Then by Lemma 1,

$$\sum_{x \in V} p(x)N(x) = \sum_{y \in G} N_G(y) \sum_{x \leq y} p(x) \left(\frac{|y|}{|x|} \right)^{-1} \quad (24)$$

By (17), $N(x) \geq \alpha(n)$ for all x . Hence

$$\sum_{x \in V} p(x)N(x) \geq \alpha(n) \quad (25)$$

Let us rewrite the inner sum in (24) in the following way:

$$\sum_{x \leq y} p(x) \binom{|y|}{|x|}^{-1} = p(y) + \sum_{x < y} p(x) \binom{|y|}{|x|}^{-1} \quad (26)$$

$$\leq p(y) + \frac{1}{2} \sum_{x < y} p(x) + \frac{1}{2} \sum_{x > y} p(x) \quad (28)$$

We now claim that if $n > 1$, and $x < y$,

$$p(x) \binom{|y|}{|x|}^{-1} \leq \frac{1}{2} p(x) \quad (27)$$

If $x \neq 0$, (27) is obvious since then the binomial coefficient will be ≥ 2 . If $x = 0$, the binomial coefficient is 1, but (27) is true anyway because $p(0) = 0$. This can be seen as follows. Let $x = 0$ in (10); we get $P\{X \leq Y\} = 1/2 + 1/2 p(0)$. Hence if $p(0) > 0$, then $P\{X \leq Y\} > 1/2$. But since $n > 1$ we can select two non-comparable elements x_1 and x_2 and define a probability distribution q by setting $q(x_1) = q(x_2) = 1/2$. For this probability distribution we clearly have $P\{X \leq Y\} = 1/2$. This shows that no distribution that minimizes $P\{X \leq Y\}$ for $n > 1$ can have $p(0) > 0$, and this completes the proof of (27).

Combining (26) and (27), we get

$$\sum_{x \leq y} p(x) \binom{|y|}{|x|}^{-1} \leq p(y) + \frac{1}{2} \sum_{x < y} p(x)$$

We now apply (10) to (28) and conclude that

$$\sum_{x \leq y} p(x) \binom{|y|}{|x|}^{-1} \leq P\{X \leq Y\}, \text{ if } y \in G \quad (29)$$

Combining (24), (25), and (29), we get

$$\alpha(n) \leq P\{X \leq Y\} \sum_{y \in G} N_G(y) \quad (30)$$

Finally we observe that each maximal chain from 0 to 1 is counted at most once in the sum (30). (If c is such a chain and if $L_G(c) = y$, it is counted by the term $N_G(y)$.) Since the total number of such chains is $n!$ (see Eq. 14), we get $\sum N_G(y) \leq n!$ and hence, finally,

$$P\{X \leq Y\} \geq \frac{\alpha(n)}{n!} = \left(\binom{n}{\lfloor n/2 \rfloor} \right)^{-1} \quad (31)$$

This completes the proof of Theorem 1.

References

1. Levitt, B. K., "Analysis of a Discrete Spectrum Analyzer for the Detection of Radio Frequency Interference," in *DSN Progress Report 42-38*, April 15, 1977, pp. 83-98.
2. Knuth, D. E., *Sorting and Searching*, Vol. 3 in *The Art of Computer Programming*, Reading: Addison-Wesley, 1973.
3. Lubell, D., "A Short Proof of Sperner's Lemma," *J. Combinatorial Theory*, 1 (1966), p. 299.
4. Motzkin, T. S., and E. G. Strauss, "Maxima for Graphs and a New Proof of a Theorem of Turan," *Canadian J. Math.* 17 (1965), pp. 535-540.
5. Cottle, R. N., and Lemke, C. E., eds., *Nonlinear Programming*, SIAM-AMS Proceedings, Vol. 9, Providence: American Math. Society, 1976.

D15-91
43-088

N78-32152

VLBI-Laser Intercomparison Project

B. D. L. Mulhall
TDA Engineering Office

The VLBI-Laser Intercomparison Project was established at the direction of NASA to assess state-of-the-art geodetic measurement systems being developed by NASA. A Project plan describing the objectives of the Project, the methods for making the assessment, and the schedule, was reviewed. The plan was approved and published. This article describes the contents of the plan.

I. Introduction

A. General

The primary objective of the DSN VLBI-Laser Intercomparison Project is the accurate measurement of baseline vectors, both length and direction, between established geodetic benchmarks.¹

A second objective is the intercomparison between both satellite and lunar laser ranging techniques with VLBI. Both geodetic and geodynamic measurement instruments are to be evaluated. This is to provide potential users with an assessment of the value of the different instruments. This assessment is to be performed in terms of accuracy of the baselines measured and/or the geodynamic parameters measured, the operability of each instrument and, finally, the cost of operations of each system. This leads to the demonstration of the suitability of the various systems to potential applications.

¹A surveyor's mark made on a permanent landmark that has a known position altitude that can be used by various geodetic measurement systems.

B. Specific Objectives

The specific objectives of the Project are divided into immediate and future objectives. The immediate objectives are to: assess current VLBI and Laser System performance, identify potential problems in the application of VLBI or Laser Systems by NASA or other agencies, assist system development to overcome problems, and finally, demonstrate readiness for technology transfer. All these objectives are intended to be accomplished by 1979, except for the intercomparison between VLBI and Lunar Laser Ranging (LURE) which is not planned to be accomplished until early 1980.

Beyond 1980 the objectives of the Project are to demonstrate performance of the five-centimeter VLBI system in an operational environment and intercomparison with LURE.

C. Assessment Criteria

The VLBI and Laser Systems will be judged on their ability to measure vectors between benchmarks in terms of relative accuracy, since no absolute scale can be found. By relative accuracy is meant the repeatability of each system's measure-

ments over the measurement session and, in cases where appropriate, the ability to close figures such as triangles.

Secondly, the operability, that is the ability to operate each system, will be assessed. This will be done by noting the differences between planned observations and actually-accomplished observations of the measurement's sources during each session.

Finally, the life-cycle cost of each system will also be a basis for judgement. By life-cycle cost is meant the implementation cost of an operational system and the operating cost over the life-cycle of the system. Operational costs will be measured in terms of man-months of effort per month, and shipping and setup costs rather than actual salary dollars to avoid evaluation dependence on salary structure of the user agency or contractor.

D. Accuracy Demonstration

The objective of demonstrating geodetic and geodynamic measurement accuracy can be satisfied by an experiment which will produce necessary and sufficient results. For example, if a more accurate measurement technique existed, then the accuracy of VLBI could be demonstrated by comparison to this more accurate technique. For short baselines where conventional surveys can provide centimeter accuracy, this comparably accurate technique does exist. However, on long baselines there is no demonstrated technique for producing comparable accuracies.

Consequently, in the absence of a more accurate measurement technique, no known test of sufficiency has been found. What can be done is to satisfy an exhaustive set of necessary conditions to infer the accuracy.

II. Error Source Evaluation Methods

The VLBI error sources can be grouped for analysis as follows. First, there are the VLBI subsystems, some of which can be isolated and examined singly. Others must be lumped together for evaluation. Table 1 lists the subsystems, the types of errors that arise, the methods for evaluating each subsystem or group of subsystems, and the measurement session in which the evaluation will occur (see paragraph III for measurement session schedule).

A second set of error sources can be called natural. These are shown in Table 2 and include the structure and position of the radio source, the ionosphere, and the troposphere. In two of these instances, ionosphere and troposphere, related research has been conducted for some years by DSN Advanced Systems. Also, more work is planned in the future to evaluate

the water vapor radiometer in an absolute sense. The Project will closely monitor these activities. But, they are not part of this Project plan since they have been or will be carried out regardless of this Project's sponsorship.

It is the intent of the Project to conduct VLBI experiments in certain environmental conditions such as variable humidity to investigate the effect on the interferometry of water vapor, for example.

System evaluations will be conducted as follows: First, short baseline closure and repeatability will be performed to investigate instrument errors. Also, comparisons with conventional surveys, such as NGS will be conducted.

Secondly, continental baseline closure and repeatability can demonstrate VLBI capability and comparisons with satellite laser ranging can be made.

Third, intercontinental baseline comparisons with LURE are planned as intercomparison with the VLBI system. The Universal Time 1 and polar motion determined by both systems will also be compared to establish the geodynamic capability of the two systems.

III. Measurement Session Schedule

The Project is organized and conducted as a series of measurement sessions. Each session is designed to achieve specific objectives as developed in later portions of this plan. Sessions are generally conducted once per year. Sufficient time should be allowed between measurement sessions to evaluate the results so that the planning for the next session can take full advantage of the knowledge obtained from the last session.

The measurement sessions evolve from the simple to complex by increasing system sensitivity and performance, by adding more calibrations and by lengthening the baseline being measured. Also, there are sessions which are intended to penetrate deeply into one aspect or subsystem of the system which may also be conducted and which may in fact be simpler measurements but performed under more highly controlled conditions to isolate error sources of the system.

Figure 1 shows the overall VLBI-Laser Intercomparison Project schedule. The top two lines indicate the periods for data acquisition for each measurement session and the schedule for project reports. As shown, each session has a pre-session plan describing the objectives of the session and a post-session report listing the results.

The planning for each session involves preparation of a pre-session report to document specific objective, measure-

ment strategy and technique, and estimate its estimated accuracies. The pre-session report also identifies the hardware and software required and the schedule for data acquisition, reduction, and analysis. The measurement is then performed.

The post-session report is published to document the results. In the post-session report the experiences learned in terms of operational difficulty and the equipment requirements for the next session should be identified. Most important of all, the accuracy actually obtained will be published.

Also, there is an overall Project plan, which is this document, and there will be a final Project report at the end of the Project.

The next line item on the schedule are flight project events and are included to show periods of peak activity and heavy loading on DSN facilities. As can be seen from the data acquisition measurement section schedule, sessions are for the most part intended to avoid these heavy deep space probe activity periods to facilitate antenna scheduling.

The next three line items show the deployment schedule for the mobile satellite laser ranging equipment (MOBLAS), the Geoceivers, which employ satellite Doppler measurements to determine their position, and the ARIES antenna which provides a mobile arm for the VLBI system. The planned deployments of these three systems require coordination and the agreement of the respective agencies before the plan can be finalized. Specifically, the deployment of the Geoceivers of the National Geodetic Survey in Session Four at Haystack, Goldstone, and Ft. Davis, needs to be agreed upon.

The next six line items, VLBI data acquisition racks, RF phase calibrators, water vapor radiometers, hydrogen masers, noise adding radiometers, and the Caltech-JPL Mark-II Correlator are major equipment items that are required for certain sessions as indicated by the cross-hatched bars. Note that the Mark II Correlator will not be employed in Session Six since

the DSN VLBI processor subsystem will be used for correlation and estimation for this final session.

The next items are surveys being conducted by the NGS as part of certain intercomparisons mainly, the survey at DSS 14 between the intersection of axes of this antenna, a benchmark or monument beside DSS 14, to the MOBLAS location pad and the ARIES pad 300 meters from the DSS 14 antenna. A second survey which is planned if the intra-complex report indicates that the anticipated accuracies are sufficient to provide a highly precise intercomparison with VLBI will be conducted over the entire Goldstone complex. This survey will primarily be used to compare the DSS 14 to DSS 13 baseline. However, since survey techniques require the establishment of a network of measuring devices the other Goldstone antennas can also be surveyed without a great additional cost. It should be noted that DSS 13 will become a wideband VLBI station before DSS 14 and consequently DSS 13 will be used in certain long baseline tests in place of DSS 14 where 14 is unavailable due to other comments. Consequently, by measuring the 13-14 baseline accurately, these DSSs can be used more or less interchangeably.

The next item is the implementation schedule of the DSN VLBI System which will be employed in Session Six for the operational demonstration. DSN VLBI will produce UT1-polar motion routinely from July 1979. The precise DSN VLBI System (5 cm) will be operational in time for Session Six. The DSS 13 VLBI configuration is the next line item and is planned to be completed by October 1978. At that time 100 MHz of spanned bandwidth at X-band would be available.

Finally, the four participating facilities not within the DSN, namely, the Haystack Observatory, the Owens Valley Radio Observatory, the Ft. Davis Observatory, and the LURE equipment at the McDonald and the Haleakala Observatories, are listed as are their required participation periods as shown by cross-hatched bars.

Table 1. Subsystem error source evaluation

Error sources	Evaluation method	Measurement session
Instrumentation		
Frequency standard ^a		
Phase stability		
Phase calibrator ^a	Short baselines and connected element interferometry	3
Phase center variations to intersection of axes		
Phase path variations due to antenna distortion or sub-reflector motion		
Off-axis pointing phase effect		
Mechanical		
Variation between intersection of axes and benchmark	Comparison with survey	2
Software		
	Comparison of independently formulated code, comparison of results with identical input data	2

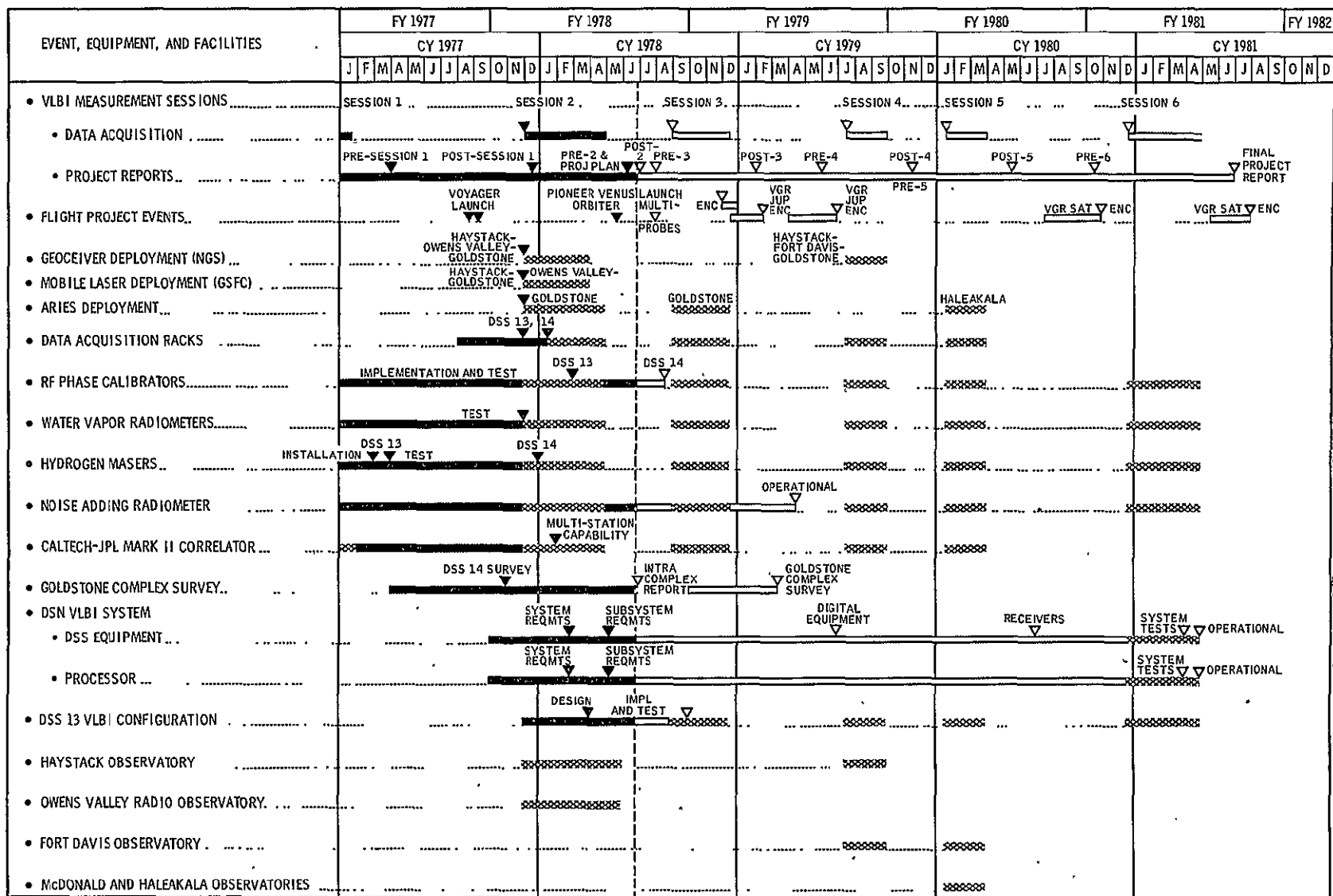
^aEvaluation provided by Advanced Systems.

Table 2. Natural error source evaluation

Error source	Evaluation method	Measurement session
Source positions and structure		
Uncertainty source positions	Baseline repeatability	2 & 4
Changing source structure	Baseline closure	2 & 4
Ionosphere^a		
	S- vs X-band solution (<1 cm)	
Troposphere		
Dry components ^a	Surface measurements (<1 cm)	
Wet component ^a	WVR (water vapor radiometer) calibration (<2 cm)	
	Measurements in highly variable humidity	

^aEvaluation provided by Advanced Systems and/or ARIES Project.

ORIGINAL PAGE IS OF POOR QUALITY



LEGEND.
 REQUIRED

Fig. 1. NASA VLBI-laser intercomparison project schedule

ORIGINAL PAGE IS
OF POOR QUALITY

A Fast Computation of Complex Convolution Using A Hybrid Transform¹

I. S. Reed

University of Southern California
Department of Electrical Engineering

T. K. Truong

TDA Engineering Office

In this article, it is shown that the cyclic convolution of complex values can be performed by a hybrid transform. This transform is a combination of a Winograd transform and a fast complex integer transform developed previously by the authors. This new hybrid algorithm requires fewer multiplications than any previously known algorithm.

I. Introduction

Several authors (Refs. 1-9) have shown that transforms over finite fields or rings can be used to compute circular convolutions without round-off error. Recently, Agarwal and Cooley (Ref. 10) used the techniques of Winograd (Refs. 11, 12) to compute cyclic convolutions. These new algorithms for convolutions of a few thousand points require substantially fewer multiplications than the conventional FFT algorithm (Ref. 13).

Previously the authors (Ref. 5) defined a class of Fourier-like transforms over the complex integers modulo q . This was a transform over the Galois field $GF(q^2)$, where $q = 2^p - 1$ is a Mersenne prime for $p = 2, 3, 5, 7, 13, 17, 19, 31, 61, \dots$. Recently these complex integer transforms were specialized to a transform length of d points, where $d \mid 8p$ (Ref. 8). The advantage of the latter transform over others is that it can be accom-

plished completely by circular shifts, i.e., no multiplications are needed (Ref. 8).

In this article, it is shown that Winograd's algorithm (Ref. 11) can be combined with the above-mentioned complex integer transform over $GF(q^2)$ to yield a new algorithm for computing the discrete cyclic convolution of complex number points. By this means a fast method for accurately computing the cyclic convolution of a sequence of complex numbers for long convolution lengths can be obtained. This hybrid algorithm is comparable in speed to that given by Agarwal and Cooley (Ref. 10) and is implemented readily on a digital computer. The dynamic range requirements for this hybrid algorithm are presented here in detail.

II. Cyclic Convolution

The following algorithm for the cyclic convolution of two sequences is based on ideas given by Winograd (Ref. 11). Let the field of rationals be R . Also let $X(u) = x_0 + x_1 u + x_2 u^2 +$

¹This work was supported in part by the U.S. Air Force Office of Scientific Research under Grant AFOSR-75-2798.

$\dots + x_n u^{n-1}$, $Y(u) = y_0 + y_1 u + y_2 u^2 + \dots + y_n u^{n-1}$ be two polynomials over R . The product $T(u) = X(u) \cdot Y(u)$ can be computed by

$$T(u) = X(u) \cdot Y(u) \bmod \prod_{i=0}^{2n-2} (u - \alpha_i) \quad (1)$$

where $\alpha_i \in R$. It is shown in Ref. 11 that a minimum of $2n - 1$ multiplications are needed to compute (1).

It is readily shown that the cyclic convolution of $X(u)$ and $Y(u)$ is the set of coefficients of the polynomial

$$T'(u) = X(u) \cdot Y(u) \bmod (u^n - 1)$$

Let the polynomial $u^n - 1$ be factored into irreducible relatively prime factors, i.e.,

$$u^n - 1 = \prod_{i=1}^k g_i(u)$$

where $(g_i(u), g_j(u)) = 1$ for $i \neq j$. Then $T'(u) \bmod g_i(u)$ for $i = 1, 2, \dots, k$ can be computed using Eq. (1). Finally, the Chinese remainder theorem is used to evaluate $T'(u)$ from these residues. The above summarizes Winograd's method for performing a cyclic convolution.

The following theorem is due to Winograd (Ref. 11).

Theorem 1: Let a and b be relatively prime positive integers and A be the cyclic $ab \times ab$ matrix, given by

$$A(x, y) = f(x + y \bmod a \cdot b), \quad 0 \leq x, y < ab$$

If π is a permutation of the set of integers $\{0, 1, \dots, ab - 1\}$, let

$$B(x, y) = A(\pi(x), \pi(y))$$

Then there exists a permutation π such that, if B is partitioned into $b \times b$ submatrices, each submatrix is cyclic and the submatrices form an $a \times a$ cyclic matrix.

It was shown previously (Refs. 10, 12) that the number of multiplications needed to perform a circular convolution of 3, 5, 7, and 9 points of complex numbers is 4, 10, 19, and 22 multiplications, respectively. In order to compute the cyclic

convolution of two longer sequences of complex integers, a d -point transform over $GF(q^2)$, where $q = 2^p - 1$ and $d \mid 8p$, will be utilized here. Since the latter transform can be evaluated without multiplications (Ref. 8), it can be used with considerable advantage to compute a cyclic convolution of two d -point complex number sequences. The number of complex integer multiplications required to perform this circular convolution over $GF(q^2)$ is precisely d , the number of multiplications needed to multiply together the transforms of the two sequences.

For the moment, let d , the transform length, be an arbitrary integer. Next let $d = p_1 \cdot p_2 \cdot \dots \cdot p_r$ be the factorization of d into prime integers. If one lets $a_1 = p_1 \cdot p_2 \cdot \dots \cdot p_{r-1}$ and $b_1 = p_r$, then by Theorem 1, a $d \times d$ cyclic matrix can be partitioned into $b_1^2 = p_r^2$ matrices of size $a_1 \times a_1$. Next let $a_1 = a_2 \times b_2$, where $a_2 = p_1 \cdot \dots \cdot p_{r-2}$ and $b_2 = p_{r-1}$. If a_2 is not a prime, then each $a_1 \times a_1$ cyclic matrix can be partitioned into b_2^2 matrices of size $a_2 \times a_2$. In general, $a_i = a_{i+1} \times b_{i+1}$, where b_{i+1} is a prime. If $a_{i+1} \neq 1$, then each $a_i \times a_i$ cyclic matrix can be partitioned into b_{i+1}^2 matrices of size $a_{i+1} \times a_{i+1}$. Otherwise, the procedure terminates. If the number of multiplications used to compute the cyclic convolution of p_i points is m_i for $i = 1, 2, \dots, r$, then Winograd has shown (Ref. 10) that the number of multiplications needed to compute a d -point cyclic convolution is equal to $N = m_1 \cdot m_2 \cdot \dots \cdot m_r$.

It is necessary to choose only certain values of d as the transform length in order to combine the Winograd transform with the fast complex integer transform over $GF(q^2)$, where $q = 2^p - 1$ is a Mersenne prime. For this purpose, let the number d have the form

$$d = a \cdot 2^m \cdot p \quad (2)$$

where $m = 0, 1, 2, 3$ and $a = 3, 5, 7$, or 9. For most practical applications, it suffices in (2) to let $p = 31$ or 61.

If d , the transform length of the cyclic convolution, is given by (2), then by Theorem 1, there exists a permutation of rows and columns so that the cyclic $d \times d$ matrix can be partitioned into blocks of $(2^m \cdot p) \times (2^m \cdot p)$ cyclic matrices in such a manner that the blocks form an $a \times a$ cyclic matrix. Now the cyclic convolutions of $a = 3, 5, 7$, or 9 complex number points can be accomplished by Winograd's algorithm. Since $2^m \cdot p \mid q^2 - 1$ for $m = 0, 1, 2, 3$, a transform of length $2^m \cdot p$ over $GF(q^2)$ can be found and used to compute the cyclic convolution of the $2^m \cdot p$ complex number points. The number of multiplications needed to perform this convolution is $2^m \cdot p$. Using this and the number of multiplications needed for Winograd's algorithm, the total number of multiplications needed to perform a convolution of d complex number points can be

computed. The results of this computation are shown in Table 1. The present algorithm, and Agarwal and Cooley's algorithm are compared in this table by giving the total number of complex number multiplications required to perform the different algorithms.

It was shown above that Winograd's algorithm can be combined with a transform over $GF(q^2)$ to yield a new rather fast hybrid algorithm for computing the cyclic convolution of complex values. In this algorithm it was necessary to compute the cyclic convolution of $2^m \cdot p$ complex number points for $m = 0, 1, 2$, or 3. This cyclic convolution of two d -point sequences of complex number points is

$$c_k = \sum_{n=0}^{d-1} e_n f_{(k-n)} \quad (3)$$

where $d \mid 8 \cdot p$ and $(k-n)$ denotes the residue of $k-n \pmod d$. To compute this convolution the components of the truncated complex numbers e_n and f_n must be converted first to integers a_n and b_n with dynamic ranges, say, A and B , respectively. Previously (Ref. 5), a sufficient dynamic range constraint for A and B was shown to be

$$A \leq \frac{q-1}{4Bd} \quad (4)$$

If $A = B$, (4) reduces to

$$A \leq \left\lfloor \sqrt{\frac{q-1}{4d}} \right\rfloor \quad (5)$$

where $\lfloor x \rfloor$ denotes the greatest integer less than x .

If the circular convolution of a_n and b_n is denoted by c'_k for $k = 0, 1, 2, \dots, d-1$, then using the procedure described in the example of Ref. 5, c'_k can be obtained by using fast transforms over $GF(q^2)$. In (3), c_k can be obtained by scaling back c'_k into the scale of the original complex numbers for $k = 0, 1, 2, \dots, d-1$. Evidently, the only error made in this computation of the c'_k s is the truncation error.

The dynamic range constraint A of the input sequence given in (5) is generally very pessimistic. By an argument similar to that used for integer convolutions (Ref. 14), one can lessen the severity for this dynamic range constraint and still maintain c_k in the interval $\pm(q-1)/2$ with a small probability of overflowing. This assertion is justified in the Appendix.

To illustrate this new hybrid algorithm, consider the following example.

Example: Let $d = 6$. Next suppose that the input function defined by

$$\begin{aligned} a_n &= 1 + i0 & n &= 0, 1 \\ &= 0 & 2 \leq n \leq 5 \end{aligned}$$

is convolved with itself. This convolution is

$$c_k = \sum_{n=0}^5 a_n b_{(k-n)}$$

where (x) denotes the residue $k-n$ of modulo 6. This convolution can be written in matrix form as

$$\begin{pmatrix} c_0 \\ c_1 \\ c_2 \\ c_3 \\ c_4 \\ c_5 \end{pmatrix} = \begin{pmatrix} a_0 & a_1 & a_2 & a_3 & a_4 & a_5 \\ a_1 & a_2 & a_3 & a_4 & a_5 & a_0 \\ a_2 & a_3 & a_4 & a_5 & a_0 & a_1 \\ a_3 & a_4 & a_5 & a_0 & a_1 & a_2 \\ a_4 & a_5 & a_0 & a_1 & a_2 & a_3 \\ a_5 & a_0 & a_1 & a_2 & a_3 & a_4 \end{pmatrix} \begin{pmatrix} b_0 \\ b_5 \\ b_4 \\ b_3 \\ b_2 \\ b_1 \end{pmatrix}$$

By Theorem 1, there exists a permutation π of rows and columns so that the above cyclic matrix can be partitioned into a 2×2 -block matrix of 3×3 cyclic blocks as follows:

$$\begin{pmatrix} c_0 \\ c_4 \\ c_2 \\ c_3 \\ c_1 \\ c_5 \end{pmatrix} = \begin{pmatrix} a_0 & a_4 & a_2 & a_3 & a_1 & a_5 \\ a_4 & a_2 & a_0 & a_1 & a_5 & a_3 \\ a_2 & a_0 & a_4 & a_5 & a_3 & a_1 \\ a_3 & a_1 & a_5 & a_0 & a_4 & a_2 \\ a_1 & a_5 & a_3 & a_4 & a_2 & a_0 \\ a_5 & a_3 & a_1 & a_2 & a_0 & a_4 \end{pmatrix} \begin{pmatrix} b_0 \\ b_2 \\ b_4 \\ b_3 \\ b_5 \\ b_1 \end{pmatrix}$$

ORIGINAL PAGE IS
OF POOR QUALITY

This matrix equation has the form

$$\begin{pmatrix} Y_1 \\ Y_2 \end{pmatrix} = \begin{pmatrix} A & B \\ B & A \end{pmatrix} \begin{pmatrix} X_1 \\ X_2 \end{pmatrix}$$

where

$$Y_1 = \begin{pmatrix} c_0 \\ c_4 \\ c_2 \end{pmatrix}, Y_2 = \begin{pmatrix} c_3 \\ c_1 \\ c_5 \end{pmatrix}, X_1 = \begin{pmatrix} b_0 \\ b_2 \\ b_4 \end{pmatrix}, X_2 = \begin{pmatrix} b_3 \\ b_5 \\ b_1 \end{pmatrix},$$

$$A = \begin{pmatrix} a_0 & a_4 & a_2 \\ a_4 & a_2 & a_0 \\ a_2 & a_0 & a_4 \end{pmatrix}, B = \begin{pmatrix} a_3 & a_1 & a_5 \\ a_1 & a_5 & a_3 \\ a_5 & a_3 & a_1 \end{pmatrix}$$

Thus

$$\begin{pmatrix} Y_1 \\ Y_2 \end{pmatrix} = 2^{-1} \begin{pmatrix} (A+B)(X_1+X_2) + (A-B)(X_1-X_2) \\ (A+B)(X_1+X_2) - (A-B)(X_1-X_2) \end{pmatrix} \\ = 2^{-1} \begin{pmatrix} D+E \\ D-E \end{pmatrix} \quad (6)$$

where $D = (A+B)(X_1+X_2)$, $E = (A-B)(X_1-X_2)$. Now

$$D = \begin{pmatrix} a_0+a_3 & a_4+a_1 & a_2+a_5 \\ a_4+a_1 & a_2+a_5 & a_0+a_3 \\ a_2+a_5 & a_0+a_3 & a_4+a_1 \end{pmatrix} \begin{pmatrix} b_0+b_3 \\ b_2+b_5 \\ b_4+b_1 \end{pmatrix}$$

$$= \begin{pmatrix} 1 & 1 & 0 \\ 1 & 0 & 1 \\ 0 & 1 & 1 \end{pmatrix} \begin{pmatrix} 1 \\ 0 \\ 1 \end{pmatrix} \quad (7)$$

Let $x_0 = 1, x_1 = 0, x_2 = 1$ and $y_0 = 0, y_1 = 1, y_2 = 1$. Then the matrix equation defined in (7) can be obtained by computing the convolution of the two sequences a_n and b_n . To do this, use a transform over $GF(q^2)$. In order to avoid overflow, one needs to choose $q = 7$ so that the integer components of a_n, b_n lie in the interval ± 1 .

Since 2 is a 3rd root of unity, the transform over $GF(7^2)$ of x_n is

$$X_k = \sum_{n=0}^{3-1} x_n 2^{nk} = 2^0 + 2^{2k} \quad \text{for } k = 0, 1, 2$$

Thus, $X_0 = 2, X_1 = 5, X_2 = 3$.

Similarly, the transform of sequence y_n is

$$Y_k = \sum_{n=0}^{3-1} y_n 2^{nk} = 2^k + 2^{2k} \quad \text{for } k = 0, 1, 2$$

That is, $Y_0 = 2, Y_1 = 6, Y_2 = 6$. But $D_k = X_k, Y_k$, i.e., $D_0 = 4, D_1 = 2, D_2 = 4$. These are the only complex integer multiplications needed to perform this transform. The inverse transform of D_k is

$$d_n = 3^{-1} \sum_{k=0}^{3-1} D_k 2^{-nk}$$

$$= 5(4 + 2 \cdot 2^{-k} + 4 \cdot 2^{-2k}) \text{ mod } 7 \quad \text{for } k = 0, 1, 2$$

since $3^{-1} \equiv 5 \text{ mod } 7$. Thus finally, $d_0 = 1, d_1 = 2, d_3 = 1$.

In a similar fashion, matrix E , given in (6), can also be obtained as $e_0 = 1, e_1 = -2, e_2 = 1$. Thus, by (6), one obtains finally $c_0 = 1, c_1 = 2, c_2 = 1, c_3 = 0, c_4 = 0$ and $c_5 = 0$.

Acknowledgement

The authors wish to thank Dr. N. A. Renzetti, Manager of Tracking and Data Acquisition Engineering, and the members of the Advanced Engineering Group in that organization at the Jet Propulsion Laboratory for their early support, suggestions, and encouragement of the research which led to this article.

References

1. Pollar, J. M., "The Fast Fourier Transform in a Finite Field," *Math. Comput.*, 1971, 25, pp. 365-374.
2. Schonhage, A., and Strassen, V., "Schnelle Multiplikation Grosser Zahlen," *Computing*, 1971, 7, pp. 281-292.
3. Rader, C. M., "Discrete Convolution Via Mersenne Transforms," *IEEE Trans. Comp.*, 1972, C-21, pp. 1269-1273.
4. Agarwal, R. C., and Burrus, C. S., "Number Theoretic Transforms to Implement Fast Digital Convolution," *Proc. IEEE*, 1975, 63, pp. 550-560.
5. Reed, I. S., and Truong, T. K., "The Use of Finite Fields to Compute Convolution," *IEEE Trans.*, 1975, IT-21, pp. 208-213.
6. Reed, I. S., and Truong, T. K., "Complex Integer Convolution Over a Direct Sum of Galois Fields," *IEEE Trans.*, 1975, IT-21, pp. 657-661.
7. Vegh, E., and Leibowitz, L. M., "Fast Complex Convolution in Finite Rings," *IEEE Trans.*, 1976, ASSP-24, pp. 343-344.
8. Reed, I. S., Truong, T. K., and Liu, K. Y., "A New Fast Algorithm for Computing Complex Number-Theoretic Transforms," *Electron. Lett.*, 1977, pp. 278-280.
9. Reed, I. S., and Truong, T. K., "Fast Mersenne-Prime Transforms for Digital Filtering," to be published in *Proceedings IEE*.
10. Agarwal, R. C., and Cooley, J. W., "New Algorithm for Digital Convolution," *IEEE Trans. Acoust. Speech Signal Processing*, Vol. ASSP-25, pp. 392-410, Oct. 1977.
11. Winograd, S., "On Computing the Discrete Fourier Transform," *Proc. Nat. Acad. Sci. USA*, 1976, 73, pp. 1005-1006.
12. Winograd, S., *On Computing the Discrete Fourier Transform*, Research Report, Math. Science Dept., IBM Thomas J. Watson Research Center, Yorktown Heights, New York.
13. Cooley, J. W., and Tukey, J. W., "An Algorithm for the Machine Calculation of Complex Fourier Series," *Math. Comput.*, Vol. 19, pp. 297-301, April 1965.
14. Reed, I. S., Kwoh, Y. S., Truong, T. K., and Hall, E.-L., "X-Ray Reconstruction by Finite Transforms," *IEEE Transactions on Nuclear Science*, Vol. NS-24, No. 1, February 1977.
15. Papoulis, A., *Probability Random Variable Stochastic Processes*, McGraw-Hill Book Co., New York, 1965.

Table 1. Complexity of New Algorithm for the Convolution of Complex Number Points

d	Factors	No. Complex Number Multiplications	No. Complex Number Multiplications of Agarwal and Cooley's Algorithm
120			560
124	4×31	124	
210			1520
244	4×61	244	
248	8×31	248	
420			3800
488	8×61	488	
744	3×248	992	
840			10640
1260			20900
1464	3×488	1952	
2520			58520
3720	$3 \times 5 \times 248$	9920	
7320	$3 \times 5 \times 488$	19520	

Appendix A

A Probabilistic Dynamic Range Constraint for the Transform Over $GF(q^2)$

Let $a_n = \alpha_n + \hat{i}\beta_n$ and $b_n = x_n + \hat{i}y_n$. Then the cyclic convolution of a_n and b_n is given by

$$\begin{aligned} c'_k &= \sum_{n=0}^{d-1} (\alpha_n + \hat{i}\beta_n) (x_n + \hat{i}y_n) \\ &= \sum_{n=0}^{d-1} \mu_n + \hat{i} \sum_{n=0}^{d-1} \nu_n \end{aligned} \quad (\text{A-1})$$

where $\mu_n = \alpha_n x_n - \beta_n y_n$, $\nu_n = \alpha_n y_n + \beta_n x_n$. In many applications, the sequences α_n , β_n , x_n , and y_n can be regarded as mutually independent. With this assumption, consider the sum

$$S_\mu = \sum_{n=0}^{d-1} \mu_n$$

in (A-1). The expected value of μ_n is given by

$$E(\mu_n) = E(\alpha_n) E(x_n) - E(\beta_n) E(y_n)$$

where E denotes the expected value operator. With no loss of generality, the means of α_n , β_n , x_n , and y_n can be assumed to be zero. With these assumptions, $E(\mu_n) = 0$, and the variance σ_μ^2 of μ_n is given by

$$\sigma_\mu^2 = E(\mu_n^2) = E(\alpha_n^2) E(x_n^2) + E(\beta_n^2) E(y_n^2) \quad (\text{A-2})$$

Finally, assume that α_n and β_n are uniformly distributed over the dynamic range A , and that x_n and y_n are uniformly distributed over the dynamic range B .

$$E(\alpha_n^2) = E(\beta_n^2) = \frac{A^2}{12}$$

$$E(x_n^2) = E(y_n^2) = \frac{B^2}{12}$$

Substituting these values in A-2,

$$\sigma_\mu^2 = 2 \cdot \frac{A^2 B^2}{12^2} \quad (\text{A-3})$$

Now by the central limit theorem (Ref. 15), the probability of exceeding a threshold λ is

$$P \left\{ \frac{S_\mu}{\sqrt{d}\sigma_\mu} > \lambda \right\} = 2(1 - \varphi(\lambda))$$

where $\varphi(\lambda)$ is the standard normal distribution. This equation can be written as

$$P \left\{ |S_\mu| > \lambda \sqrt{d}\sigma_\mu \right\} = 2(1 - \varphi(\lambda)) \quad (\text{A-4})$$

To keep S_μ from overflowing, one needs the inequality

$$|S_\mu| \leq \frac{q-1}{2}$$

Hence if one sets

$$\lambda \sqrt{d}\sigma_\mu = \frac{q-1}{2} \quad (\text{A-5})$$

then (A-4) is the probability of overflow.

For example, if $\lambda = 3$, then the probability of overflowing is

$$P \left\{ |S_\mu| > \lambda \sqrt{d\mu} \right\} = 2(1 - \varphi(3)) = 0.0026$$

$$-2^{k_1} \leq \alpha_n, \beta_n \leq 2^{k_1}$$

$$-2^{k_2} \leq x_n, y_n \leq 2^{k_2}$$

which is very small. Substituting (A-3) into (A-5) yields

$$A \cdot B = \frac{6(q-1)}{\sqrt{2d\lambda}} \quad (\text{A-6})$$

the dynamic ranges A and B are 2^{k_1+1} and 2^{k_2+1} , respectively. For most applications the two Mersenne prime $2^{31} - 1$ and $2^{61} - 1$ will provide enough bit accuracy and dynamic range for computing two $2^m \cdot p$ -point sequences of complex numbers. To illustrate this, if d is chosen to be $d = 2^8$, $\lambda = 3$, $q = 2^{31} - 1$ and $k_1 = k_2$, then by (A-6)

$$A = 2^{k_1+1} = \sqrt{\frac{6(q-1)}{\sqrt{2d\lambda}}} \cong 2^{14}$$

Equation (A-6) is the required relation among the parameters A , B , q , d , and λ . Similarly, one obtains the same result defined in (A-6) for the sum

$$S_\nu = \sum_{n=0}^{d-1} \nu_n$$

Thus one needs approximately $k_1 = k_2 = 13$ bits to satisfy (A-4) with an overflow probability equal to 0.0026. This is a considerably better bound than one obtains using formula (5) for A . In fact, the dynamic range constraint (5) yields $A \cong 2^{k_1} = 2^{10}$.

Let 2^{k_1} and 2^{k_2} be binary scale factors for a_n and b_n , respectively. Then since

The Gravitational Wave Detection Experiment: Description and Anticipated Requirements

A. L. Berman
TDA Engineering Office

One of the most exciting challenges facing gravitational theoreticians and experimenters in the remaining decades of this century will be the search for "gravitational waves" as predicted by Einstein's General Theory of Relativity. Proposals have been advanced to search for gravitational waves in ultraprecise two-way Doppler data. In such an experiment, the total measurement system includes the Deep Space Network Tracking System, the spacecraft, the intervening media, and the data processing system. Preliminary estimates of gravitational wave characteristics are used to define a baseline experiment, with a total measurement system fractional frequency fluctuation of 1×10^{-15} , and a desirable experiment, with a total measurement system fractional frequency fluctuation of 1×10^{-17} .

The experiment to detect gravitational waves in ultraprecise two-way Doppler data is described, as are the anticipated requirements for the Deep Space Network, the spacecraft, and the data processing system. The article concludes by describing the steps necessary to provide the capability to perform this experiment.

I. Introduction

One of the most exciting challenges facing gravitational theoreticians and experimenters in the remaining decades of the 20th century will be the attempted detection and measurement of "gravitational waves" as predicted by Einstein's General Theory of Relativity. Gravitational waves are spatial strains propagating at the speed of light which are (expected to be) generated by the violent collapse of stars, star clusters, galaxy cores, quasars, and seyfert galaxies into supermassive black holes (for instance, see Thorne and Braginsky, Ref. 1).

Proposals have been advanced to use "ultraprecise" two-way Doppler data while tracking spacecraft at large distances (i.e., >1 AU) to detect very-low-frequency ($\sim 10^{-3}$ Hz) gravitational waves (for instance, see Davies, Ref. 2, and Estabrook and Wahlquist, Ref. 3). Although such a scheme appears to be one of the more promising suggested, substantial improvements in current Deep Space Network (DSN) and spacecraft performance will have to be achieved, as well as provision of new capabilities, to bring to fruition the utilization of ultraprecise Doppler data in the search for gravitational waves. It is thus the purpose of this article to provide a brief description

of the experiment to detect gravitational waves in ultraprecise Doppler data, and to establish anticipated requirements for the spacecraft, DSN, and subsequent data processing.

II. Definition of "Baseline" and "Desirable" Experiments

As already noted, gravitational waves are expected to be produced by the violent collapse of stellar bodies into supermassive black holes; these waves are expected to be evidenced as spatial strains propagating at the speed of light. Specifically, one expects (Refs. 1 and 3) that the waves will:

- (1) Alter the distance between separated free masses.
- (2) Produce a fractional frequency shift in ultraprecise Doppler data, on the order of the wave amplitude.

Thorne and Braginsky (Ref. 1) have estimated possible gravitational wave characteristics; these are presented in Fig. 1. As can be seen, the wave duration (τ) is proportional to the wave amplitude (h) and the expected ranges of durations and amplitudes¹ are:

$$40 \text{ seconds} < \tau < 40,000 \text{ seconds}$$

$$10^{-17} < h < 10^{-14}$$

In Section III it will be shown that the scheme to utilize ultraprecise Doppler data requires:

$$\tau < \text{Round-Trip-Light-Time (RTLT)}$$

Since the next decade of funded and proposed deep space missions have maximum distances of either Jupiter (Galileo Mission, Solar Polar Mission) or Saturn (Saturn Orbiter Mission), it is immediately apparent from Fig. 1 that one is constrained to search for waves in which the amplitude is $\sim 10^{-15}$ or less. It is also obvious that one would like to search for waves with amplitudes as low as 10^{-17} ($\tau = 40$ seconds). This then motivates the selection of a "baseline" experiment to look for the strongest expected waves, and a "desirable" experiment to search for a wide variety of waves. Using this rationale, and noting that there are stringent requirements throughout the entire measurement system, consisting of

- (1) DSN Tracking System
- (2) Intervening media

- (3) Spacecraft
- (4) Data processing

one proceeds to define the baseline experiment as follows:

- (1) Search for waves with amplitude $h \gtrsim 10^{-15}$.
- (2) Require total measurement system fractional frequency fluctuation ($\sigma(\Delta F/F)$) of 10^{-15} or less.²
- (3) Require each identifiable independent element of the total measurement system to have a fractional frequency fluctuation of 3×10^{-16} or less.³
- (4) Require averaging times (τ_a) between 50 and 5000 seconds.

Similarly, one defines a desirable experiment as follows:

- (1) Search for waves with amplitudes $h \gtrsim 10^{-17}$.
- (2) Require total measurement system fractional frequency fluctuation ($\sigma(\Delta F/F)$) of 10^{-17} or less.
- (3) Require each identifiable independent element of the total measurement system to have a fractional frequency fluctuation of 3×10^{-18} or less.
- (4) Require averaging times (τ_a) between 5 and 5000 seconds.

While it is considered technologically possible to achieve a baseline system in the 1980s, the desirable system may not be achievable until the 1990s, if then.

While fractional frequency fluctuation is most appropriate for the basic description of ultraprecise two-way Doppler (frequency) data, certain elements of the measurement system are more conveniently thought of in terms of phase fluctuation ($\sigma(\Delta\phi)$) or path length fluctuation ($\sigma(\Delta L)$). For the remainder of the article, the following equivalents will be assumed:

$$\sigma(\Delta\phi) = \sigma(\Delta F/F) \cdot d\phi/dt \cdot \tau_a$$

$$\sigma(\Delta L) = \sigma(\Delta F/F) \cdot c \cdot \tau_a$$

²The symbol σ will be used to represent a "generalized" measure of fluctuation which ultimately may be determined to most appropriately be the Allan variance, RMS, etc.

³Since there are numerous independent elements, it is assumed appropriate to require each independent element to be specified at a level one-half order of magnitude below the total measurement system requirement.

¹It should be emphasized that these are *highly tentative* estimates

where

ϕ = phase

F = frequency

t = time

τ_a = averaging time

L = length

c = speed of light

Some typical conversions are

(1) $\sigma(\Delta F/F) = 1 \times 10^{-15}$

τ_a	100 seconds	1000 seconds
$\sigma(\Delta\phi)$, X-band	0.3 deg	3.0 deg
$\sigma(\Delta L)$	0.03 mm	0.3 mm

(2) $\sigma(\Delta F/F) = 1 \times 10^{-17}$

τ_a	100 seconds	1000 seconds
$\sigma(\Delta\phi)$, X-band	0.003 deg	0.03 deg
$\sigma(\Delta L)$	0.0003 mm	0.003 mm

III. Experiment Description

The special feature which allows the usage of ultraprecise Doppler data for the possible detection of gravitational waves is a unique "three-pulse" signature which is a function of the spacecraft, Earth, and gravitational wave propagation direction geometry (Ref. 3). The pulses (fractional frequency shifts) result from effects which are conveniently described as follows:

- (1) "Clock speed-up" (Earth only effect)
- (2) "Buffeting" (equal Earth and spacecraft effect)

Consider a case where θ defines the angle between the gravitational wave propagation direction and the Earth-spacecraft line, as seen in Fig. 2. Clock speed-up is evidenced as pulses of maximum amplitude $-h$ and $+h$ at the time the wave impinges on Earth and a RTLT later, respectively. This is shown schematically in Fig. 3. Similarly, Earth

buffeting is seen as pulses of maximum amplitude $+h \cos \theta$ when the wave impinges on Earth and a RTLT later. In addition, spacecraft buffeting produces a pulse of $-2h \cos \theta$ in the Doppler data a one-way-light-time (OWLT) after the wave strikes the spacecraft. Earth and spacecraft buffeting effects are schematically illustrated in Fig. 4. Finally, combining the clock speed-up and Earth and spacecraft buffeting effects, one obtains the unique three-pulse signature which is expected to be seen in ultraprecise two-way Doppler data. The characteristics of this signature are as follows:

- (1) Pulse amplitudes
 - (a) $h(\cos \theta - 1)$
 - (b) $h(-2 \cos \theta)$
 - (c) $h(\cos \theta + 1)$
- (2) Pulse separation times (r = Earth-spacecraft distance)
 - (a) $\frac{r}{c}(1 + \cos \theta)$
 - (b) $\frac{r}{c}(1 - \cos \theta)$

Figure 5 schematically demonstrates the combination of clock speed-up and buffeting effects for $\theta = 60$ degrees.

Finally, it is noted that the above exercise is for a single spacecraft measurement. Should dual spacecraft measurements be made, one could obtain the two-dimensional propagation direction of the gravitational wave — certainly a most valuable bit of additional information.

IV. Anticipated Gravitational Wave Detection Experiment Requirements

The major categories identified as constituents of the gravitational wave detection measurement system are:

- (1) DSN Tracking System
- (2) Intervening media
- (3) Spacecraft
- (4) Data processing

In general, requirements are necessary for multiple independent elements in each category. As already noted, each independently identifiable element will be "specified" at a performance level 1/2 order of magnitude better than the entire system requirement, under the assumption that they will combine in a fashion similar to root-sum-square. Each major category is discussed below.

A. DSN Tracking System

The central element of the DSN Tracking System is obviously the frequency standard of the DSS Frequency and Timing Subsystem. The performance of the new hydrogen masers currently being implemented is considered to be

$$\sigma(\Delta F/F) \approx 3 \times 10^{-15}$$

$$\tau_a > 100 \text{ seconds}$$

so that a decrease of about an order of magnitude will be required to achieve the baseline experiment defined in Section II:

$$\sigma(\Delta F/F) = 3 \times 10^{-16}$$

$$50 \text{ seconds} < \tau_a < 5000 \text{ seconds}$$

Numerous other DSN Tracking System elements will have to be evaluated as to their current performance, and the technology developed to obtain the desired frequency stability. Below are listed the various pertinent subsystems, with the appropriate performance parameter indicated in parentheses:

- (1) DSS Frequency and Timing Subsystem (Frequency)
 - (a) Hydrogen maser (or other frequency standard)
 - (b) Frequency distribution
- (2) DSS Receiver-Exciter Subsystem (Phase)
 - (a) Closed-loop receiver
 - (b) Doppler extractor
 - (c) Exciter
- (3) DSS Tracking Subsystem (Phase)
Metric Data Assembly
- (4) Antenna Mechanical Subsystem (Length)
- (5) Antenna Microwave Subsystem (Phase)
- (6) Transmitter Subsystem (Phase)
- (7) System Cabling (Frequency)

Table 1 summarizes the required performance for the above elements for both the baseline and desirable experiment cases.

B. Intervening Media

In passing between the Deep Space Station (DSS) and spacecraft, the signal passes through the following interactive media:

- (1) Solar Wind (dispersive)
- (2) Troposphere (neutral)
- (3) Ionosphere (dispersive)

In the discussion to follow, the ionosphere, consisting of charged particles, will be considered jointly with the similar, but generally much larger effect of the Solar Wind.

- (1) Solar Wind. The Solar Wind effect on the gravitational wave detection experiment has been explored in detail in a previous article (Ref. 4). The results from Ref. 4 are summarized as follows (for $\tau_a = 1000$ seconds):
 - (a) Current S-band (both uplink and downlink) Solar Wind limitation:

$$\sigma(\Delta F/F) = 3 \times 10^{-13}$$

- (b) Expected optimum X-band (uplink and downlink) Solar Wind limitation:

$$\sigma(\Delta F/F) = 1 \times 10^{-14}$$

It is a major conclusion of Ref. 4 that to achieve a Solar Wind fractional frequency fluctuation of $\sigma(\Delta F/F) = 3 \times 10^{-16}$, one would require simultaneous S- and X-band uplink and downlink frequency band capability. To achieve the desirable experiment level (3×10^{-18}), it is speculated that the spacecraft will require sophisticated new capabilities, such as an onboard frequency standard and a Doppler counter.

- (2) "Wet" Troposphere. An extremely preliminary estimate (Ref. 5) for the wet troposphere at an elevation of 30 degrees (20 cm total signal retardation assumed) and an averaging time $\tau_a = 1000$ seconds is:

$$\sigma(\Delta L/L) \approx 1 \times 10^{-14}$$

It is considered that to meet the baseline experiment requirements, water vapor radiometer calibration of the wet component of the troposphere will be required. For the desirable experiment level, new spacecraft capabilities are envisioned.

- (3) “Dry” Troposphere. Again, an extremely preliminary estimate (Ref. 5) for the dry troposphere at an elevation of 30 degrees (400 cm total signal retardation assumed) and an averaging time $\tau_a = 1000$ seconds is:

$$\sigma(\Delta L/L) \approx 7 \times 10^{-15}$$

It is considered that to meet the baseline experiment requirements, extremely accurate surface barometric pressure calibration of the dry component of the troposphere will be required.

Media calibration capabilities required for the baseline and desirable experiment are summarized in Table 2.

C. Spacecraft

Similarly to the DSN Tracking System, individual critical path elements within the Spacecraft Radio Subsystem, such as the receiver, transponder, transmitter, need to be specified at $\sigma(\Delta F/F)$ levels of 3×10^{-16} and 3×10^{-18} for the baseline and desirable experiments, respectively.

D. Data Processing

Data processing numerical accuracies will need to be commensurate with the $\sigma(\Delta F/F)$ levels of 3×10^{-16} and 3×10^{-18} for the baseline and desirable experiments, respectively. Translated into units of cycles, the appropriate requirements for data processing numerical accuracies are as follows:

- (1) Baseline Experiment
 - (a) S-band — 3×10^{-5} cycle $\cdot (\tau_a/50)$
 - (b) X-band — 1×10^{-4} cycle $\cdot (\tau_a/50)$
- (2) Desirable Experiment
 - (a) S-band — 3×10^{-8} cycle $\cdot (\tau_a/5)$
 - (b) X-band — 1×10^{-7} cycle $\cdot (\tau_a/5)$

V. Discussion and Summary

In order to progress towards a gravitational wave detection capability in regard to the proposed usage of ultraprecise Doppler data, a series of actions will need to be undertaken, as follows:

- (1) Development of gravitational wave detection experiment “drivers,” such as:
 - (a) $\sigma(\Delta F/F) = 3 \times 10^{-16}$ frequency standard
 - (b) X-band uplink capability
- (2) Identification of all critical path elements in the Spacecraft and DSN Tracking System, including evaluation of current frequency stability performance and development of the appropriate technology to achieve a fractional frequency fluctuation of 3×10^{-16} .
- (3) Additional study of the fractional length fluctuation of the troposphere, and development of the appropriate tools necessary to calibrate the troposphere to $\sigma(\Delta L/L) = 3 \times 10^{-16}$.

Prior to obtaining a total measurement system of $\sigma(\Delta F/F) = 1 \times 10^{-15}$, it is suggested that “demonstrations” in the early 1980s might be possible at about the $\sigma(\Delta F/F) \approx 1 \times 10^{-14}$ level. Significant features of such a demonstration would be:

- (1) $\sigma(\Delta F/F) \approx 3 \times 10^{-15}$ frequency standard^a
- (2) X-band uplink and downlink

Possible missions for such a demonstration would be the Solar Polar and the Galileo missions.

References

1. Thorne, K. S., and Braginsky, V. B., "Gravitational-Wave Bursts from Nuclei of Distant Galaxies and Quasars: Proposal for Detection Using Doppler Tracking of Interplanetary Spacecraft," *The Astrophysical Journal*, Volume 204: L1-L6, February 15, 1976.
2. Davies, R. W., "Issues in Gravitational Wave Detection With Space Missions," *Transactions of the International Conference on Gravitational Waves and Radiations*, Paris, 1973.
3. Estabrook, F. B., and Wahlquist, H. D., "Response of Doppler Spacecraft Tracking to Gravitational Radiation," *General Relativity and Gravitation*, Volume 6, No. 5, 1975.
4. Berman, A. L., "Solar Wind Density Fluctuation and The Experiment to Detect Gravitational Waves in Ultraprecise Doppler Data," in *The Deep Space Network Progress Report 42-44*, Jet Propulsion Laboratory, Pasadena, California, 15 April 1978.
5. Private communication, S. D. Slobin.

Table 1. Required performance summary

Element	Baseline Experiment Requirement	Desirable Experiment Requirement
Total system, $\sigma(\Delta F/F)$	1×10^{-15}	1×10^{-17}
DSN Tracking System, $\sigma(\Delta F/F)$	$< 1 \times 10^{-15}$	$< 1 \times 10^{-17}$
Averaging time, seconds	$50 < \tau_a < 5000$	$5 < \tau_a < 5000$
Frequency and Timing Subsystem		
Frequency standard (H_2 maser), $\sigma(\Delta F/F)$	3×10^{-16}	3×10^{-18}
Frequency distribution, $\sigma(\Delta F/F)$	3×10^{-16}	3×10^{-18}
Receiver-Exciter Subsystem		
Closed-loop receiver, $\sigma(\Delta\phi)$, X-band	$0.05^\circ \cdot \{\tau_a/50\}$	$0.00005^\circ \cdot \{\tau_a/5\}$
Doppler extractor, $\sigma(\Delta\phi)$, X-band	$0.05^\circ \cdot \{\tau_a/50\}$	$0.00005^\circ \cdot \{\tau_a/5\}$
Exciter, $\sigma(\Delta\phi)$, X-band	$0.05^\circ \cdot \{\tau_a/50\}$	$0.00005^\circ \cdot \{\tau_a/5\}$
Antenna Mechanical Subsystem, $\sigma(\Delta L)$	$0.005 \text{ mm} \cdot \{\tau_a/50\}$	$0.000005 \text{ mm} \cdot \{\tau_a/5\}$
Antenna Microwave Subsystem, $\sigma(\Delta\phi)$, X-band	$0.05^\circ \cdot \{\tau_a/50\}$	$0.00005^\circ \cdot \{\tau_a/5\}$
Transmitter Subsystem, $\sigma(\Delta\phi)$, X-band	$0.05^\circ \cdot \{\tau_a/50\}$	$0.00005^\circ \cdot \{\tau_a/5\}$
System cabling, $\sigma(\Delta F/F)$	3×10^{-16}	3×10^{-18}
Data processing software		
Numerical accuracy, X-band	$1 \times 10^{-4} \text{ cycle} \cdot \{\tau_a/50\}$	$1 \times 10^{-7} \text{ cycle} \cdot \{\tau_a/5\}$
Spacecraft		
Radio Subsystem, $\sigma(\Delta F/F)$	3×10^{-16}	3×10^{-18}

ORIGINAL PAGE IS
OF POOR QUALITY

Table 2. Required capabilities summary

Media Effect	Baseline Experiment Requirement	Desirable Experiment Requirement
Solar Wind		
• DSN	Receive and transmit simultaneous S- and X-band	Multiple one-way and two-way Doppler links
• Spacecraft	Receive and transmit simultaneous S- and X-band	On-board frequency standard and Doppler counter; Multiple one-way and two-way Doppler links
Wet troposphere		
• DSN	Water vapor radiometer	Multiple one-way and two-way Doppler links
• Spacecraft		On-board frequency standard and Doppler counter; Multiple one-way and two-way Doppler links
Dry troposphere		
• DSN	Surface barometric pressure	Multiple one-way and two-way Doppler links
• Spacecraft		On-board frequency standard and Doppler counter; Multiple one-way and two-way Doppler links

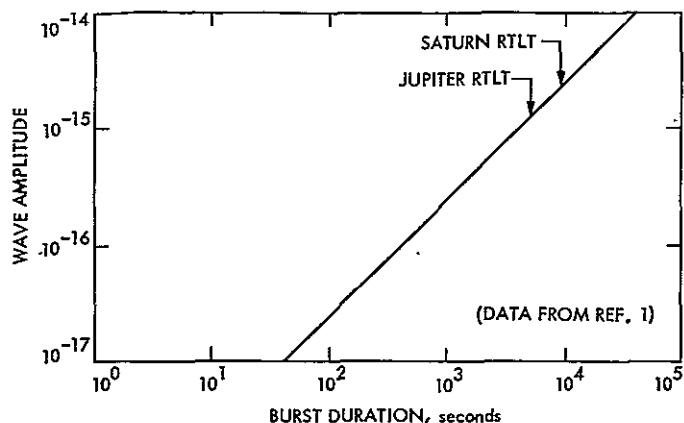


Fig. 1. Relationship between gravitational wave amplitude and burst duration

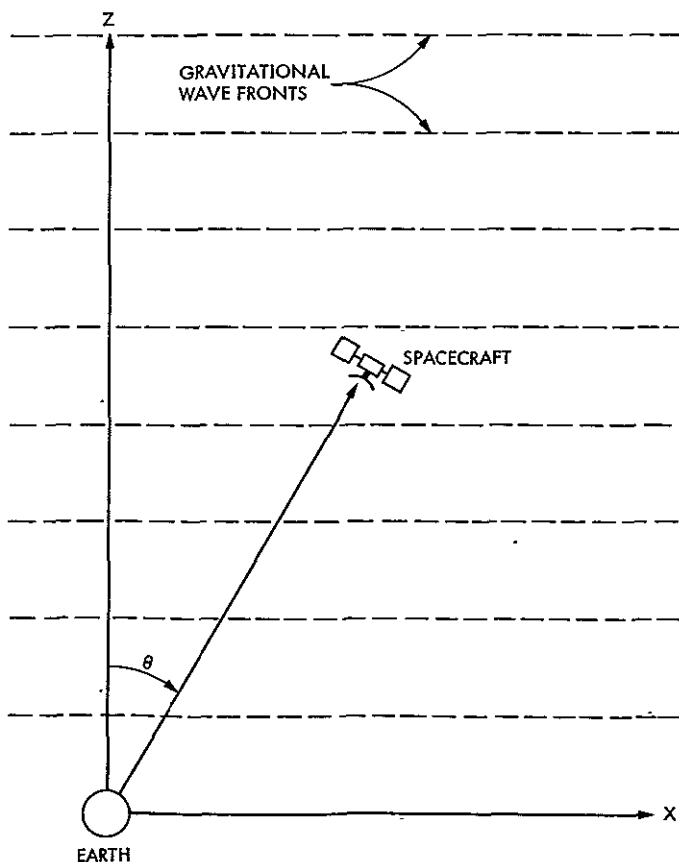


Fig. 2. Gravitational wave geometry

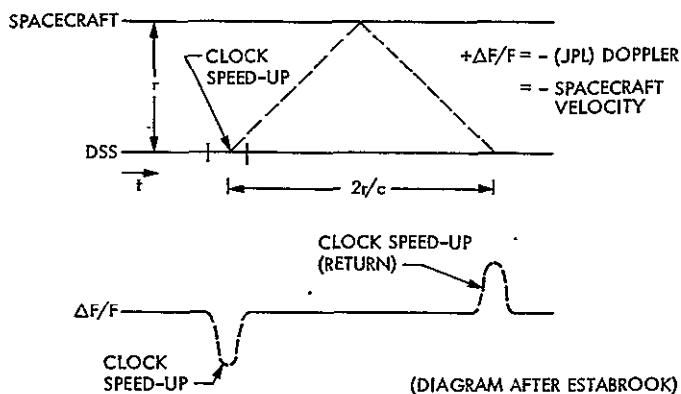


Fig. 3. Clock speed-up signature in ultraprecise Doppler data

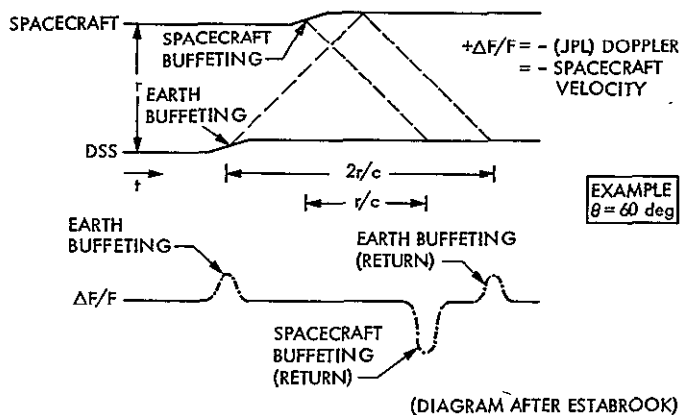


Fig. 4. Earth and spacecraft buffeting signature in ultraprecise Doppler data

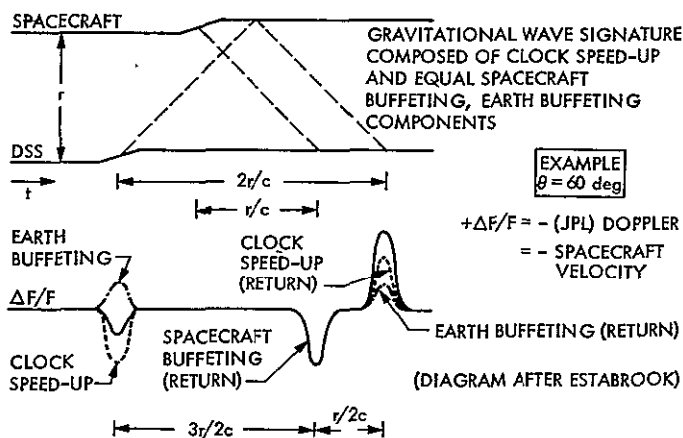


Fig. 5. Unique gravitational wave signature in ultraprecise Doppler data

ORIGINAL PAGE IS OF POOR QUALITY

D, 8-114
33-09C

N78-32155

Preliminary Analysis of the Impact of Power Cycling on CTA-21 Equipment Reliability

E. R. Cole
DSN Engineering Section

This article presents the preliminary findings of a study being made at CTA-21 to determine whether Deep Space Station control room equipment power may be turned off to conserve energy. The results of reliability analysis indicate that there may be some correlation between the observed increase in failure rate and cycling of equipment power in the eight-month study period.

I. Introduction

The DSN Energy Conservation Project has been investigating modifications to Deep Space Stations at Goldstone, California, in regard to energy conservation and cost reduction. One of these modifications is to selectively turn off certain electronic equipment during periods of nonuse or low activity. Significant energy savings are expected to result, especially when equipment control is automated in the future via the computer-based Utility Control System. However, a key question in considering this procedure is whether cycling of electrical power will change equipment reliability and thus impact DSN maintenance and operations activities or cost.

The DSN Equipment Compatibility Test Area (CTA-21) at JPL, Pasadena, was selected as a test site. This is the CTA-21 control room in building 125 where electronic and air conditioning equipment is presently turned off on weekends. The use of the CTA-21 control room provides field observations of equipment reliability under conditions closely representing a Deep Space Station's environment.

Tentatively the study is divided into two phases. Phase one, which is the substance of this article, consists of data collection and performance of a preliminary analysis. It covers the period of April through November 1977, examining overall failure trends. Phase two is a detailed correlation analysis of failures with possible causes. Each phase will be discussed in detail later.

II. Field Observations and Data Collection

After examining CTA-21 past failure and maintenance records, it was decided that the existing records were not of sufficient detail or comprehensiveness to support the study. Therefore, in conjunction with CTA-21 management and staff, a special equipment event log was implemented. This form, as shown in Fig. 1, provides both the DSN Energy Conservation Project and CTA-21 with an unique source of information consisting of:

- (1) Equipment failures, including references to equipment event reports (EER's) when applicable

- (2) Power turnoff periods
- (3) Commercial power outages
- (4) Air handler failures
- (5) High ambient control room temperatures
- (6) Equipment modifications through engineering change orders (ECO's)
- (7) Other installations, removals, calibrations, and maintenance

The log utilizes two coding groups to assist in data processing and interpretation. The first group is the event code, which specifically identifies the nature of the event reported. The second group code provides categorization of the type of equipment involved. The equipment event log serves not only the purposes of the study but also makes available to CTA-21 management and engineering a useful maintenance record. Since outstanding events are referenced in subsequent order in the log, relevant actions can be traced and monitored for optimum performance.

The equipment at CTA-21 represents nearly ninety percent of the equipment located in the control room of a typical Deep Space Station. At times, this consists of over one hundred individual cabinets of widely varying types of electronic equipment. Therefore, the equipment was divided into ten system categories to simplify analysis:

- (1) Telemetry
- (2) Communication
- (3) Radio frequency
- (4) Command
- (5) Monitor and control
- (6) Radio metric
- (7) Simulation and test
- (8) Timing
- (9) Facility
- (10) Software

No special turnoff procedure is used at CTA-21. However, individual cabinets and systems are turned off in no particular sequence before general power is removed. The control room air handlers are allowed to run an additional thirty minutes after equipment turnoff to remove residual heat. This procedure was initiated when a significant rise in temperature-related failure rates was noted prior to the preliminary study period. Likewise, individual equipment is turned on after general power is restored.

III. Data Study and Analysis

Initial CTA-21 equipment event data have been processed for the thirty-four-week period from April 4, 1977, until November 23, 1977, and were divided into seven subperiods designated as either "experimental" or "control" periods.

Experimental periods are defined as those time intervals during which equipment power was turned off on weekends. That is, those contiguous groups of weeks where equipment power is off for nominally two days (weekends) and equipment power is on for five days. In control periods, the power was on all seven days of the week. The control periods, listed in Table 1, start with a weekend during which power was left on and cover the period until power is next turned off.

Only failure and power turnoff events were included in this preliminary phase one analysis. No attempt was made to determine possible causes of individual failures. Turnoff of power at CTA-21 is conducted on a noninterference basis with the operations schedule, which leads to widely varying study period lengths. The statistics of hourly failure frequency (or rate) was computed to allow comparison of control and experimental study periods.

The distribution of daily failure rates occurring in each subperiod over the entire study period is shown in the time-line bar charts in Fig. 2. The time-line bar chart was produced to reveal any significant distribution patterns, and to display overall trend. Tables 1 and 2 compare failure rates to indicate any significant effect of power turnoff on equipment reliability.

IV. Results of the First Phase Study

Inspection of the above time-line bar chart does not directly indicate any particular repetitive pattern. However, the overall 34-week failure trend was downward as shown by Table 1. Furthermore, the failure rates in both period types decreased over the duration of the study. One explanation could be that turning off equipment power over long time periods extends equipment life and is manifest in lowered failure rates. Other possibilities include reduced station activity and unreported failures. These hypotheses will be examined in more detail during the second phase.

Table 1 indicates that failure rate increased during periods of weekend power turnoff, and that the overall experimental period failure rate exceeds the aggregate control period failure rate by 73%. Table 2 shows that the majority of failures occurred in the telemetry and communication systems equipment. However, the greatest sensitivity to power turnoff was exhibited in the monitor and control system, although all systems show an increase in failure rate during experimental periods.

Figure 3 shows the time distribution density of failures as a function of elapsed time. The distribution for control periods exhibits a somewhat uniform density with considerable random variation. Since CTA-21 is normally manned during the

week, usually no observations are made of failures that occur on weekends. They are reported when discovered during the five-day work week. This explains the marked decrease in failures on weekends. The distribution of failures after power turnoff shows an apparent 2.5-day cycle of unknown significance, whereas a simple "one cycle" exponential distribution would tend to suggest a strong relationship between equipment failure and power turnoff. This phenomenon will be further explored in detail during phase two of the study.

V. Significance of Results

The initial phase of this study shows an increase in failure rate during weekend turnoff periods. However, the results are based on only 282 failures occurring over 34 weeks. The adequacy of the data sample was tested, and data confidence intervals were determined to the 95% confidence level as shown in Table 3.

The resulting confidence intervals indicate that the computed failure rates are at best rough approximations. With an objective of reaching a 20% confidence interval ($\pm 10\%$ confidence limit) it was determined that a possible 13 additional months of data would be required. Since new data may have a major effect upon final results, conclusions at this stage are undecided.

The next phase of study not only will benefit from a larger data base, but also detailed correlation analysis will be performed. Correlation analysis will indicate relationships between failures and other events such as air handler malfunctions, high ambient temperatures, equipment modifications, life-cycle, etc. Failures thus identified may be eliminated from data being investigated for relationships to turnoff periods. The objective of phase two will be to identify equipment that is sensitive to power turnoff, thereby providing a criterion by which electronic equipment may be selectively chosen for power shutoff to conserve energy.

Acknowledgement

The cooperation and assistance of G. H. Winn and A. Salazar of CTA-21 in making this study are acknowledged.

Table 1. Total CTA-21 failure rate for 34-week study period

Period type	Weeks	Failures	Total hours	Pwr on hours	Failures/hour	
					Control	Expt
Control 1 ^a	8	72	1344	1344	0.0536	
Expt 1 ^b	8	91	1344	875		0.1040
Control 2	6	52	984	984	0.0528	
Expt 2	5	29	864	563		0.0515
Control 3	2	11	336	336	0.0327	
Expt 3	1	7	168	118		0.0596
Control 4	4	20	624	624	0.0321	
Total percentage	34	282	5664	4844	0.0471 100%	0.0816 173.1%

^aControl periods (eqpt. not turned off): 1. April 2–May 27, 2. July 23–September 1; 3. October 8–October 21; 4. October 29–November 23.

^bExperimental periods (eqpt. turned off on weekends): 1. May 28–July 22; September 2–October 7; 3. October 22–October 28.

Table 2. Failure rates for the ten system categories

System	Failures	Percent of total	Failures/hour		Percent difference
			Control period	Expt period	
Telemetry	85	30.1	0.0143	0.0244	70.8
Communication	58	20.6	0.0110	0.0141	29.1
RF	34	12.1	0.0058	0.0096	66.8
Command	31	11.0	0.0055	0.0084	52.6
Monitor	31	11.0	0.0040	0.0116	192.6
Metric	16	5.7	0.0024	0.0052	111.3
Simulation	14	5.0	0.0024	0.0051	58.5
Timing	11	3.9	0.0015	0.0039	153.6
Facility	2	0.7	0.0003	0.0006	111.3
Software	0	NA	NA	NA	NA
Total	282	100%	0.0471	0.0816	+73.1%

Table 3. Data confidence and sample adequacy

Period type	Failures/hour	Confidence interval	
		Limit	% of rate
Control 1	0.0536	±0.0152	±28.5%
Expt 1	0.1040	0.0260	25.0
Control 2	0.0528	0.0167	31.5
Expt 2	0.0515	0.0232	45.1
Control 3	0.0327	0.0269	82.1
Expt 3	0.0596	0.0222	37.4
Control 4	0.0321	0.0161	50.4
Total control	0.0471	±0.0090	±19.1%
Total expt.	0.0816	±0.0174	±21.4%

ORIGINAL PAGE IS
OF POOR QUALITY

EQUIPMENT EVENT LOG

STATION: CTA-21

DATE: 8/01/77 DAY: MON

EVENT CODE:

B = BROKEN E = ECO M = MISC
C = CALIBRATION F = FAILURE
D = DEFECTIVE I = INTERMITTENT

GROUP CODE:

A = ANALOG FAC = FACILITIES
CA = CABLES L = LOGIC P = PWR SUPPLY
CO = CONNECTOR M = MECH O = OTHER

LOG NO. REF. DATE	GMT	EQUIPMENT	EER #	WA	EVENT CODE	GROUP CODE	HISTORY LOG	DESCRIPTION OF EVENT	ACTION
1229 6/26	1900	CPA 1			F	L	CMD	SIA #17 (UNUSED PORT) FAILED WRAPAROUND TEST	
1230 6/10	2130	PRA COMP INTERFACE			F	L/O	METRIC	COMPUTER INTERFACE FAILED WRAP- AROUND TEST	UNIT FROM 14, WORKED ON BY DAVIES (SPARE)
1231 6/30	1930	COMM BUFF 3			F	L/O	COMM	CB#3 DF LIGHT FAILS TO LIGHT. UNIT APPEARS TO PASS DATA PROPERLY	LED ON ORDER 07/29/77
1232 7/17	1400	DIS 1 MAG TAPE			C	A	MONITOR	READ ERROR ON BOTH MAG TAPE UNITS	MASTER OK
1233 7/21	1800	DIS 2 LP			F	L	MONITOR	L/P INOPERATIVE	
1234 7/21	1100	COMM BUFF 2			E	L/O	COMM	ECO 77.177 STARTED	
1235 7/21	0300	TPA 3 SEQ DECODER			F	L	TELEM	SEQ DECODER INOPERATIVE	
1236 08/01	1400	TCP PAPER PUNCH	38550		F	L/O	TELEMETRY	UNABLE TO PUNCH TAPE, ERRATIC	CORRECTED
1237 8/01	1430	CMF VARIAN			M	O	COMM	PREVENTIVE MAINT. PERFORMED ON PRINTER/PLOTTER	
1238 8/01	1500	TCP PHOTO READER	38549		F/I	L/O	TELEMETRY	ERROR IN LOADING PROGRAMS	CORRECTED
1239 8/01	1530	MDA OPS. SW.	38552		E	O	SOFTWARE	RECEIVED LATEST VERSION OF PROGRAM. DMK-5106-OP-B	ERROR TO ECO 76,042
1240 8/01	2000	RF LINK	38551		E	FAC/O	RF	CLOSEOUT OF ECO 77.027. INSTALL RF LINK JPL TO HUGHES	

Fig. 1. CTA-21 equipment event log

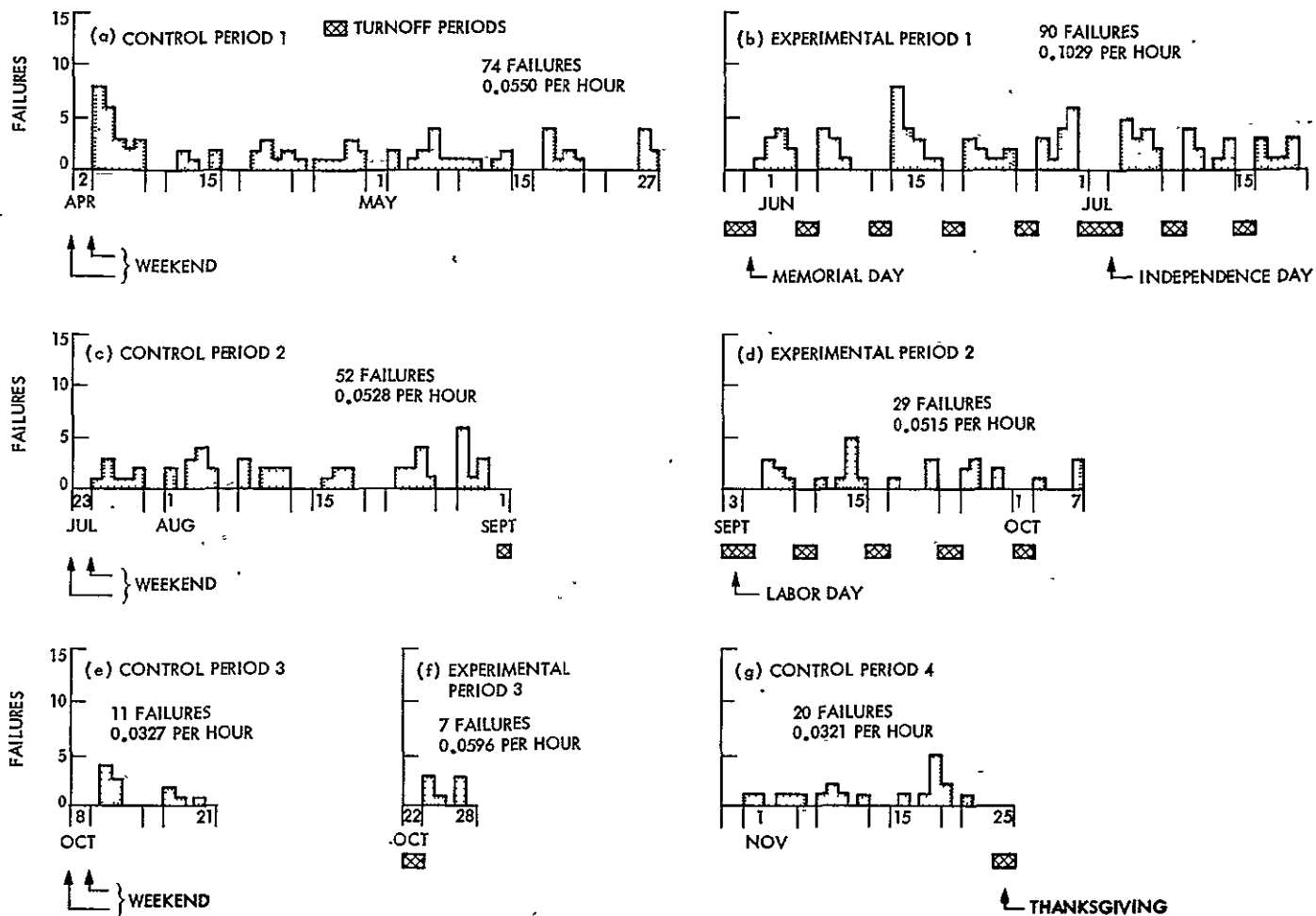


Fig. 2. CTA-21 equipment failure time-line chart

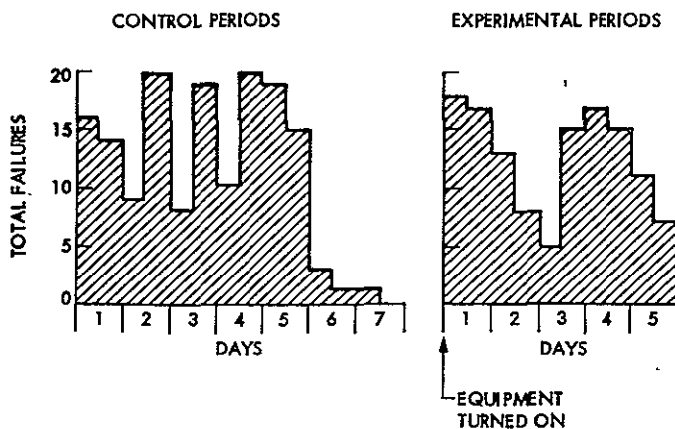


Fig. 3. Time distribution of CTA-21 failures for first phase data (April - November 1977)

311-142
 32-176

The DSS Radio Science Subsystem — Data Handling of Very Long Baseline Interferometry (VLBI) Data

A. L. Berman
 TDA Engineering Office

The DSS Radio Science Subsystem, originally implemented to provide the data handling capabilities for the DSN Radio Science System, will be modified and augmented to provide similar capabilities for the newly created DSN Very Long Baseline Interferometry (VLBI) System. This article describes the key characteristics, functional requirements, and operation of the DSS Radio Science Subsystem (DRS) as they pertain to usage of the DRS by the DSN VLBI System.

I. Introduction

The DSN Very Long Baseline Interferometry System was recently instituted as a DSN data system, following a successful review of DSN VLBI System requirements on February 28, 1978. Very Long Baseline Interferometry is a method of measuring the difference in the time of arrival of a signal produced by a distant natural radio source at two or more mutually distant antennas via simultaneous signal reception and recording. Because of the difference in signal ray paths between the antennas, the signal will evidence small time delays in reception between any pair of antennas. By cross correlating the recorded signals, the time delay and its derivative may be established for each pair of antennas. Because the natural radio source is extragalactic, and hence can be considered a fixed object, the measured time delay and its derivative provide information on the earth's motion and the baseline vectors between the various antennas. The DSN intends to use VLBI to determine Universal Time one (UT1; the instantaneous rotational angle of the earth), polar motion, and the relative positions of the Deep Space Stations (DSS), as

well as the time offsets and rates of change between the various DSS clocks.

The DSN VLBI System will be a phased implementation with the first two phases identified as "Block 1" and "Block 2." Block 1 VLBI will provide for clock synchronization between the DSS and is characterized by usage of strong radio sources and a relatively low data rate of 500 kbits/s. Block 2 VLBI will provide the radio source catalog for Block 1 operations, as well as the earth motion and baseline vector parameters required for the Block 1 data processing. Block 2 VLBI can operate with weak radio sources as well as strong sources, and is characterized by a relatively high data rate of 32 Mbits/s.

The DSS Radio Science Subsystem provides the data handling capabilities for the recently created DSN Radio Science System, and was described in detail in a previous article (Ref. 1). VLBI data is quite similar to radio science data in that both are generated via open loop receivers, and hence

the DSS Radio Science Subsystem will be modified and augmented to additionally provide the data handling capabilities for the DSN VLBI system. This article provides a description of the key characteristics, functional requirements, and operation of The DSS Radio Science Subsystem in specific regard to DRS usage by the DSN VLBI System.

II. Functional Description of the DSS Radio Science Subsystem

A. Definition

The DSS Radio Science Subsystem, an integral element of the DSN VLBI System, performs the following functions:

- (1) Receives, digitizes and records narrowband open-loop receiver data, and transmits via wideband data line to the Network Operations Control Center (NOCC).
- (2) Receives, digitizes and records wideband open-loop receiver data, and transmits via magnetic tape to the NOCC.
- (3) Receives calibration and ancillary data and transmits in real-time via High-Speed Data Line (HSDL) to the NOCC.

DSS Radio Science Subsystem functions and interfaces are shown in Fig. 1, while Fig. 2 presents functions and data flow.

B. Key Characteristics

tem are listed below for functions of the Occultation Assembly (ODA) and the Digital Recording Assembly (DRA).

- (1) VLBI Block 1 (ODA) Key Characteristics
 - (a) Hardware and software compatibility with the DSN Mark III configuration.
 - (b) A to D conversion of narrowband open-loop receiver data with 1-bit quantization.
 - (c) Total data rate of 500 kbits/s.
 - (d) Merging of open-loop receiver data with calibration and ancillary data ("VLBI data") in real-time.
 - (e) Reconstruction of analog signals for verification of calibration tones.
 - (f) Temporary storage of VLBI data on magnetic tape at the DSS with subsequent transmission via Wideband Data Line (WBDL) to the NOCC.
 - (g) Real-time transmission of VLBI calibration and status data to NOCC via High-Speed Data Line.

- (2) VLBI Block 2 (DRA) Key Characteristics

- (a) Hardware compatibility with the DSN Mark III configuration.
- (b) Provision for recording eight wideband open-loop receiver channels of 4 Mbit/s data rate each.
- (c) Provision for time tagging of recorded data to one microsecond or better resolution.
- (d) Reconstruction of analog signal for verification of calibration tones.
- (e) Automated control of the DRA by the ODA.

C. Functional Operation

1. VLBI Block 1 Phase 1. Natural radio source signals are received by the Block IV closed-loop receivers and processed by the Advanced System Equipment (ASE). Multiplexed signals from the ASE are received by the VLBI Converter Subassembly and digitized. The ODA Modcomp Computer receives the data from the VLBI Converter Subassembly and records it on magnetic tape. Concurrently, the ODA receives calibration and ancillary data from the DSS Tracking Subsystem (DTK). In real-time the ODA formats the calibration and ancillary data for HSDL transmission to the NC Radio Science Subsystem (NRS) via the Communications Monitor and Formatter (CMF). Post pass, the ODA formats the digitized receiver data, calibration data, and ancillary data for Wideband Data line transmission to the GCF Data Records Subsystem. During VLBI operations, a reconstructed analog signal is passed to the Spectrum Signal Indicator (SSI) for verification.

The DSS is configured and controlled by the DSS Monitor and Control Subsystem (DMC), while the DRS status is routed to both the DMC and NRS. Figure 3 presents a functional block diagram of the ODA while performing VLBI Block 1 Phase 1 operations.

2. VLBI Block 1 Phase 2. Natural Radio source signals are received by the Wideband Multi-mission Receiver (MMR) and pass through VLBI Intermediate Frequency (IF) Converters. The ODA configures both the VLBI IF Converters (Bandwidth selection) and the Wideband MMR synthesizer (fixed frequency information). From the VLBI IF converters, the signals are received by the VLBI Converter Subassembly, where they are multiplexed and digitized. The Occultation Data Assembly Modcomp computer receives the data from the VLBI Converter Subassembly and records it on magnetic tape. Concurrently, the ODA receives calibration and ancillary data from the DSS Tracking Subsystem (DTK). In real-time the ODA formats the calibration and ancillary data for High-Speed Data transmission to the NC Radio Science Subsystem via the Communications Monitor and Formatter. Post pass, the ODA

formats the digitized receiver data, calibration data, and ancillary data for Wideband Data line transmission to the GCF Data Records Subsystem. During VLBI operations, a reconstructed analog signal is passed to the SSI for verification of the calibration tones in the recorded receiver data. The DSS Radio Science Subsystem is configured and controlled by the DSS Monitor and Control Subsystem, while DRS status is routed to both the DMC and NRS. Figure 3 presents a functional block diagram of the ODA while performing VLBI Block 1 Phase 2 operations.

3. **VLBI Block 2.** Natural radio source signals are received by the Wideband Multi-mission Receiver and pass through VLBI Intermediate Frequency Converters. The ODA configures both the VLBI IF Converters (Bandwidth selection) and the Wideband MMR synthesizer (fixed frequency information). From the VLBI IF converters, the signals are received by the VLBI Converter Subassembly, where they are multiplexed and digitized. The Digital Recording Assembly receives the data from the VLBI Converter Subassembly and records it on magnetic tape. The DRA is controlled by the ODA; for example, recording is halted during slew between radio sources. Concurrently, the ODA receives and records calibration and ancillary data from the DMC. These data are formatted for HSDL transmission to the NRS via the CMF. During VLBI operations, a reconstructed analog signal is passed to the SSI for verification of the calibration tones in the recorded receiver data. The DRS is configured and controlled by the DMC, while DRS status is routed to both the DMC and NRS. Post pass, the DRA and ODA recorded tapes are shipped via Network Information Control (NIC) to the Network (NWK) VLBI Processor Subsystem. Figure 4 presents a functional block diagram of the DRA while performing VLBI Block 2 operations.

III. Functional Requirements of the DSS Radio Science Subsystem

A. Functional Requirements for Block 1 VLBI (ODA)

Block 1 VLBI system requirements on the ODA are as follows:

- (1) 250 kHz bandwidth
- (2) 1 bit/sample
- (3) 500 kbit/s data rate
- (4) 10^9 bits data volume
- (5) 1×10^{-6} bit error rate

- (6) 2-nanosecond maximum sampling jitter of any bit with respect to station reference
- (7) 10-microsecond time tag accuracy

B. Functional Requirements for Block 2 VLBI (DRA)

Block 2 VLBI system requirements on the DRA are as follows:

- (1) 8 parallel channels
- (2) 2 MHz bandwidth/channel
- (3) 1 bit/sample
- (4) 32 Mbit/s data rate
- (5) 5×10^{12} bits data volume
- (6) 1×10^{-6} bit error rate
- (7) 2-nanosecond maximum sampling jitter of any bit with respect to station reference
- (8) 5-microsecond time tag accuracy
- (9) Control of the DRA by the ODA

IV. DRS Planned Implementation Schedule

The planned implementation dates for the various DRS capabilities are presented below:

VLBI Block 1 Phase 1

(Includes VLBI Converter Subassembly, modification of ODA hardware and software, DTK interface, wideband interface.)

DSS 14	July 1, 1979
DSS 43	July 1, 1979
DSS 63	July 1, 1979

VLBI Block 1 Phase 2

(Includes MMR interface and ODA software modifications.)

DSS 14	July 1, 1980
DSS 43	July 1, 1980
DSS 63	July 1, 1980

VLBI Block 2

(Includes modification of DRA, ODA, VLBI Converter Subassembly, and DMC interface.)

DSS 14	April 1, 1981
DSS 43	April 1, 1981
DSS 63	April 1, 1981

Reference

1. Berman, A. L., "The DSS Radio Science Subsystem – Real-Time Bandwidth Reduction and Wideband Recording of Radio Science Data," in *The Deep Space Network Progress Report 42-44*, Jet Propulsion Laboratory, Pasadena, California, April 15, 1978.

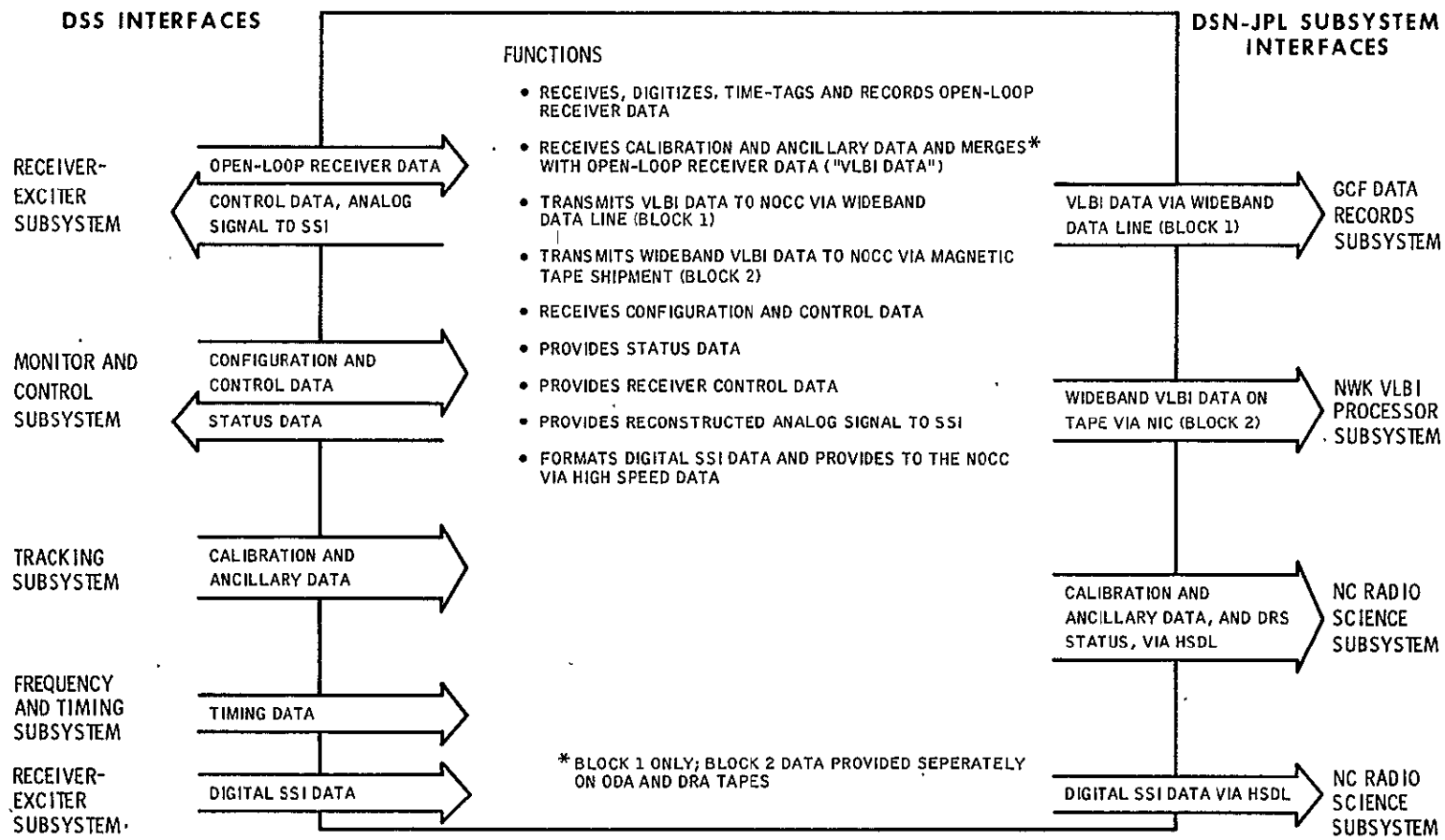


Fig. 1. DSS Radio Science Subsystem functions and interfaces

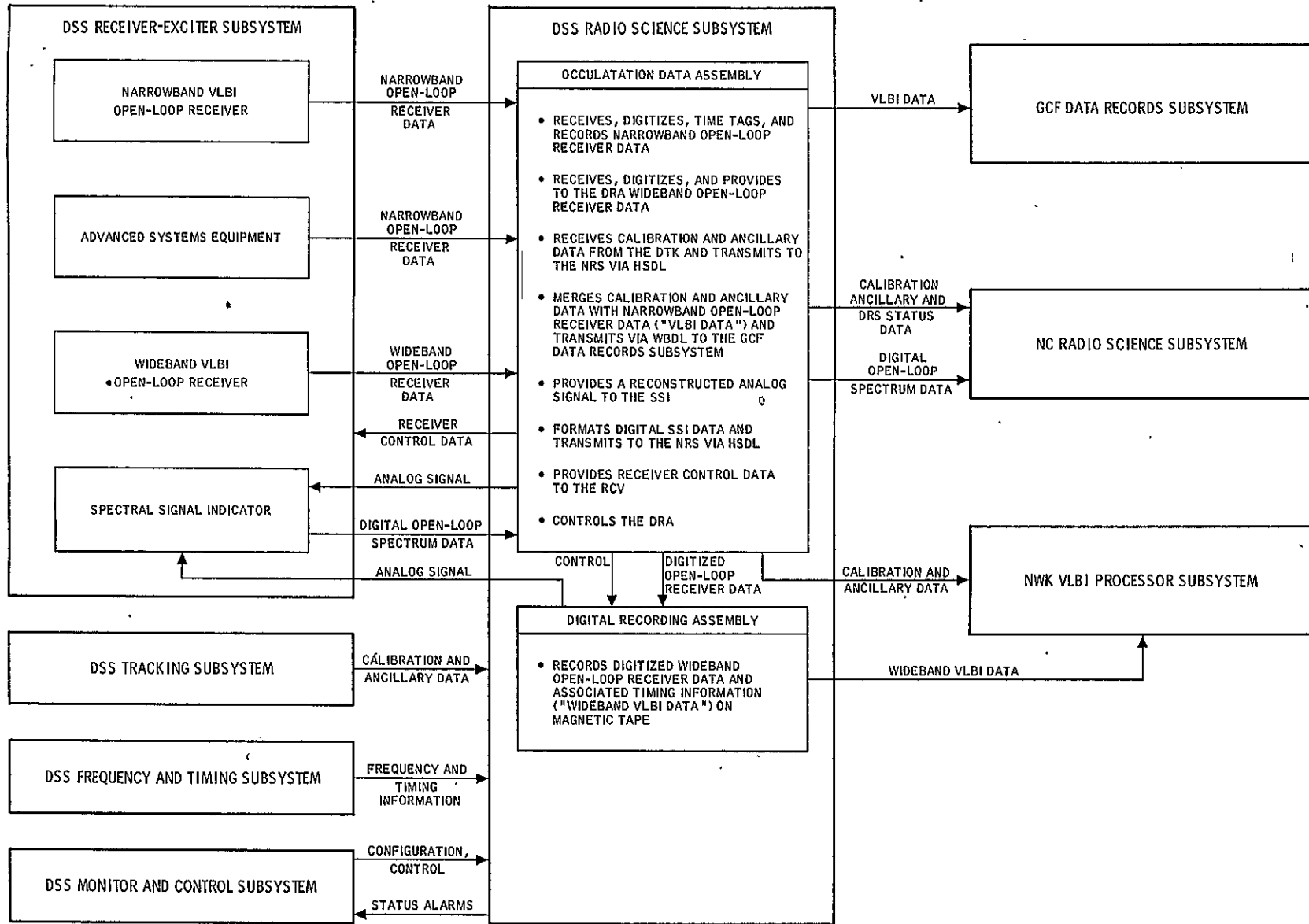


Fig. 2. DSS Radio Science Subsystem functions and data flow

ORIGINAL PAGE IS
OF POOR QUALITY

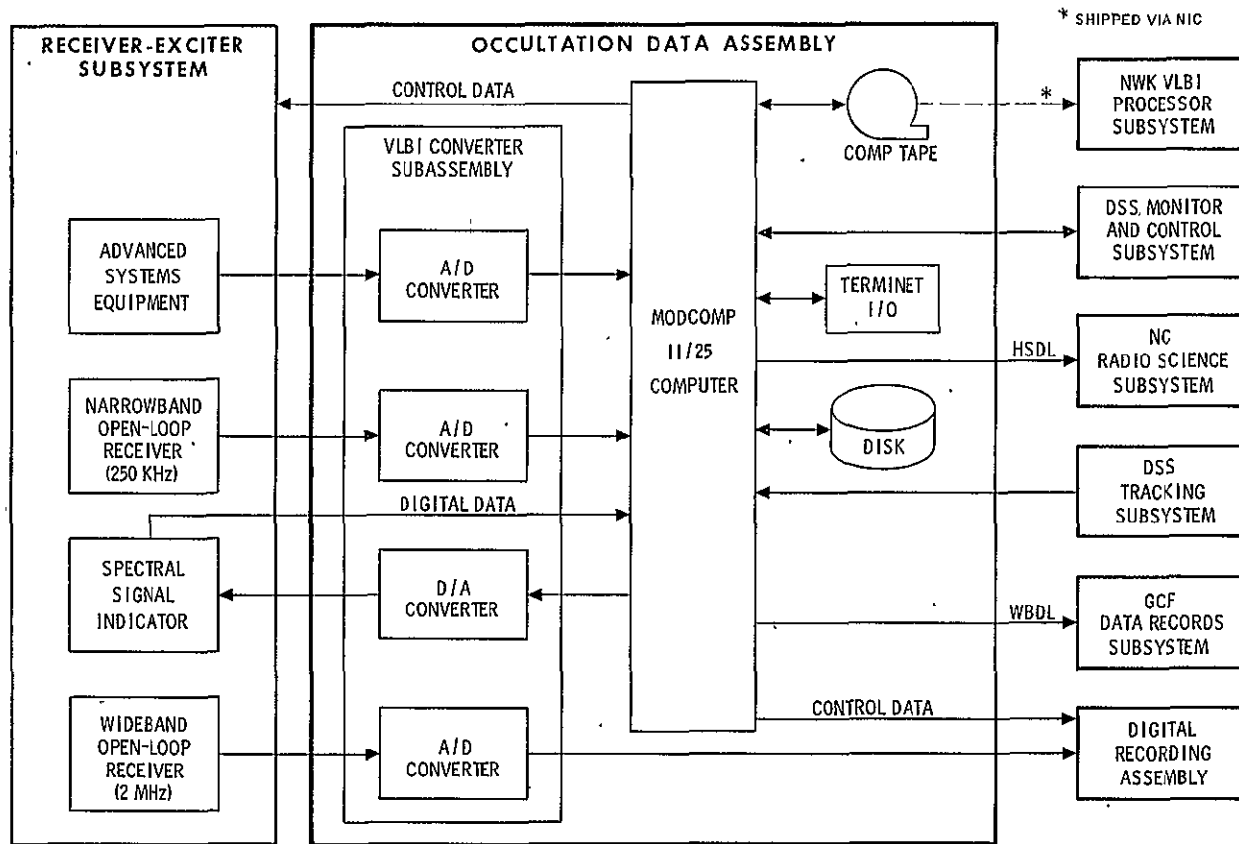


Fig. 3. Occultation Data Assembly functional block diagram

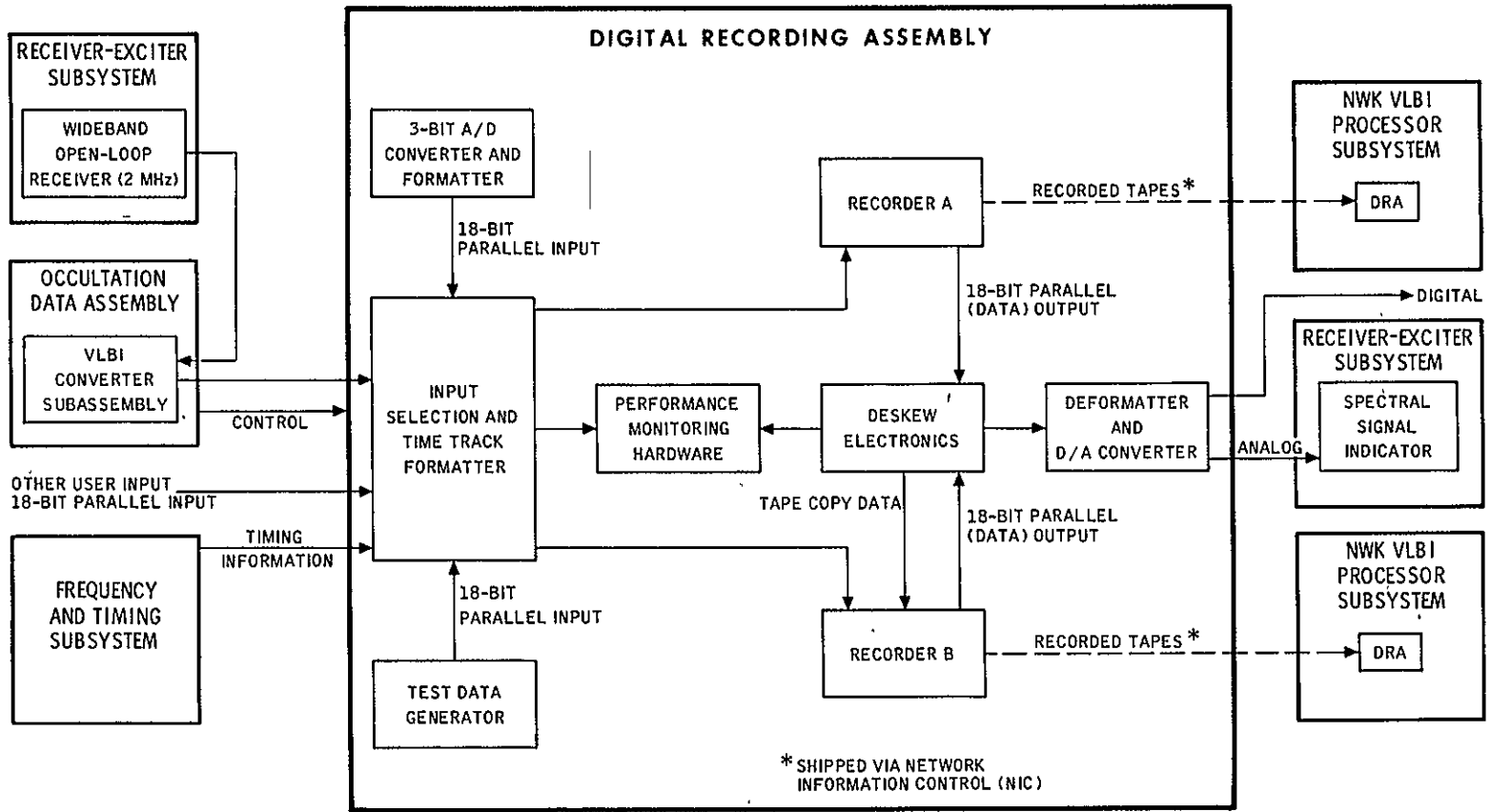


Fig. 4. Digital Recording Assembly functional block diagram

Absolute Flux Density Calibrations: Receiver Saturation Effects

A. J. Freiley, J. E. Ohlson¹ and B. L. Seidel
Radio Frequency and Microwave Subsystems Section

The effect of receiver saturation is examined for a total power radiometer which uses an ambient load for calibration. Extension to other calibration schemes is indicated. The analysis shows that a monotonic receiver saturation characteristic could cause either positive or negative measurement errors, with polarity depending upon operating conditions. A realistic model of the receiver is made using a linear-cubic voltage transfer characteristic. The evaluation of measurement error for this model then provides a means for correcting radio source measurements. It also provides the means for assuring that this source of error is small in a particular situation.

I. Introduction

The Jet Propulsion Laboratory's Antenna Gain Calibration Program has demonstrated the feasibility of accurately determining the gain performance of large aperture antennas using radio metric measurements of natural radio sources (Ref. 1). One phase of this program examined systematic errors and their effects on the radio metric measurements. The measurement of low system operating temperature and ambient noise reference temperature demands operation of the radiometer receiving system over a fairly large dynamic range. This necessitated examination of receiver saturation. The saturation may be small, but it can have impact on radio source temperature measurements at the 1% error level.

Consider a classical total power radiometer which goes through the sequence shown in Table 1. The parameters shown are defined as

T_{OP} = System operating noise temperature (cold sky).

T_s = Increase in system operating noise temperature due to radio source.

T_{AMB} = System operating noise temperature when terminated in an ambient load.

G = System power gain through the receiver. This value is assumed to only be known nominally prior to use of T_{AMB} as a reference.

P_1, P_2, P_3 = Output powers of an ideal linear receiver as indicated by an ideal detector.

¹Dr. Ohlson, a consultant to Section 333, is a Professor at the U.S. Naval Postgraduate School, Monterey, CA.

P'_1, P'_2, P'_3 = Observed output powers of a real receiver as indicated by an ideal detector.

First, consider an ideal linear receiver. Step 1 (Table 1) gives us GT_{op} when the antenna is pointed slightly away from the source. Step 2 gives us $G(T_{op} + T_s)$ when on source. Step 3 gives us a calibration value of GT_{AMB} . The value of T_{AMB} is known from physical temperature measurement of the load and other RF hardware calculations. Using a prime to denote estimated values, the estimated gain factor is

$$G' = \frac{P_3}{T_{AMB}} \quad (1)$$

However, since we are starting by assuming a linear receiver, we have $P_3 = GT_{AMB}$ and thus $G' = G$. Then the estimated value of T_s is measured in the classical manner as

$$T'_s = \frac{P_2 - P_1}{G} \quad (2)$$

and we clearly obtain $T'_s = T_s$.

II. Real Receiver Analysis

Let the real receiver be described by the compression factors C_1, C_2 and C_3 which have values between 0 and 1. These represent the reduction of receiver output due to saturation so that (see Table 1)

$$P'_1 = C_1 P_1 < P_1 \quad (3)$$

$$P'_2 = C_2 P_2 < P_2 \quad (4)$$

$$P'_3 = C_3 P_3 < P_3 \quad (5)$$

We assume that the saturation is not in the detector, but in the intermediate frequency (IF) amplifier prior to the detector. To insure that this is the case, most accurate radiometers use a very accurate adjustable calibrated IF attenuator prior to the detector. The detector is used simply as an indicator and the IF attenuator is adjusted so the indicator is returned to a standard reading. This technique eliminates nonlinearity error in the detector because the detector always operates at the same level for each measurement step. The data is then the difference of the attenuation readings from the attenuator dial, for Steps 1, 2 and 3 in Table 1.

From (1) with P'_3 substituted for P_3 the measurement of gain for the real receiver is

$$G' = \frac{P'_3}{T_{AMB}} = C_3 G \quad (6)$$

Then from (2) and (6), with $P_2 \rightarrow P'_2, P_1 \rightarrow P'_1$ and $G \rightarrow G'$, we have the measurement of source temperature as

$$T'_s = \frac{P'_2 - P'_1}{G'} = \frac{C_2}{C_3} T_s - \frac{(C_1 - C_2)}{C_3} T_{op} \quad (7)$$

The error in measurement is

$$\Delta T = T'_s - T_s = \left(\frac{C_2}{C_3} - 1 \right) T_s - \frac{(C_1 - C_2)}{C_3} T_{op} \quad (8)$$

Observe that C_1, C_2 and C_3 are specific values of the function $C(GT_{IN})$ where T_{IN} is total system temperature, i.e.,

$$C_1 = C(GT_{op})$$

$$C_2 = C[G(T_{op} + T_s)] \quad (9)$$

$$C_3 = C(GT_{AMB})$$

We now define a *monotonic compression characteristic* for a receiver as one for which $C(x)$ is monotonically decreasing with x . Thus, if for example

$$T_{op} \leq T_{op} + T_s \leq T_{AMB} \quad (10)$$

then if a receiver had monotonic compression, it would have

$$1 \geq C_1 \geq C_2 \geq C_3 > 0 \quad (11)$$

i.e., C_1 has less compression and is closer to unity.

The first conclusion will now be made. The error in (8) can be positive or negative. To show this consider two special cases, satisfying (10) and (11).

(1) Let $T_{op} + T_s = T_{AMB}$. Then $C_2 = C_3$ and from (8) ΔT is *negative* since $C_1 > C_2$.

- (2) Assume compression occurs only for T_{AMB} . Then $1 = C_1 = C_2 > C_3 > 0$ and from (8) ΔT is positive.

For any radiometer we will usually have $T_{op} < T_{AMB}$. Assuming T_{op} is less than T_{AMB} , two operating conditions exist. One condition is in (10). It and the other one possible are tabulated in Table 2. The error of the first was shown to possibly be positive or negative. For the second in Table 2, the error is always negative, under the monotonic assumption in (11). The breakpoint between positive and negative errors is difficult to find by simply setting (8) equal to zero, since we have not yet developed an analytic function for (9). The main result of this section is in (8). This is useful when the compression factors are known because we can then calculate the measurement error ΔT .

III. Modeling of Compression

The result above is useful only when C_1 , C_2 and C_3 are each known. This is usually not the case. Usually a radiometer user knows only that he is operating some amount (backoff) below a reference compression point, e.g., the -0.1 dB point. In this section we consider a linear-cubic model and can calculate the measurement error when given only the backoff value.

The voltage input-output relationship of an amplifier is often modeled with the linear-cubic model²:

$$v_{out} = v_{in} - v_{in}^3 \quad (12)$$

This model is widely used for intermodulation product calculation, and seems appropriate here as well. We assume a bandpass filter to follow the amplifier prior to the detector. Thus, second and fourth order terms could be included in (12) but their output would be rejected by the filter and have no effect. The gain is unity for small v_{in} . Saturation increases for larger v_{in} . We assume that we will operate far below the point at which (12) has its maximum value and starts decreasing for very large v_{in} .

²A more general form for a real amplifier which incorporates a gain parameter α and a saturation parameter β is

$$v_{out} = \alpha v_{in} - \beta v_{in}^3$$

With no loss of generality in what is to follow, α and β can be taken to be unity as in (12).

An amplifier is usually characterized for sine wave inputs and outputs. Let $v_{in} = A \cos \omega t$, where ω is the IF center frequency. Substitution of this in (12), and manipulation gives

$$v_{out} = \left[A - \left(\frac{3A^3}{4} \right) \right] \cos \omega t - \frac{A^3}{4} \cos 3\omega t \quad (13)$$

The second term is rejected by the bandpass filter so the envelope voltage amplitude of the output sine wave is

$$e = A - \frac{3A^3}{4} \quad (14)$$

We now choose a standard reference compression point, C_r . Commonly, this is expressed in decibels so C_r (in dB) = $10 \log_{10} C_r$, e.g., -0.1 dB from $C_r = 0.97724$. Since C_r is a power ratio, $C_r^{1/2}$ then is the factor by which e in (14) is reduced below the amplitude A obtained with a linear receiver. We wish to find the input envelope $A = A_o$ where this compression occurs. Thus

$$A_o - \frac{3A_o^3}{4} = A_o C_r^{1/2} \quad (15)$$

and hence

$$A_o^2 = \frac{4}{3}(1 - C_r^{1/2}) \quad (16)$$

Since power comes from the envelope as $A_o^2/2$, we have the input power giving compression C_r for a sine wave is

$$P_s = \frac{2}{3}(1 - C_r^{1/2}) \quad (17)$$

We now examine compression for a noise input. For Gaussian noise the envelope A has the Rayleigh probability density

$$p(A) = \frac{A}{P_n} \exp(-A^2/2P_n), A \geq 0 \quad (18)$$

where P_n = average input power of the noise. The output envelope after the filter is in (14) so the output power (observed by the detector) is

$$P_o = \overline{e^2}/2 = \frac{1}{2} \int_0^\infty \left(A - \frac{3A^3}{4} \right)^2 p(A) dA$$

$$= P_n - 6P_n^2 + \frac{27}{2} P_n^3 \quad (19)$$

The compression factor for noise C_n , is implicitly defined as $P_o = C_n P_n$ to give

$$C_n = \frac{P_o}{P_n} = 1 - 6P_n + \frac{27}{2} P_n^2 \quad (20)$$

Now let the input noise power P_n be below the sine wave compression point P_s by the backoff $B < 1$:

$$P_n = B P_s \quad (21)$$

We then have, by (21), (20) and (17)

$$C_n = 1 - 4B(1 - C_r^{1/2}) + 6B^2(1 - C_r^{1/2})^2 \quad (22)$$

We have already presumed small saturation, so C_r is very close to unity. Thus $(1 - C_r^{1/2})$ is $\ll 1$ and since $B < 1$, the third term in (22) is second order in $B(1 - C_r^{1/2})$ and is negligible with respect to the second term. Thus

$$C_n \approx 1 - 4B(1 - C_r^{1/2}) \quad (23)$$

This is the main result of this section.

An important question may now be answered. At some reference level the compression for a sine wave input is C_r . At what backoff from this reference level will a noise input have the same compression? We start with (23) and set $C_n = C_r = C$. Since $B(1 - C_r^{1/2}) \ll 1$, we use $(1 + x)^{1/2} \approx 1 + x/2$ to get from (23)

$$C^{1/2} = 1 - 2B(1 - C_r^{1/2}) \quad (24)$$

Solving for B gives $B = 1/2$. Thus we conclude that a noise input must be backed off a factor of 2 (= 3 dB) from a sinusoidal input to have the same compression. This is reasonable since the noise input has large excursions which are compressed more than a sinusoidal input.

IV. Application to Radiometer Error

In (8) we have the error in measurement of T_s in terms of the compression factors C_1 , C_2 and C_3 . In (23) we now have an expression for these factors under the assumption of a linear-cubic receiver model.

We first characterize the receiver for a sinusoidal input by establishing the reference level at which a compression of C_r occurs, say -0.1 dB. This reference level can be determined by use of a signal generator and precision attenuators. For use as a radiometer, with a noise input, this same compression occurs for a reference temperature T_r . This temperature represents an input noise power reduced by a backoff of 1/2 with respect to the reference sinusoid. Thus for total input temperature T_{in} , backoff is given by

$$B = \frac{T_{in}}{2T_r} \quad (25)$$

From (23) we thus have

$$C_n = 1 - 2 \frac{T_{in}}{T_r} (1 - C_r^{1/2}) \quad (26)$$

This gives the compression vs input temperature T_{in} under the condition that a compression of C_r occurs at reference temperature T_r . Square-rooting (26) and using the argument prior to (24) easily shows that $C_n = C_r$ when $T_{in} = T_r$.

For simplicity, define

$$\delta = 2(1 - C_r^{1/2})/T_r \quad (27)$$

Then the compression factors needed for (8) are of the form in (9):

$$C_1 = 1 - \delta T_{op}$$

$$C_2 = 1 - \delta(T_{op} + T_s)$$

$$C_3 = 1 - \delta T_{AMB} \quad (28)$$

Substitution into (8) gives

$$\frac{\Delta T}{T_s} = \frac{2(1 - C_r^{1/2})(T_{AMB} - 2T_{op} - T_s)}{T_r[1 - 2(1 - C_r^{1/2})T_{AMB}/T_r]} \quad (29)$$

Since $(1 - C_r^{1/2})$ will be small, and assuming T_{AMB} is not much larger than T_r , we can drop the second term in the denominator bracket to give

$$\frac{\Delta T}{T_s} \approx 2(1 - C_r^{1/2}) \frac{T_{AMB} - 2T_{op} - T_s}{T_r} \quad (30)$$

This is the main result of this section. In this form it can be used to calculate correction factors for measurements.

Several observations can be made:

- (1) The fractional error $\Delta T/T_s$, linearly decreases as T_s increases.
- (2) The error goes to zero when

$$T_s = T_{AMB} - 2T_{op} \quad (31)$$

- (3) The error is positive or negative depending upon whether T_s is below or above the value in (31).

A special case is of considerable value: Let T_{op} and T_s be very small compared to T_{AMB} . Then

$$\frac{\Delta T}{T_s} = 2(1 - C_r^{1/2}) \frac{T_{AMB}}{T_r} \quad (32)$$

Further, as long as

$$T_s + 2T_{op} \leq T_{AMB} \quad (33)$$

the result in (30) is bounded by (32). Thus, we obtain the useful result which can be used to provide an upper bound on saturation effects (condition 33 must apply):

$$\frac{\Delta T}{T_s} \leq 2(1 - C_r^{1/2}) \frac{T_{AMB}}{T_r} \quad (34)$$

V. Example

To illustrate the above calculations, consider the following example parameters representative of a high performance radiometer using a maser:

$$T_{op} = 15 \text{ K}$$

$$T_s = 100 \text{ K}$$

$$T_{AMB} = 300 \text{ K} \quad (35)$$

Let the receiver be set so that a temperature $T_r = 400 \text{ K}$ gives a compression of -0.1 dB ($C_r = 0.97724$). The error is, from (30), at the 1% level:

$$\frac{\Delta T}{T_s} = 0.0097 \quad (36)$$

The maximum error for any T_s satisfying (33) with $T_s \leq 270$, is, from (34)

$$\frac{\Delta T}{T_s} \leq 0.0172$$

VI. System Constraint for Small Error

Let us now find the constraint on the receiver compression so that the system error will be small. Assume that (33) holds and let us use the bound in (34) so that our constraint will hold for any value of T_s in (33). Let us take a value of $\Delta T/T_s = E_{MAX}$ as the worst case error we can accept. Then for equality in (34) we have the tradeoff in T_{AMB}/T_r vs C_r :

$$E_{MAX} = 2(1 - C_r^{1/2}) \frac{T_{AMB}}{T_r} \quad (37)$$

Examples of this tradeoff are shown in Table 3 for a value of $E_{MAX} = 0.003$. This Table shows that -0.026 dB compression at a value of T_r which is 3 dB above T_{AMB} guarantees that $\Delta T/T_s$ is below 0.003. This is also true if there is -0.131 dB compression when T_r is 10 dB above T_{AMB} . Clearly there is an infinite number of pairs of values satisfying (34). The usefulness of (34) is that only one value of

compression need be specified and this can be done for a nearly arbitrary value of T_r .

In many radiometers, the system calibration is done by use of a calibrated active noise source reference (gas discharge tube or noise diode) which adds a precise amount of noise to the system input. This is as opposed to the use of an ambient load for calibration as done above. With small changes, it is straightforward to apply the technique above to the case of an active reference. The key point is that Step 3 in Table 1 now has "off source--noise reference on" and temperature $T_{op} + T_C$, where T_C is the calibrated noise reference contribution. Also the gain estimate in (6) becomes

$$G' = \frac{P'_3 - P'_1}{T_C}$$

The remainder of the analysis closely follows the above and is omitted for brevity.

VII. Conclusions

An analysis has been made of measurement error in a radiometer due to receiver saturation. The general result is in (8). A linear-cubic model of receiver saturation was then assumed and an explicit result was obtained in (30).

The measurement error is characterized by only one measurement of compression which can be made at nearly any reference temperature. The work here is useful for calculating correction factors, or at the very least, verifying that error is insignificant for a particular situation.

Reference

1. Freiley, A. J., P. D. Batelaan and D. A. Bathker, *Absolute Flux Density Calibrations of Radio Sources: 2.3 GHz*, Technical Memorandum 33-806, Jet Propulsion Laboratory, Pasadena, California, December 1, 1977 (available from authors upon request).

Table 1. Summary of measurement

Step	Description	Temperature	Output power of ideal receiver	Output power of real receiver
1	Off source (cold sky)	T_{op}	$P_1 = GT_{op}$	$P'_1 = C_1 GT_{op}$
2	On source	$T_{op} + T_s$	$P_2 = G(T_{op} + T_s)$	$P'_2 = C_2 G(T_{op} + T_s)$
3	Ambient load	T_{AMB}	$P_3 = GT_{AMB}$	$P'_3 = C_3 GT_{AMB}$

Table 2. Error polarity

Condition	Error, ΔT
$T_{op} + T_s < T_{AMB}$	Positive/negative
$T_{op} + T_s > T_{AMB}$	Negative

Table 3. Saturation tradeoff

Case	T_{AMB}/T_r	Worst case compression
A	0.5 (-3.0 dB)	0.99401 (-0.026 dB)
B	0.1 (-10.0 dB)	0.97023 (-0.131 dB)

DSN Portable Zero Delay Assembly

E. J. Serhal, Jr., and T. Y. Otoshi

Radio Frequency and Microwave Subsystems Section

This article presents design and test data on portable zero delay assemblies that have recently been delivered to DSS 14, 43, and 63. These portable assemblies are field-use delay standards that will be used to periodically calibrate the Block IV Translator ranging paths at each 64-m antenna Deep Space Station.

I. Introduction

The Block IV Translator Method (Ref. 1) is currently being used to determine the ground station range delays at all 64-m antenna Deep Space Stations (DSS). The validity and accuracy of this method are dependent upon the Block IV Translator ranging paths being recalibrated (1) at periodic intervals (once or twice each year) or (2) whenever significant component or configuration changes have been made in the translator ranging path.

The calibrations of the translator ranging path delays have been performed in the past years with an R & D Zero Delay Device (ZDD) (Ref. 2). The ZDD was shipped at various times to the three 64-m antenna DSS and has been used successfully to make translator delay measurements. Recently, the design features of the R & D ZDD have been improved and incorporated into a field-worthy version called the Portable Zero Delay Assembly (PZDA). PZDAs have been fabricated for the DSN and a calibrated unit has now been supplied to DSS 14, DSS 43, and DSS 63. Operational test procedures for translator measurements with the PZDA have been written by DSN Network Operations and are currently being verified. The purpose of this article is to present pertinent design information as well as calibration test data on the PZDA.

II. Description

Figures 1 and 2 respectively show the original R & D ZDD and the new PZDA. For the PZDA, pads and step attenuators were made to be internal components of the assembly to simplify test procedures for field use. In addition, the PZDA includes some broadband filters and isolators (see Figs. 3 and 4) to suppress potential mismatch and higher order harmonic distortion errors. Suppressing these errors is especially important when calibrating the PZDA delays by the back-to-back method to be described later in this article. The tradeoff for a more accurate unit for field use is a longer delay through the PZDA because of the additional built-in components. All components including filters and isolators have at least ± 40 MHz bandwidths at their approximate uplink-downlink center frequencies of 2113 MHz, 2295 MHz, and 8415 MHz.

Figure 5 shows the S¹ and X-band mixer subassembly for the PZDA. This subassembly is a standard mixer assembly being used in the Block IV Doppler Translator Assembly and is also very similar to the mixer assembly in the R & D ZDD.

The test cables supplied with the PZDA as shown in Fig. 2 are phase-stabilized F282 cables made by the Flexco Co. in Denville, New Jersey. These cables were selected (instead of

the smaller diameter F182 cable used for the R & D ZDD) because of their lower loss and superior mechanical durability with flexing, especially at the type N-to-cable transition joints. Three 7.62-m (25 ft) F282 cables are supplied with each PZDA for the S-X signal paths and two 3.05-m (10 ft) F282 cables for the L.O. paths. The F282 cable has a delay characteristic of about 4.72 ns/m and attenuations of 0.66 dB/m in the 2.1 to 2.3-GHz range and 1.25 dB/m at 8.4 GHz.

III. Test Method

The PZDAs were calibrated by use of the back-to-back method which is depicted in Fig. 6. The PZDA on the right-hand side is the unit under test while the unit on the left is the comparison standard. The comparison standard is also a PZDA but differs in that the S-X isolators are reversed to permit signal to flow in the reverse direction (J6 and J7 ports to J3 port). When making S-S delay calibrations, the 182-MHz L.O. drive is turned on and simultaneously feeds port J1 of each unit. The uplink test signal (of approximately 2113 MHz) is fed into port J3 of the unit being tested. This uplink signal becomes up-converted to approximately 2295 MHz in the test unit and then down-converted back to 2113 MHz when it passes through the standard comparison unit. When measurements are to be made for S-X band delays, the 182-MHz L.O. drive is turned off and the 6.3-GHz L.O. drive is turned on to simultaneously feed port J5 of each unit. The 2113-MHz test signal becomes up-converted to approximately 8415 MHz in the test unit and down-converted back to 2113 MHz when passing through the standard comparison unit.

Insertion phase versus frequency measurements are made for an input test frequency range of 2113.5 ± 8.5 MHz using an HP 8410A Network Analyzer and a microwave source driven by a frequency synthesizer. Group delay is calculated from the slope of the insertion phase versus frequency data. It is necessary to (1) measure the delay of the total insertion delay of the back-to-back assemblies as shown in Fig. 6 and (2) measure separately the delays of any test cables (including pads) that were used to interconnect the test unit to the standard unit in the back-to-back configuration. The delay of the unit under test is then determined by subtracting the delay of the test cables and delay of the standard comparison unit from the total measured insertion delay. If the delay of the standard comparison unit is not known, then the delay of the unit under test can be determined by subtracting out the test cable delays from the total measured insertion delay and then dividing the net result by two. This latter method is valid only if both the test and standard units were built to the same specifications and are therefore electrically identical to within an acceptable tolerance.

For the test results of the article, the delay of the standard comparison PZDA was known and determined previously by connecting it to an improved R & D ZDD and calibrating it in the back-to-back configuration. The R & D ZDD (improved version) in this configuration was the basic primary standard and was used because it has S-S and S-X delays of 2.3 ns in each path which are known to accuracies of ± 0.2 ns (1σ). These accuracies were established previously from extensive testing and cross-comparisons.

After completion of the PZDA calibrations, the two 3-dB pads in the test unit as shown in Fig. 6 were replaced by two 20-dB pads (of nearly the same physical lengths and electrical delays) to restore the PZDA to its operational configuration of Fig. 3. The lower value (6 dB) padding was temporarily needed during the calibration because a relatively strong test signal level is required for the Network Analyzer insertion phase measurements.

IV. Test Results

Table 1 shows the final calibrated delays of the PZDAs that were sent to various DSSs. The applicable serial numbers and DSS identification are also tabulated. The accuracy of the delays are estimated to be better than ± 1.0 ns (1σ). Due to the fact that all components in the PZDA including isolators and filters are wide-band (see Section II of this article), the delay calibrations in Table 1 are applicable over a wide-band and apply to all S-S and S-X frequencies for DSN channels 5 through 27 listed in DSN documents.

The insertion losses of the PZDA in the final operational configuration were determined to be 54 ± 2 dB for the (S-S) path going from port J3 to J6 and 55 ± 2 dB for the (S-X) path going from port J3 to J7. The high insertion losses are mainly due to the two 20-dB pads (see Fig. 3) that are needed to attenuate an anticipated test signal level of +19 dBm to a level of about -20 dBm so that internal S- and X-band mixers will be operated in their linear regions. The strong test signal level of +19 dBm is derived at each 64-m DSS from the output of a 54-dB waveguide coupler which samples the 20-kW transmitter power.

V. Conclusion

A PZDA that is field-worthy, operationally easy to use, and accurately calibrated has been developed. A PZDA has been shipped to DSS 14, DSS 43, and DSS 63. Preliminary results

of Translator delay measurements from DSS 43 and 63 indicate the results obtained with the PZDA agree reasonably well with test data obtained in previous years with the R & D ZDD.

The standard comparison PZDA as well as calibration procedure documentation have been sent to the DSN Maintenance Center (DMC). Recalibrations of the PZDA in the future can be done by shipping the units to DMC.

References

1. Komarek, T., and Otoshi, T., "Terminology of Ranging Measurements and DSS Calibrations" in *The Deep Space Network Progress Report 42-36*, pp. 35-40, Dec. 15, 1976.
2. Otoshi, T. Y., Batelaan, P. D., Wallace, K. B., and Ibanez, F., "Calibration of Block 4 Translator Path Delays at DSS 14 and CTA 21" in *The Deep Space Network Progress Report 42-37*, pp. 188-197, Feb. 15, 1977.

Table 1. Calibrated PZDA delays

DSS	SN	S-S (ns)	S-X (ns)
14	2	18.8	14.3
43	3	18.1	14.2
63	4	18.2	13.9

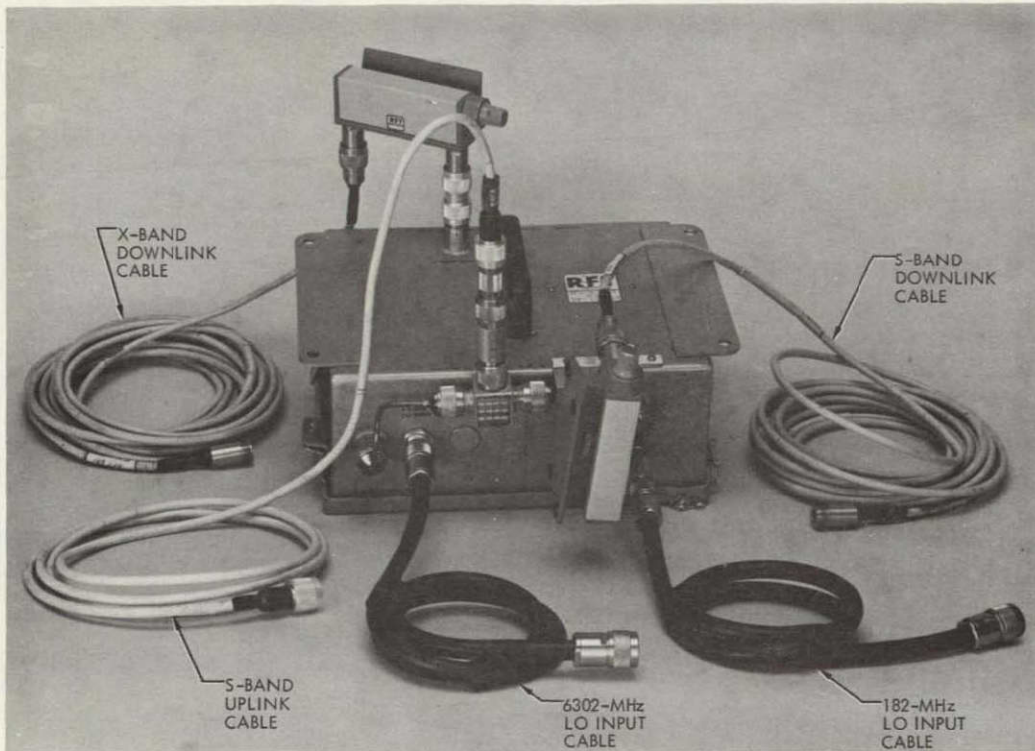


Fig. 1. R&D Portable Zero Delay Device with external test cables and attenuators



Fig. 2. DSN Portable Zero Delay Assembly

FOLDOUT FRAME 1

FOLDOUT FRAME 2

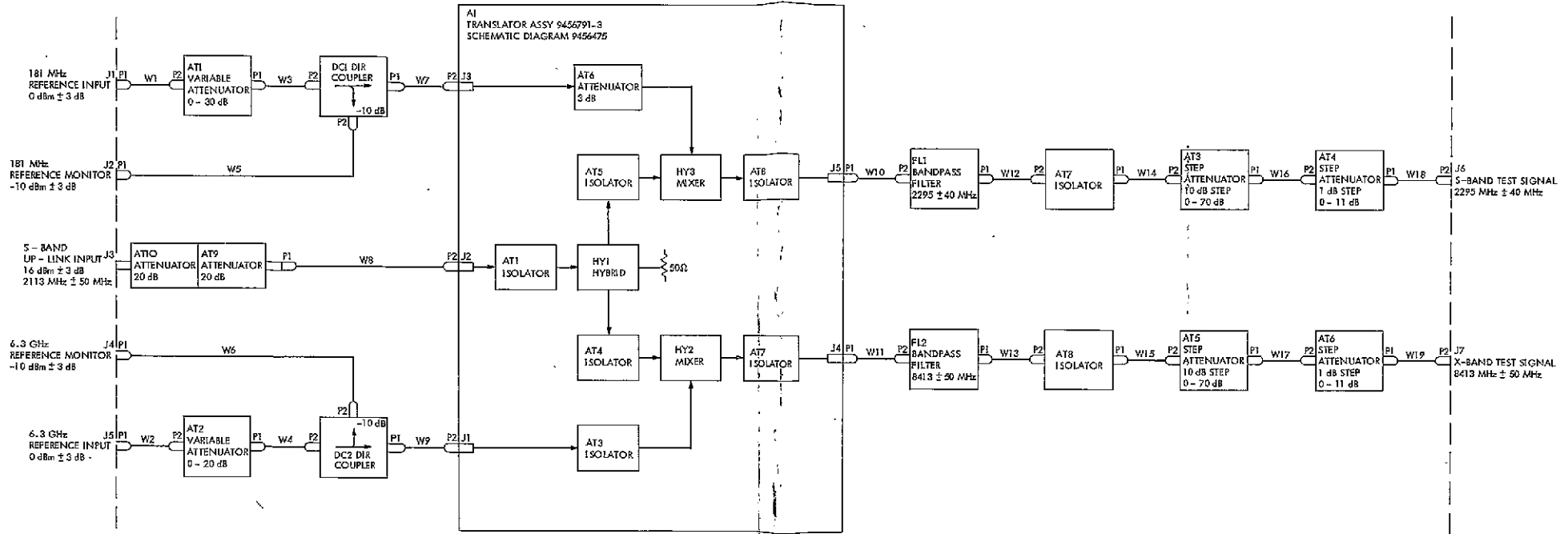


Fig. 3. Block diagram of Portable Zero Delay Assembly

ORIGINAL PAGE IS
OF POOR QUALITY

ORIGINAL PAGE IS
OF POOR QUALITY

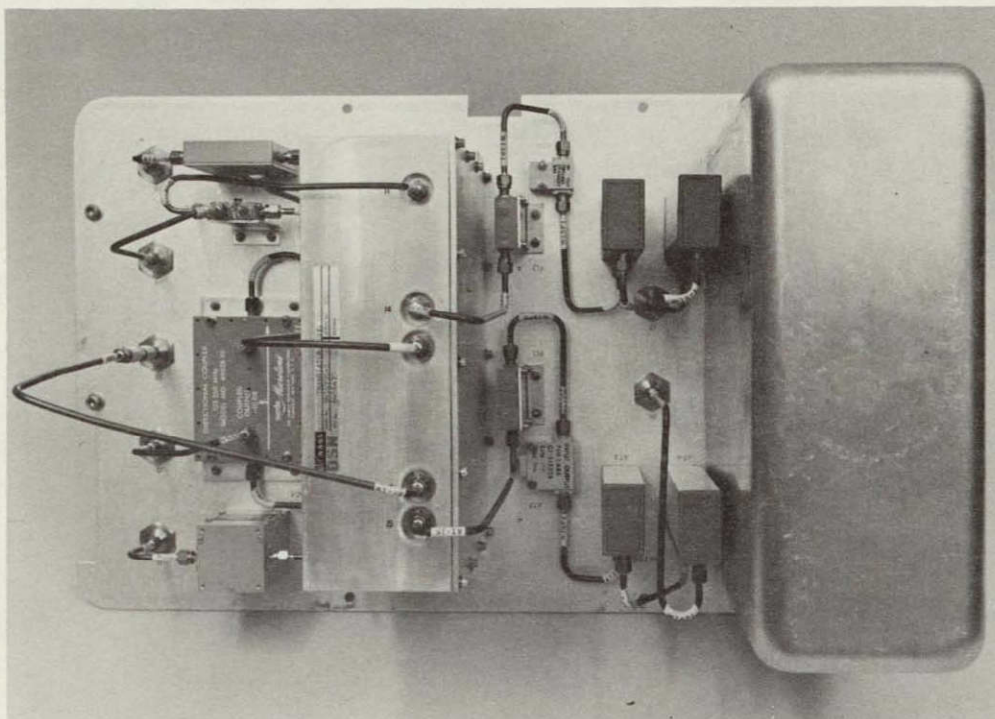


Fig. 4. Microwave components mounted on underneath side of front panel of Portable Zero Delay Assembly

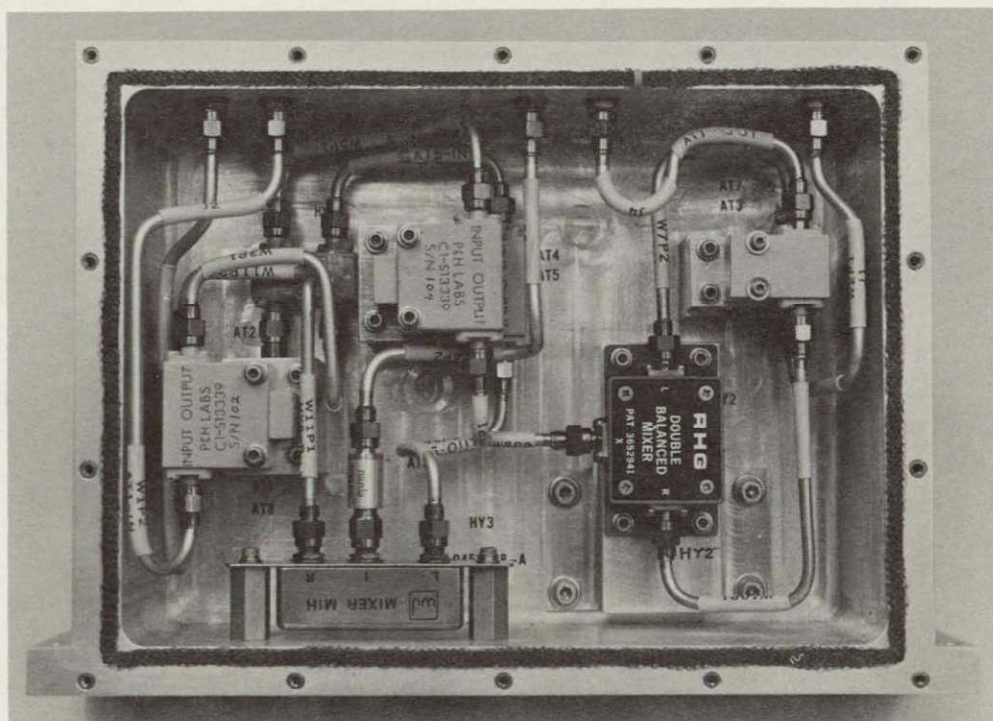


Fig. 5. S- and X-band mixer subassembly of Portable Zero Delay Assembly. Same as Translator Assembly 9456791-3

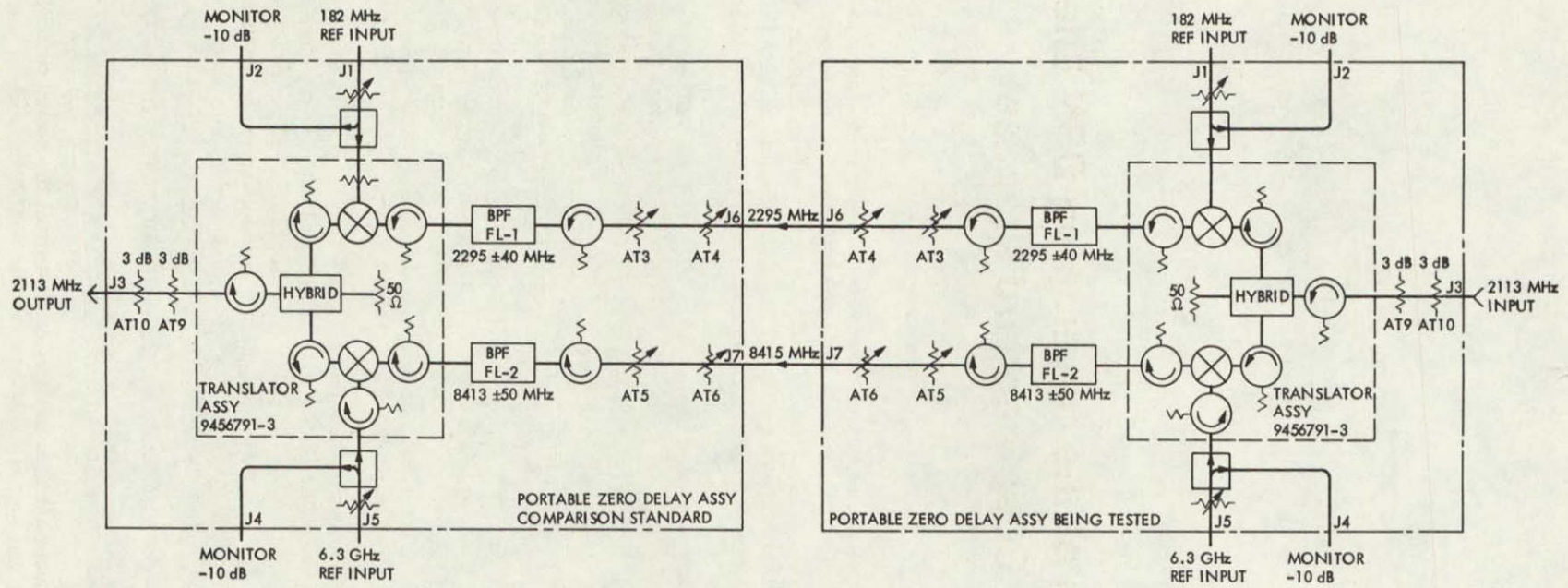


Fig. 6. Back-to-back test configuration

ORIGINAL PAGE IS
OF POOR QUALITY

Evaluation of the Developing DSN Life-Cycle Cost Standard Practice

M. McKenzie
TDA Planning

The DSN is developing a Life-Cycle Cost Standard Practice. This report compares the developing Practice to those of industry and the Department of Defense. Results show that the DSN uses the accepted concept of Life-Cycle Costing, tailoring the concept to DSN specific needs, but does not push the concept past the point of prevailing theory.

I. Introduction

The DSN is developing a Life-Cycle Cost (LCC) Standard Practice. At this stage of development, it is useful to compare the Practice to those of industry and the Department of Defense (DOD). Specifically, three questions are posed for study:

- (1) How widely used is the Life-Cycle Cost concept?
- (2) Is the DSN LCC Practice, at this stage of development, in accordance with generally accepted standards?
- (3) How does the DSN LCC Practice compare with those of industry and the military; i.e., is the DSN at the state-of-the-art?

These questions are addressed in the following report.

II. Use of Life-Cycle Costing

A. Department of Defense

LCC is clearly used by the Department of Defense (DoD). An investigation of the LCC concept was made in the early

1960's by the Logistics Management Institute for the Assistant Secretary of Defense for Installations and Logistics (Ref. 1). Since that time, numerous DoD and service directives have clarified and ordered the use of Life-Cycle Cost analysis. An example is the DoD Directive 5000.28 which states:

"Life-cycle cost estimates will be used as a basis for cost trade-off analyses when considering acquisition versus O&S costs, comparing competing prototypes or comparing current versus new systems" (Ref. 2).

Furthermore, in using LCC,

"Life-cycle cost objectives shall be established for each acquisition and separated into cost elements within the broad categories of development, production, operation, and support. As system definition continues, the cost elements are firmed into cost goals to which the system will be designed and its cost controlled" (Ref. 3).

Thus, the Department of Defense uses Life-Cycle Costing to select a system, and then uses "design to Life-Cycle Cost elements" to control costs. One source reports that use of Life-Cycle Cost analysis has resulted in "significant cost

savings,” validated by the Air Force Auditor General’s Office (Ref. 4).

B. Military-Related Industries

A sampling of military-related industries was conducted by the author to determine the extent to which LCC is used. Martin Marietta, Northrop, and Hughes Aircraft were contacted, and all use some form of Life-Cycle Cost analysis. One of the three has a documented standard LCC approach (Ref. 5), two have centralized LCC departments, and all three use approaches which are tailored to specific use.

Numerous industrial articles have been written on LCC analysis, and will be referenced throughout the remainder of this report. The general conclusion is that military-related industries do use some form of LCC analysis, but no single approach is standard.

C. Other Industries

Other industries use the LCC technique for purposes such as comparing alternatives:

“In comparing alternative solutions to accomplish a particular goal, the system showing the lowest life-cycle cost will usually be the first choice, assuming the performance requirements defined by the goal are adequately met” (Ref. 6).

Industrial articles on LCC analysis were found in the following magazines and journals:

Industrialization Forum

Logistics SPECTRUM

Professional Engineer

Proceedings Annual Reliability and Maintainability Symposium

Management Accounting

The articles will be referenced, as appropriate, in the following pages. The same conclusion is reached through review of these articles; the use of the Life-Cycle Cost concept is widespread, but the specific approaches and models used are not standardized.

III. Accepted Life-Cycle Cost Standards

A. Definition of “Life-Cycle Cost”

General agreement exists on the meaning of “Life-Cycle Cost.” The Department of Defense Directive 5000.28 states:

“The Life Cycle Cost of a system is the total cost to the Government of acquisition and ownership of that system over its full life. It includes the cost of development, acquisition, operation, support, and where applicable, disposal” (Ref. 7).

Similarly, a student of the Air Force Institute of Technology writes that Life-Cycle Cost is:

“... a method for evaluating and considering the total costs of ownership, including the costs of acquiring, operating, supporting, and disposing of an item, less its residual or scrap value, during its useful life” (Ref. 8).

A Martin Marietta representative states:

“Life-Cycle Costing (LCC) is a Department of Defense (DoD) acquisition or procurement technique that considers operating, maintenance, and other costs of ownership, as well as acquisition price, in the award of contracts for hardware and related support. The object of this technique is to insure that the hardware procured will result in the lowest overall ownership cost to the Government during the life of the hardware” (Ref. 9).

A similar concept is referenced in *Professional Engineer*:

“Life-cycle costing is an analysis of the total cost of a system, machine, device, building, and the like over its anticipated useful life” (Ref. 10).

Thus the DSN definition — Life-Cycle Cost is implementation cost, plus M&O costs over the life of the capability, plus deimplementation cost — is in accordance with the generally accepted definition.

B. Life-Cycle Cost Uses and Purposes

Although the definition of Life-Cycle Costing is standard, its uses vary with the background of those employing it. Donald Earles of Raytheon Company explains it:

“... over the past ten years, Life-Cycle Costing has evolved into four things; a costing discipline, a procurement technique, an acquisition consideration, and a design trade-off tool.”

The specific use depends on the user. The DSN employs LCC analysis as an acquisition consideration and a trade-off tool (Ref. 1).

C. Costing Philosophies

Just as LCC uses vary among users, costing philosophies vary with the specific application. Costs of a system may be full costs, delta costs projected from some baseline, or even

variable costs For example, a RAND weapon case study remarks:

"It is important to note that this definition of weapon system LCCs is intended to capture only the variable costs associated with the weapon system. We make no attempt to reflect any of the "fixed" costs which are necessary for the management of the organization (e.g., HQ/USAF) which uses the system, but which are not incurred by or for the weapon" (Ref. 11).

This is the costing philosophy assumed for the DSN pathfinder LCC analysis (Ref. 12). Other companies use different approaches. Hughes Aircraft Corporation, for example, uses absolute costs, while Northrop employs absolute or delta costs, as the situation demands.

D. Project Life-Cycle Period

Another Life-Cycle Cost concept which varies in use is that of project life-cycle period. An Air Force publication notes that the LCC period may be 10-20 years for a DoD weapon system (Ref. 13). A specific cost analysis done by the U.S. Army Electronics, Communications, and Material Commands uses a 10-year period (Ref. 14). This variability is summed up in *Professional Engineer*:

"The Life-Cycle of the system or machine must be realistically appraised. It can be defined as the expected physical life or the estimated period to obsolescence, whichever occurs first" (Ref. 10).

The variability of the life-cycle period is recognized by the DSN.

E. Life-Cycle Cost Definitions

Included in the DSN LCC Standard Practice is the requirement of definitions. Careful definitions insure fair comparisons and allow validation that no cost has been forgotten (Ref. 15). Although this is a generally accepted standard in government and industry, it is not practiced as thoroughly as is wise. Nevertheless, examples of LCC reports accompanied by careful definitions can be found. Two examples are *A Summary and Analysis of Selected Life-Cycle Costing Techniques and Models* of the Air Force Institute of Technology (Ref. 16), and *Life-Cycle Costing Emphasizing Energy Conservation, Guidelines for Investment Analysis* of ERDA (Ref. 17).

F. Cost Estimation Procedure

It is clear from even a cursory examination of the Life-Cycle Cost literature, that there are a number of cost estimating methods. Some of the titles of these methods are

per unit catalog price, cost-to-cost estimating relationships, non-cost-to-cost estimating relationships, specific analogy, expert opinion, simulation (Ref. 18), accounting, and parametric. It is the last two which express the organizational nature of cost estimating and which concern us here.

In general, the DSN uses the accounting approach, which lists all cost elements for a project over its life and, with a specific procedure, sums the costs. This method is explained:

"The most frequently referenced of the life-cycle cost models in use today are the additive accounting models." They are useful for projects characterized by dollars and provide managerial visibility, comparison of costs, identification of specific differences in bidders' proposals, and visibility of high support costs (Ref. 19).

In comparison, the parametric approach is useful for estimating effects of learning curves, provisioning policies, management factors, repair and replacement policies, and system characteristics (Ref. 20). Only a few parametric models are sufficiently tested for DSN use.

There are numerous cost models which incorporate these methods. For example, an Air Force Institute of Technology study lists twenty such models (Ref. 21). None of these can be used as a standard cost model. As a Honeywell employee states:

"The state-of-the-art of cost modeling, however, is not to the point where existing cost models can be used universally in whole or in part for wide varieties of applications. They are highly tailored in terms of systems treated, scope of elements covered, and categories of costs included" (Ref. 22).

Thus, there are generally accepted cost estimation procedures, one of which is used by the DSN. There are no models incorporating these methods which can be used as a standard LCC model.

G. Cost Elements

Within the accounting cost estimation method are the cost elements themselves. Again, there is no single list of detailed cost elements applicable to all projects. Examples of cost element lists are given in Tables 1 and 2 and more can be found in the literature (Refs. 13, 20, 23). At this time, however, DSN cost elements must be determined for each cost study by those familiar with the project.

H. Monetary Adjustment

Another part of Life-Cycle Costing is the monetary adjustment of projected costs. Review of the literature shows a

lack of standardization here also. The Office of Management and Budget suggests the use of comparative inflation and a general discount rate of 10% (Ref. 24). A RAND study, however, uses a discount rate of 5% (Ref. 25). Northrop prefers to work solely in constant dollars and inflate only if required for bidding purposes. The Martin Marietta LCC process allows total discretion in the inflating and discounting procedures used on each cost estimation.

Thus, the monetary adjustment used in LCC estimation will depend upon the project, the intended use of the estimation, and any applicable laws.

I. Life-Cycle Cost Presentation

The form in which a LCC estimate is presented is dependent upon the project and the purpose of the estimate. The DSN pathfinder LCC analysis used a reporting format designed to reflect the specific cost elements and algorithm used in that project. Other formats can be found in the literature (Ref. 26). An example is in Table 3.

J. Standard Practice

As stated previously, the DSN is developing a Life-Cycle Cost Standard Practice. The question arises: Are LCC standard practices common in industry and government? The answer is that in reviewing sixty sources, the author encountered only four sets of documents which could be considered as standard practices. ERDA published the *Life-Cycle Costing Emphasizing Energy Conservation, Guidelines for Investment Analysis* (Ref. 17), and Martin Marietta has the *Computerized Costing Methodology* which incorporates Life-Cycle Costing (Ref. 5). The Navy has an *Economic Analysis Handbook* (Ref. 27), and the DoD has a series of documents published as guidelines for various weapon procurements (Ref. 28).

The need for standard practices, however, is well documented. A 1975 Air Force working group found that:

“At least five actions are required in order to establish an adequately effective life cycle cost analysis capability in program offices.”

- “1. Program offices must be provided with a source of personnel familiar with analytical techniques.”
- “2. These engineers and analysts must be given general guidance on how to develop, adapt and use life cycle cost models for specific applications.”
- “3. Program office and supporting personnel should have access to a short course in the subject of

development and application of life cycle cost models and methods.”

- “4. Periodic life cycle cost methods workshops should be held. . . .”
- “5. Finally, program office personnel should be provided with a central focus of expertise where lessons learned in each new life cycle application are integrated with existing life cycle cost models and methods. . . .” (Ref. 29).

Similarly, a RAND study states:

“In order to advance the current state-of-the-art of LCC estimating, at least the following improvements” are needed:

- “1. Operational consistency of LCC procedures”
- “2. Better cost allocation rules”
- “3. A nomenclature directory”
- “4. Project LCC decision requirements”
- “5. An LCC data base” (Ref. 30)

Thus, the need for standard practices is generally accepted, and some such documents already exist. The DSN, with others, is responding to this need.

IV. General Conclusions

Life-Cycle Costing is a popular technique, widely used in the military and industry. It is generally accepted that Life-Cycle Costing is a specific concept whose use should be accompanied by LCC definitions, a stated costing procedure, a stated project life-cycle period, monetary adjustment procedures suited to need, and at least a locally accepted LCC standard practice. The DSN is in accord with these generally accepted standards. The specific application of the standards is user and project dependent, as found in both the LCC literature and the DSN.

The DSN is not at the state-of-the-art of Life-Cycle Costing. The state-of-the-art is an advanced and fluctuating position including such things as economic risk analysis, performance effectiveness measurement, multiple regression analysis, and unproven parametric models. These advances are not being ignored by the DSN, but rather will be incorporated as appropriate with the DSN environment. The DSN is using an accepted tool, adapted to local needs, to reduce project costs.

References

1. Donald R. Earles, "LCC – Commercial Application, Ten Years of Life-Cycle Costing," *Proceedings of the Annual Reliability and Maintainability Symposium*, 1975, p. 74.
2. U. S. Department of Defense, *Design to Cost*, Directive No. 5000.28 (May 23, 1975), p. 4.
3. DoD Directive 5000.28, p. 3.
4. James H. Hammond, "Life-Cycle Costing for Government Procurement," *Industrialization Forum*, Vol. 5, No. 1-2, 1974, pp. 77-78.
5. Aaron N. Silver, *Computerized Costing Methodology* (Martin Marietta proprietary information), March 1976.
6. G. F. Pearson, "Life-Cycle Costing in an Energy Crises Era," *Professional Engineer*, Vol. 44, No. 7, July 1974, p. 27.
7. DoD Directive 5000.28, p. 2.
8. Lawrence E. Dover et al., *A Summary and Analysis of Selected Life-Cycle Costing Techniques and Models*, Air Force Institute of Technology Report No. SLSR 18-7 (Master's Thesis), Aug. 1974, p. 4.
9. Martin B. Goldman and Robert W. Tipton, "Accurate LCC Estimating Early in Program Development," *Proceedings of the Annual Reliability and Maintainability Symposium*, 1974, p. 256.
10. Pearson, "Life-Cycle Costing in an Energy Crisis Era," p. 26.
11. Marco R. Fiorello, *Getting "Real" Data for Life-Cycle Costing*, RAND Corporation, No. AD-A010 960, Jan. 1975, p. 6.
12. A pathfinder LCC analysis was performed for the Large Advanced Antenna Station. Results of this analysis will be published as a separate DSN Progress Report.
13. Dover, *A Summary and Analysis*, p. 2.
14. Harry Rosenberg and James H. Witt, "Effects of Test Equipment Standardization," *Proceedings of the Annual Reliability and Maintainability Symposium*, 1976, p. 287.
15. E. Posner, D. Herrman, and M. McKenzie, "LAASP Tutorial on Life-Cycle Cost" (unpublished), p. 2.
16. Dover, *A Summary and Analysis*, pp. 156-159.
17. *Life-Cycle Costing Emphasizing Energy Conservation, Guidelines for Investment Analysis*, ERDA Publication, September 1976.
18. Earles, "LCC – Commercial Application," p. 79.
19. Dover, *A Summary and Analysis*, p. 19.
20. Philip S. Kilpatrick and Arthur L. Jones, "Life-Cycle Cost Comparisons of Avionic System Design Alternatives," *Proceedings of the National Aerospace and Electronics Conference*, 1974, p. 515.
21. The modules can be found in: Dover, *A Summary and Analysis*.
22. Kilpatrick and Jones, "Life-Cycle Cost Comparisons," p. 514.

23. Examples of further cost element lists are found in:
- Dean B. Dickinson and Lyman Sessen, "Life-Cycle Cost Procurement of Systems and Spares," *Proceedings of the Annual Reliability and Maintainability Symposium*, 1976, p. 282.
 - Allen Dushman, "Effects of Reliability on Life Cycle Inventory Cost," *Proceedings of the Annual Reliability and Maintainability Symposium*, 1969, p. 550.
 - Goldman and Tipton, "Accurate Life-Cycle Costing Early in Program Development," p. 258.
 - Dover, *A Summary and Analysis*, pp. 20, 25.
 - Earles, "LCC – Commercial Application," p. 78.
 - Kilpatrick and Jones, "Life-Cycle Cost Comparisons," p. 541.
 - Fiorello, *Getting "Real" Data*, p. 3.
24. Office of Management and Budget of the Executive Office of the President, Circular No. 9-94 Revised, March 27, 1972, p. 4.
25. Fiorello, *Getting "Real" Data*, p. 81.
26. Other reporting formats can be found in:
- Fiorello, *Getting "Real" Data*, p. 13.
 - Marco Fiorello, *Estimating Life-Cycle Costs: A Cost Study of the A-70*, Air Force Report F-1518-PR, Feb. 1975, p. 19.
 - Gary White and Phillip Ostwald, "Life-Cycle Costing," *Management Accounting*, Vol. 57, No. 7, Jan. 1976, p. 40.
27. Richard S. Brown and Kenneth M. Shachmut, *Economic Analysis Handbook*, Navy Facilities Engineering Command HQ, Report No. P-442, June 1975.
28. The documents are:
- U.S. Department of Defense, *DoD Life Cycle Costing Procurement Guide (Interim)*, LCC-1, July 1970.
 - U.S. Department of Defense, *DoD Casebook – Life Cycle Costing in Equipment Procurement*, LCC-2, July 1970.
 - U.S. Department of Defense, *DoD Life Cycle Costing Guide for Systems Acquisitions (Interim)*, LCC-3, Jan. 1973.
29. Dwight E. Collins, *Analysis of Available Life Cycle Cost Models and Actions Required to Increase Future Model Applications*, Joint AFSC/AFLC Commanders' Working Group, Technical Report No. ASD-TR-75-25, Dec. 1974, pp. 15-16.
30. Fiorello, *Getting "Real" Data*, p. 16.

ORIGINAL PAGE IS
OF POOR QUALITY

Table 1. Life-cycle cost categories^a

Major categories	Subcategories
Research & Development	Engineering Prototype Fabrication System Test & Evaluation Data Total Systems Management Training Producibility Engineering & Planning
Investment, Nonrecurring	Initial Production Facilities Effort Data Tooling Instruction Training Total Systems Management
Investment, Recurring	Hardware Cost Attrition Initial Spares & Repair Parts Support Equipment Auxiliary Equipment First Destination Transportation Initial Training Engineering Changes System Test & Evaluation Total Systems Management
Operating	Personnel Personnel, Replacement Training Consumption Integrated Logistics Support Depot Overhaul Transportation

^aSource: Thomas W. Otto, Jr., *Life-Cycle Cost Model*, U.S. Army Electronics Command Report ECOM-4338, July 1975, p. 8.

Table 2. Weapon system life-cycle cost categories^a

Major categories	Subcategories
RDT&E	Research & Development Test & Evaluation (RDT&E)
Procurement	Aircraft (Flyaway Cost) Support Equipment Training Equipment Technical Manuals SPO-Personnel Test & Evaluation (IOT&E)
Ownership	Spares: Initial, Replenishment, Engines, WRM (HDWR) Maintenance: On-Equipment Maintenance: Off-Equipment Management Personnel: System/Item Managers Training: Tech Training Operations: Crew, CMD PERS – Military and Civilian – Base Only Base Operating Support Fuel Modifications (HDWR) Testing & Evaluation (OT&E) Item Transportation (2nd DSTNTN) Munitions and Missiles – Training Personnel PCS Attrition New Facilities
Salvage & Disposal	Disposal Modifications

^aSource: Marco R. Fiorello, *Getting "Real" Data for Life-Cycle Costing*, RAND Corporation, No. AD-A010 960, Jan. 1975, p. 7.

Table 3. LCC trade-off analysis of two competitive products for two years^a

Cost	Vendor A	Vendor B
Product Price	\$200,000	\$170,000
Installation	3,000	4,000
Manning Labor (2 Yrs)	46,720	93,440
Preventive Maintenance (2 Yrs)	912	1,632
Corrective Maintenance (2 Yrs)	2,800	9,344
Power Requirements (@ 0.025/kW)	1,168	1,314
Parts & Supplies Cost (@ 1% & 2% of Product Price Respectively)	2,000	3,400
TOTAL	\$256,600	\$283,130

^aSource: Gary White and Phillip Ostwald, "Life-cycle Costing," *Management Accounting*, Vol. 57, No. 7, Jan. 1976, p. 42.

A Brief Historical Introduction to Very Long Baseline Interferometry

B. Benjauthrit
TDA Engineering Office

This article provides a short historical account of Very Long Baseline Interferometry, including the rationale, development, and experiments.

I. Introduction

The technique of Very Long Baseline Interferometry (VLBI) has been employed to achieve extremely high angular resolution in the study of radio sources. Unprecedented accuracies may be obtained for values of various geophysical quantities. As an example, it is now possible to compare time scales on separate continents with an uncertainty of only one nanosecond (10^{-9} sec). The main purpose of this article is to provide a short history of VLBI starting from the Michelson-Pease experiment of 1920 up to the present time. This includes the rationale, development, and various experiments behind the subject of VLBI. However, due to a large volume of references¹ on the subject, only certain aspects are covered here.

II. The Rationale Behind Radio Interferometry

Until recently images of celestial objects obtained from radio telescopes lacked the detail of those obtained from optical telescopes. The reason is that the resolution of a telescope increases with the ratio of its aperture to the wavelength of the received signal, and radio wavelengths are

about a million times longer than light wavelengths. Thus, radio telescopes are fundamentally confined to a poor angular resolution when compared to optical telescopes. However, in practice this is not the case for two reasons (Ref. 164):

- (1) The resolution of large optical telescopes is confined not by their size but by irregularities in the earth's atmosphere. The limit is about 1 arc second. This is about 100 times better than the unaided human eye. Also, due to longer wavelength, the fluctuation of the incoming signal path length through the atmosphere at radio frequencies is much smaller than that at light frequencies.
- (2) The signal must be coherent, or in phase, over the entire dimensions of the telescope. Coherent radio waves are much easier to obtain than coherent light signals, so that radio telescopes can operate much closer to the theoretical resolution limit than optical telescopes.

III. Early Need for Radio Interferometry

Although resolution increases as wavelength decreases, the performance begins to deteriorate significantly when the wavelength approaches the dimensions of the structural imperfections in the antenna. Further, the largest antennas

¹All references in this article refer to "An Extensive Bibliography on Long Baseline Interferometry" following this article.

available were paraboloidal type; they had the least precise surfaces. Thus, the best resolution that had been obtained with paraboloidal antennas did not depend strongly on wavelength and was about 1 arc minute. Although it is possible to build a more precise large antenna, it would not provide better resolution than 0.1 arc minute (Ref. 177). This is the reason why radio astronomers turned to interferometry, where in effect two relatively small antennas function as opposite edges of a single huge radio telescope.

The development of interferometry began as early as 1890 when Albert A. Michelson published a paper (Ref. 237) describing a technique of modifying an optical telescope to receive star light along two paths, and determining the angular diameter of a star by means of interference of its own light waves. However, it was not until 1920 that his technique was successfully demonstrated on the 100-inch telescope of Mt. Wilson, in collaboration with F. G. Pease. Figure 1 shows a sketch of the Michelson-Pease stellar optical interferometer. Here, a light wave is intercepted by two separated mirrors which reflect two beams to a common point where the beams are combined. If the path of one beam is made slightly longer or shorter than that of the other beam, the light waves in one beam will be out of phase with the waves in the other beam. When the beams are combined, one sees a pattern of alternating light and dark "fringes."

Attempts to extend the optical interferometer to longer baselines in order to achieve higher resolution have not been very successful, mainly due to the difficulty in obtaining coherent light waves from the system and in maintaining the alignment of the mirrors within a fraction of the wavelength. It is much simpler to solve this problem by using radio waves. Two or more antennas can be used to synthesize large apertures and achieve high angular resolution. With such an instrument, one can determine not only the size and shape of discrete radio sources but also their precise positions in the sky.

IV. Early Development of Radio Interferometry

Early radio interferometers were essentially radio analogs of the above well-known optical device. However, in radio interferometers, the signals are combined and compared (or cross-correlated) electrically. This idea had evolved from the discovery of extraterrestrial radio-frequency radiation by Jansky² in the early 1930's. Figure 2 depicts the radio equivalent first employed by Ryle and Vonberg for solar

observations in the late 1940's.³ In the same period, a radio Lloyd's mirror interferometer was set up in Australia. Meanwhile, McCready and colleagues (Ref. 230) used a similar technique to study solar radiation and its relation to sunspots.

Resolution obtained by radio instruments has been steadily upgraded by advanced technology in short wavelengths and increases in baseline lengths. Many radio sources are well resolved by an interferometer with a baseline of about one kilometer (km) and a resolution of the order of one arc minute. However, by the late 1950's, it was realized that further increases in resolution would be required to study the structure of those sources in more detail and to resolve the smaller sources.

V. Modifications to the Basic Interferometry

The basic interferometer system can be modified in many ways. One way is to employ several intermediate frequencies, each generated by an independent local oscillator. Another way is to use complicated local oscillator chains for greater frequency versatility and phase-compensating systems. Detailed discussions on four modifications, namely, lobe rotation, spectral-line interferometry, Very Long Baseline Interferometry, and intensity interferometry were given by E. B. Fomalont and M. C. H. Wright.⁴ We deal here solely with the subject of VLBI.

VI. Type of Radio Source

It is now generally accepted that the radio emission of discrete sources such as radio galaxies and quasars is "synchrotron" radiation from electrons moving in a weak cosmic magnetic field at relativistic speeds, i.e., speeds close to the speed of light. Also, radio sources may essentially be classified into two different types. One has a large angular extent and is strongest at the longer wavelengths. The other is relatively compact and is strongest at the shorter wavelengths. There is no simple relation between the angular extent of the radio emission and the optical emission from galaxies and quasars, however compact radio sources are not confined to quasars; many are identified with the nuclei of galaxies. Furthermore, many quasars are large extended radio sources.

The large radio sources have a complex distribution of radio emission that typically extends over several hundred thousand light years of space, corresponding to angular dimensions of

²Jansky, K. G., "Electrical Disturbances Apparently of Extraterrestrial Origin," *Proc Inst. Radio Engineers*, N.Y., Vol. 21, p. 1387, 1933.

³Ryle, M., and D. D. Vonberg, *Nature*, pp. 158-339, 1946.

⁴See Chapter 10 of *Galactic and Extragalactic Radio Astronomy*, edited by G. L. Verchuur and K. I. Kellermann, 1974.

between a few arc seconds to a few arc minutes. On the other hand, the compact radio sources are so small and their particle densities are so great that, since relativistic particles absorb radiation as well as emit it, the source becomes opaque to its own radiation at long wavelengths. The self-absorption cutoff frequency depends only on the flux density, the angular size, and weakly on the magnetic-field strength. The smaller the source, the shorter the wavelength at which it becomes opaque.

Since the compact sources are relatively weak at the long wavelengths, where most of the early observations of extragalactic radio sources were made, they remained essentially unnoticed for many years until sensitive receivers for short wavelengths became available. Further, William A. Dent (Ref. 95) discovered in 1965 that some compact sources such as the quasar 3C273 are variable as observed from their radio emissions.

VII. Development of VLBI

Longer baselines for conventional interferometers were not feasible partly because of the increased cost of the cable between the interferometer elements and partly because of human and natural obstructions such as roads, rivers, mountains, and ultimately oceans. To overcome such problems, radio relay links were employed (see Fig. 3). The idea is to join the radio telescopes by a microwave-relay link. Here the local-oscillator signal is transmitted to the mixers to reduce the high frequency signal down to an intermediate level for returning for correlation. In order for the intermediate frequency signals from each antenna to be coherent, they are generally derived from a common source. This technique was first used by Australian and British radio astronomers to obtain baselines of more than 100 km and resolutions better than one second of arc. By the early 1960's the efforts to extend the interferometer baseline were carried out successfully at the University of Manchester (Ref. 274). Various interferometric techniques have also been applied to polarization measurement^{5,6} and the mapping of source brightness distributions (Refs. 142 and 321). However, in order to resolve the compact variable sources with expected dimensions of about 0.001 arc second, baselines of size comparable to the dimensions of the earth were needed. Moreover, large improvements in the resolution of radio link interferometers were not practical because radio links are limited to line-of-sight

operation, and installation of large numbers of repeater stations was both costly and technically complex.

For many years radio astronomers had considered the possibility of completely eliminating the direct electrical connection between interferometer elements by separately recording the signals at each end on magnetic tape and later cross-correlating the two recorded signals. In order to utilize this technique successfully, the following requirements are necessary:

- (1) The recordings of the two tapes must be synchronized so that the time when a given wavefront is received at each station is precisely known. Also, the time tags on the recordings should permit reasonably short searches for fringes in the correlation process.
- (2) The actual radio signal frequencies are generally too high to be recorded directly on magnetic tape. Independent local oscillators must be employed to "heterodyne" the radio signal frequency (typically several gigahertz) to a much lower frequency so that it can be recorded on magnetic tape. If the two lower frequency signals are to be cross-correlated, then the oscillators must remain coherent over the observing time (or integration time). This implies that the relative phase change of the two oscillators must remain small during this period so that the change in frequency is less than the reciprocal of the recording time. For example, at a radio signal frequency of 10 GHz and a 100-second integration time, a frequency stability better than one part in one trillion ($\Delta f/f = 10^{-12}$) is required.
- (3) Due to the time delay after heterodyning, phase rotation is also necessary.

A typical tape-recording interferometer system and a more sophisticated one may be seen in Ref. 164.

The idea of employing independent-local-oscillator tape recording interferometers was considered in the U.S.S.R. as early as 1961. However, stable frequency standards and wide-band tape recorders needed for high sensitivity were not generally available then. The frequency standards generally perform two functions (Ref. 340):

- (1) To generate sufficient phase stability that will ensure no significant loss of coherence in the two signal streams to be cross-correlated.
- (2) To keep time with sufficient accuracy to insure that the clock offset error remains constant over the interval required for the determination of the instantaneous baseline vector.

⁵Ko, H. C., "Theory of Tensor Aperture Synthesis," *IEEE Trans. Antennas and Propagation*, Vol. AP-15, pp. 188-190, Jan. 1967.

⁶Morris, D. V., et al., "Preliminary Measurements on the Distribution of Linear Polarization Over Eight Radio Sources," *Astrophys. J.*, Vol. 139, pp. 560-569, Feb. 1964.

A tape-recording interferometer was first used in radio astronomy by a group at the University of Florida to study the dimensions of the radio storms on the planet Jupiter at a frequency of 18 MHz in 1965 (Ref. 40). Since the Jovian bursts are so intense, an integration time of considerably less than a second and a bandwidth of about one kilohertz (kHz) give an adequate sensitivity (requires $\Delta f/f = 10^{-3}$). Hence, a frequency stability of only one in a million and a time synchronization of about 1 millisecond from the National Bureau of Standards Station WWV were sufficient to maintain coherence at the two ends of the interferometer system. With this it was possible to determine on the surface of Jupiter the dimension of the radio emitting regions less than 1 arc second or about 320 km. This resolution is considerably better than the highest resolution in photographs made of Jupiter at optical wavelengths.

Tape-recording interferometers for studying the much weaker radio emission of radio galaxies and quasars had to wait until stable atomic frequency standards and wideband tape recorders were commercially available. At that time, two systems for tape-recording interferometry were developed independently in the United States (Refs. 12 and 248) and in Canada (Refs. 26 and 27).

A. Analog VLBI Development

The joint Canadian team from the National Research Council and the University of Toronto built an analog recording and processing system employing television tape recorders. At each site data were recorded at 4 MHz on video recorders (down converted from 408 MHz received frequency) on a 90-minute reel tape. Then rubidium frequency standards and a special analog correlator were used to process the data to simultaneously provide fringe patterns from a number of delays. These fringe patterns were then displayed on a multipen recorder.

B. Digital VLBI Development

A system built by two U.S. groups from the National Radio Astronomy Observatory and Cornell University (NRAO-Cornell) used a standard computer tape drive to record digital data in a 360 kHz band. Rubidium frequency standards were also employed here. The incoming signal (down converted from 610 MHz received frequency) was first bandlimited, infinitely clipped, sampled at 720 kilobits per second (kbps) and finally recorded on standard 7-track computer tape at a per-track density of 315 bits per centimeter; hence, a full reel of tape held three minutes of data. This system preserves only the zero crossing information (i.e., the phase) of the signal. The normalized cross-correlation function can still be estimated from this infinitely clipped data by applying a correc-

tion factor derived first by Van Vleck in 1943 (Ref. 382). A large general purpose computer was used to process the data.

VIII. Further Developments and Experiments on VLBI

The Canadian system has a greater bandwidth advantage but requires more complex special equipment to synchronize the tape on playback. In the U.S. system digital data were simply fed into a large general purpose computer which stored and correlated the two data streams. In early experiments 90 minutes of computer time was typically required to process a pair of tapes over 15 delays. Lately, only 50 seconds of computer time has been required to search over 7 delays. By using special-purpose digital correlators further reductions in computer time are possible.

Both the Canadians and Americans had experienced difficulties in their early attempts. The Canadians obtained their fringes first, both on a baseline in Ontario between Shirley Bay and Algonquin Park (183 km) and on a much longer baseline between Algonquin Park and Penticton, B.C. (3074 km).⁷ The NRAO-Cornell group obtained fringes at 610 MHz between Riverside, Md. and Green Bank, W. Va. (228 km), followed by a successful experiment at 1.665 MHz between Westford, Mass., and Green Bank, W. Va. (845 km), with the same digital equipment, by a group at the Massachusetts Institute of Technology. A hydrogen maser frequency standard was used at the Massachusetts site.

The MIT group (Ref. 408), in cooperation with the Northeast Radio Observatory Corporation, Haystack Observatory, Westford, Massachusetts, undertook a program to improve the instruments to allow accurate measurements of group delays (the frequency derivative of the phase delay) to make possible precise determinations of vector baseline (Ref. 138), radio source positions (Ref. 18), polar motion, universal time, and earth tides (Ref. 346).

To measure the group delays with an accuracy greatly exceeding the inverse of the recorded bandwidth, the method of bandwidth synthesis was devised (Refs. 310 and 408) where the receiver passband is switched to sample signals over a wideband. This bandwidth synthesis technique is also employed in the VLBI development at JPL (Refs. 273, 368-376).

First long-baseline measurements with tape-recording were made in 1967 on the baseline across Canada and the U.S. at

⁷Their experimental results were presented at the Ottawa meeting of the International Scientific Radio Union on May 23, 1967 (Refs. 26 and 27).

radio wavelengths of 75, 50, and 18 centimeters. The results confirmed many small size galaxies and quasars. But many were still unresolved and higher resolution was needed. This was rapidly extended in a series of cooperative intercontinental experiments conducted in 1968 and 1969 by American, Swedish, and Australian radio astronomers. With a 6-centimeter wavelength, a 0.001-arc second resolution was obtained on the longest baselines. In spite of this, some small sources still remain unresolved. The 10^4 km California-Australia baseline was already more than 80% of the earth's diameter, so further significant increases in the physical baseline were not feasible without expensive procedures of setting up stations in space or on the moon.

A cheaper and simpler alternative was to observe at shorter wavelengths. Outside North America, however, only two radio telescopes were suitable for operation at short wavelengths and large enough to yield sufficient sensitivity for long-baseline interferometry, both of which were in the U.S.S.R. Due to distance, government regulations, lack of exchange in technology, and other problems, arranging such joint experiments was both difficult and formidable.

The first U.S.-U.S.S.R. experiment was completed late in 1969, using the baseline between the 43-meter radio telescope at NRAO and the 22-meter radio telescope on the shore of the Black Sea in the Crimea (Ref. 388). Later in Spring of 1971, a second experiment was conducted, involving, in addition to the above, the 64-meter radio telescope at Goldstone,⁸ California and the "Haystack" telescope in northern Massachusetts.⁹ More than 20 investigators from eight institutions in both countries participated and it included observations of interstellar clouds of water vapor as well as of radio galaxies and quasars.

The data from the Goldstone-Crimea baseline obtained at a wavelength of 3.5 cm (X-band) provided the highest resolution (about 0.0003 arc sec) achieved so far in the study of radio galaxies and quasars. The measurements of the water vapor clouds which were made at shorter wavelengths gave even higher resolution.

From the various data taken, it was evident that some quasars appear to expand faster than the speed of light. Martin J. Rees (Ref. 297) of the University of Cambridge has suggested the "super light velocity" theory for interpreting such a phenomenon. If the radio source expands at a velocity close to the speed of light, then since it takes a finite time for radio signals to reach an observer, the signal arriving from the

receding part of the source will have originated at an earlier time, when it was closer to the point of origin than the signals from the approaching parts. Under these conditions the apparent velocity of expansion may in fact exceed the speed of light.

Evidence that this might be important in the quasar 3C279 was first obtained in a series of transpacific observations made between 1968 and 1970 by a joint team from Australia (at Tidbinbilla) and the California Institute of Technology (at Goldstone). This group found that a component of the source that had first appeared in 1966 had reached a diameter of about 0.001 arc second by the end of 1969. This corresponds to a linear diameter of about 12 light-years. Thus, the apparent expansion velocity was indeed about twice the speed of light, as theorized by Rees.

More detailed measurements were made of 3C279 in October, 1970, by a group from MIT, NASA, and the University of Maryland employing a transcontinental baseline. These observations were originally designed to measure the gravitational bending of the radio signals from 3C279 as it approached the sun on October 8, but they showed clearly that the compact source in 3C279 was complex and appeared to have at least two components separated by 0.00155 arc second, or about 20 light-years. This source was observed again in February 1971 by the same group and also by investigators from the NRAO, Caltech, and Cornell group, using the same baseline and techniques. The source appeared to double in only four months, but the separation was greater by two light-years. Hence the two components seem to be receding from a common point of origin with an apparent velocity about three times the speed of light.

Although the sensitive long-baseline interferometer systems were initially developed to study the compact extragalactic radio source, the technique has also been used to study the radio emission from interstellar clouds of hydroxyl radicals (OH) and water vapor. Typically the clouds are dispersed over a volume of several light-years across, although the individual components are as small as one astronomical unit (the average distance between the sun and the earth).

One limitation of tape-recording interferometry has been the lack of sufficient oscillator stability to determine the phase of the interference pattern; the improvement is to be expected from the use of hydrogen masers as frequency standards. Even with infinitely stable oscillators, there are still problems (Ref. 339) resulting from fluctuations in the path length through the atmosphere and ionosphere at the two widely separated observing sites.

⁸Managed by JPL for NASA.

⁹Managed by MIT.

Another limitation is the antenna flexure, but this type of limitation is often small and can be calibrated with a residual error of less than 1 mm.

IX. Limitations on Baseline Length

Extension of the baseline cannot always solve the resolution problem. The present evidence indicates that only for wavelengths less than about 10 cm can baselines much greater than the diameter of the earth be effectively used. Hence, hydroxyl emission regions, which radiate at 18 cm, and pulsars, which radiate most strongly at meter wavelengths, are not likely to be targets for a space interferometer.

There is an even more fundamental limit to the maximum baseline when dealing with the synchrotron sources. If the dimensions of the synchrotron system are below a critical size, the relativistic particles quickly lose all their energy by inverse Compton scattering and so do not have time to radiate radio energy. This critical angular size is proportional to the wavelength at which the flux density is the highest. Since the resolution of a fixed length interferometer is inversely proportional to the wavelength of observation, the two effects cancel each other if the observations are made near the wavelength of maximum intensity (as they usually are to achieve the highest sensitivity). Thus, the maximum baseline needed to resolve synchrotron sources is nearly independent of the wavelength of observation; in fact, it is comparable to the diameter of the earth for the stronger radio galaxies and quasars. Baselines in space or on the moon will therefore probably not be necessary to study even the smallest radio nuclei and quasars.

Besides extending the baseline to achieve high resolution, intermediate baselines may be made very effective by linking together to form an ultra-high-resolution array (Refs. 74 and 171); but this can be difficult. Moreover, the task of collecting all the tape recordings at a common location and correlating all possible pairs of telescopes is formidable. An attractive alternative is to telemeter the data from each antenna to a common site by means of synchronously orbiting satellites, dispensing with the tape recording system completely. This technique was successfully demonstrated via the Harnes satellite as reported in Ref. 422.

X. Radio Interferometry for Earth Physics

The techniques of VLBI have also been applied to geophysical studies at JPL. The study of various faults, earthquakes, and other geophysical applications often requires a wide range of baseline lengths. A project that concentrates on this aspect of VLBI is referred to as the Astronomical Radio Interferometric Earth Survey (ARIES) Project (Ref. 218). The essence of the project is to use a pair of antennas, one fixed and the other portable, to provide the desired wide range of baseline lengths. The system characteristics, error sources, and other system details and requirements are given in Refs. 218, 272 and 273.

A mobile VLBI geodetic system¹⁰ is currently under development at JPL for NASA application to earth crustal dynamics studies, as well as for technology transfer to the National Geodetic Survey (NGS), the U.S. Geological Survey (USGS), and other geodetic user communities. This system consists of a 4-meter high mobility station and a 13-meter transportable base station. The system characteristics are given in Table 1. The various error sources (both random and systematic) for the mobile VLBI geodetic system are tabulated in Table 2. Certain applications of such a geodetic system are:

- (1) Environmental monitoring related to natural resource extraction such as subsidence resulted from geothermal field heat removal, oil drillings, and ground water pumping.
- (2) Global tectonics and regional crustal deformations for uses in the development of a fundamental scientific understanding of geodynamic processes and earthquake precursory model development in the pursuit of a reliable productive capability.

Other possible VLBI applications to earth physics are global geodesy, tidal oscillations, crustal-block motions (including continental drift), polar motion, earth rotation, precession and nutation (including a test of general relativity), obliquity of ecliptic, shape of sea surface geopotential and global time and frequency synchronization. More detailed discussions on these applications are given in Ref. 339.

¹⁰Renzetti, N. A., "Radio Interferometric Geodetic System Applications," A JPL internal interoffice memo, dated June 1, 1978.

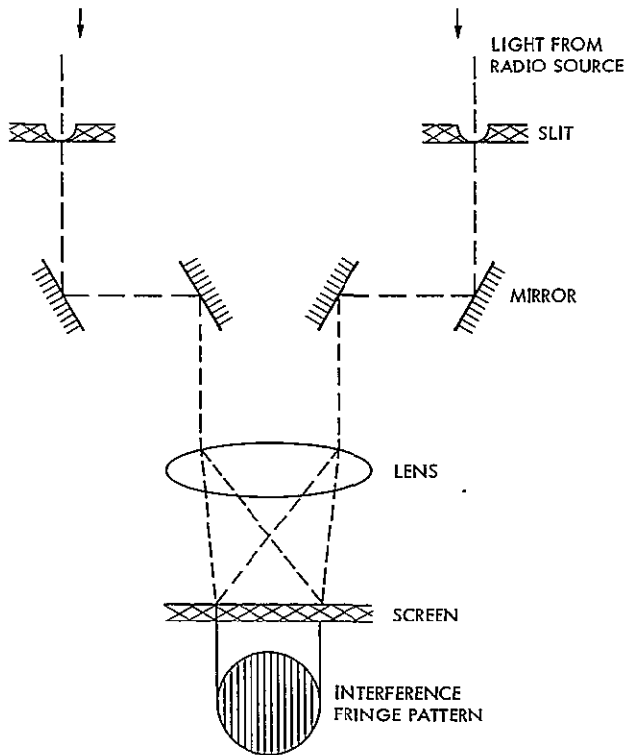
Table 1. Mobile VLBI geodetic system characteristics

Characteristic	Mobile	Transportable base
Antenna diameters	4 m	13 m
Antenna efficiency	50%	50%
Receiver temperature (X-band)	70 Kelvin	30 Kelvin
Bandwidth synthesized	400 MHz	400 MHz
Radio source strength	2 Jansky	2 Jansky
Digital data recording rate ^a	112 Mb/s	112 Mb/s
Observation time per source	720 sec	720 sec
Note: Signal-to-noise ratio		
	25:1	
Average delay precision	22 psec (7 mm)	
Baseline measurement precision limit	5 mm given 6 hr of data (single work shift)	
^a 3-channel bandwidth synthesis		

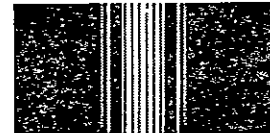
Table 2. Errors in mobile VLBI geodetic system

Errors	Distance equivalent, mm
Random Errors	
Delay precision	7
Time and frequency (H-masers, $\Delta f/f = 5 \times 10^{-15}$)	10
Troposphere	
Dry (surface meteorology)	10
Wet (water vapor radiometers)	10
Ionosphere (8.4 GHz, X-band)	5
Radio source catalog (0.003 arc sec)	7
Root sum square	21
Baseline vector precision given 12 hours of data	10
Systematic Error Sources (Baseline \leq 500 km)	
UT1/polar motion (10-cm accuracy, supplied by external sources)	8
Radio source catalog (0.003 arc sec accuracy to be held essentially constant for monitoring missions)	4
Troposphere	
Dry (surface meteorology)	10
Wet (water vapor radiometry)	7
Ionosphere (X-band)	5
Antenna positioning relative to geodetic marks	5
Root sum square	17
Combined random and systematic error sources accuracy)	20

ORIGINAL PAGE IS
OF POOR QUALITY



ORIGINAL PAGE IS
OF POOR QUALITY



AN ACTUAL DOUBLE-SLIT
INTERFERENCE PHOTOGRAPH

Fig. 1. Michelson-Pease Optical Interferometer. (Light from a distant radio source is reflected from the outer mirrors to the inner mirrors and then optically combined at the projection screen. Moving one of the mirrors makes one light path longer than the other. The two out-of-phase beams, when combined at the screen, will interfere with each other to provide "fringes." A photograph of actual double-slit interference fringes is shown on the right.)

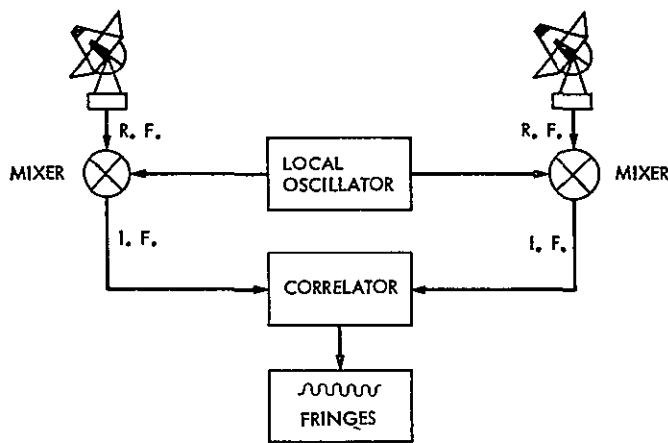


Fig. 2. Basic Radio Interferometer. (Two radio telescopes, separated by a few kilometers, are linked by cables. The high radio frequency (R.F.) signal from the radio source is mixed with a local oscillator signal to provide an intermediate frequency (I.F.) signal which is suitable for further data processing.)

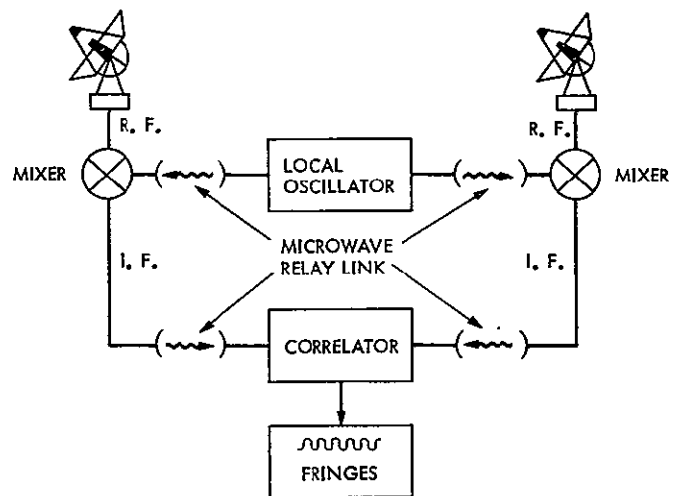


Fig. 3. General Radio-link Interferometer Concept. (The local-oscillator signal is transmitted to the mixers and the I.F. signals are returned via microwave-relay links. The local-oscillator signal at each end is derived from a common source so as to provide coherent (in phase) I.F. signals from each antenna.)

An Extensive Bibliography on Long Baseline Interferometry

B. Benjauthrit

Office of Tracking and Data Acquisition

This article presents an extensive bibliography on the subject of long baseline interferometry, starting from the time of Albert A. Michelson (1890) up to the present time. It contains over 400 references, including areas of long baseline interferometry applications.

Over the past few decades, the subject of long baseline interferometry has grown from a simple concept of an optical device for detecting light fringes to a highly theoretical and sophisticated system assisted by computers and modern electronic components. Interest in this subject is still increasing. The areas of applications are rapidly widening. These include radio astronomy, radio science, geodesy¹, tectonics², space navigation, and seismology.

¹A branch of applied mathematics that determines the exact positions of points and the figures and areas of large portions of the earth's surface, the shape and size of the earth, and the variations of terrestrial gravity and magnetism (*Webster's New Collegiate Dictionary*, 1975).

²A branch of geology concerned with structure, especially with folding and faulting (*ibid.*)

With the above wide applications, it is not surprising that the number of references on the subject is almost inexhaustible. As one searches through the literature, one often wonders which references one should select. The references selected here were considered most relevant to the subject of long baseline interferometry. However, certain papers and texts which have been found helpful in understanding the subject have also been included.

Although there are over four hundred references listed in this bibliography, it is by no means complete. It may, however, be considered one of the most extensive bibliographies on the subject. The bibliography is based on a computer data base search performed by the JPL Library. It is currently stored on the DACONICS computer system at the Laboratory.

In addition to searching through the appropriate references on the subject in the literature, the NASA/RECON computer printouts (the primary and alternate data banks and engineering index from 1962 to April 20, 1978), the INSPEC data base, and a Report Bibliography of the Defense Document Center were utilized. Several references were obtained through private communications with researchers in the field.

One can generally obtain a bibliography on the subject from computer data banks such as those mentioned above, with abstracts and other additional information. However, due to the volume of the data, one is often discouraged from looking through the printouts. With this present bibliography, one should find it much more expeditious and convenient to identify appropriate material. The references are listed alpha-

betically by the principal authors' names. Papers by the same author are listed chronologically. If an article is published in more than one journal (with the same title and authors), the alternative sources are also noted at the end of the reference. Moreover, those papers which can be obtained from the National Technical Information Service (NTIS) are indicated by the words, "Avail. NTIS." Also, the Defense Document Center's identification numbers should be found useful.

According to the computer data banks mentioned above, over 1800 references have been published on VLBI and its related topics. Clearly, it was impossible to include all the available references in this bibliography. Many excellent papers on the subject have had to be omitted, as have the majority of the papers written on applications of VLBI.

1. Aitken, G. J. M., "A signal processing system for a long-baseline interferometer," *IEEE Transactions on Antennas and Propagation*, Vol. AP-16, p. 112, January 1966.
2. Alekseev, V. A., E. D. Gatilyuk, B. N. Lipatov, V. N. Nikonov, A. S. Sizov, A. I. Chikin, and B. V. Shchekotov, "Synchronization of Time Scales at Sites of a Very Long Base Interferometer from Observations of Maser Sources of Cosmic Radio Emission," *Izv. Vuz Radiofiz.*, 18, 1777-85, 1975.
3. Alekseev, V. A., N. S. Blinov, B. N. Lipatov, and E. N. Fedoseev, "Analog of the Tsinger Method in Radio Astrometry," *Astron. Zh.*, 52, 1089-95, 1975.
4. Alekseev, V. A., et al., "Radiospectrometry Using Differential Very Long Baseline Interferometric Measurements," *Radiofizika*, Vol. 19, No. 11, pp. 1669-1677 (in Russian), 1976.
5. Allan, D. W., "Statistics of Atomic Frequency Standards," *Proc. IEEE*, Vol. 54, pp. 221-230, February 1966.
6. Allan, D. W., and J. E. Gray, "Comments on the October 1970 Metrologia paper 'The U.S. Naval Observatory clock time reference and the performance of a sample of atomic clocks'," *Metrologia*, vol. 7, pp. 79-82, April 1971.
7. "All-Union Conference on Radio Astronomy," 8th, Pushchino, USSR, June 18-20, 1975, Papers, Conference sponsored by the Akdemiia Nauk SSSR, *Radiofizika*, Vol. 19, No. 11 (in Russian), 1976.
8. Anderson, B., "Applications of Very Long Baseline Interferometry to Geodesy and Geodynamics," Royal Society (London), *Philosophical Transactions*, Series A, Vol. 284, No. 1326, pp. 469-473, May 11, 1977.
9. Andrew, B. H., "Models of VRO 42.22.01 (BL Lacertae)," *Astrophysical Jnl., (Letters)*, 186, L3, 1973.
10. Arzac, J., "Etude théorique des réseaux d'antennes en radioastronomie et réalisation expérimentale de l'un d'eux" ("Theoretical study of the spacings of radio-astronomical antennas and experimental realization of one of them"), Ph.D. dissertation, University of Paris, Paris, France, 1956.
11. Audion, C., and P. Grivet, "Atomic Clocks in Long Baseline Radio Astronomical Interferometry," *Revue Phys. Appl. (France)*, Vol. 6, No. 2, pp. 247-54, June 1971.

12. Bare, C. C., B. G. Clark, K. I. Kellermann, M. H. Cohen, and D. L. Jauncey, "Interferometer experiment with independent local oscillators," *Science*, vol. 157, pp. 189-191, July 1967.
13. Barton, D. K., "Interferometer Phase Measurements: Comparison with Theory," *IEEE Trans. Antennas and Propagation*, Vol. AP-19, No. 4, pp. 566-9, July 1971.
14. Basart, J. P., et al., "A Phase Stable Interferometer of 100000 Wavelengths Baseline," *Publ. Astron. Soc., Pacific*, Vol. 80, No. 474, pp. 273-80. June 1968.
15. Basart, J. P., et al., "Phase Measurements with an Interferometer Baseline of 11.3 km," *IEEE Trans. Antennas and Propagation*, Vol. AP-18, No. 3, pp. 375-9, May 1970.
16. Batchelor, R. A., et al., "The Parkes Interferometer," *Proc. Instn. Radio Electronics Engrs., Australia*, Vol. 30, No. 10, pp. 305-13, Oct. 1969.
17. Blinov, N. S., and E. N. Fedoseev, "Use of Long Baseline Radio Interferometers for Astrometric Work," *Sov. Astron.*, 17, 383-385, 1973.
18. Blinov, N. S., et al., "Application of Long-Baseline Radio Interferometers to Astrometric Tasks," *Astronomicheskii Zhurnal*, Vol. 50, pp. 601-605 (in Russian), May-June 1973.
19. Block, W. F., M. P. Paul, T. D. Carr, G. R. Lebo, V. M. Robinson, and N. F. Six, "Interferometry of Jupiter at 18 MHz with a 52,800 Lambda Baseline," *Astrophysical Letters*, 5, 133-136, 1970.
20. Broderick, J. J., et al., "Interferometric Observation on the Greenbank-Crimea Baseline," *Radio Sci.*, Vol. 5, No. 10, p. 1281, Oct. 1970.
21. Broderick, J. J., et al., "High-Resolution Observations of Radio Sources Near 8 GHz," *Bull. Am. Astron. Soc.*, Vol. 3, No. 4, Pt. 1, p. 465, 1971.
22. Broderick, J. J., V. V. Vitkevich, et al., "Observations of compact radio sources with a radio interferometer having a Green Bank-Crimea baseline," *Soviet Astronomy-AJ* 14, 4, 627-629, 1971.
23. Broderick, J. J., K. I., Kellermann, D. B. Shaffer, and D. L. Jauncey, "High-Resolution Observations of Compact Radio Sources at 13 Centimeters," *Astrophysical Jnl.*, 172, 299-305, 1972.
24. Broderick, J. J., and J. J. Condon, "Compact Components in a Complete Sample of Extragalactic Radio Sources," *Astrophysical Jnl.*, 202, 596-602, 1975.
25. Broten, N. W., T. H. Legg, J. L. Locke, C. W. McLeish, R. S. Richards, R. M. Chisholm, H. P. Gush, J. L. Yen, and J. A. Galt, "Observations of Quasars Using Interferometer Baselines Up to 3074 km," *Nature*, 215, 38, 1967.
26. Broten, N. W., T. H. Legg, J. L. Locke, C. W. McLeish, R. S. Richards, R. M. Chisholm, H. P. Gush, J. L. Yen, and J. A. Galt, "Long baseline interferometry: a new technique," *Science*, vol. 156, pp. 1592-1593, June 1967.
27. Broten, N. W., R. W. Clarke, T. H. Legg, J. L. Locke, C. W. McLeish, R. S. Richards, J. L. Yen, R. M. Chisholm, and J. A. Galt, "Diameters of some quasars at a wavelength of 66.9 cm," *Nature*, vol. 216, pp. 44-45, Oct. 1967.
28. Broten, N. W., R. W. Clarke, T. H. Legg, J. L. Locke, J. A. Galt, J. L. Yen, and R. M. Chisholm, "Long Baseline Interferometric Observations at 408 and 448 MHz-I," *MNRAS*, 146, 313-327, 1969.

29. Broten, N. W., "The Role of Long Baseline Interferometry in the Measurements of Earth's Rotation," NATO Advanced Study Institute, University of Western Ontario, 1969. *Earthquake Displacement Fields and the Rotation of the Earth*, pp. 279-283, 1970.
30. Brown, G. W., "Long Baseline Interferometry of Jupiter's Decametric Radiation," Ph.D. Thesis, Univ. of Florida, Gainesville, 1970.
31. Brown, G. W., T. D. Carr, and W. F. Block, "Long Baseline Interferometry of S Bursts from Jupiter," *Astrophysical Letters*, 1, 89-94, 1968.
32. Burke, B. F., "Long baseline interferometry," *Phys. Today*, 22, 54-63, 1969.
33. Burke, B. F., "Summer Study Group," Final Report, 1 April 1969-30 June 1970, MIT (Avail. NTIS).
34. Burke, B. F., D. C. Papa, G. D. Papadopoulos, P. R. Schwartz, S. H. Knowles, W. T. Sullivan, M. L. Meek and J. M. Moran, "Studies of H₂O Sources by Means of a Very Long Baseline Interferometer," *Astrophysical Jnl.*, Vol. 160, pp. L63-L68, May 1970.
35. Burke, B. F., K. J. Johnston, V. A. Efanov, B. G. Clark, L. R. Kogan, V. I. Kostenko, K. Y. Lo, L. I. Matveenko, I. G. Moiseev, J. M. Moran, S. H. Knowles, D. C. Papa, G. D. Papadopoulos, A. E. E. Rogers, and P. R. Schwartz, "Observations of Maser Radio Sources with an Angular Resolution of 0.0002," *Sov. Astron-Astronomical Jnl.*, 16, 379-382, 1972.
36. Burke, B. F., "Summer Study Group," DDC# AD-737 689, Feb 1972. Research Lab of Electronics, Mass. Inst. of Tech., Cambridge, Mass.
37. Burke, B. F., "Radio Pictures of the Sky," *Technology Review*, Vol. 78, pp. 44-55, Dec. 1975.
38. Butkevich, A. V., "Application of Long-Base Radio Interferometry for Geodetic Purposes," DDC# AD-B017924L, Defense Mapping Agency Aerospace Center St. Louis Air Force Station, April 1977.
39. Cannon, W. H., R. B. Langley, and W. T. Petrachenko, "Transatlantic Geodesy by Long Baseline Interferometry," *Trends in Modern Geodesy*, Proc. of the Canadian Geophysical Union Symposium, Quebec, 1976. Dept. of Physics and C.R.E.S.S. York University, Toronto, Ontario, Canada.
40. Carr, T. D., J. May, C. N. Olsson, and G. F. Walls, "Post-detector correlation interferometry of Jupiter at 18 Mc/s," *IEEE NEREM Rec.*, Vol. 7, pp. 222-223, Nov. 1965. (This is the first paper written on VLBI.)
41. Carr, T. D., M. A. Lynch, M. P. Paul, G. W. Brown, J. May, N. F. Six, V. M. Robinson, and W. F. Block, "Very Long Baseline Interferometry of Jupiter at 18 MHz," *Radio Sci.*, 5, 1223-1226, 1970.
42. Chao, C. C., "QVLBI Doppler Demonstrations Conducted During Pioneer 2 Encounter and Solar Conjunctions," *DSN Progress Report 42-31*, Feb. 15, 1976, pp. 54-66, (see N76-18163 09-12).
43. Chow, Y. L., and J. L. Yen, "The Spatial Frequency Coverage of Satellite-to-Earth Interferometers," (Univ. of Waterloo) National Radio Sci. Meeting, Univ. of Colorado, Boulder, Colorado, Jan. 9-13, 1978.
44. Clark, B. G., M. H. Cohen, and D. L. Jauncey, "Angular Size of 3C 273B," *Astrophysical Jnl. (Letters)*, 149, L151-L152, 1967.

45. Clark, B. G., "Radio Interferometers of Intermediate Type," *IEEE Trans. on Antennas and Propagation*, Vol. AP-16, No. 1, January 1968.
46. Clark, B. G., K. I. Kellermann, C. C. Bare, M. H. Cohen, and D. L. Jauncey, "High-Resolution Observations of Small-Diameter Radio Sources at 18-centimeter Wavelength," *Astrophysical Jnl.*, 153, 705-714, 1968.
47. Clark, B. G., K. I. Kellermann, C. C. Bare, M. H. Cohen, and D. L. Jauncey, "Radio Interferometry Using a Baseline of 20 Million Wavelengths," *Astrophysical Jnl. (Letters)*, 153, L67-L68, 1968.
48. Clark, B. G., "Information-Processing Systems in Radio Astronomy," *Ann. Rev. Astron. & Ap.*, V.8, pp. 115-38, 1970.
49. Clark, B. G., R. Weimer, and S. Weinreb, *The Mark II VLB System*, NRAO Electronics Division Internal Report 118, 1972.
50. Clark, B. G., "The NRAO Tape-Recorder Interferometer System," *Proceedings of the IEEE*, Vol. 61, No. 9, pp. 1242-1248, 1973.
51. Clark, B. G., K. I. Kellermann, M. H. Cohen, D. B. Shaffer, J. J. Broderick, D. L. Jauncey, L. I. Matveyenko, and I. G. Moiseev, "Variations in the Radio Structure of BL Lacertae," *Astrophysical Jnl. (Letters)*, 182, L57-L60, 1973.
52. Clark, B. G., K. I. Kellermann, and D. Shaffer, "High-Resolution Observations of the Radio Emission from Beta Persei," *Astrophysical Jnl. (Letters)*, 198, L123-L124, 1975.
53. Clark, R. R., F. H. Glanz, and A. D. Frost, "Satellite Verification of an Interferometer Direction Finder for Meteor Radar Echoes," DDC# AD-720 865, Rept. No. Scientific-3, ASL-70-3, New Hampshire Univ., Antenna Systems Lab., Durham, Aug. 1970.
54. Clark, R. W., N. W. Broten, T. H. Legg, J. L. Locke, and J. L. Yen, "Long Baseline Interferometer Observations at 408 and 448 MHz-II," *MNRAS*, 146, 381-397, 1969.
55. Clark, T. A., "Very Long Baseline Interferometry," NASA Goddard Space Flight Center, Greenbelt, MD., 1972 (Avail. NTIS).
56. Clark, T. A., "Precision Timing and Very Long Baseline Interferometry (VLBI) — Application for Measuring Small Angular Features in Galactic and Extragalactic Radio Sources," NASA Goddard Space Flight Center, *Proc. of the 4th PTTI Planning Meeting*, pp. 74-89 (see N75-11249 02-35), 1973.
57. Clark, T. A., et al., "Long Wavelength VLBI," *Proc. IEEE*, Vol. 61, No. 9, pp. 1230-1233, Sept. 1973.
58. Clark, T. A., "Time, Geodesy, and Astrometry Results from Radio Interferometry," *Proc. of the 5th Ann. NASA & DOD PTTI Planning Meeting*, pp. 33-46, 1974.
59. Clark, T. A., et al., "Application of VLBI to Astrometry and Geodesy Effect of Frequency Standard Instability on Accuracy," *PTTI*, pp. 349-359, 1974.
60. Clark, T. A., C. C. Counselman III, I. I. Shapiro, H. F. Hinteregger, A. E. E. Rogers, and A. R. Whitney, "Very Long Baseline Interferometry for Centimeter Accuracy in Geodetic Measurements," *Tectonophys.*, 29, (1-4):9-18, 1975.

61. Clark, T. A., et al., "Meter-Wavelength VLBI. II – The Observations – Astronomical Very Long Baseline Interferometry," *Astronomical Jnl.*, Vol. 80, pp. 923-930, Nov. 1975.
62. Clark, T. A., et al., "An Unusually Strong Radio Outburst in Algol – VLBI Observations," *Astrophysical Jnl.*, Vol. 206, Pt. 2, pp. L107-L111, June 1, 1976.
63. Clark, T. A., et al., "Radio Source Positions from Very Long Baseline Interferometry Observations," *Astronomical Jnl.*, Vol. 81, pp. 599-603, Aug. 1976.
64. Coates, R. J., T. A. Clark, C. C. Counselman, III, I. I. Shapiro, H. F. Hinterreger, A. E. E. Rogers, and A. R. Whitney, "Very long baseline interferometer for centimeter accuracy geodetic measurements," *Tectonophysics*, Vol. 29, No. 1-4, pp. 9-18, 1975, from 5th Int. Symp. on Recent Crustal Movements, Zurich, Switzerland, pp. 9-18, Aug. 26-31, 1976.
65. Cohen, M. H., "High-Resolution Observations of Radio Sources," *Ann. Rev. Astr. and Astrophysics*, 7, 619-660, 1969.
66. Cohen, M. H., et al., "Compact Radio Source in the Nucleus of M87," *Astrophys. J. Letters*, pp. L83-L85, 1969.
67. Cohen, M. H., D. L. Jauncey, C. C. Bare, B. G. Clark, and K. I. Kellerman, "High Resolution Radio Interferometry at 610 MHz," *Astrophysical Jnl.*, V160, pp. 337-339, Apr., 1970.
68. Cohen, M. H., and D. R. Shaffer, "Positions of Radio Sources from Long-Baseline Interferometry," *Astronomical Jnl.*, V76 N2, pp. 91-100, No. 1387, March 1971.
69. Cohen, M. H., W. Cannon, G. H. Purcell, D. B. Shaffer, J. J. Broderick, K. I. Kellerman, and D. L. Jauncey, "The small-scale structure of radio galaxies and quasi-stellar sources at 3.8 centimeters," *Astrophysical Journal*, 170, 207-217, December 1, 1971.
70. Cohen, M. H., "Accurate Positions for Radio Sources," *Astrophysics Letters*, 12, 81-85, 1972.
71. Cohen, M. H., "Introduction to Very-Long-Baseline Interferometry," *Proc. IEEE*, V. 61, No. 9, pp. 1192-1197, Sept. 1973 (Also Rept. No. 1973-7, Owens Valley Radio Observatory, Pasadena, Calif., 1973 and NTIS).
72. Cohen, M. H., "Small Scale Structure of Quasars and Galactic Nuclei at Radio Wavelengths," *Annals NY Acad. Sci.*, 262, 428-435, 1975.
73. Cohen, M. H., A. T. Moffet, J. D. Romney, R. T. Schilizzi, D. B. Shaffer, K. I. Kellermann, G. H. Purcell, G. Grove, G. W. Swenson, Jr., J. L. Yen, I. I. K. Pauliny-Toth, E. Preuss, A. Witzel, and D. Graham, "Observations with a VLB Array. I. Introduction and Procedures," *Astrophysical Jnl.*, 201, 249-255, 1975.
74. Cohen, M. H., et al., "A VLBI Network Using Existing Telescopes: A Report and Proposal Submitted by The Network Group," 1975.
75. Cohen, M. H., A. T. Moffet, J. D. Romney, R. T. Schilizzi, G. A. Seielstad, K. I. Kellermann, G. H. Purcell, D. B. Shaffer, I. I. K. Pauliny-Toth, E. Preuss, A. Witzel, and R. Rinehart, "Rapid Increase in the Size of 3C 345," *Astrophysical Jnl. (Letters)*, 206, L1-L3, 1976.
76. Cohen, E. J., J. L. Fanselow, G. H. Purcell, Jr., D. H. Rogstad, and J. B. Thomas, "Recent Astrometric Observations on Intercontinental Baselines," (Advanced VLBI System Group, Jet Propulsion Lab., Pasadena, California). National Radio Sci. Meeting, Univ. of Colorado, Boulder, Colorado, Jan 9-13, 1978.

77. Corbin, T. E., and S. J. Goldstein, Jr., "Interferometer Baselines and Poles Obtained by Linking Radio Observatories," Leander McCormick Observatory, Charlottesville, Va., 1972 (Avail. NTIS).
78. Counselman, C. C., III, H. F. Hinteregger, and I. I. Shapiro, "Astronomical Applications of Differential Interferometry," *Science*, Vol. 178, pp. 607-608, 1972.
79. Counselman, C. C., III, et al., "Lunar Baselines and Libration from Differential VLBI Observations of ALSEPS," *The Moon*, Vol. 8, pp. 484-489, 1973.
80. Counselman, C. C., III, "Very-Long Baseline Interferometry Techniques Applied to Problems of Geodesy, Geophysics, Planetary Science, Astronomy, and General Relativity," *Proc. IEEE*, Vol. 61, No. 9, pp. 1225-1230, Sept. 1973.
81. Counselman, C. C., III, H. F. Hinteregger, R. W. King, and I. I. Shapiro, "Precision Selenodesy Via Differential Interferometry," *Science*, 181, 772-774, 1973.
82. Counselman, C. C., III, "Positions of Extragalactic Sources from Very Long Baseline Interferometry," *New Problems In Astrometry*, Ed: Gliese, et al. Reidel, Dordrecht-Holland, 1974, pp. 119-124 (IAU Symposium No. 61, Perth, 1973).
83. Counselman, C. C., III, S. M. Kent, C. A. Knight, I. I. Shapiro, T. A. Clark, H. F. Hinteregger, A. E. E. Rogers, and A. R. Whitney, "Solar gravitational deflection of radio waves measured by very-long baseline interferometry," *Phys. Rev. Letters*, Vol. 33, pp. 1621-1623, 1974.
84. Counselman, C. C., III, "Precision Selenodesy and Lunar Libration Through VLBI Observations of Alseps," "Final Technical Report, 1 Jan. 1974-31 Jan. 1975, Dept. of Earth and Planetary Sciences, MIT, Cambridge (Avail. NTIS).
85. Counselman, C. C., III, "Geodesy by Very Long Baseline Interferometry," *Rev. Geophys. Space Phys.*, 13, 270-271, 1975.
86. Counselman, C. C., III, "Radio Astronomy," *Annual Review of Astronomy and Astrophysics*, Vol. 14, Palo Alto, Calif., Annual Reviews, Inc., pp. 197-214, 1976.
87. Counselman, C. C., III, "VLBI Observations of ALSEP Transmitters," Final Report, Dept. of Earth and Planetary Sciences, M.I.T., Sept. 30, 1977 (Avail. NTIS).
88. Counselman, C. C., III, et al., "VLBI clock synchronization - for atomic clock rate," *IEEE Proceedings*, Vol. 65, pp. 1622-1623, Nov. 1977.
89. Cronyn, W. M., "Long Baseline Interferometry at a Decametric Wavelength," *Bull. Am. Astron. Soc.*, Vol. 3, No. 3, Pt. II, p. 416, 1971.
90. Cronyn, W. M., "Interferometry: Effects of Irregular Propagation Media," *Bull. Am. Astron. Soc.*, Vol. 4, No. 2, Pt. 1, p. 216, 1972.
91. Cronyn, W. M., "Interferometer Visibility Scintillation," *Astrophysical Journal*, 174, 181-200, May 15, 1972.
92. Cutler, L. S., and R. F. C. Vessot, "Present Status of Clocks and Frequency Standards, in 1968 NEREM Record, Boston, Mass. 6-8 Nov. 1968" (IEEE, New York, pp. 68-9, 1968).
93. Dachel, P. R., et al., "Hydrogen Maser Frequency Standards for the Deep Space Network," *DSN Progress Report 42-40*, pp. 76-83, August 15, 1977. (Also PTTI Conference, Proceedings, December 1976).

94. Dennison, B. K., "Astronomical Polarization Studies at Radio and Infrared Wavelengths, Part I. Gravitational Deflection of Polarized Radiation," Cornell Univ., Ithaca, N. Y., Aug. 1976, (NTIS HC A05/MF A01).
95. Dent, W. A., "Variation in the radio emission from the Seyfert Galaxy NGC 1275," *Astrophysical Jnl.*, Vol. 144, p. 843, 1966.
96. Dent, W. A., "3C 279: Evidence for a Non-Superrelativistic Model," *Science*, 175, 1105, 1972.
97. Dent, W. A. "Evidence for Spatially Independent Outbursts in Compact Radio Sources," *Astrophysical Jnl.*, 175, L55, 1972.
98. Dicke, R. H., "The Secular Acceleration of the Earth's Rotation and Cosmology," *The Earth-Moon System*, eds. B. G. Marsden and A. G. W. Cameron, pp. 98-164, Plenus, New York, 1966.
99. Dickinson, D. F., M. D. Grossi, and M. R. Pearlman, "Refractive Corrections in High-Accuracy Radio Interferometry," *Journal of Geophysical Research*, Vol. 75, pp. 1619-1621, 1970.
100. Dieter, N. H., et al., "A Very Small Interstellar Neutral Hydrogen Cloud Observed with VLBI Techniques," *Astrophysical Jnl.*, Vol. 206, Pt. 2, pp. L113-L115, June 1, 1976.
101. Donaldson, W., et al., "Interferometric Observations with a Baseline of 127 Kilometers II," *Monthly Notes Roy. Astron. Soc.*, Vol. 152, No. 2., pp. 145-58, 1971.
102. Dravskikh, A. F., et al., "On the Possibility of Creating a Radio-Astronomical Inertial Coordinate System Based on the Measurement of Arcs between QSOs with the aid of VLBI," *Astrophysics and Space Science*, Vol. 38, pp. 255-266, Dec. 1975.
103. Dravskikh, A. F., "Tropospheric limits to the accuracy of radio-interferometer measurements of coordinates with the aid of interference frequency," *Radio-tekhnika I Elektronika*, Vol. 22, pp. 2305-2311, Nov. 1977 (in Russian).
104. Dulk, G. A., "Characteristics of Jupiter's decametric radio source measured with arc-second resolution," *Astrophys. J.*, vol. 159, pp. 671-684, Feb. 1970.
105. Epstein, R. I., and M. J. Geller, "A Model for Superlight Velocities of Extragalactic Radio Sources," *Nature*, 265, 219-222, 1977.
106. Erickson, W. C., T. B. H. Kuiper, T. A. Clark, S. H. Knowles, and J. J. Broderick, "Very Long Baseline Interferometer Observations of Taurus A and Other Sources at 121.6 MHz," *Astrophysical Jnl.*, 177, 101-114, 1972.
107. *Explanatory Supplement to the Astronomical Ephemeris and the American Ephemeris and Nautical Almanac*, London, Her Majesty's Stationery Office, p. 83, 1961.
108. Fajemirokun, F. A., "Applications of Laser Ranging and VLBI Observations for Selenodetic Control," Dept. of Geodetic Science, Ohio State University Research Foundation, Columbus, Nov. 1971 (Avail. NTIS).
109. Fanselow, J. L., P. F. MacDoran, J. B. Thomas, J. G. Williams, C. J. Finnie, T. Sato, L. Skjerve, and D. J. Spitzmesser, "The Goldstone interferometer for earth physics," *DSN Technical Report 32-1526*, vol. V, pp. 45-57, Jet Propulsion Lab., Oct. 15, 1971.
110. Findlay, J. W., Ed., "Charlottesville symposium on very long baseline interferometry," *Radio Sci.*, vol. 5, pp. 1221-1292, Oct. 1970.

111. Finnie, C., R. Sydnor, and A. Sward, "Hydrogen maser frequency standard," in *Proc. 25th Ann. Freq. Contr. Symp.* (Ft. Monmouth, N.J.), pp. 348-351, Apr. 1971.
112. Fliegel, H. F., et al., "Frequency Standards Requirements of the NASA DSN to Support Outer Planet Missions," in *NASA Goddard Space Flight Center Proc. of the 6th Ann. Precise Time and Time Interval Planning Meeting*, pp. 381-393, 1974.
113. Fomalont, E. B., "Earth Rotation Aperture Synthesis," *Proc. IEEE*, Vol. 61, p. 1211, 1973.
114. Fort, D. N., "Studies of Small Diameter Radio Sources with a Tape Recording Interferometer," University of Manchester, Thesis, 1971.
115. Fort, D. N., "The Brightness Distribution of 3C 84," *Astrophysical Jnl. (Letters)*, 207, L155-L157, 1976.
116. Fort, D. N., and H. K. C. Yee, "A Method of Obtaining Brightness Distributions From Long Baseline Interferometry," *Astr. and Astrophysical J.*, 50, 19, 1976.
117. Fort, D. N., "Radio Source Structures from Long Baseline Interferometry," National Radio Sci. Meeting, Univ. of Colorado, Boulder, Colorado, Jan 9-13, 1978.
118. Frost, A. D., et al., "The long-base-line interferometer at Jodrell Bank," *Sky and Telescope*, Vol. 32, pp. 21-24, July 1966. (Also in *NEREM Record*, 1965, Vol. 7.)
119. Frost, A. D., and R. R. Clark, "Observations of Large Scale Ionospheric Irregularities Using a Long Baseline Interferometer," Final Report, 1 Feb. 1972 - 31 Jan. 1972, New Hampshire University, Durham, No. ASL-72-A (Avail. NTIS).
120. Fujita, et al., "Baseline arrangement of radio interferometer array for tracking artificial satellites," *Electron. Commun. Japan*, Vol. 55, No. 5, pp. 102-108, May 1972.
121. Galt, J. A., N. W. Broten, T. H. Legg, J. L. Locke, and J. L. Yen, "Long Baseline Observations of CPO 329," *Nature*, 225, 530-531, 1970.
122. Galt, J. A., N. W. Broten, and T. H. Legg, "Simultaneous Interferometric and Spectrometric Observations of Pulsar 0329+54," *Astronomical Jnl.*, 80, 311-317, 1975.
123. Galt, J. A., N. W. Broten, T. H. Legg, H. J. A. Leparskas, and J. L. Yen, "Long-Baseline Interferometer Observations at 430 MHz," *MNRAS*, 178, 1977.
124. Garner, E., "Air Force Research Review. Number 2, March-April 1971," DDC# AD727338, Rept. No. AFSCR-80-2, Air Force Systems Command, Washington D.C., April 1971.
125. Gay, J., and A. Journet, "Infrared Interferometry," *Nature Physical Science*, Vol. 241, pp. 32, 33, Jan. 8, 1973.
126. Giuffrida, T. S., B. J. Rossin, R. L. Fiedler, A. Parrish, and B. F. Burke, "The M.I.T. Radio Interferometer On-Line Data Processing System," National Radio Science Meeting, Univ. of Colorado, Boulder, Colorado, Jan. 9-13, 1978.
127. Gold, T., "Radio method for the precise measurement of the rotation period of the earth," *Science*, 157, 302-304, 1967.
128. Gubbay, J. S., A. J. Legg, D. S. Robertson, A. T. Moffet, R. D. Ekers, and B. Seidel, "Variations of Small Quasar Components at 2300 MHz," *Nature*, 224, 1094, 1969.

129. Gubbay, J. S., A. J. Legg, D. S. Robertson, A. T. Moffet, and B. Seidel, "Trans-Pacific Interferometer Measurements at 2300 MHz," *Nature*, 222, 730, 1969.
130. Gubbay, J. S., et al., "Comparison of Two Intercontinental Baselines by VLBI - Very Long Baseline Interferometry," in *Symposium on Earth's Gravitational Field and Secular Variations in Position*, Sydney, Australia, University of New South Wales, pp. 396-404, 1974.
131. Gubbay, J. S., A. J. Legg, D. S. Robertson, W. Gliese, C. A. Murray, and R. H. Tucker, "Position Solution of Compact Radio Sources Using Long Coherence VLBI," *IAU Symposium No. 61 on New Problems in Astrometry*, 125-9, 1974.
132. Gubbay, J. S., A. J. Legg, D. S. Robertson, G. D. Nicolson, A. T. Moffet, and D. B. Shaffer, "Variations in the Intensities and Sizes of Compact Radio Sources at 13 cm Wavelength," *Astrophysical Jnl.* 1977.
133. Gush, H. P., "A Long Baseline Radio Interferometer for the Measurements of Quasar Diameters," *Physics in Canada*, 22, No. 5, 14, 1966.
134. Hemenway, P. D., *The Measurement of Position, Baseline, and Time Using 4-Antenna Interferometry*, Ph.D. Thesis, Virginia Univ., Charlottesville, 1974.
135. Heppenheimer, T. A., "Spaceborne VLB radio astronomy interferometry," *Journal of Spacecraft and Rockets*, Vol. 11, p. 268-270, Apr. 1974.
136. Hildebrand, C. E., V. J. Ondrasik, and G. A. Ransford, "Earthbased navigation capabilities for outer planet missions," in *AIAA/AAS Astrodynamics Conference*, Palo Alto, Calif., AIAA Paper 72-925, Sept. 11-12, 1972.
137. Hinteregger, H. F., "A long baseline interferometer system with extended bandwidth," *IEEE NEREM Rec.*, vol. 10, pp. 66-67, Nov. 1968.
138. Hinteregger, H. F., I. I. Shapiro, D. S. Robertson, G. A. Knight, R. A. Ergas, A. R. Whitney, A. E. E. Rogers, J. M. Moran, T. A. Clark, and B. F. Burke, "Precision geodesy via radio interferometry," *Science*, 178, 396-398, 1972.
139. Hinteregger, H. F., G. W. Catuna, C. C. Counselman III, R. A. Ergas, R. W. King, C. A. Knight, D. S. Robertson, A. E. E. Rogers, I. I. Shapiro, A. R. Whitney, T. A. Clark, L. K. Hutton, G. E. Marandino, R. A. Perley, G. Resch, and N. R. Vandenberg, "Cygnus-X-3 Radio Sources: Lower Limit on Size and Upper Limit on Distance," *Nature, Phys. Sci.*, 240, 159-160, 1972.
140. Hjellming, R. M., "Beta Persei - Radio Star and Probable X-Ray Star," *Nature, Physical Science*, Vol. 238, pp. 52-55, July 24, 1972.
141. Hjellming, R. M., B. Balick, and C. Bignell, "Early VLA Maps of Four Planetary Nebulae" (National Radio Astronomy Observatory, Socorro, NM), National Radio Sci. Meeting, Univ. of Colorado, Boulder, Colorado, Jan. 9-13, 1978.
142. Hogg, D. E., G. H. MacDonald, R. G. Conway, and C. M. Wade, "Synthesis of brightness distribution in radio sources," *Astron. J.*, vol. 74, pp. 1206-1213, Dec. 1969.
143. Hung, N. T., et al., "Magnitude of 64-m Elevation Axis Movements Due to Alidade Temperature Changes," *DSN Progress Report 42-36*, pp. 41-44, Dec. 15, 1976 (NTIS HC A08/MF A01).
144. Hurd, W. J., "DSN station clock synchronization by maximum likelihood VLBI," *DSN Technical Report 32-1526*, vol. X, pp. 82-95, Aug. 15, 1972.

145. Hurd, W. J., "Demonstration of Intercontinental DSN Clock Synchronization by VLBI," *NASA Goddard Space Flight Center Proc. of the 5th Ann. NASA and DOD PTTI Planning Meeting*, pp. 59-73, 1973 (N75-11275 Oz-35).
146. Hurd, W. J., "An Analysis and Demonstration of Clock Synchronization by VLBI," *IEEE Transactions Instrumentation and Measurement*, Vol. IM-23, No. 1, pp. 80-89, March 1974.
147. Hurd, W. J., "VLBI SNR: Definitions and Comparisons," JPL IOM 331-76-57, Aug. 16, 1976 (JPL internal document).
148. Hurd, W. J., "Preliminary Demonstration of Precision DSN Clock Synchronization by Radio Interferometry," *DSN Progress Report 42-37*, pp. 57-68, Feb. 15, 1977.
149. Hutton, L. K., T. A. Clark, W. C. Erickson, G. M. Resch, N. R. Vandenberg, S. H. Knowles, and A. B. Youmans, "Meter-Wavelength VLBI, I-Cassiopeia A," *Astronomical Jnl.*, 79, 1248, 1974.
150. Hutton, L. K., et al., "High Resolution Observations of Cassiopeia A at Meter Wavelengths — Pulsar Source in Supernova Remnant," NASA Goddard Space Flight Center, Greenbelt, Md., May 1974 (Avail. NTIS).
151. Hutton, L. K., "Fine Structure in 3C 120 and 3C 84," Ph.D. Thesis, Maryland Univ., 24 Aug. 1976 (Avail. NTIS).
152. Jauncey, D. L., C. C. Bare, B. G. Clark, K. I. Kellermann, and M. H. Cohen, "High-Resolution Radio Interferometry at 610 MHz," *Astrophysical Jnl.*, 160, 337-339, 1970.
153. Jennison, R. C., "A Phase Sensitive Interferometer Technique for the Measurement of the Fourier Transform of the Spatial Brightness Distribution of Small Angular Extent," *Monthly Notes Roy. Astron. Soc.*, Vol. 118, p. 276, 1958.
154. Johnston, K. J., S. H. Knowles, W. T. Sullivan, III, J. M. Moran, and C. A. Knight, "An Interferometer Map of the Water-Vapor Sources in W49," *Astrophysical Jnl.*, V. 166, pp. L21-L26, 15 May 1971.
155. Johnston, K. J., "Radio Astrometry," in *NASA Goddard Space Flight Center Proc. of the 6th Ann. Precise Time and Time Interval (PTTI) Planning Meeting*, pp. 373-379, 1974.
156. Johnston, K. J., "Astrometry Via Connected Element Interferometry," National Radio Sci. Meeting, Univ. of Colorado, Boulder, Colorado, Jan. 9-13, 1978.
157. Jones, H. S., "The Rotation of the Earth and the Secular Acceleration of the Sun, Moon and Planets," *Mon. Not. Roy. Astron. Soc.*, Vol. 99, pp. 541-558, 1939.
158. Kaidanovskii, N. L., "Design of radio interferometers with a super-longbase," *Radio Engineering and Electronic Physics*, Vol. 11, pp. 1531-1534, Oct. 1966.
159. Kaula, W. M., and A. W. Harris, "Dynamics of Lunar Origin and Orbital Evolution," *Reviews of Geophysics and Space Physics*, Vol. 13, pp. 363-371, 1975.
160. Kellermann, K. I., B. G. Clark, C. C. Bare, O. Rydbeck, J. Ellder, B. Hansson, E. Kollberg, B. Hoglund, M. H. Cohen, and D. L. Jauncey, "High-Resolution Interferometry of Small Radio Sources Using Intercontinental Base Lines," *Astrophysical Jnl. (Letters)*, 153, L209-L214, 1968.

161. Kellermann, K. I., et al., "High resolution observations of compact radio sources at 13 centimeters," *Astrophys. J.*, Vol. 161, pp. 803-809, Sept. 1970.
162. Kellermann, K. I., D. L. Jauncey, M. H. Cohen, D. B. Shaffer, B. G. Clark, J. Broderick, B. Ronnang, O. E. H. Rydbeck, L. Matveyenko, I. Moiseyev, V. V. Vitkevitch, B. F. C. Cooper, and R. Batchelor, "High-resolution observations of compact radio sources at 6 and 18 cm," *Astrophys. J.*, vol. 169, pp. 1-24, Oct. 1971.
163. Kellermann, K. I., "Joint Soviet-American Radio Interferometry," *Sky and Tel.*, 42, 132-133, 1971.
164. Kellermann, K. I., "Intercontinental radio astronomy," *Scientific American*, 226, 2, 72-83, 1972.
165. Kellermann, K. I., B. G. Clark, M. H. Cohen, D. B. Shaffer, J. J. Broderick, and D. L. Jauncey, "Absence of variations in the nucleus of Virgo A," *Astrophysical Jnl. (Letters)*, 179, L141-L144, 1973.
166. Kellermann, K. I., B. G. Clark, D. L. Jauncey, J. J. Broderick, D. B. Shaffer, M. H. Cohen, and A. E. Niell, "Observations of Further Outbursts in the Radio Galaxy 3C 120," *Astrophysical Jnl. (Letters)*, 183, L51-L55, 1973.
167. Kellermann, K. I., B. G. Clark, D. B. Shaffer, M. H. Cohen, D. L. Jauncey, J. J. Broderick, and A. E. Niell, "Further Observations of Apparent Changes in the Structure of 3C 273 and 3C 279," *Astrophysical Jnl. (Letters)*, 189, L19-L22, 1974.
168. Kellermann, K. I., B. G. Clark, A. E. Niell, and D. B. Shaffer, "Observations of Compact Radio Nuclei in Cygnus A, Centaurus A, and Other Extended Radio Sources," *Astrophysical Jnl. (Letters)*, 197, L113-L116, 1975.
169. Kellermann, K. I., et al., "Observations of a Radio Source in the Nucleus of M81 with Dimensions Less than 1300 Astronomical Units," *Astrophysical Jnl.*, Vol. 210, Pt. 2, pp. L121-L122, Dec. 15, 1976.
170. Kellermann, K. I., D. B. Shaffer, G. H. Purcell, I. I. K. Payliny-Toth, E. Preuss, A. Witzel, D. Graham, R. T. Schilizzi, M. H. Cohen, A. T. Moffet, J. D. Romney, and A. E. Niell, "Very High Resolution Observations of the Radio Sources NRAO 150, OJ 287, 3C 273, M87, 1633+38, BL Lac and 3C 454.3," *Astrophysical Jnl.*, 1977.
171. Kellermann, K. I., "An Intercontinental Very Long Baseline Array," *VLBI Network Studies III*, National Radio Astronomy Observatory, Green Bank, W. Va., May 1977.
172. Kellermann, K. I., D. B. Shaffer, B. G. Clark, and B. J. Geldzahler, "The Small Radio Source at the Galactic Center," *Astrophysical Jnl.*, Part 2 — Letters to the Editor, Vol. 214, pp. L61-L62, June 1, 1977.
173. King, R. W., *Precision Selenodesy via Differential Very-Long Baseline Interferometry*, Ph.D. Thesis, Massachusetts Institute of Technology, Cambridge, Mass., 1975.
174. King, R. W., C. C. Counselman, III, and I. I. Shapiro, "Lunar Dynamics and Selenodesy — Results from Analysis of VLBI and LASER Data," *Jnl. of Geophysical Research*, Vol. 81, pp. 6251-6256, Dec. 10, 1976.
175. King, R. W., C. C. Counselman, III, I. I. Shapiro, and H. F. Hinteregger, "Study of Lunar Librations Using Differential Very Long Baseline Observations of Alseps," *Recent Advances in Engineering Science*, Vol. 8, pp. 431-438, 1977.

176. Klemperer, W. K., et al., "Long Baseline Interferometry with Large Meter-Wavelength Antenna Arrays," *IEEE, Int. Conf. on Commun. Conf. Rec.*, Montreal, Canada, pp. 20-22, June 14-16, 1971.
177. Klemperer, W. K., "Long-Baseline Radio Interferometry with Independent Frequency Standards," *Proceedings of the IEEE*, 60 No. 5, 602-609, 1972.
178. Knight, C. A., D. S. Robertson, A. E. E. Rogers, I. I. Shapiro, A. R. Whitney, T. A. Clark, R. M. Goldstein, G. E. Marandino, and N. R. Vandenberg, "Quasars: millisecond-of-arc structure revealed by very long baseline interferometry," *Science*, vol. 172, pp. 52-54, Apr. 1971.
179. Knight, C. A., "Accurate Radio Source Positions from Four-Antenna Long Baseline Interferometry," Massachusetts Institute of Technology, 1976.
180. Knight, C. A., et al., "Astrometry Via Long Baseline Interferometry," National Radio Sci. Meeting, Univ. of Colorado, Boulder, Colorado, Jan. 9-13, 1978.
181. Knowles, S. H., K. J. Johnston, J. M. Moran, and J. A. Ball, "Interferometric Observations of the $2\pi 3/2$, $J=5/2$ State of Interstellar OH," *Astrophysical Jnl. (Letters)*, 180, L117-L121, 1973.
182. Knowles, S. H., et al., "Applications of Radio Interferometry to Navigation," *NASA Goddard-Space Flight Center Proc. of the 5th Ann. NASA and DOD PTTI Planning Meeting*, pp. 47-58, 1973 (see N75-11275 02-35).
183. Knowles, S. H., K. L. Johnston, J. M. Moran, B. F. Burke, K. Y. Lo, and G. D. Papadopoulos, "Further Interferometer Observations of the Water Vapor Sources in W49," *Astronomical Jnl.*, 79,925, 1974.
184. Koehler, R. L., "Radio propagation measurements of pulsed plasma streams from the sun using pioneer spacecraft," *J. Geophys. Res.*, 73, 15, 4883-4894, 1968.
185. Kogan, L. R., et al., "System for recording and processing data for VLBI," *Radio-phys. Quantum Electron.*, Vol. 19, No. 9, pp. 889-892, Sept. 1976.
186. Kolaczek, B., and G. Weiffenbach, "On Reference Coordinate Systems for Earth Dynamics," *Proceedings of the Colloquium*, Uniwersytet Torunski, Torun, Poland, Aug. 26-31, 1974.
187. Krasinskii, C. A., "On Constructing the Inertial System of High Accuracy by VLBI Methods," *Proceedings of the Colloquium on Reference Coordinate Systems for Earth Dynamics*, Torun, Poland, pp. 381-393, Aug. 26-31, 1974.
188. Landgren, P. G., and B. O. Roennaeng, "An Astronomical Computer Program Package for the Onsala Space Observatory," Chalmers University of Technology, Goteborg, Sweden, 1971 (Avail. NTIS).
189. Lawson, J. L., and G. E. Uhlenbeck, *Threshold Signals*, vol. 24, MIT Radiation Laboratory Series, New York, McGraw-Hill, 1950.
190. Lay, R., "Phase and Group Delay of S-band Megawatt Cassegrain Diplex and S-band Megawatt Transmit Filter," *DSN Progress Report 47-37*, p. 198-203, Feb. 15, 1977.
191. Layland, J. W., "Threshold Analysis for VLBI Delay and Doppler," *DSN Progress Report 42-31*, pp. 67-74, Feb. 15, 1976.
192. Layland, J. W., "Very Long Baseline Interferometry Covariance," *DSN Progress Report 42-31*, pp. 21-29, Feb. 15, 1976. (see N76-18163 09-12).

193. Layland, J. W., and A. N. Mathews, "VLBI Clock Sync and the Earth's Rotational Instability," *DSN Progress Report 42-42*, pp. 81-84, JPL, Pasadena, California, Dec. 15, 1977.
194. Layland, J. W., and W. J. Hurd, "VLBI Instrumental Effects, Part I," *DSN Progress Report 42-42*, pp. 54-80, JPL, Pasadena, California, Dec. 15, 1977.
195. Lee, W., and M. A. Geller, "Preliminary Design Study of a High Resolution Meteor Radar," Aeronomy Report No. 52, Illinois University, Urbana, March 1, 1973 (Avail. NTIS).
196. Legg, T. H., "Smoothing for phase-switched radiotelescopes," *IEEE Trans. Antennas Propagat. (Commun.)*, vol. AP-12, pp. 803-804, Nov. 1964.
197. Legg, T. H., N. W. Broten, D. N. Fort, J. L. Yen, F. V. Bale, P. C. Barber, and M. J. S. Quigley, "Long Baseline Interferometry of the Seyfert Galaxy 3C 84," *Nature*, 244, 18-19, 1973.
198. Legg, T. H., et al., "The Small-Scale Structure and Variability of 3C 273 B", *Astrophysical Jnl.*, Vol. 211, Pt. 1, pp. 21-30, Jan. 1, 1977.
199. Levine, M. W., and R. F. C. Vessot, "Hydrogen-Maser Time and Frequency Standard at Agassiz Observatory," *Radio. Sci.*, Vol. 5, No. 10, pp. 1287-92, Oct. 1970.
200. Little, L. T., "Refraction Effects and Position Stability in Components of Water Source W49," *Royal Astronomical Society, Monthly Notices*, Vol. 175, pp. 245-255, May 1976.
201. Litvak, M. M., "The Meaning of the OH H₂O Maser Maps," *Astrophysical Jnl.*, 170, 71-80, 1971.
202. Lo, K. Y., R. C. Walker, B. F. Burke, J. M. Moran, K. J. Johnston, and M. S. Ewing, "Evidence for Zeeman Splitting in 1720-MHz OH Line Emission," *Astrophysical Jnl.*, 202, 650-654, 1975.
203. Lo, K. Y., et al., "VLBI Observations of the Compact Radio Source in the Center of the Galaxy -- Very Long Baseline Interferometer," *Astrophysical Jnl.*, Vol. 202, Pt. 2, pp. L63-L65, Dec. 1, 1975.
204. Lo, K. Y., et al., "An angular size for the compact radio source at the galactic center," *Astrophysical Journal*, Part 1, Vol. 218, pp. 668-670, Dec. 15, 1977.
205. Locke, J. L., "Very Long Baseline Interferometry," *Science Jnl.*, V5A, N5, pp. 41-46, Nov. 1969.
206. Lushbaugh, W. A., and J. W. Layland, "Preliminary Design Work on a DSN VLBI Correlator," *DSN Progress Report 42-43*, Jet Propulsion Laboratory, Pasadena, Calif., pp. 90-98, Feb. 15, 1978.
207. Lynch, M. A., et al., "Intercontinental Interferometry of Jupiter at 18 MHz," *Bull. Am. Astron. Soc.*, Vol. 3, No. 1, Pt. 1, p. 4, 1971.
208. Lynch, M. A., and T. D. Carr, "Transhemispheric VLB Interferometry of a Jovian Decametric L. Burst," *Bull. Am. Astron. Soc.*, Vol. 3, No. 4, Pt. 1, p. 476, 1971.
209. Lynch, M. A., *Observations of Jupiter's Decametric Radiation with a Very Long Baseline Interferometer*, Ph.D. Thesis, Florida University, Gainesville, 1972.
210. Lynch, M. A., T. C. Carr, J. May, W. F. Block, V. M. Robinson, and N. F. Six, "Long-Baseline Analysis of a Jovian Decametric L Burst," *Astrophysical Letters*, 10, 153-158, 1972.

211. Lynch, M. A., et al., "VLBI Measurements of Jovian S Bursts," *Astrophysical Jnl.*, Vol. 207, Pt. 1, pp. 325-328, July 1, 1976.
212. Lynn, K. J. W., and J. S. Gubbay, "The Effect of the Earth's Atmosphere on Baseline Determinations by Very Long Baseline Interferometry — Radio Frequencies/Frequency Shift," Weapons Research Establishment, Salisbury, Australia, WRE-TN-1312 (WR/D), Jan. 1975. (Avail. NTIS).
213. Lynn, K. J. W., et al., "Atmospheric phase path corrections for VLBI," *Monitor Proc. Inst. Radio Electron. Eng. Aust.*, V. 37, No. 12, pp. 361-368, Dec. 12, 1976.
214. MacDonald, G. J. F., "Implications for geophysics of the precise measurement of the earth's rotation," *Science*, 157, 304-305, 1967.
215. MacDoran, P. F., "A First-Principles Derivation of the Differenced Range Versus Integrated Doppler (DRVID) Charged-Particle Calibration Method," *DSN Space Programs Summary 37-62*, Vol. II, Jet Propulsion Laboratory, Pasadena, Calif., p. 28, February 15, 1970.
216. MacDoran, P. F., "Very Long Baseline Interferometry (VLBI) Earth Physics — Application to Radio Astronomy and Interferometric Earth Surveys," *NASA Goddard Space Flight Center Proc. of the 4th PTTI Planning Meeting*, pp. 62-73, Nov. 16, 1972 (see N75-11249 02-35).
217. MacDoran, P. F., "Radio Interferometry for Study of the Earthquake Mechanism," *Proc. of the Conference on Tectonic Problems of the San Andreas Fault System*, Stanford University, Publications of the University Series: Geological Sciences, 13, 104-123, 1973.
218. MacDoran, P. F., "Radio Interferometry for International Study of the Earthquake Mechanism," *Acta Astronautica*, Vol. 1, pp. 1427-1444, 1974.
219. MacDoran, P. F., "VLBI applications to secular geodynamic and earth strain measurement," International Ass. of Geodesy and Australian Academy of Science, *Earth's Gravitational Field and Secular Variations in Position.*, Univ. of New South Wales.
220. Mader, G. L., "The Relative Positions of the Hydroxyl and Water Vapor Astrophysical Masers," University of Maryland, 1975.
221. Mader, G. L., K. J. Johnston, J. M. Moran, S. H. Knowles, S. A. Mango, P. R. Schwartz, and W. B. Waltman, "The Relative Positions of the OH and H₂O Masers in W49N and W3 (OH)," *Astrophysical Jnl. (Letters)*, 200, L111-L114, 1975.
222. Maksimov, V. I., and V. S. Troitskii, "Influence of Relativity Theory Effects on VLBI Clock Synchronization," *Radiofizika*, Vol. 19, No. 10, pp. 1455-1458 (in Russian), 1976.
223. Markowitz, W., "Timing for Geodetic Satellites," in *The Use of Artificial Satellites for Geodesy*, Proceedings of the 3rd International Symposium, Wash., D. C., American Geophysical Union, 1972, pp. 245-246, Apr. 15-17, 1971.
224. Marscher, A. P., "Effects of Non Uniform Structure on the Derived Physical Parameters of Compact Synchrotronsources," *Astrophysical Jnl.*, Part 1, Vol. 216, pp. 244-256, Aug. 15, 1977.
225. Martin, C. F., and D. M. Walls, "Tracking Station Coordinates from Range Rate Tracking of a Lunar Transponder," in *The Use of Artificial Satellites for Geodesy and Geodynamics*, Proceedings of the International Symposium, Athens, Greece, May 14-21, 1973.

226. Mathur, N. C., M. D. Grossi, and M. R. Pearlman, "Atmospheric effects in very long baseline interferometry," *Radio Sci.*, vol. 5, pp. 1253-1261, Oct. 1970.
227. Matveenko, L. I., L. R. Kogan, V. I. Kostenko, I. G. Moiseev, V. A. Efanov, B. G. Clark, K. I. Kellermann, G. Grove, M. H. Cohen, J. J. Broderick, and D. L. Jauncey, "Ultrafine Structure of Some Compact Radio Sources," *Sov. Astron. - Astronomical Jnl.*, 17, 731-736, 1973-1974.
228. Matveenko, L. I., et al., "A Receiver System for a Very Long Baseline Radio Interferometer," *Soviet Astronomy Letters*, Vol. 2, pp. 159-161, Translation, July-August 1976.
229. May, J., and T. D. Carr, "Interferometry of Jupiter at 18 Mc/s," *Quarterly Journal of the Florida Academy of Sciences*, 30, 1-9, 1967.
230. McCready, L. L., J. L. Pawsey, and R. Payne-Scott, "Solar radio radiation and its relation to sunspots," *Proc. Roy. Soc., Ser. A*, Vol. 190, pp. 357-375, Aug. 1947.
231. Meeks, M. L., *Astrophysics, Part C - Radio Observations*, New York, Academic Press, Inc., 367 pp., 1976.
232. Melbourne, W. G., et al., "Constants and Related Information for Astrodynamical Calculations, 1968," Technical Report 32-1306, Jet Propulsion Laboratory, Pasadena, Calif., July 15, 1968.
233. Michael, W. H., Jr., "Radio Science Experiments: The Viking Mars Orbiter and Lander," *Icarus*, Vol. 16, 57-73, 1972.
234. Michellini, R. D., "One-bit VLBI Recording and Playback System Using Video-Tape Recorders," *Radio Sci.*, V. 5, N. 10, pp. 1263-70, Oct. 1970.
235. Michellini, R. D., and M. D. Grossi, "Very Long Baseline Interferometry Observations of Radio Emissions from Geostationary Satellites," in *Space Research XII*, Proceedings of the Fourteenth Plenary Meeting, Seattle, Wash., Volume 1, June 18-July 2, 1971.
236. Michellini, R. D., "The Application of VLB Interferometry to Earth Measurements," Final Report, Smithsonian Astrophysical Observatory, Cambridge, Mass., April 1973 (Avail. NTIS).
237. Michelson, A. A., "On the applications of interference methods to astronomical measurements," *Phil. Mag.* 30, 1-21, 1890.
238. Middleton, D., "The response of biased, saturated linear and quadratic rectifiers to random noise," *J. Appl. Phys.*, vol. 17, p. 778, 1946.
239. Middleton, D., "Some general results in the theory of noise through nonlinear devices," *Quart. Appl. Math.*, vol. 5, p. 445, 1948.
240. Middleton, D., *An Introduction to Statistical Communication Theory*, New York; McGraw-Hill, 1960.
241. Miller, J. K., and K. M. Rourke, "The application of differential VLBI to planetary approach orbit determination," *DSN Progress Report 42-40*, JPL, pp. 84-90, August 15, 1970.
242. Miller, R. B., "Pioneer Venus 1978 Mission Support - Interferometry Experiment," *DSN Progress Report 42-31*, pp. 11-14, Feb. 15, 1976 (see N76-18163 09-12).
243. Miller, R. B., "Pioneer Venus 1978 Mission Support," NTIS HC A03/MF A01, *DSN Progress Report 42-36*, pp. 22-27, Dec. 15, 1976.

244. Moffet, A. T., "Minimum-redundancy linear arrays," *IEEE Trans. Antenna Propagat.*, Vol. AP-16, pp. 172-175, Mar. 1968.
245. Moffet, A. T., "The Whole-Earth Array-Developments in Very-Long-Baseline Interferometry," in the *1971 IEEE Group on Antennas and Propagation International Symposium*, Los Angeles, Calif., pp. 2-4, September 1971.
246. Moffet, A. T., J. S. Gubbay, D. S. Robertson, and A. J. Legg, "High Resolution Observation of Variable Radio Sources," *External Galaxies and Quasi-Stellar objects*, IAU Symposium No. 44 (held in Uppsala, Sweden, August 1970), Ed. by David S. Evans, D. Reidel, Dordrecht-Holland, pp. 228-229, 1972.
247. Molinder, J. I., "A tutorial introduction to VLBI using bandwidth synthesis," *DSN Progress Report 42-46*, August 15, 1978.
248. Moran, J. M., P. P. Crowther, B. F. Burke, A. H. Barrett, A. E. E. Rogers, J. A. Ball, J. C. Carter, and C. C. Bare, "Spectral line interferometry with independent time standards at stations separated by 845 kilometers," *Science*, vol. 157, pp. 676-677, Aug. 1967.
249. Moran, J. M., "Interferometric Observations of Galactic OH Emission," Massachusetts Institute of Technology, Thesis, 1968.
250. Moran, J. M., B. F. Burke, A. H. Barrett, A. E. E. Rogers, J. A. Ball, J. C. Carter, and D. D. Cudaback, "The Structure of the OH Source in W3," *Astrophysical Jnl. (Letters)*, 152, L97-L101, 1968.
251. Moran, J. M., "Recent Advances in the Study of Radio Emission from Galactic H₂O Sources," DDC# AD-721063, Nov. 1970, Rept. No. MS-2940, Mass. Inst. of Tech., Lincoln Lab, Lexington. (Also in *NEREM-70*, pp. 192-193.)
252. Moran, J. M., "Some Characteristics of an Operational System for Measuring UT1 Using VLBI," in *Space Research XIII, Proceedings of the 15th Plenary Meeting*, Madrid, Spain, Vol. 1, pp. 73-82, May 10-24, 1972.
253. Moran, J. M., "Spectral-line analysis of very-long-baseline interferometric data," *Proc. IEEE*, 61, 1236-1242, 1973.
254. Moran, J. M., G. D. Papadopoulos, B. F. Burke, K. Y. Lo, P. R. Schwartz, D. L. Thacker, K. J. Johnston, S. H. Knowles, A. C. Reisz, and I. I. Shapiro, "Very Long Baseline Interferometric Observations of the H₂O Sources in W49 N, W3 (OH), Orion A, and VY Canis Majoris," *Astrophysical Jnl.*, 185, 535-567, 1973.
255. Moran, J. M., "Geodetic and Astrometric Results of Very Long Baseline Interferometric Measurements of Natural Radio Sources," *Proc. of Open Meeting of Work Group on Phys. Sci. of the Plenary Meeting of Cospar*, 17th Space Res. 15, Sao Paulo, Brazil, pp. 33-47, June 1974.
256. Moran, J. M., and B. R. Rosen, "The Estimation of Tropospheric Propagation Path Length from Ground-Based Microwave Measurements," presented at the Annual Meeting of the U.S. National Comm. International Union of Radio Science, Boulder, Colorado, 1975.
257. Moran, J. M., "Very Long-Baseline Interferometric Observations and Data Reduction," Center for Astrophysics, Harvard College Observatory and Smithsonian Astrophysical Observatory, Preprint Series No. 108, May 1974. (Also, *Methods of Experimental Physics* by M. L. Meeks, 12, Part C, 228, 1976.)
258. Moran, J. M., "Radio Observations of Galactic Masers," *Frontiers of Astrophysics* (Harvard University Press), pp. 385-437, 1976.

259. Moran, J. M., "Very Long Baseline Interferometer Systems," *Methods of Experimental Physics* by M. L. Meeks, 12, Part C, 174, 1976.
260. Moran, J. M., J. A. Ball, J. L. Yen, P. R. Schwartz, K. J. Johnston, and S. H. Knowles, "Very Long Baseline Interferometric Observations of OH Masers. Associated with Infrared Stars," *Astrophysical Jnl.*, 211, 160, 1977.
261. Moyer, T. D., "Transformation from Proper Time on Earth to Coordinate Time in Solar System Barycentric Space – Time Frame of Reference," JPL-TM-33-786, JPL, Calif. Inst. of Tech. (NTIS HC A041MF A01).
262. Mutel, R. L., J. J. Broderick, T. D. Carr, M. Lynch, M. Desch, W. W. Warnock, and W. K. Klemperer, "VLB Observations of the Crab Nebula and the Wavelength Dependence of Interstellar Scattering," *Astrophysical Jnl.*, 193, 279-282, 1974.
263. Mutel, R. L., "Theory and Observations of Interferometer Visibility Scintillation with Application to the Interplanetary Medium," University of Colorado, Ph.D. Thesis, 1975.
264. Niell, A. E., K. I. Kellermann, B. G. Clark, and D. B. Shaffer, "Milli-Arcsec Structure of 3C 84, 3C 273 and 3C 279 at 2 Centimeter Wavelength," *Astrophysical Jnl. (Letters)*, 197, L109-L112, 1975.
265. Niell, A. E., et al., "Comparison of a radio interferometric differential baseline measurement with conventional geodesy," submitted to *Tectonophysics*, Dec. 30, 1977.
266. Niell, A. E., et al., "VLBI Baseline Measurements to a Transportable Antenna with Decimeter Accuracy," National Radio Sci. Meeting, Univ. of Colorado, Boulder, Colorado, Jan. 9-13, 1978.
267. Notvedt, H., "The correlation function in the analysis of directive wave propagation," *Phil. Mag.*, vol. 42, pp. 1022-1031, Sept. 1951.
268. Nur, A., "Dilatancy, pore fluids, and premonitory variations of t_s/t_p travel times," *Bull. Seim. Soc. Am.*, 62, 1217-1222, 1972.
269. O'Neill, G. K., "A high-resolution orbiting telescope," *Science*, Vol. 160, pp. 843-847, May 1968.
270. Ondrasik, V. J., and K. H. Rourke, "Application of New Radio Tracking Data Types to Critical Spacecraft Navigation Problems," *JPL Quart. Tech. Rev.*, Vol. 1, No. 4, pp. 116-132, Jan. 1972.
271. Ondrasik, V. J., C. E. Hildebrand, and G. A. Ransford, "Preliminary evaluation radio data orbit determination capabilities for the Saturn portion of a Jupiter-Saturn-Pluto 1977 mission," *DSN Technical Report 32-1526*, Vol. X, pp. 59-75, Aug. 15, 1972.
272. Ong, K. M., P. F. MacDoran, J. B. Thomas, H. F. Fliegel, L. J. Skjerve, D. J. Spitzmesser, P. D. Batelaan, S. T. Paine, and M. G. Newsted, "A demonstration of radio interferometric surveying using DSS 14 and the Project Aries Transportable antenna," *DSN Progress Report 42-26*, pp. 41-53, Jet Propulsion Laboratory, Pasadena, CA, April 15, 1975.
273. Ong, K. M., P. F. MacDoran, J. B. Thomas, H. F. Fliegel, L. J. Skjerve, D. J. Spitzmesser, P. D. Batelaan, and S. R. Paine, "A Demonstration of a Transportable Radio Interferometric Surveying System with 3-cm Accuracy on a 307-m Base Line," *J. Geophys. Res.*, 81, 3587-3593, 1976.

274. Palmer, H. P., B. Rowson, B. Anderson, W. Donaldson, G. K. Miley, H. Gent, R. L. Algie, O. B. Slee, and J. H. Crawther, "Radio diameter measurements with interferometer baselines of one million and two million wavelengths," *Nature*, vol. 213, pp. 789-790, Feb. 1967.
275. Papadopoulos, G. D., "Ku-Band Interferometry," DDC# AD-721574, Rept. No. TR-481, Mass. Inst. of Tech. Cambridge Research Lab-of Electronics, Dec. 1970.
276. Papadopoulos, G. D., and B. F. Burke, "The M. I. T. Ku-Band Radio Interferometer," *Radio Sci.*, Vol. 7, No. 6, pp. 667-74, June 1972.
277. Papadopoulos, G. D., "A Statistical Technique for Processing Radio Interferometer Data Using Maximum Likelihood Algorithm," *IEEE Trans. on Antennas and Propagation*, Vol. AP-23, pp. 45-53, Jan. 1975.
278. Papoulis, A., *Probability, Random Variables, and Stochastic Processes*, Sec. 12-2, McGraw-Hill Book Company, New York, 1965.
279. Pariiskii, Y. N., and A. A. Stotskil, "On the Possibility of Obtaining Radio Images of Celestial Bodies with Resolution Better than 10^{-2} Seconds of Arc," Main Astronomical Observatory, *Isvestia*, 188, 195-211, 1972.
280. Parrish, A., T. Guiffrida, B. Allen, and A. Haschick, G. Papadopoulos, and B. F. Burke, "The M.I.T. Aperture Synthesis Interferometer System," National Radio Science Meeting, Univ. of Colorado, Boulder, Colorado, Jan. 9-13, 1978.
281. Pauliny-Toth, I. I. K., E. Preuss, A. Witzel, K. I. Kellermann, D. B. Shaffer, G. H. Purcell, G. W. Grove, D. L. Jones, M. H. Cohen, A. T. Moffet, J. Romney, R. T. Schilizzi, and R. Rinehart, "High Resolution Observations of NGC 1275 with a Four-Element Intercontinental Radio Interferometer," *Nature*, 259, 17-20, 1976.
282. Pauliny-Toth, I. I. K., et al., "Observations of Compact Radio Sources by Means of Very-Long-Baseline Interferometry," *Kleinheubacher Berichte*, Vol. 19, pp. 327-331, 1976.
283. Pauliny-Toth, I., and A. Witzel, "Discovery of a High-Energy Double Source in the Nucleus of a Radio Galaxy," *Zeitschrift fuer Flugwissenschaften und Weltraumforschung*, Vol. 1, pp. 222-223 (in German), May-June 1977.
284. "Pioneer Venus Experiment Descriptions," *Space Science Reviews*, Vol. 20, pp. 451-525, June 1977.
285. Preston, R. A., R. Ergas, H. F. Hinteregger, C. A. Knight, D. S. Robertson, I. I. Shapiro, A. R. Whitney, A. E. E. Rogers, and T. A. Clark, "Interferometric Observations of an Artificial Satellite," *Science*, 178, 407-409, 1972.
286. Preston, R. A., "Accurate Satellite Tracking with Very Long Baseline Interferometry," Massachusetts Institute of Technology, Ph.D. Thesis, 1973.
287. Preston, R. A., "Dual-Spacecraft Radio Metric Tracking," *DSN Progress Report 42-22*, Jet Propulsion Laboratory, Pasadena, Calif., August 15, 1974.
288. Preston, R. A., et al., "JPL Catalog of VLBI Radio Sources," *Bull. AAS*, 1975.
289. Preuss, E., et al., "Interferometry with Intercontinental Baseline Lengths – Status of Experiments Involving a 100-m Radio Telescope," *Astronomische Gesellschaft, Mitteilungen*, No. 35, pp. 237-243 (in German), 1974.
290. Preuss, E., "High-Resolution Radio Interferometry-Specific Features of VLBI," *Sterne und Weltraum*, Vol. 15, pp. 392-396 (in German), Dec. 1976.

291. Preuss, E., "High-Resolution Radio Interferometry /VLBI/-Technical-Organizational Implementation," *Sterne und Weltraum*, Vol. 16, pp. 86-90 (in German), March 1977.
292. Purcell, G. H., Jr., "The Structure of Compact Radio Sources at 606 MHz," Ph.D. Thesis, Calif. Inst. of Tech., 1973.
293. Purcell, G. H., "A Procedure for Preliminary Reduction of Bandwidth Synthesis Data," Jet Propulsion Laboratory *DSN Progress Report 42-33*, April 1976.
294. Ratner, M. R., "Very Long Baseline Observations of Jupiter's Millisecond Radio Bursts," University of Colorado, Ph.D. Thesis, 1976.
295. Readhead, A. C. S., P. N. Wilkinson, and G. H. Purcell, "Very Long Baseline Interferometry Observations at 610 MHz of Sources which are Suspected of Showing Decimetric Flux Density Variations," *Astrophysical Jnl., Part 2 - Letters to the Editor*, Vol. 215, pp. L13-L15, July 1, 1977.
296. Reasenberg, R. D., and I. I. Shapiro, "Bound on the Secular Variation of the Gravitational Interaction," in *Proceedings of the 5th Conference on Atomic Masses and Fundamental Constants*, Paris, 1975.
297. Rees, M. J., "Appearance of Relativistically Expanding Radio Sources," *Nature*, Vol. 211, p. 468, 1966.
298. Reid, M. J., and D. O. Muhleman, "Very Long Baseline Interferometric Observations of OH/IR Stars," *Astrophysical Jnl.*, Vol. 196, Pt. 2, pp. L35-L37, Feb. 15, 1975. (Also, Rept. No. 1974-14, Owens Valley Radio Observatory, Pasadena, Ca., 1974 (Avail. NTIS)).
299. Reid, M. J., "The Structure of Hydroxyl Masers and Circumstellar Envelopes of Long Period Variable Stars," Ph.D. Thesis, Calif. Inst. of Tech., Order No. 76-16377, 1976.
300. Reid, M. J., D. O. Muhleman, J. M. Moran, K. J. Johnston, and P. R. Schwartz, "The Structure of Stellar Hydroxyl Masers," *Astrophysical Jnl.*, 1977.
301. Reid, M. J., et al., "Observations of Hydroxyl Masers with a VLB Network." National Radio Sci. Meeting, Univ. of Colorado, Boulder, Colorado, Jan. 9-13, 1978.
302. Reisz, A. C., I. I. Shapiro, J. M. Moran, G. D. Papadopoulos, B. F. Burke, K. Y. Lo, and P. R. Schwartz, "W3 (OH): Accurate Relative Positions of Water Vapor Emission Features," *Astrophysical Jnl.*, 186, 537-544, 1973.
303. Reisz, A. C., "A Study of H₂O Masers Associated with Galactic H_{II} Regions," Massachusetts Institute of Technology, 1976.
304. Resch, G. M., "Comparison of Microwave Radiometric and In-Situ Measurements of Tropospheric Water Vapor," presented at the Annual Meeting of the U.S. National Comm. International Union of Radio Science, Boulder, Colorado, 1975.
305. Resch, G. M., "Low-Frequency Spectra of Compact Sources," Ph.D. Thesis, Florida State University, Tallahassee, 1974.
306. Robertson, D. S., J. S. Gubbay and A. T. Legg, "VLBI in the southern hemisphere," *Proceedings of Astronomical Society of Australia*, Vol. 2, pp. 184-187, Oct. 1973.
307. Robertson, D. S. "Special Relativity and Very Long Baseline Interferometers," *Nature*, 257, 467-468, 1975.

308. Robertson, D. S., *Geodetic and Astrometric Measurements with Very-Long Baseline Interferometry*, Ph.D. Thesis, Massachusetts Institute of Technology, Cambridge, Mass., 1975.
309. Rogers, A. E. E., "Spectral line interferometry and interferometer noise analysis," MIT Lincoln Labs., Tech. Rep. 441, pp. 20-21, Jan. 1968.
310. Rogers, A. E. E., "Very Long Baseline Interferometry with Large Effective Bandwidth for Phase-Delay Measurements," *Radio Sci.*, Vol. 5, No. 10, pp. 1239-1247, October 1970.
311. Rogers, A. E. E., "Broadband passive 90° RC hybrid with low component sensitivity for use in the video range of frequencies," *Proc. IEEE*, 59, 1617-1618, 1971.
312. Rogers, A. E. E., C. C. Counselman III, H. F. Hinteregger, C. A. Knight, D. S. Robertson, I. I. Shapiro, A. R. Whitney, and T. A. Clark, "Extragalactic Radio Sources: Accurate Positions from Very Long Baseline Interferometer Observations," *Astrophysical Jnl.*, 186, 801-806, 1973.
313. Rogers, A. E. E., H. F. Hinteregger, A. R. Whitney, C. C. Counselman, I. I. Shapiro, J. J. Wittels, W. K. Klemperer, W. W. Warnock, T. A. Clark, L. K. Hutton, G. E. Marandino, B. O. Ronnang, O. E. H. Rydbeck, and A. E. Niell, "The Structure of Radio Sources 3C 273B and 3C 84 Deduced from the "Closure" Phases and Visibility Amplitudes Observed with Three-Element Interferometers," *Astrophysical Jnl.*, 193, 293-301, 1974.
314. Rogers, A. E. E., *A Receiver Phase and Group Delay Calibration System for Use in VLBI*, Haystack Observatory Technical Report 1975-6, Feb 15, 1976.
315. Rogers, A. E. E., et al., "Very Long Baseline Interferometry as a Means of Worldwide Time Synchronization," Report No. TR-478, M.I.T., Feb. 1970.
316. Rogers, A. E. E., et al., "Very Long Baseline Interferometry Hardware," Final Report for Contract #NAS5-20777, Part 13 "A Receiver Phase and Group Delay Calibration System," Haystack Technical Note 1975-6, Feb. 1976.
317. Rogers, A. E. E., et al., "Geodesy by Radio Interferometry: Determination of a 1.24-km Base Line Vector with 5-mm Repeatability," *Journal of Geophysical Research*, Vol. 83, No. B1, pp. 325-333, January 10, 1978.
318. Ronnang, B. O., O. E. Rydbeck, and J. M. Moran, "Very Long Baseline Interferometry of Galactic OH Sources," *Radio Science*, V5, N10, pp. 1227-1231, Oct. 1970.
319. Ross, S., "VLBI Determination of Synchronous Equatorial Satellite Orbits," American Institute of Aeronautics and Astronautics and American Astronautical Society, Astrodynamics Conference, Palo Alto, Calif., Sept. 11-12, 1972.
320. Rumford Symposium on Recent Developments in the Field of Long-Baseline Interferometry, Boston, Mass., Apr. 13-14, 1971.
321. Ryle, M., B. Elsmo, and A. C. Neville, "High resolution observations of radio sources in Cygnus and Cassiopeia," *Nature*, vol. 205, pp. 1259-1262, Mar. 1965.
322. Salzberg, I. M., "Very Long Baseline Interferometry," NASA Goddard Space Flight Center, Greenbelt, Md. in its *Significant Accomplishments in Technol.*, pp. 116-120, 1972.
323. Sanders, R. H., "Super-Relativistic Phase Velocities of Radio Source Components," *Nature*, 248, 390-392, 1974.

324. Sargent, H. H., and W. K. Klemperer, "A Decametric Long Baseline Interferometer System," *Radio Sci.*, Vol. 5, No. 10, pp. 1283-6, Oct. 1970.
325. Schain, H. O., "Geodetic Application of Long Baseline Interferometry," DDC# AD-709 868, Rept. No. ORA-70-0005, Office of Research Analyses, Holloman AFB, N. Mex., May 1970.
326. Schaper, L. W., D. H. Staelin, and J. W. Waters, "The Estimation of Tropospheric Electrical Path Length by Microwave Radiometry," *Proc. Inst. Elec. Electron. Eng.*, Vol. 58, No. 2, pp. 272-273, 1970.
327. Schilizzi, R. T., M. H. Cohen, J. D. Romney, D. B. Shaffer, K. I. Kellermann, G. W. Swenson Jr., J. L. Yen, and R. Rinehart, "Observations with a VLB Array. III. The Sources 3C 120, 3C 273B, 2134+004, and 3C 84," *Astrophysical Jnl.*, 201, 263-274, 1975.
328. Schilizzi, R. T., "VLBI Detection of Compact Central Components in 17 Extended Radio Sources," *Astronomical Jnl.*, 81, 946-951, 1976.
329. Scott, M. A., "Structural Variations of Extragalactic Radio Sources over Large Frequency Ranges," *Royal Astronomical Society, Monthly Notices*, Vol. 179, pp. 377-388, May 1977.
330. Seielstad, G. H., "The Rapidly Changing Variable Radio Source 3C 120," *Astrophysical Jnl.*, 193, 55, 1974.
331. Shaffer, D. B., M. H. Cohen, D. L. Jauncey, and K. I. Kellermann, "Rapid Change in the Visibility Function of the Radio Galaxy 3C 120," *Astrophysical Jnl. (Letters)*, 173, L147-L150, 1972.
332. Shaffer, D. B., *The Structure of Compact Radio Sources at 10.7 GHz - Using Very Long Baseline Interferometry*, Ph.D. Thesis, Calif. Inst. of Tech., 1974.
333. Shaffer, D. B., and R. T. Schilizzi, "18 cm Visibility Functions of High-Frequency Compact Sources," *Astronomical Jnl.*, 80, 753-758, 1975.
334. Shaffer, D. B., et al., "Observations with a VLB Array. II. The Sources 4C39.25, NRA0150, VRO42.11.01, 3C345, and 3C454.3, 342 - Radio Interferometers for Measuring Extraterrestrial Radio Waves," Rept. No. 1975-5, Owens Valley Radio Observatory, Pasadena, California, 1975 (Avail. NTIS).
335. Shaffer, D. B., "Modelling Autocorrelation, Phaseless Iteration, Phase-Closure, and Relative Phase 18 cm VLB Mapping," National Radio Sci. Meeting, Univ. of Colorado, Boulder, Colorado, Jan. 9-13, 1978.
336. Shapiro, A., E. A. Uliana, and B. S. Yapple, "Very-Long-Baseline Interferometry Navigation Using Natural H₂O Sources, Part 1," DDC# AD-901 999L, Naval Research Lab., Washington, D.C., July 1972.
337. Shapiro, I. I., "New method for the detection of light deflection by solar gravity," *Science*, vol. 157, p. 806, Aug. 1967.
338. Shapiro, I. I., "Possible experiments with long-baseline interferometers, 1968 *NEREM Record*, Boston, Mass, 6-8 Nov. 1968, (IEEE, New York, pp. 70-1, 1968).
339. Shapiro, I. I., and C. A. Knight, "Geophysical Applications of Long Baseline Radio Interferometry," NATO Advanced Study Institute, University of Western Ontario, 1969, *Earthquake Displacement Fields and the Rotation of the Earth*, pp. 284-301, 1970.

340. Shapiro, I. I., and C. A. Knight, "Geophysical applications of long-baseline radio interferometry," in *Earthquake Displacement Fields and Rotation of the Earth*, L. Mansinha et al., Eds., Dordrecht, The Netherlands: D. Reidel Pub. Co., 1970, pp. 284-301.
341. Shapiro, I. I., "Astrometric Applications of VLBI," *Bull. Am. Astron. Soc.*, Vol. 4, No. 2, Pt. 2, p. 266, 1972.
342. Shapiro, I. I., "Very Long Baseline Interferometry, the Impact on Astronomy and Geophysics," *Adv. Astronaut. Sci., Suppl., Sci. Technology Ser.*, V. 28, p. 133, 1972.
343. Shapiro, I. I., "Wind Speeds in Lower Atmosphere of Venus. Status Report on Possible Measurement via Differential VLBI Tracking of Entry Probes," Final Report, Dept. of Earth and Planetary Sciences, M.I.T., Cambridge, May 1972 (Avail. NTIS).
344. Shapiro, I. I., H. F. Hinteregger, C. A. Knight, J. J. Punskey, D. S. Robertson, A. E. E. Rogers, A. R. Whitney, T. A. Clark, G. E. Morandino, R. M. Goldstein, and D. J. Spitzmesser, "3C 120: Intense Outbursts of Radio Radiation Detected with the Goldstone-Haystack Interferometer," *Astrophysical Jnl. (Letters)*, 183, L47-L50, 1973.
345. Shapiro, I. I., and R. W. King, "Analysis of Luna Laser and ALSEP VLBI Data for Geodetic Purposes," Final Report, Dept. of Earth and Planetary Sciences, M.I.T., July 31, 1974 (Avail. NTIS).
346. Shapiro, I. I., D. S. Robertson, C. A. Knight, C. C. Counselman, III, A. E. E. Rogers, H. F. Hinteregger, S. Lippincott, A. R. Whitney, T. A. Clark, A. E. Niell, and D. J. Spitzmesser, "Transcontinental baselines and the rotation of the earth measured by radio interferometry," *Science*, 186, 920-922; 191-451, 1974.
347. Shapiro, I. I., et al., "Very Long Baseline Interferometry for Centimeter Accuracy Geodetic Measurements," *Tectonophysics*, V. 29, N. 1-4, 1975, for 5th Int. Symp. on Recent Crustal Movements, Zurich, Switz., pp. 4-18, Aug. 26-31, 1974.
348. Shapiro, I. I., "Estimation of Astrometric and Geodetic Parameters," *Methods of Experimental Physics* by M. L. Meeks, 12, Part C, 261, 1976.
349. Shapiro, L. D., et. al., "Using Loran-C Transmissions for Long Baseline Synchronization," *Radio Sci.*, V. 5, N. 10, pp. 1233-8, Oct. 1970.
350. Shawhan, S. D., T. A. Clark, W. H. Cronyn, and J. P. Basart, "Upper Limit to the 11.4 M Flux of Saturn Using VLBI," *Nature (Phys. Sci.)*, 243, 65-6, 1973.
351. Shnidman, D., "Tracking the Lunar Rover Vehicle with Very Long Baseline Interferometry Techniques," *NASA Goddard Space Flight Center Proc. of the 4th PTTI Planning Meeting*, pp. 90-99, 1973 (see N75-11249 02-35).
352. Siry, J. W., "A Systems Plan for an Earth and Ocean Dynamics Satellite Applications Program," NASA Goddard Space Flight Center, Greenbelt, MD, Nov. 1970 (Avail. NTIS).
353. Slade, M. A., *The Orbit of the Moon*, Ph.D. Thesis, Massachusetts, Institute of Technology, Cambridge, Mass., 1971.
354. Slade, M. A., P. F. MacDoran, and J. B. Thomas, "Very Long Baseline Interferometry (VLBI) Possibilities for Lunar Study," *DSN Technical Report 32-1526*, Vol. XII, pp. 35-39, Jet Propulsion Laboratory, Pasadena, Calif., 1972.

355. Slade, M. A., et al., "The Mariner 9 Quasar Experiment: Part I," *DSN Technical Report 32-1526*, Vol. XIX, pp. 31-35, Jet Propulsion Laboratory, Pasadena, Calif., 1974.
356. Slade, M. A., et al., "Quasar Differential VLBI," *DSN Progress Report 42-33*, pp. 37-54, June 15, 1976 (see N76-27262, 18-12).
357. Smith, A. G., "Radio Astronomy of the Planets," DDC# AD-730090, Florida Univ., Gainesville, Dept. of Physics and Astronomy, Sept. 1971.
358. Smith, D. E., "Precision Tracking Systems of the Immediate Future – A Discussion," *NOAA Sea Surface Topography from Space*, Vol. 1, February 1972.
359. Snow, W. R., "Atmospheric Refraction Errors in DLBI Observations at Low Elevation Angles," MIT, Sept. 1977.
360. Sramek, R. A., "A measurement of the gravitational deflection of microwave radiation near the sun," *Astrophys. J.*, Vol. 167, No. 2, Pt. 2, pp. L55-60, 15 July 1971. (Also in *Bull. Am. Astron. Soc.*, Vol. 3, No. 3, Pt. II., p. 416, 1971.)
361. Staelin, D. H., "Passive remote sensing at microwave wavelengths," *Proc. IEEE*, vol. 57, pp. 427-439, Apr. 1969.
362. Stannard, K. M., et al., "Very Long Baseline Interferometry of Decametric Radiation from Jupiter," *Radio Sci.*, V. 5. N. 10, pp. 1271-80, Oct. 1970.
363. Swenson, G. W., Jr., and N. C. Mathur, "The interferometer in radio astronomy," *Proc. IEEE*, vol. 56, pp. 2114-2130, Dec. 1968.
364. Swenson, G. W., Jr., "An Intercontinental Array, A Next-Generation Radio Telescope," *Science*, Vol. 188, pp. 1263-1268, June 27, 1975.
365. Swenson, G. W., Jr., "Optional station locations for VLBI aperture synthesis," (Univ. of Illinois) National Radio Sci. Meeting, Univ. of Colorado, Boulder, Colorado, Jan. 9-13, 1978.
366. Swerling, P., "Parameter Estimation for Waveforms in Additive Gaussian Noise," *J. SIAM*, Vol. 7, pp. 154-166, 1959.
367. Teague, D. D., "Analysis of Acoustic Navigation System Concepts as Compared to Precision Navigation System Technology", DOC# AD-B015383L, Zetetic Inc., Alexandria, Va., Mar. 1976.
368. Thomas, J. B., et al., "An Analysis of Long Baseline Radio Interferometry: The Goldstone Interferometer for Earth Physics," *DSN Progress Report 32-1526*, Vol. V, p. 45 (1971).
369. Thomas, J. B., "An Analysis of Long Baseline Radio Interferometry," *DSN Technical Report 32-1526*, Vol. VII, pp. 37-50, Jet Propulsion Laboratory, Pasadena, Calif., Feb. 15, 1972.
370. Thomas, J. B., "An Analysis of Long Baseline Radio Interferometry, Part II," *DSN Technical Report 32-1526*, Vol. VIII, Jet Propulsion Laboratory, Pasadena, Calif., pp. 29-38, April 15, 1972.
371. Thomas, J. B., and H. F. Fliegel, "Time Frequency Requirements for Radio Interferometric Earth Physics," *NASA Goddard Space Flight Center Proc. of the 5th Ann. NASA and DOD PTTI Planning Meeting*, pp. 15-31, 1973 (see N75-11275 02-35).

372. Thomas, J. B., "An analysis of long baseline radio interferometry, Part III," *DSN Technical Report 32-1526*, Vol. XVI, Jet Propulsion Laboratory, Pasadena, Calif., pp. 47-64, June 15, 1973.
373. Thomas, J. B., J. L. Fanselow, P. F. MacDoran, J. J. Spitzmesser, and L. J. Skjerve, "Radio interferometry measurements of a 16-km baseline with 4-cm precision," *DSN Technical Report 32-1526*, Vol. XIX, pp. 36-54, Jet Propulsion Laboratory, Pasadena, CA, February 15, 1974.
374. Thomas, J. B., "Reformulation of the Relativistic Conversion Between Coordinate Time and Atomic Time," *Astronomical Jnl.*, 80, 405-411, 1975.
375. Thomas, J. B., J. L. Fanselow, P. F. MacDoran, L. J. Skjerve, D. J. Spitzmesser, and H. F. Fliegel, "A Demonstration of an Independent-Station Radio Interferometry System with 4-cm Precision on a 16-km Base Line,"
376. Thomas, J. B., "The Tone Generator and Phase Calibration in VLBI Measurements," *DSN Progress Report 42-44*, Jet Propulsion Laboratory, Pasadena, Calif., pp. 63-74, April 15, 1978.
377. Tseitlin, N. M., *Antenna Engineering and Radio Astronomy*, Moscow, *Izdatel'stvo Sovetskoe Radio* (in Russian), 1976.
378. Tsubokawa, I., "Anomalous changes in heights by levelling surveys before and after the 1964 Niigata earthquake", *Journal of the Geodetic Society of Japan* 15, 75-81, 1969.
379. Urech, J. M., et al., "S-Band Maser Group Delay Measurements and Stability Report," Madrid Deep Space Station, Oct. 1976.
380. Utukuri, R. R. N., and R. H. MacPhie, "Coincident arrays for the direct measurement of the principal solution in radio astronomy," *IEEE Trans. Antennas Propagat.*, Vol. AP-15, pp. 49-59, Jan. 1967.
381. Van Flandern, T. C., "A Determination of the Rate of Change of G," *Mon. Not. Roy. Astron. Soc.*, Vol. 170, No. 2, pp. 333-342, Feb. 1975.
382. Van Vleck, J. H., and D. Middleton, "The spectrum of clipped noise," *Proc. IEEE*, vol. 54, No. 1, pp. 2-19, Jan. 1966.
383. Vanbun, F. O., "Earth and Ocean Dynamics Satellites and Systems," presented at International Astronautical Federation (IAF), 20th Congr. Lisbon, 21-27, Sept., 1975 (Avail. NTIS).
384. Vandenberg, N. R., et al., "VLBI Observations of the Crab Nebula Pulsar," *Astrophysical Jnl.*, Vol. 180, Pt. 2, pp. L27-L29, Feb. 15, 1973.
385. Vandenberg, N. R., "Meter-Wavelength Observations of Pulsars Using Very Long Baseline Interferometry — Concentrating on the Crab Nebula," Ph.D. Thesis, Maryland Univ., College Park, Order No. 75-7371, 1974.
386. Vandenberg, N. R., "Meter Wavelength VLBI — Part 4 — Temporal and Spatial Scattering of the Crab Nebula Pulsar's Radiation," *Astrophysical Jnl.*, 209, 578, 1976.
387. Vandenberg, N. R., et al., "Meter-Wavelength VLBI. III — Pulsars," *Astrophysical Jnl.*, Vol. 207, Pt. 1, pp. 937-948, Aug. 1, 1976.
388. Vitkevich, V. V., J. J. Broderick, et al., "Observations of compact radio sources with a radio interferometer having a Greenbank-Crimea baseline," *Astronomicheskii Zhurnal*, 47, 4, 784-786, 1970 (in Russian).

389. *VLBI Validation Report*, Pre-Session No. 1, Document 890-60, 1 April 1977.
390. Wade, C. M., "Precision Positions of Radio Sources I. Radio Measurements," *Astrophysical Jnl.*, 162, 381, 1970.
391. Walker, R. C., K. Y. Lo, B. F. Burke, K. J. Johnston, and J. M. Moran, "6-cm Observations of Radio Galaxies Over a 228-KM Baseline," *Astrophysical Jnl.*, 208, 296, 1976.
392. Walker, R. C., et al., "VLBI Observations of High-Velocity H₂O Emission in W49 N," *Astrophysical Jnl*, Part 2 – *Letters to the Editor*, Vol. 211, pp. L135-L138, Feb. 1, 1977.
393. Walter, H. G., "An Extension of the Astronomical Fundamental Catalog Related to Radio Sources," *Astronomische Gesellschaft, Mitteilungen*, No. 38, pp. 185-188 (in German), 1976.
394. Walter, H. G., "Astrometrical Applications of Long Baseline Interferometry," *Geodesie Spatiale*, Paris, Groupe de Recherches de France, Aug. 1973 (Avail. NTIS).
395. Walter, H. G., "Comments on Observations with Very Long Baseline Radio Interferometers for Position Determination," European Space Operations Center, Darmstadt, West Germany (Avail. NTIS).
396. Walter, H. G., "Precision estimation of precession and nutation from radio interferometer observations," *Astronomy and Astrophysics*, Vol. 59, No. 3, pp. 433-440, Aug. 1977.
397. Warwick, R. S., "High-Resolution Observations at 408 MHz of Sources From the B2 Catalogue – Radio Astronomy," *Royal Astronomical Society, Monthly Notices*, Vol. 179, pp. 1-11, Apr. 1977.
398. Weaver, D. K., "Design of RC Wide-Band 90-Degree Phase-Difference Network," *IRE Proc.*, pp. 671-676, Apr. 1954.
399. Weiler, R. A., "A Measurement of Solar Gravitational Microwave Deflection with the Westerbork Synthesis Telescope," *Astron. Astrophysics*, 30, 241, 1974. (This provides references to all prior short baseline determinations of the deflection.)
400. Weinberg, S., "Gravitation and Cosmology," *Principles and Applications of the General Theory of Relativity*, John Wiley, New York, 1972.
401. Weinreb, S., "A digital spectral analysis technique and its application to radio astronomy," Tech. Rep. 412, MIT Fes. Lab. Electron., Cambridge, Massachusetts, 1963.
402. Whitcomb, J. H., "New Vertical Geodesy-VLBI Measurements for Earthquake Prediction," *J. of Geophysical Research*, Vol. 81, pp. 4937-4944, Sept. 10, 1976.
403. Whitney, A. R., B. F. Burke, T. A. Clark, H. F. Hinteregger, C. A. Knight, D. S. Robertson, A. E. E. Rogers, and I. I. Shapiro, "Long-baseline interferometric measurement of gravitational bending of radiation from 3C279 in the solar gravitational field," *Bull. Amer. Astron. Soc.*, vol. 2, pt. I, pp. 356-357, 1970.
404. Whitney, A. R., et al., "High-Accuracy Determination of 3C273-3C279 Position Difference from Long-Baseline Interferometer Fringe Phase Measurements," *Bull. Am. Astron. Soc.*, Vol. 3, No. 4, Pt. 1, p. 465, 1971.
405. Whitney, A. R., I. I. Shapiro, A. E. E. Rogers, D. S. Robertson, C. A. Knight, T. A. Clark, R. M. Goldstein, G. E. Marandino, and N. R. Vandenberg, "Quasars

- revisited: rapid time variations observed via very-long-baseline interferometry,” *Science*, vol. 173, No. 3993, pp. 225-230, July 1971.
406. Whitney, A. R., “Precision Geodesy and Astrometry via Very Long Baseline Interferometry,” Ph.D. Thesis, Mass. Inst. of Tech., Cambridge, Mass., 1974.
 407. Whitney, A. R., et al., “A Very Long Baseline Interferometry for Geodetic Applications,” *Proceedings of the IEEE*, 1975.
 408. Whitney, A. R., A. E. E. Rogers, H. F. Hinteregger, C. A. Knight, J. I. Levine, T. A. Clark, I. I. Shapiro, D. S. Robertson, and S. Lippincott, “A very long baseline interferometer system for geodetic applications,” *Radio Sci.*, Vol. 11, No. 5, pp. 420-432, May 1976.
 409. Wielebinski, R., “Receivers in Radio Astronomy,” *Kleinheubacher Berichte*, Vol. 15, pp. 371-378 (in German), 1972.
 410. Wilkinson, P. N., “Observations of Radio Sources with an Interferometer of 24 KM Baseline. 3. The Angular Structures at 408 and 1423 MHz of 44 Relatively Intense Radio Sources,” *Jodrell Bank Ann.*, Ser. 1, Vol. 2, Pt. 1, pp. 58-78 (Manchester University, England), Sept. 1973.
 411. Wilkinson, P. N., et al., “Radio structure of 3C147 determined by multi-element VLBI,” *Nature*, Vol. 269, pp. 764-768, Oct. 27, 1977.
 412. Williams, J. G., “Very Long Baseline Interferometry and Its Sensitivity to Geophysical and Astronomical Effects,” *DSN Space Programs Summary 37-62*, Vol. II, pp. 49-55. Jet Propulsion Laboratory, Pasadena, Calif., March 31, 1970.
 413. Williams, J. G., et al., “Lunar Physical Libration and Laser Ranging,” *The Moon*, Vol. 8, pp. 469-483, 1973.
 414. Wilson, W. J., A. H. Barrett, and J. M. Moran, “OH Radio Emission Associated with Infrared Stars,” *Astrophysical Jnl.*, 160, 545-571, 1970.
 415. Wittels, J. J., C. A. Knight, I. I. Shapiro, H. F. Hinteregger, A. E. E. Rogers, A. R. Whitney, T. A. Clark, L. K. Hutton, G. E. Marandino, A. E. Niell, B. O. Ronnang, O. E. H. Rydbeck, W. K. Klemperer, and W. W. Warnock, “Fine Structure of 25 Extragalactic Radio Sources,” *Astrophysical Jnl.*, 196, 13-39, 1975.
 416. Wittels, J. J., *Positions and Kinematics of Quasars and Related Radio Objects Inferred from VLBI Observations*, Ph.D. thesis, Massachusetts Institute of Technology, Cambridge, Mass., 1975.
 417. Wittels, J. J., W. D. Cotton, C. C. Counselman III, I. I. Shapiro, H. F. Hinteregger, C. A. Knight, A. E. E. Rogers, A. R. Whitney, T. A. Clark, L. K. Hutton, B. O. Ronnang, O. E. H. Rydbeck, and A. E. Niell, “Apparent ‘Superrelativistic’ Expansion of the Extragalactic Radio Source 3C 345,” *Astrophysical Jnl. (Letters)*, 206, L75-L78, 1976.
 418. Wittels, J. J., et al., “Time-Dependent Radio Fine Structure of the Quasar 3C 345,” *Astronomical Jnl.*, Vol. 81, pp. 933-945, Nov. 1976.
 419. Wittels, J. J., et al., “Mapping Radio Sources with VLBI,” National Radio Sci. Meeting, Univ. of Colorado, Boulder, Colorado, Jan. 9-13, 1978.
 420. Wolfe, A. M., J. J. Broderick, J. J. Condon, and K. J. Johnston, “3C 286: A Cosmological QSO?” *Astrophysical Jnl. (Letters)*, 208, L47-L50, 1976.

421. Yen, J. L., "A Long Baseline Interferometer System with Extended Bandwidth," *1968 NEREM Record*, Boston, Mass., 6-8 Nov. 1968 (IEEE, New York, pp. 64-5, 1968).
422. Yen, J. L., et al., "Real-Time, Very-Long-Baseline Interferometry Based on the Use of a Communication Satellite," *Science*, Vol. 198, pp. 289-291, Oct. 21, 1977.
423. Zhongolovich, I., "The Role of VLBI in the Establishment of Coordinate Systems," *Reference Coordinate Systems for Earth Dynamics*, IAU Colloquium No. 26 (held in Torun, Poland 1974), ed. Kolaczek & Weiffenbach, pub. in Warsaw, Poland, pp. 293-295, 1975.
424. Zverev, M. S., "Astrometry Under New Conditions — Review of Recent Developments and Future Possibilities," *Geodeziia i Aerofotos'emka*, No. 5, pp. 57-62 (in Russian), 1976.

Acknowledgment

The author is most grateful for ideas and encouragement from Dr. Nicholas A. Renzetti, Manager of Tracking and Data Acquisition Engineering, B. D. L. Mulhall, Manager of Advanced Engineering, and Dr. T. K. Truong. Thanks are due to Dr. Robert L. Miller for his many hours of patient work in scrounging through computer printouts from the NASA data bank and the Defense Document Center in order to make this bibliography as complete as it is.

Special thanks are also due to Professor M. H. Cohen of Caltech for his excellent bibliography of VLBI papers through December 1976, from which over one hundred references were taken. Finally, the author is indebted to many useful comments from Dr. G. M. Resch. —

